NASA CR-132537

MODEL OF HUMAN DYNAMIC ORIENTATION

By Charles C. Ormsby

Prepared under Contract No. NGR-22-009-701

Massachusetts Institute of Technology
Cambridge, Massachusetts

for

NATIONAL AERONAUTICS AND SPACE ADMINISTRATION

MODEL OF

HUMAN DYNAMIC ORIENTATION

by

Charles C. Ormsby

Submitted to the Department of Aeronautics and Astronautics, Massachusetts Institute of Technology, on January 16, 1974, in partial fulfillment of the requirements for the degree of Doctor of Philosophy.

ABSTRACT

The dynamics associated with the perception of orientation were modelled for near-threshold and suprathreshold vestibular stimuli. A model of the information available at the peripheral sensors which was consistent with available neurophysiologic data was developed and served as the basis for the models of the perceptual responses. As a preliminary assumption the central processor was assumed to utilize the information from the peripheral sensors in an optimal (minimum mean square error) manner to produce the perceptual estimates of dynamic orientation. This assumption, coupled with the models of sensory information, determined the form of the model for the central processor. Comparison of model responses with data from psychophysical experiments indicated that while little or no central processing may be occuring for simple suprathreshold canal stimulation, a significant portion of the dynamic response to translational accelerations must be attributed to the central processing of otolith information.

The fundamental mechanism which underlies the phenomenon of vestibular thresholds was studied experimentally by testing the response of subjects to a near threshold stimulus consisting of a velocity step-ramp proportional to the sum of the subject's velocity step and acceleration step thresholds. Experimental results indicated that canal thresholds could be accounted for by a model of central processing consisting only

of an optimal processing of afferent firing rates in additive noise with no necessity for peripheral dead zone nonlinearities. Quantitative models of threshold detection were developed which correctly predicted threshold levels (75% correct detection) and response latencies for rotational stimuli. It was found that the same detector could be used to model the threshold responses resulting from translational stimuli.

The illusions of static orientation were studied and it was shown that they were consistent with a simple vector transformation which could be associated with differences in the processing of signals arising from stimuli in and stimuli perpendicular to the "utricle plane". A model was developed which incorporated this difference and which was capable of predicting the perception of orientation in an arbitrary static specific force environment.

The problem of integrating information from the semicircular canals and the otoliths to predict the perceptual response to motions which stimulate both organs was studied. A model was developed which was shown to be useful in predicting the perceptual response to multi-sensory stimuli.

Thesis Supervisors: Laurence R. Young, Chairman
Professor of Aeronautics and Astronautics

Renwick E. Curry
Assistant Professor of Aeronautics and Astronautics

Charles M. Oman
Assistant Professor of Aeronautics and Astronautics

John J. Deyst
Associate Professor of Aeronautics and Astronautics

ACKNOWLEDGMENTS

I wish to express my gratitude to Professor Laurence R. Young who encouraged this research and who offered his aid and advice whenever it was requested. In addition I would like to thank Professor Renwick E. Curry, Professor Charles M. Oman and Professor John J. Deyst, each of whom made significant contributions to the success of this investigation.

The experimental work on rotational thresholds could not have been performed without either the experimental facilities or the technical assistance offered by NASA at the Langeley Research Center. Therefore, I would like to thank Mr. Ralph W. Stone who made the arrangements for the use of these facilities and Mr. Hugh Bergeron and his fellow workers who assisted in carrying out the experimental program.

Finally, I would like to dedicate this thesis to my wife Barbara who has without doubt borne the greatest burden of graduate life.

This research was supported by NASA grant NGR 22-009-701.

TABLE OF CONTENTS

Chapter Number		Page Number
CHAPTER I	INTRODUCTION	13
1.1	Motivation for Research	14
1.2	Approach to the Problem of Vestibular Modelling	16
1.3	Thesis Organization	21
CHAPTER II	THE HUMAN VESTIBULAR SYSTEM	23
2.1	Semicircular Canal System	23
2.2	Otolith System	26
CHAPTER III	MODELLING OF FIRST ORDER AFFERENTS AND RESPONSE TO NONINTERACTING SUPRATHRESHOLD STIMULI	33
3.1	Semicircular Canals	35
3.1.1	Dynamic Response of Cupula	35
3.1.2	Afferent Processing and Random Signal Variations	41
3.1.3	Optimal Processing and Model Predictions	50
3.2	Otolith System	62
3.2.1	Division of Afferent Response and Higher Order Processing	63
3.2.2	Otolith Model Specification and Predictions	71
CHAPTER IV	QUALITATIVE NATURE OF PROCESSOR FOR DETECTION OF NEAR-THRESHOLD HORIZONTAL ROTATION	81

Chapter Number		Page Number
4.1	Processor Hypotheses	81
4.2	Threshold Characteristics of the Hypothesized Models	86
4.3	Experimental Description	91
4.4	Analysis of Experimental Results	97
4.5	Conclusions	106
CHAPTER V	STOCHASTIC MODEL FOR DETECTION OF NEAR THRESHOLD ROTATIONAL STIMULI	108
5.1	*First Order Processing*	109
5.2	Detection Using Information From the Suprathreshold Optimal Estimator	121
5.3	Simplified Detector Model	128
5.4	Summary of Model Predictions for Detection Probabilities and Latencies	134
CHAPTER VI	STOCHASTIC MODEL FOR DETECTION OF NEAR THRESHOLD CHANGES IN SPECIFIC FORCE	139
6.1	Necessity for First Order Processing	141
6.2	Simplified Detector Model	150
6.3	Summary of Model Predictions for Detection Probabilities and Latencies	152
CHAPTER VII	PERCEPTION OF STATIC ORIENTATION IN A CONSTANT SPECIFIC FORCE ENVIRONMENT	157
7.1	Perceptual Illusions of Static Orientation	159
7.2	Model Based on Altered Saccular Information	173

Chapter Number		Page Number
7.3	Model Predictions in Various Constant Specific Force Environments	182
7.4	Summary	191
CHAPTER VIII	INTEGRATION OF SEMICIRCULAR CANAL AND OTOLITH INFORMATION FOR MULTISENSORY STIMULI	192
8.1	Discussion of Modelling Problems and Philosophy	193
8.2	DOWN Estimator	204
8.3	Quantitative Model Predictions	219
8.3.1	Dynamic Elevator Illusion	219
8.3.2	Rotation to Lateral Tilt of 5 Degrees	221
8.3.3	Catapult Launch	221
8.3.4	Frequency Response for Small Pitch and Roll Oscillations	227
8.4	Summary	230
CHAPTER IX	CONCLUSIONS AND SUGGESTIONS FOR FURTHER RESEARCH	231
9.1	Summary of Threshold Modelling	231
9.2	Summary of Suprathreshold Modelling	234
9.3	Suggestions for Further Research	237
Appendices		
A	Summary of Parameters for Perceptual Models	241
References		247
Biographical Sketch		254

LIST OF FIGURES

Figure No.		Page No.
2.1	Diagram of Human Inner Ear	24
2.2	Orientations and Polarizations of the Semicircular Canals	25
2.3	Horizontal Semicircular Canal	27
2.4	Cross Section of Otolith Organ	29
2.5	Orientation of Otolith Organs	30
2.6	Morphological Polarization Maps for the Saccule and Utricle of the Squirrel Monkey	32
3.1	Afferent Model of Semicircular Canals	46
3.2	Internal Model of the Stimulus Process	51
3.3	Internal Model of Stimulus and Canal Dynamics	53
3.4	Predicted Subjective Response to 1.5 Degree/Second ^{2} Acceleration Step	59
3.5	Amplitude and Phase Plots for Second Order Systems	66
3.6	Model of Otolith Perception	69
3.7	Comparison of Phase Predictions for Otolith Models	77
3.8	1G Step Response of Otolith Afferent Model	79
3.9	Predicted Subjective Response to 1G Step	79
4.1	Simple Threshold Model	83
4.2	Signal in Noise Model	83

Figure No.		Page No.
4.3	Displacement of the Cupula for Velocity Step and Acceleration Step Stimuli	85
4.4	Stimulus Diagram and Threshold Predictions of Hypothesized Models	92
4.5	Strip Chart Recording for Velocity Step Stimulus to the Left	96
4.6	Threshold Data for Six Subjects	98
4.7	Comparison of Learning Model and Data	101
4.8	Comparison of Data to Thresholds Predicted by Hypotheses	105
5.1	Comparison of Afferent Response to Threshold Velocity Step and Acceleration Step	110
5.2	First Order Processor	112
5.3	Model of Information Available to Detector	118
5.4	Signals Available for Detection After First Order Processing for Threshold Steps in Angular Velocity and Acceleration	120
5.5	Decomposition of Probability Density Function	123
5.6	Decision Boundaries	126
5.7	Typical Correct Response and Incorrect Response Trials	126
5.8	Simplified Detector	131
5.9	Model Predictions of Performance Variations as a Function of Stimulus Magnitudes	135
5.10, 5.11, 5.12	Model Simulations of Velocity, Acceleration and Combination Steps	136

Figure No.		Page No.
5.13, 5.14, 5.15	Latency Histograms of Velocity, Acceleration and Combination Steps	138
6.1	Simple First Order Processor	142
6.2	Alternate First Order Processor	142
6.3	First Order Processor Based on a Spectral Separation	144
6.4	Signal Available for Detection for Various Values of τ	146
6.5	Normalized Detection Parameter for Various Values of τ	148
6.6	Model Predictions of Performance Variations as a Function of Stimulus Magnitudes	153
6.7, 6.8	Threshold Acceleration Step Simulations (τ = 3, 30 seconds)	154
6.9, 6.10	Latency Histogram for Threshold Step in Acceleration (τ = 3, 30 seconds)	156
7.1	Illustration of Specific Force Stimulus Categorization	164
7.2	Perceived Tilt Angle as a Function of Actual Tilt Angle for 1G and 2G Specific Force Environments	168
7.3	Perceived Pitch Angle as a Function of True Pitch Angle and Magnitude of Specific Force	170
7.4	Illustration of Specific Force Stimuli for Categories A, N and E	177
7.5	Alteration of $\hat{SF}_z$	179
7.6	Model of Perceived Orientation	180

Figure No.		Page No.
7.7	Orientation of $\underline{SF}$ with Respect to Head Axes	183
7.8	Orientation of $\underline{\hat{DOWN}}$ with Respect to Head Axes	183
7.9	Model Predictions for Perceived Tilt Angle as a Function of Actual Tilt Angle in 1G and 2G Specific Force Environments	185
7.10	Model Predictions for Perceived Pitch Angle as a Function of True Pitch Angle in 1G and 2G Specific Force Environments	187
7.11	Model Predictions for Perceived Pitch Angle as a Function of True Pitch Angle in Various Specific Force Environments	188
7.12	Additional Alteration of $\hat{SF}_z$ Necessary to Fit Category E Experimental Data	189
8.1	Orientation and Sensitive Axes of Cyclopian Semicircular Canal System	201
8.2	Information Available to $\underline{DOWN}$ Estimator	203
8.3	$\underline{DOWN}$ Estimator	205
8.4	$\underline{\omega}$ Estimator	206
8.5	Approximate Time Course of Model Parameters and Response to 1G Step in Lateral Acceleration	216
8.6	Dynamic Elevator Illusion (1.75g)	220
8.7	Perception of Lateral Tilt	222
8.8	Comparison of the G_x Accelerations Recorded in Catapult Launch and Centrifuge Simulation (Cohen et al)	224
8.9	Schematic Representation of a Catapult Simulation on the Human Centrifuge (from Cohen et al)	224

Figure No.		Page No.
8.10	Movement of $\hat{DOWN}$ for Catapult Launch Simulation	225
8.11	Pitch Perception for Catapult Launch Simulation	226
8.12	Phase Response of Combined Model to Small Tilts (<10°) in Pitch and/or Roll	228

Chapter I

INTRODUCTION

The research effort which is described in this thesis was undertaken to increase our understanding of the phenomenology associated with vestibular perception. More specifically, this thesis attempts to separate the processes which underlie this perception into two cascaded but fundamentally distinct elements, namely:

1. the peripheral sensors and the associated neural processes which determine the afferent response to external stimuli; and
2. the processing by the higher centers of the information available from the first order afferent responses.

These elements can be considered as both physically separable and, in terms of our methodological approach to modelling them, philosophically separable. In the case of the first element the mechanical dynamics of the sensors can be and are distinguished from the dynamic effects associated with the first order afferent processes. In the case of the second element a distinction is made between the threshold stimuli which must be processed by a detector and suprathreshold stimuli which must be processed by an estimator. Suprathreshold stimuli are further divided into those which involve the integration of more than one sensory modality and those which do not. The motivation for this research

and the methodology used to approach the fundamental problems involved in the modelling of vestibular perception are discussed in this chapter followed by a brief introduction to the contents of the remaining chapters.

1.1 Motivation for Research

The products of modern technology, especially those associated with the advancements made in aerospace vehicles, have engendered a rapid increase in the need to understand man's reactions to motion environments which are completely alien to his pre-twentieth century experiences. Obvious examples of such environments are the prolonged zero-g environments made possible by space vehicles and the rapidly varying high g environments of modern military aircraft and rocket launch vehicles. Less obvious but equally important are man's reactions to the motions arising from commercial and general aviation aircraft, ships, tall buildings (sway) and motion based simulators. Since the vestibular system is man's primary non-visual inertial orientation sensor, its central importance to any understanding of man's capability to function effectively in these motion environments is clear.

If a model of stimulus detection is developed for vestibular perception which is capable of giving reasonable estimates of the detection probabilities as a function of

time for arbitrary near threshold stimuli then predictions can be made which have significant importance for several seemingly unrelated problems. Among the most prominent of these are the following:

1. How does one maximize the fidelity of a motion-based simulator while minimizing the requirements for translational motion so that simulator costs can be reduced? While the techniques involved in optimally utilizing a given amount of lateral motion capability can become quite sophisticated a thorough understanding of the dynamics of threshold perception is necessary if maximum fidelity is to be achieved.

and

2. What are the constraints which must be placed on the structural motions of tall buildings to insure the comfort of the buildings' occupants? This question is of great importance in the design of tall buildings since that design (and therefore the construction costs) will be very sensitive to the constraints imposed. Since these motions are typically quite small it is necessary to have a general model for the detection of near threshold motions if reasonable trade offs are to be made.

The need for a model to predict the subjective perception of dynamic orientation for suprathreshold stimuli which

involve stimulation of both the semicircular canals and the otoliths is even greater. Such a model could be used to study postural control, to evaluate the ride quality of a wide variety of transportation vehicles, to predict the reactions of pilots during unusual maneuvers, to predict the incidence of motion sickness, and to evaluate many of the illusions of motion or orientation which arise due to unusual g forces or sustained rotations. In addition, the development of such a model draws upon and may contribute to knowledge of sensory/neural physiology . For example investigators who are studying the neural processing centers of the brain may find interesting parallels between the interactions of sensory information they discover and the mathematical transformations required by the model. If the time comes that a one-to-one correspondence can be made between a mathematical model of man's perceptual responses and the processes seen in the brain then it might be possible to predict the site of neurological disorders based upon the response of patients to controlled stimuli.

1.2. Approach to the Problem of Vestibular Modelling

Since this research is concerned with the processing of information which is relevant to the perception of dynamic orientation it is important to elucidate carefully exactly what information is being considered. While the

problem of integrating the signals available from every sensory system which provides information pertinent to the perception of dynamic orientation is an important one, it is a task which, due to its extremely broad scope must await the solution of more restricted problems. The models developed in this thesis exclude any information gained from non-vestibular sensors during the time of stimulus exposure. Specifically excluded are visual, tactile, proprioceptive, kinesthetic and aural information. Information gained prior to the stimulus exposure is considered a priori information and in most cases can be handled by the general mathematical framework of the models if care is taken to account fully for the nature of that information and how it is affected by any pre-stimulus instructions. In addition to a priori information the higher centers have at their disposal two other types of information. The first of these is the afferent signal available from the vestibular sensors which must be processed to obtain the perceptual estimates of orientation. To process these sensory signals and to mix them optimally with the a priori information requires some knowledge of the processes which give rise to the afferent signals. It is this knowledge (which includes an internal model of both the sensory dynamics and the measurement noise processes) that completes the information base available to the higher centers.

In the process of developing models for the information available from the vestibular sensors and for the processing of that information by the higher centers a number of issues arise which can be dealt with as methodological problems. Several of these issues will be dealt with here as illustrations of the approach to perceptual modelling taken in this research.

One question which arises immediately in any modelling effort concerns the criteria which will be used to select the form of the model and its parameters. The answer to this question depends on the amount of knowledge available about the physical system being modelled. Since a significant amount of qualitative and quantitative knowledge is available concerning the mechanical and afferent dynamics of the vestibular sensors this information will be used as much as possible in modelling their dynamic response. On the other hand the knowledge available about the internal structure and organization of the central processor is much more limited. So much so in fact that any attempt to develop a viable model of subjective perception as a function of afferent responses based upon the known neurophysiological structure of the brain would probably be fruitless. Upon what information then can a model of the central processor be based? In any modelling effort in which the physical structure is considered completely unknown, a "black box" approach is taken to produce

a model which is consistent with the known responses of the system to selected inputs. In this case it is reasonable to presume that the neural net which forms the central processor has evolved to use the available sensory information in a roughly optimal way. This assumption of optimality serves to suggest the form of the processor and eliminates any problem of non uniqueness (the fact that more than one processor might have been capable of producing the required predictions). The model which proceeds from this assumption of optimality must then be checked against the known output of the system--namely the subjective responses determined from psychophysical experiments.

Another problem which arises involves the issue of efferent signals from the higher centers which may dramatically alter the afferent response. The mechanism by which efferent discharges affect afferent responses is, as of yet, unknown. Whatever that mechanism, if the transformation of the afferent signal has a unique inverse then the point of view taken in this research is that the total information available to the higher centers concerning the dynamic orientation of the head is unchanged since the higher centers initiated the efferent signaland are aware of its effect on the afferent response. Since the goal of this research is to develop a model of the available afferent vestibular information and its subsequent optimal processing by the higher

centers any invertible alteration of the afferent information will not affect the models predictions and therefore can be ignored in the development of the model.

Finally the problem of active versus passive head movements is an issue which deserves attention. Since an active movement of the head is initiated by the higher centers, the resultant motion (to the extent that it can be predicted open loop by the higher centers) is available as a priori knowledge. Therefore the equivalent information available from the peripheral sensors is redundant and adds nothing to the a priori knowledge available to the higher centers. Since the open loop estimate of head motion is bound to contain some errors the afferent response from the peripheral sensors should be used to check these a priori estimates. One way to accomplish this is to take the difference between the expected sensory response (based upon the open loop estimate of motion and the internal model of the sensory dynamics) and the actual sensory response. This is one interpretation of the corollary efferent discharge or "efferent copy." The resulting signal can then be processed to estimate the errors associated with the movement. The models developed in this thesis should therefore only be used in an error correcting mode for motions which are initiated by the higher centers.

Additional problems similar to those described above are dealt with in a similar fashion when they arise in the course of developing the models.

1.3. Thesis Organization

Chapter Two summarizes the structure, function and orientation of the semicircular canals and the otoliths.

Chapter Three derives a model of the information available at the first order afferent level of both the semicircular canal system and the otoliths. These models are then coupled with optimal estimators to yield predictions of subjective perception for simple noninteracting stimuli.

Chapters Four, Five, and Six develop models for the detection of near threshold stimuli. Chapter Four describes an experiment which was conducted to determine the fundamental mechanism underlying the threshold phenomenon. Chapters Five and Six develop quantitative models for the detection processes associated with rotational and translational motions respectively.

The seventh chapter investigates the illusions of static orientation as a function of body position and the strength of the gravito-inertial field. A simple mechanism is proposed which accurately predicts these illusions and indicates that they most likely have a common origin.

The problem of integrating the information from both

the semicircular canals and the otoliths to arrive at a single set of preceptual responses is investigated in Chapter Eight. A model of sensory integration is proposed which can be used either qualitatively or quantitatively to predict the subjective perceptions associated with interacting stimuli.

Finally, Chapter Nine summarizes the conclusions which can be drawn from this research and suggests possibilities for further experimental and analytical investigation.

Chapter II

THE HUMAN VESTIBULAR SYSTEM

The purpose of this chapter is to introduce the reader who is unfamiliar with the vestibular sensors to the basic structural organization and physiologic function of these organs. A more in-depth introduction is available in references 9,61 and 80.

2.1. Semicircular Canal System

The semicircular canals are the primary nonvisual sensors of rotational motion with respect to inertial space. They consist of three approximately circular toroidal canals whose axes form a roughly orthogonal set. The membranous canals are suspended in a fluid (perilymph) in the temporal bone of the skull adjacent to the auditory portion of the inner ear. Figure 2.1 illustrates the entire inner ear (including vestibular and auditory portions) and Figure 2.2 indicates the orientation of the canals relative to the head. The semicircular canals are filled with a water-like fluid called endolymph which, due to its inertia, tends to lag behind the motion of the canal walls when the head undergoes angular acceleration. When the endolymph moves relative to the canal it tends to displace the cupula which obstructs an expanded section of the canal called the ampulla. This displacement of the cupula is detected by sensory hair cells at the base of the cupula which in turn produce a change in

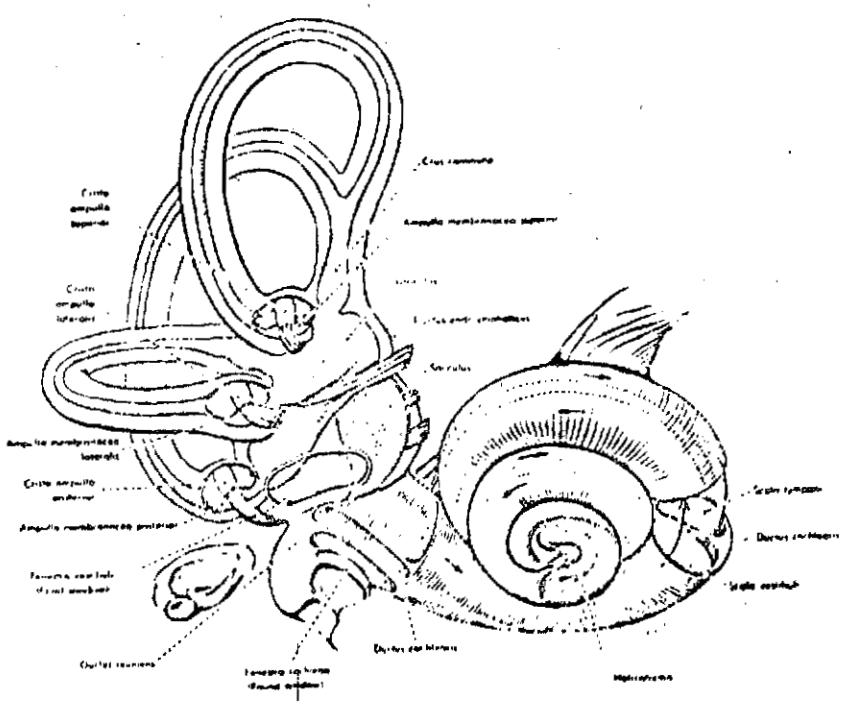

Figure 2.1 Diagram of Human Inner Ear
(Abbott Laboratories Ref. 1)

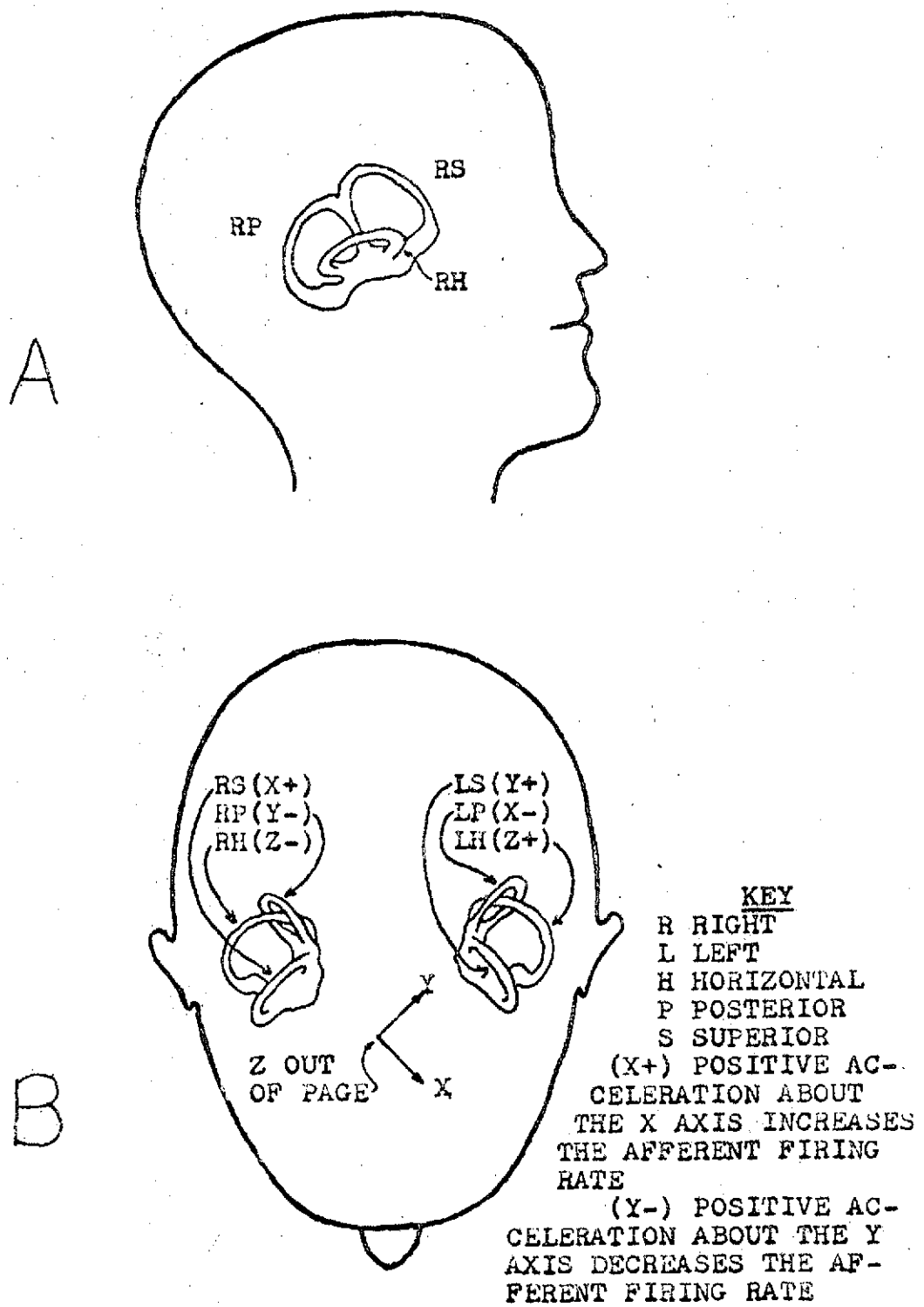

Figure 2.2 Orientations and Polarizations of the Semicircular Canals

the firing frequency of the first order afferents which provide information to the central nervous system. Figure 2.3 illustrates this process for the horizontal canal. All of the hair cells associated with a particular canal have the same polarization, i.e., displacement of the cupula due to endolymph flow in one direction will either excite all of the sensory hair cells or inhibit them all.

Since the canals on the right side are essentially coplanar with the canals on the left side they are pairwise sensitive to angular accelerations about the same axes. Investigation of the afferent responses of these sensors indicates that a pair of canals which are sensitive to acceleration about the same axis (e.g. the right posterior canal and the left superior canal) have opposite sensitivities (see Figure 2.2B), so it is presumed that the higher centers respond to the difference of their responses. The detailed dynamic response of the afferent firing of the semicircular canals to an angular acceleration of the head is discussed in section 3.1.

2.2. Otolith System

In addition to the semicircular canals, the nonauditory portion of each inner ear contains two otolith organs which are sensitive to changes in the gravitoinertial reaction force (referred to here as specific force). The approximate

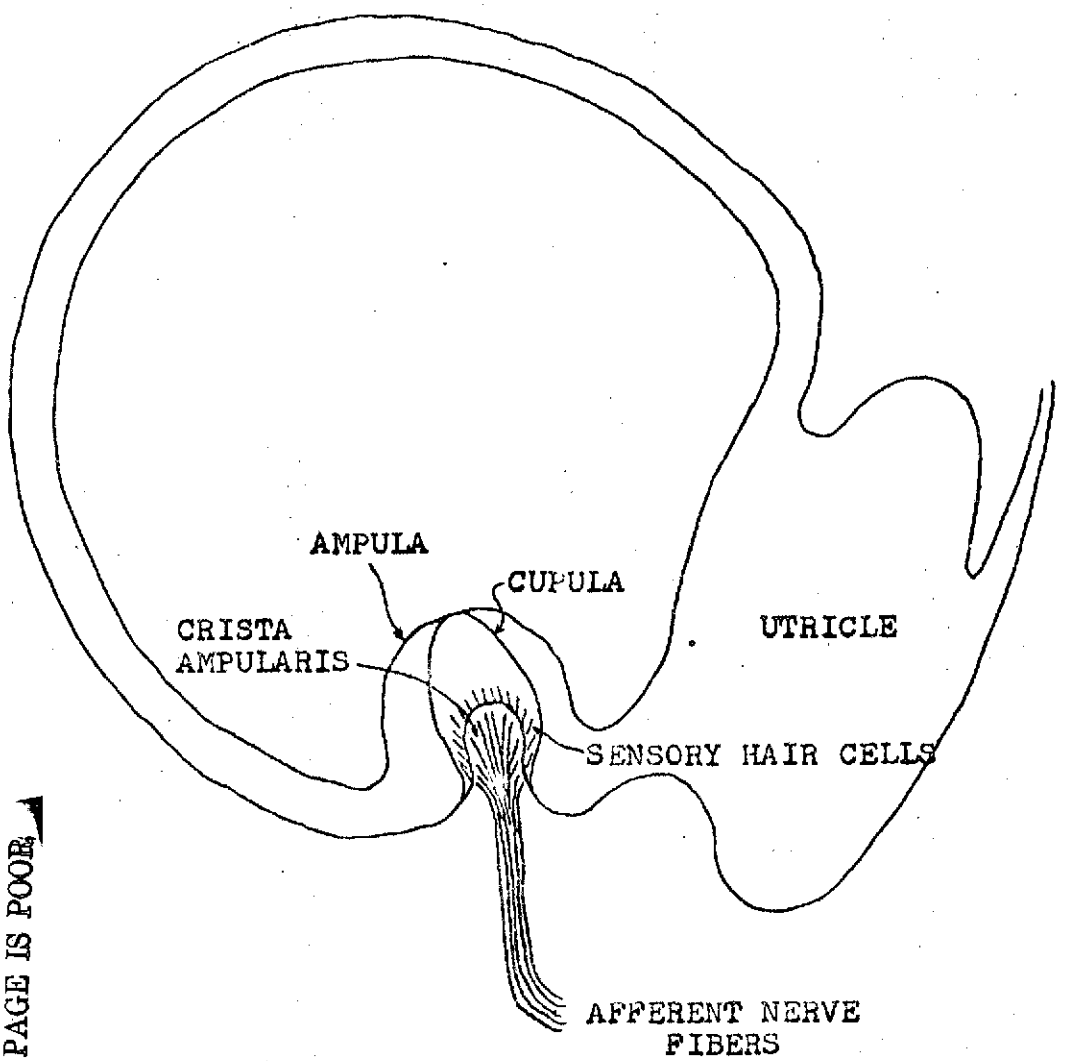

Figure 2.3 Horizontal Semicircular Canal

location of each of these organs, known as the utricular otolith and the saccular otolith, is shown in Figure 2.1. Each otolith organ contains a gelatinous layer interspersed with calcium carbonate crystals and supported by a large number of sensory hair cells. Since the calcium carbonate crystals (known as otoconia) have a higher specific gravity than the surrounding fluid (endolymph) an appropriate accleration of the head will tend to shift the otoconia relative to the bed of sensory cells (known as the macula). When this shifting motion occurs the sensory hairs are bent and the afferent fibers which innerviate these hair cells change their firing rate. Figure 2.4 illustrates the basic structure of the otoliths.

Motion of the otoconia parallel to the bed of sensory hairs (in Figure 2.4: motion right and left or into and out of the page) is normally assumed to be the effective agent in eliciting a change in afferent firing. The utricles are oriented such that the major plane of their sensitivity is parallel to the plane of the horizontal semicircular canals. The saccular organs are oriented so that their plane of sensitivity is perpendicular to the horizontal canals (and therefore the utricles) and roughly parallel to the median plane. Figure 2.5 illustrates the approximate orientation of the otolith organs. Unlike the semicircular canals, the hair cells in the otolith organs do not all have the

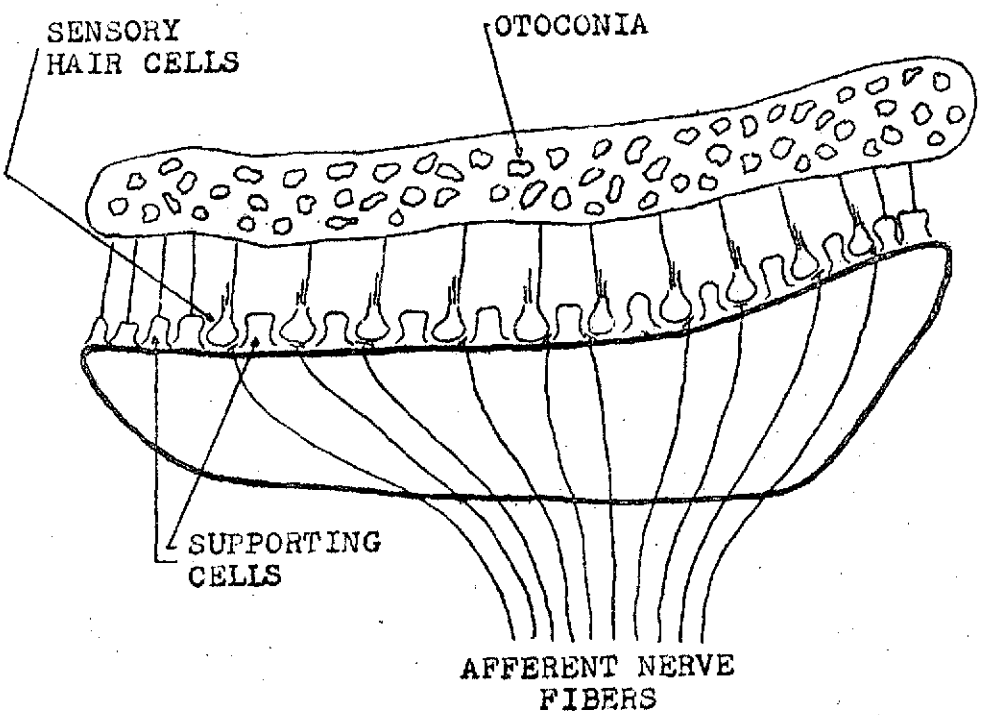

Figure 2.4 Cross Section of Otolith Organ

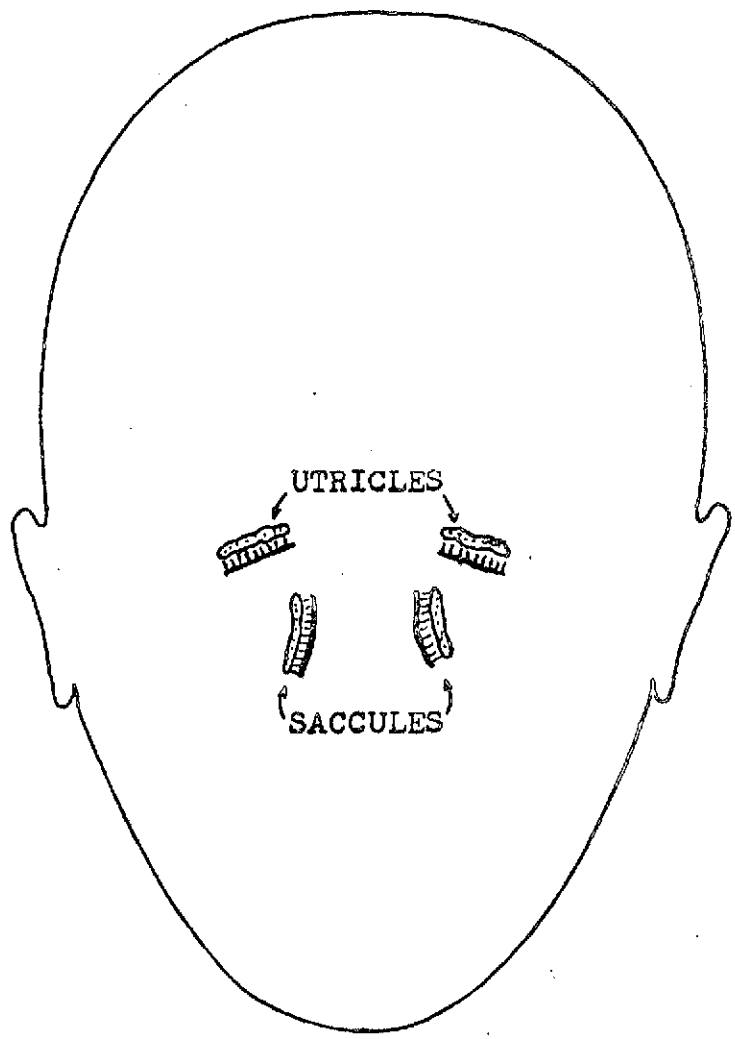

Figure 2.5 Orientation of Otolith Organs

same directional polarization. Figure 2.6 illustrates the general morphological distribution of hair cell polarizations for the utricle and saccule. The directional distribution of polarizations in the utricle is reasonably uniform and thus the utricular otolith can be considered approximately equally sensitive to shear forces in any direction in the utricular plane. The distribution of polarizations in the saccule is much more restricted, with the major axis of sensitivity roughly perpendicular to the utricular plane. Therefore the saccule can be considered as an accelerometer sensitive to changes in the specific force perpendicular to the average plane of the utricles.

The detailed dynamic response of the otolith afferents is discussed in section 3.2.

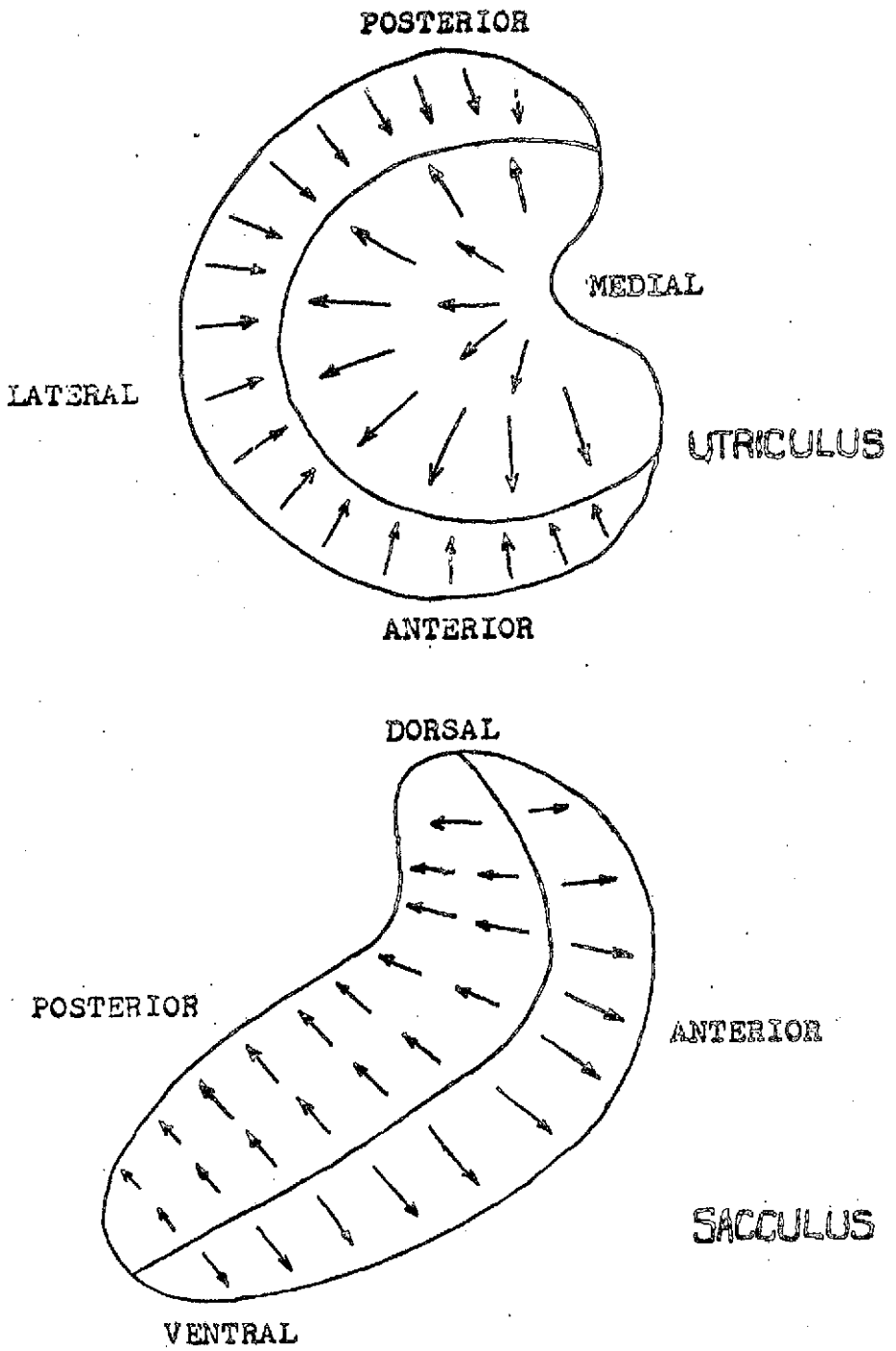

Figure 2.6 Morphological Polarization Maps for the Saccule and Utricle of the Squirrel Monkey (After Lindeman, Ref. 42)

Chapter III

MODELLING OF FIRST ORDER AFFERENTS AND RESPONSE TO NONINTERACTING SUPRATHRESHOLD STIMULI

The purpose of this chapter is to develop models of the sensory information available at the first order afferent level for both the semicircular canal and the otolith systems. The resulting models will serve as the informational link between the true motion with respect to inertial space and higher processing centers in the brain. Since we take the view that the higher centers have most likely evolved as optimal or near optimal processors of this information, a specification of the relevant sensory dynamics plays a major role in determining the overall dynamics of the subjective response to vestibular stimulation. Once the first order afferent response is modelled for each of the vestibular sensors and these models are coupled with reasonable models of process noise (which represent the a priori information concerning the statistical nature of the expected input) and measurement noise, then the optimal processor can be formulated and predictions made concerning the subjective response to noninteracting suprathreshold stimuli. The phrase "noninteracting suprathreshold stimuli" refers to any suprathreshold stimuli which involves no change in the orientation

of the subject with respect to the gravitational vertical and for which the subject is consciously aware that no such change will take place. Generally, this means rotations which are performed about an axis parallel to the local g vector and accelerations which are performed in a device which the subject knows is incapable of rotations out of the vertical. The reasons for these limitations will become clear when stimuli not meeting this description are considered in Chapter Eight.

3.1 Semicircular Canals

The specification of afferent dynamics for the semicircular canal system is divisible into several parts. The first involves a modelling of the mechanical movement of the cupula within the ampullary lumen. The second part of the specification concerns itself with how this mechanical movement is reflected in the neural firing rate in the first afferent nerve. Finally, an assessment must be made of that portion of the afferent signal which is found to be independent of the stimulus input and which therefore is considered to be measurement noise in the context of this modelling effort.

3.1.1 Dynamic Response of Cupula

The structure and fundamental mechanical operation of the semicircular canal is described in section 2.1 and illustrated in Figure 2.3. Two forces act to accelerate the endolymphatic fluid (which fills the canals) with respect to inertial space. The first of these is a viscous drag which is proportional to the rate of movement of the fluid with respect to the walls of the canal. The second is presumed to be a linear elastic restoring force which arises from the spring-like tendency of the cupula and/or the membranous canal to maintain its resting position or shape.

If it is assumed that for normal physiologic motions no endolymphatic fluid is allowed to leak between the cupula and the inner wall of the ampulla, then the amount of movement of the cupula is proportional to the angular motion of the fluid with respect to the canal walls. This assumption seems to be warranted on the basis of observations by Steinhausen (Ref. 66) and injection micrographs performed by Groen, Lowenstein and Vendrik (Ref. 32). Using this assumption, the motion of the endolymph relative to the canal can be expressed as follows:

$$M(\ddot{\theta}_{ec} + \ddot{\theta}_{ci}) = -V\dot{\theta}_{ec} - K\theta_{ec} \qquad (3.1)$$

where θ_{ec} = angular deflection of the endolymph with respect to the canal

θ_{ci} = angular position of the canal with respect to inertial space about an axis normal to the plane of the canal

M = moment of inertia of the endolymph

V = coefficient of viscous drag

K = coefficient of linear restoring force due to displacement of the fluid within the canal.

Equation 3.1 is referred to as the torsion pendulum model and was first developed (using different conventions) by Steinhausen (Ref. 67) after observing the motion of the cupula in the pike. The equation is arranged to illustrate

that the acceleration of the endolymph with respect to the inertial space ($\ddot{\theta}_{ec} + \ddot{\theta}_{ci}$) is due to the sum of a viscous drag force ($-V\dot{\theta}_{ec}$) and an elastic restoring force ($-K\theta_{ec}$). Equation 3.1 is time invariant and can be Laplace transformed to yield the following transfer function relating endolymph displacement to acceleration of the canal ($\alpha_{ci}(s)$):

$$\frac{\theta_{ec}(s)}{s^2\theta_{ci}(s)} = \frac{\theta_{ec}(s)}{\alpha_{ci}(s)} = \frac{-1}{s^2 + (\frac{V}{M})s + (\frac{K}{M})} \qquad (3.2)$$

Available evidence indicates that the system is overdamped and $\frac{K}{V} << \frac{V}{M}$. Therefore equation 3.2 can be approximated by

$$\frac{\theta_{ec}(s)}{\alpha_{ci}(s)} = \frac{-1}{(s + \frac{K}{V})\ (s + \frac{V}{M})} \qquad (3.3)$$

The short time constant, $\tau_s = \frac{M}{V}$, can be calculated from hydrodynamic considerations if the Navier Stokes equations for the canal/cupula system can be solved. Steer (Ref. 65) solved these equations for a somewhat simplified situation and concluded that to first order the short time constant should be proportional to the endolymph density, the square of the canal's minor radius and inversely proportional to the endolymph viscosity. Using the results of Igarashi (Ref. 38) for the toroidal radius yields an estimate of 0.005 seconds for the short time constant in man.

The long time constant, $\tau_L = \frac{V}{K}$, has been estimated at approximately 10 seconds using subjective responses (Ref. 68) and approximately 16 seconds using nystagmus records (Ref. 33) following step changes in angular velocity. Calculations of τ_L using the audiogyral illusion (Mayne, Ref. 49) yield values from 8 to 11 seconds. The difference between these estimates may be presumed to be due to adaptative processes which are more active in the subjective pathways than in those associated with nystagmus (Ref. 78). The adaptation dynamics will be discussed in the next section, but the important point to note here is that neither the subjective reports nor nystagmus are merely a consequence of the mechanical movement of the cupula described by the torsion pendulum model. Therefore any estimate of the long time constant for the torsion pendulum model which depends on subjective responses must also include the possible effect of neural processing. If the presumption were made that no neural processing takes place in the vestibular-ocular pathway and thus that vestibular nystagmus correctly reflects cupular motion, then we would set the long time constant at approximately 16 seconds. In fact, nystagmus slow phase velocity records taken from subjects exposed to steps in angular acceleration do seem to show weak adaptation (Young and Oman Ref. 62, Malcolm and Jones Ref. 48) and thus 16 seconds

might be considered a lower bound. Schmid, Stefanelli and Mire (Ref. 62) calculated the value of τ_L by fitting a model for the vestibular-ocular dynamics which included an adaptation term of the form $\tau_A s/(\tau_A s + 1)$ to nystagmus records and found the best fit when τ_A = 61.1 seconds and τ_L = 18.2 seconds. Based on this work and its agreement with previously cited works, we have chosen a value of τ_L = 18 seconds as a good estimate.

Up to this point, the description of cupular motion has been purposely kept vague. It is clear that if the endolymph moves within a rigid canal, is incompressible, and no leakage occurs around the cupula, then the cupula must move in such a way as to sweep out a volume equal to the net volumetric displacement of the endolymph. The classical description of this movement is that of a swinging motion in which the cupula slides freely against the ampula wall and bends near its base at the crista. This description was supported by Dohlman's experiments in which the cupula stained with china ink, was observed while pressure was applied unilaterally to the fluid and then released (Ref. 23). While this procedure might indicate that such motion of the cupula is possible under application of the pressures employed in this experiment, it can not be inferred that such motions occur during normal physiologic movement of the head. Steady state pressure differences across the cupula have been estimated

by Oman and Young (Ref. 59) to range from 1.25×10^{-4} dyne/cm^2 at threshold (.1°/sec^2) to approximately 3.8×10^{-2} dyne/cm^2 for steps of 30°/sec^2. Using a short time constant of 0.005 seconds and a long time constant of 20 seconds and presuming a rigid body rotation of the cupula about the crista, they calculated a steady state deflection of 0.025 degree for a sustained stimulus of 30°/sec^2. It is clear from these calculations, even if they are only correct within an order of magnitude that the cupula motion observed by Dohlman must have resulted from distinctly non-physiological pressures. Oman and Young concluded on the basis of these results that the cupula might move angularly, lineraly, or both. It should be noted that a linear movement of the cupula would give superior sensitivity since for a given displacement, it would be more effective in bending the sensory hair cells.

In summary we can conclude that the displacement or bending of the sensory hair cells, which is the effective agent for illiciting a change in afferent firing rate, should be related to angular acceleration of the head as follows

$$\text{Hair cell deflection} \propto \mathcal{L}^{-1}\left[\frac{-\alpha(s)}{(\tau_L s+1)(\tau_S s+1)}\right] \qquad (3.4)$$

where $\tau_S \approx 0.005$ sec

$\tau_L \approx 18$ sec

and $\mathcal{L}^{-1}$ indicates the inverse Laplace Transform Operator.

A proportional relationship is sufficient for our purposes at this point, since the overall gain from head acceleration to firing rate can best be estimated from records of afferent firing which will be discussed in the next section.

3.1.2 Afferent Processing and Random Signal Variations

The most desirable data upon which a model of afferent vestibular responses in humans could be based would, of course, be in vivo recordings in the canals' afferent nerve in humans. Since man is not suitable for experimental surgery, such data is not and may never be available. There are two other sources of data which can be used to make reasonable estimates of afferent processes in man. The first of these consists of psychophysical data taken from human subjects, which of course will include whatever dynamics are present in the afferent processing. The second source is recordings of peripheral afferents in animals. The sum of data from these two sources is not sufficient to argue conclusively that a particular dynamic effect is peripheral in man, but if such an effect is seen in human subjective responses and is also present in the afferent recordings of animals which are phylogenically similar to man, then such a conclusion seems reasonable.

An analysis of vestibular nystagmus and reports of subjective perception of rotation indicate the need for dynamics in addition to the torsion pendulum model to account for rate sensitivity and adaptation. The need for rate sensitivity shows up principally in cases when there are abrupt changes in the rate of rotation. Nashner (Ref.54,55) in studying human postural control, found it necessary to include a small lead term (.017s + 1) in the semicircular canal dynamics to predict the response times of subjects exposed to large impulsive stimuli. A behavior consistent with such a rate sensitivity was seen by Benson (Ref. 6) in analyzing nystagmus records for sinusoidal stimuli between 0.01 Hz and 5 Hz. A consistent increase in amplitude ratio for vestibular nystagmus was unexpectedly observed starting at about 0.5 Hz. An increase in the amplitude ratio of 3 db is seen at approximately 2.6 Hz which would imply a lead term of the form (0.06s + 1).

The phenomenon of adaptation is much more clearly evident in subjective responses than is rate sensitivity. Adaptation can be thought of as a fatiguing of sensation which occurs in addition to that which arises due to the long time constant of the torsion pendulum model. As an example, the torsion pendulum model predicts a steady state sensation of constant velocity in response to a step in acceleration while subjective data (Ref. 14,35) indicates a gradual decline in the sensation of velocity. For steps in angular velocity, sub-

jective data and nystagmus data (Ref. 2) indicate not only a diminishing of response to zero (consistent with the torsion pendulum model) but also a reversing of the response. Finally, as noted in the previous section attempts to fit the torsion pendulum model to the responses from impulsive velocity changes yielded different long time constants for subjective and nystagmus data. Young and Oman (Ref. 82) were able to account for this behavior by adding an adaptation operator of the form

$$\frac{30s}{30s + 1}$$

to the subjective pathway and

$$\frac{120s}{120s + 1}$$

to the nystagmus pathway. The difference in adaptation time accounts for the discrepancy in estimation of the long time constant.

Combining the terms proposed for rate sensitivity and adaptation, we conclude that in addition to the torsion pendulum model, we should have dynamics of the form

$$\frac{\tau_A s(\tau_R s + 1)}{(\tau_A s + 1)} \qquad (3.5)$$

$\tau_R \simeq .017$ seconds (lead time constant)

$\tau_A \simeq 30$ seconds (subjective adaptation time constant)

To decide if it is reasonable to ascribe these dynamics to the peripheral afferents, we must resort to data taken from the first order afferents in animals. Lowenstein and Sand (Ref. 43, 44) and Groen, Lowenstein and Vendrick (Ref. 32) made recordings in the vestibular afferent of the thornback ray. Groen et. al. made recordings in the isolated end organ to preclude the possible effects of efferent innervation. These experiments confirmed the fundamental features of the torsion pendulum model, but make no comment regarding additional rate sensitivity or adaptation. The most thorough study of the vestibular afferents in a mammal were conducted by Goldberg and Fernandez (Ref. 27) using the squirrel monkey. in these experiments a thorough evaluation of afferent responses to constant angular accelerations and sinusoidal stimuli was made. The firm conclusion reached was that significant rate sensitivity and adaptation was present in a large percentage of the cells studied. After eliminating the dynamics which can be attributed to the mechanical operation of the endolymph cupula system, Goldberg and Fernandez found afferent dynamics of exactly the same form as those given in 3.5. They found that τ_R ranged from .013 to .094 seconds with a mean value of .049 seconds. τ_A ranged from about 30 seconds to infinity (no adaptation) with a typical value being 80 seconds.

It is clear from these results that the attributes of both rate sensitivity and adaptation are present in the peri-

pheral vestibular neurons of the squirrel monkey. Since these effects, with roughly the same time constants, are observed in human subjective responses we will also consider them to be present in the afferent processes of the human vestibular system. In addition to the afferent response which depends upon the rotational stimulus there is a spontaneous afferent discharge and a noise component which is essentially independent of the stimulus. Adding these terms we arrive at the model for afferent firing rate shown in Figure 3.1. A very conservative figure was chosen for the rate time constant τ_R since its existence in subjective responses is very difficult to detect and because it is possible that the most rate sensitive cells would be used mainly for eye stabilization and consequently only show up in nystagmus records.

The constants H and F (see fig. 3.1) have not been determined separately but the product HF can be calculated based on the magnitude of the afferent response to a controlled stimulus. Afferent data from Ref. 27 indicates that a typical initial response to a step in velocity of 1 deg/sec (approximately .0175 rad/sec) is about .55 impulses/sec. Substituting the values for the time constants into the model and using the initial value theorem we obtain a value for HF of -6303. The sign of HF can be considered arbitrary as long as the processing centers in the brain interpret the sign correctly. The value for the spontaneous discharge (SFR) is of little consequence for our purposes since it is presumed that the

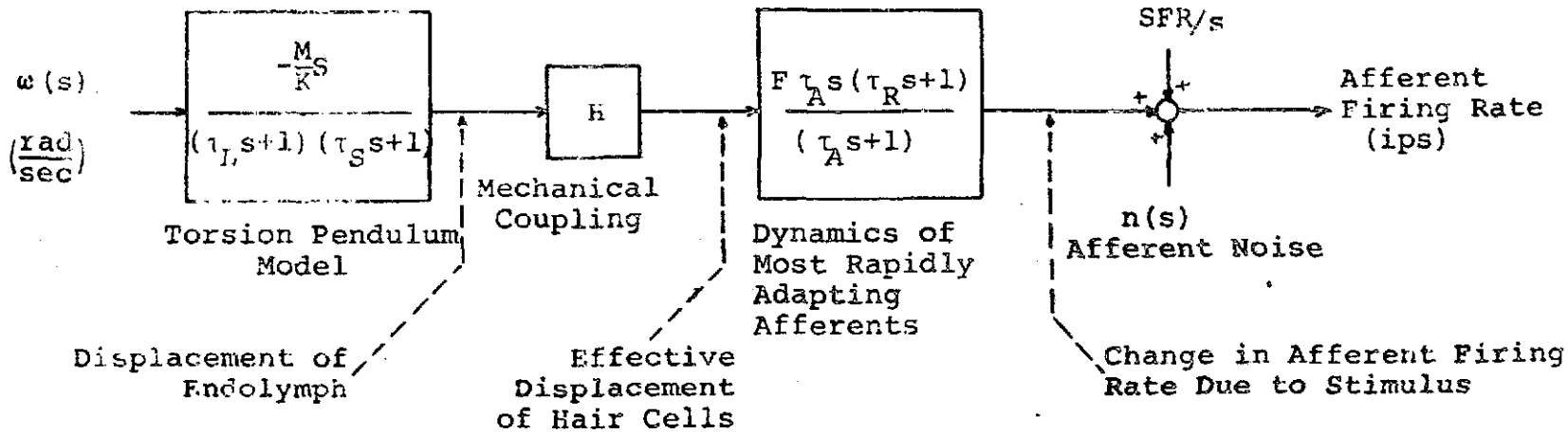

$\omega(s)$ = Stimulus (rad/sec)

$M/K = \tau_L \tau_S = .09 \text{ sec}^2$

τ_L = 18 seconds

τ_S = .005 seconds

τ_A = 30 seconds

τ_R = .01 seconds

H — Mechanical coupling of endolymph to effective hair cell displacement

F — Constant which relates hair cell displacement to change in firing rate

SFR — Spontaneous firing rate of typical afferent cell (90 ips)

Figure 3.1 Afferent Model of Semicircular Canals

higher centers only process differences from the resting level, but for completeness we will assign a value of 90 ips which is typical of the cells seen by Goldberg and Fernandez.

Lastly, we must address the problem of specifying the statistics of the afferent noise, n. The presumption is made that n is a stationary, gaussian process with zero mean. No information is available concerning the autocorrelation of n, but the variance of n for different afferent cells has been calculated. Goldberg and Fernandez show a histogram for the coefficient of variation (CV) for 142 different cells. The CV for a particular unit is defined as

$$CV \equiv \frac{E^{1/2}\{(\Delta T - E\{\Delta T\})^2\}}{E\{\Delta T\}} \tag{3.6}$$

where ΔT = time in msec between impulses

and $E\{x\}$ denotes the expected value of x.

CVs varied from about 0.03 to as high as 0.64. The distribution of CVs showed a sharp peak around CV = 0.06 with two thirds of the units falling below CV = 0.25. If the higher centers were capable of distinguishing between regular and irregular units then it would be reasonable to assume that a greater weighting would be placed on units with regular discharge patterns. For this reason, a value of 0.06 will be used as the coefficient of variation typical of the most regular

cells found (≈ 1/3 of the total population). Using this value we can calculate what one standard deviation in firing rate would be for a typical cell.

$$E^{1/2}\,[n^2(t)] = \frac{.06}{1 + .06}\,90. \;=\; 5.1 \text{ ips} \qquad (3.7)$$

Gacek (Ref. 26) estimates that there are approximately 12,000 afferent fibers in the vestibular nerve of the cat. Since this would include the otoliths and all three canals a figure for one crista of 2400 would be reasonable. The equivalent one channel representation of a 2400 channel system each with independent additive noise of magnitude σ, would be one channel with

$$E^{1/2}[n^2(t)] \;=\; \sigma/\sqrt{2400} \qquad (3.8)$$

This reduction in σ must be tempered by the following considerations

1) We chose CV = .06 which was representative of the most regular 1/3 of the total cell population and thus the value of 2400 should be reduced to approximately 800.
2) We presumed in the above analysis that the noise on each channel was independent of the noise on the other channels. If the noise were exactly the same on each channel then there would be no reduction in effective noise at all. What the actual correlation might be is unknown but it is not unreasonable to assume that some correlation exists (especially if the noise were related to random movements of the cupula).

and finally

3) We cannot assume that the higher centers are perfect in their ability to weed out irregular cells or in their ability to combine the resulting regular cells in such a way as to minimize the effective noise level.

In chapter V the noise level necessary to yield 75% correct detection for the case of experimentally determined threshold stimuli is calculated based on a near optimal model of the detection capabilities of the higher centers. This results in value of $E^{1/2}[n^2]$ equal to .223 ips which is roughly equivalent to 520 independent channels each with a noise standard deviation of 5.1 ips. In light of the considerations listed above this seems to be a reasonable noise reduction capability.

The results of this chapter, to this point, can be summarized by the following model of afferent firing in response to a rotation stimulus:

$$\begin{matrix}\text{Afferent}\\ \text{Firing}\\ \text{Rate}\\ \text{(ips)}\end{matrix} = \mathcal{L}^{-1}\left\{\frac{(57.3)\ 300s^2(.01s+1)}{(18s+1)(.005s+1)(30s+1)}\right\}\omega(s) + SFR + n(t) \qquad (3.9)$$

$E^{1/2}[n^2(t)] = .223$ ips

$\omega(s)$ = rotational rate normal to the plane of the canal (rad/sec).

SFR = spontaneous firing rate (ips)

3.1.3 Optimal Processing and Model Predictions

Now that a linear model is available for the afferent firing rate, it is relatively easy to develop a model for the processing done by the higher centers. An optimal estimate can be formulated for any linear combination of the internal states of the sensory dynamics if the processor receives periodic measurements of the afferent firing rate and has a knowledge of the sensory dynamics and the statistical characteristics of both the measurement noise and the input process. So far we have specified models for both the linear dynamics and for the measurement noise but we have yet to model the processors' a priori knowledge of the stimulus. Once this is done the optimal processor can be formulated and the entire system including cupula dynamics, afferent dynamics and processing dynamics can be tested and its predictions checked against subjective responses.

It is reasonable to postulate that in most situations where a person is exposed to passive motion he has some estimate of the magnitude of the motion which he expects to experience and to a lesser degree an idea of the motions frequency context. One model for the subject's a priori information which incorporates both of these notions quite simply, consists of a first order filter driven by white noise. This is equivalent to modelling the stimulus as an exponentially correlated process. The only parameters to be specified

in such a model are the filter's cut off frequency and the magnitude of the white noise. Figure 3.2 illustrates the higher centers' internal model of the input statistics which, together with a model of the sensory mechanism, describes the afferent firing which the processor samples periodically. One way to communicate to the mathematics of our model that very little is known about the frequency content of the stimulus is to make τ_I small and thus render the bandwidth of the input spectrum very large. With this in mind τ_I is set to a value less than or equal to one second. Q(t) is typically set to a constant such that the expected standard deviation of the input process given by $Q/\sqrt{2\tau_I}$ is essentially of the correct magnitude for the actual stimulus being tested. Setting Q to a value which correctly represents the stimulus magnitude can be justified both on the grounds that one usually has a reasonably correct estimate of the magnitude of incipient motions and on the grounds that an approximately

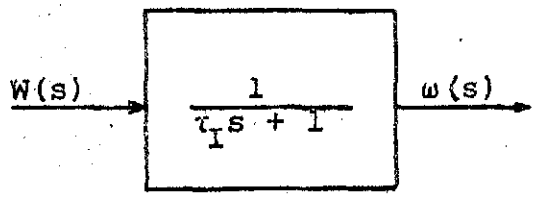

$E\{W(t_1)W(t_2)\} = Q^2(t_1)\delta(t_1-t_2)$

$E[\omega(t)] = 0$

If $Q(t) = Q$ then

$E[\omega(t_1)\omega(t_2)] = \frac{Q^2}{2\tau_I} e^{\frac{-|t_1-t_2|}{\tau_I}}$

Figure 3.2 Internal Model of the Stimulus Process

correct value for Q could be inferred on line based upon the level of afferent firing.

Formulation of the optimal estimate is most conveniently presented if the mathematical notation is changed from the frequency domain (Laplace transform notation) to the time domain (state vector notation). The processor's internal model of the processes which give rise to the afferent firing from the semicircular canals can then be written as follows:

$$\dot{\underline{x}}(t) = \underline{A}\,\underline{x}(t) + \underline{B}\,W(t)$$
$$y(t) = \underline{C}\,\underline{x}(t) + SFR + n(t) \qquad (3.10)$$

where $\underline{x}(t)$ is a state vector which represents the state of the canal-stimulus system at time t (4 dim)

$y(t)$ is the afferent firing rate at time t (scalar)

$W(t)$ is the white input process shown in figure 3.2

SFR is the spontaneous firing rate (90 ips)

and $n(t)$ is the measurement noise.

The choice of $\underline{A}$, $\underline{B}$ and $\underline{C}$ used to represent a given linear system is not unique. Figure 3.3 illustrates the state space realization used here. The standard controllable realization (Ref. 8) is used to model the mechanical dynamics of the cupula and the dynamics of the hair cells. $x_1(t)$, $x_2(t)$ and $x_3(t)$ represent the state of the sensor at time t. $x_4(t)$ is the stimulus angular velocity in rad/sec.

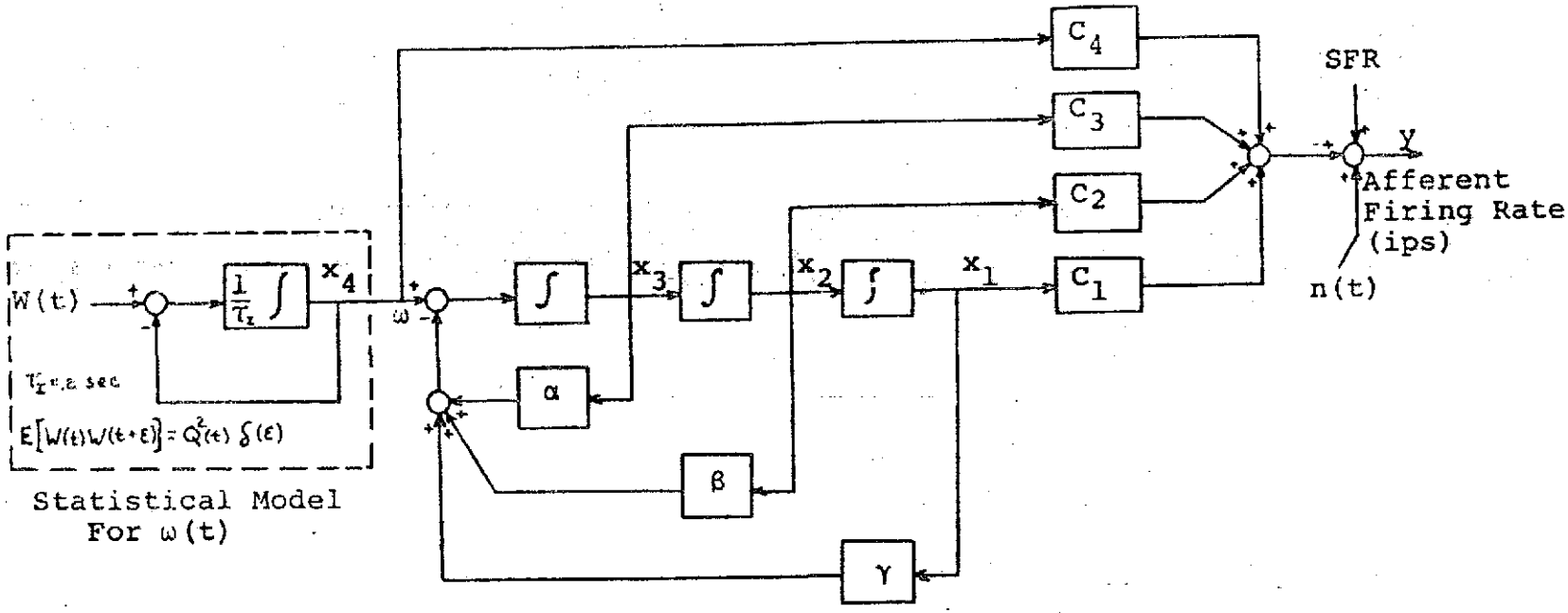

$$\begin{bmatrix} \dot{x}_1 \\ \dot{x}_2 \\ \dot{x}_3 \\ \dot{x}_4 \end{bmatrix} = \begin{bmatrix} 0 & 1 & 0 & 0 \\ 0 & 0 & 1 & 0 \\ -\gamma & -\beta & -\alpha & 1 \\ 0 & 0 & 0 & -1/\tau_1 \end{bmatrix} \begin{bmatrix} x_1 \\ x_2 \\ x_3 \\ x_4 \end{bmatrix} + \begin{bmatrix} 0 \\ 0 \\ 0 \\ 1/\tau_1 \end{bmatrix} W(t)$$

$$y = \begin{bmatrix} C_1 & C_2 & C_3 & C_4 \end{bmatrix} \underline{x} + SFR + n(t)$$

SFR = 90 ips		C_1 =	-23.58
α = 200		C_2 =	-1132.
β = 17.80		C_3 =	-6372.
γ = .3704		C_4 =	63.66

Figure 3.3 Internal Model of Stimulus and Canal Dynamics

To simulate the process of perception of rotation on a digital computer requires first, the simulation of the sensor's response $y(t)$ to a given input process $\omega(t)$ and then a simulation of the processing by the higher centers of $y(t)$. After balancing the need for a simulation with good sensory fidelity and the need for reasonable computational efficiency it was decided to update the state of the sensor every tenth of a second and to update the central processor's estimate of the rotational rate, $\hat{\omega}(t)$, every second. The central processor is now faced with the problem of estimating $\omega(t) = x_4(t)$ given the measurement history of the afferent firing rate $y(t)$, $y(t-1)$, $y(t-2)\ldots y(t-n)\ldots$. The minimum mean squared error (mmse) estimate of $\underline{x}(t)$ is given by the following sequential filter (called a Kalman Filter, Ref. 41 39,76).

$$\hat{\underline{x}}(t_n) = \underline{\Phi}_A(t_n, t_{n-1})\hat{\underline{x}}(t_{n-1}) + K(t_n)\left[(y(t_n)\text{-SFR}) - \underline{C}\underline{\Phi}_A(t_n, t_{n-1})\underline{x}(t_{n-1})\right] \qquad (3.11)$$

where $\underline{\Phi}_A(t_n, t_{n-1})$ is the state transition matrix for the system given in 3.10.

and $\underline{K}(t_n)$ are the Kalman gains at time t_n.

Since the sensory dynamics are time invariant $\underline{\Phi}_A(t_n, t_{n-1})$ can be expressed as $\underline{\Phi}_A(t_n - t_{n-1})$ and can be calculated as follows

$$\underline{\Phi}_A(\tau) = \mathcal{L}^{-1}\{(\underline{I}s - A)^{-1}\} \tag{3.12}$$

where $\underline{A}$ is defined by equation 3.10 and figure 3.3

The optimal estimate $\hat{\underline{x}}(t_n)$ differs from the true state $\underline{x}(t_n)$ by an error $\underline{\xi}(t_n)$ which is zero mean and has a covariance given by:

$$\underline{P}(t_n) = E[\underline{\xi}(t_n)\ \underline{\xi}^T(t_n)] = (\underline{I} - \underline{K}(t_n)\underline{C})\underline{P}'(t_n) \tag{3.13}$$

where $\underline{P}'(t_n)$ is the covariance of the processor's knowledge of $\underline{x}(t_n)$ given all past measurements of the afferent firing $y(t_{n-1})$, $y(t_{n-2})$... but not $y(t_n)$. $\underline{P}'(t_n)$ is given by

$$\underline{P}'(t_n) = \underline{\Phi}_A(t_n - t_{n-1})\underline{P}(t_{n-1})\underline{\Phi}_A^T(t_n - t_{n-1}) + \int_0^{(t_n - t_{n-1})} \underline{\Phi}_A(\tau)\underline{B}\, Q^2(\tau)\underline{B}^T\underline{\Phi}_A^T(\tau)\, d\tau \tag{3.14}$$

The Kalman gains $\underline{K}(t_n)$ are calculated from $\underline{P}'(t_n)$ as follows:

$$\underline{K}(t_n) = \underline{P}'(t_n)\underline{C}\left\{\underline{C}\underline{P}'(t_n)\underline{C}^T + E[n^2(t_n)]\right\}^{-1} \tag{3.15}$$

Although a full exploration of equations 3.11 - 3.15 cannot be given here, some motivation for the form of equations 3.11, 3.14 and 3.15 can be given.

Equation 3.11 shows that the minimum mean squared error (mmse) estimate of $\underline{x}(t_n)$ is made up of two terms. The first term $\underline{\Phi}(t_n, t_{n-1})\hat{\underline{x}}(t_{n-1})$ merely propagates the optimal estimate at time t_{n-1} forward in time and represents the state which would exist at time t_n if the estimate $\hat{\underline{x}}(t_{n-1})$ were errorless and the system had no inputs during the interval (t_{n-1}, t_n).

Alternatively this term can be thought of as the best estimate of $\underline{x}(t_n)$ based on the measurements $y(t_{n-1})$, $y(t_{n-2})$,.... The second term represents the difference between the expected afferent signal $\left\{E[(y(t_n) - SFR)/y(t_{n-1}),....] = \underline{C}\underline{\Phi}_A(t_n, t_{n-1})\hat{\underline{x}}(t_{n-1})\right\}$ based on the old measurements and the new measurement of the afferent signal $(y(t_n) - SFR)$. This second term therefore summarizes the relevant new information from the latest measurement. Note that the afferent signal is always measured from the spontaneous firing rate (SFR) since SFR is independent of the state $\underline{x}(t_n)$. With these interpretations of the terms in equation 3.11 the Kalman gains $\underline{K}(t_n)$ can be interpreted as the weighting factors which indicate the relative importance or usefulness of the new information as compared to the old information in estimating the state vector at time t_n.

$\underline{P}'(t_n)$ given by 3.14 represents the error covariance of an estimate of $\underline{x}(t_n)$ based only upon measurements taken before time t_n. The term $\underline{\Phi}_A(t_n - t_{n-1})\underline{P}(t_{n-1})\underline{\Phi}_A^T(t_n - t_{n-1})$ represents the covariance of the estimate error $\underline{\xi}'(t_n) = \underline{x}(t_n) - \underline{\Phi}(t_n, t_{n-1})\hat{\underline{x}}(t_{n-1})$ due to the error $\underline{\xi}(t_{n-1}) = \underline{x}(t_{n-1}) - \hat{\underline{x}}(t_{n-1})$ propagated forward in time. The integral term represents the covariance of $\underline{\xi}'(t_n)$ arising from the unknown stimulus during the interval (t_{n-1}, t_n).

Roughly speaking equation 3.15 can be looked upon as the ratio of the variance of the old information divided by the sum of the variance of the old information plus the variance

of the new information. Note that the leading term is not quadratic in $\underline{C}$ since the term which $\underline{K}(t_n)$ multiplies in equation 3.11 is already linear in $\underline{C}$. Thus $\underline{K}(t_n)$ increases if $E[n^2(t_n)]$ decreases and therefore weighs more heavily a measurement with a smaller noise component. Alternatively $\underline{K}(t_n)$ decreases if $P'(t_n)$ decreases since this indicates that the accumulated old information is relatively more useful than the new information gained from $y(t_n)$.

Implementation of equations 3.11-3.15 is relatively simple once it is recognized that most of the expressions can be calculated in advance. For the simulations carried out here measurements of the afferent firing rate are made available once every second which implies that $\tau = t_n - t_{n-1} = 1$ second. Equation 3.12 is used to calculate $\Phi_A(\tau = 1)$ and the result (a 4 X 4 matrix of constants) is stored for future calculations. The integral term in equation 3.14 (call it $\underline{P}_I(t_n)$) is also a 4 X 4 matrix of constants which can be calculated if $Q(\tau)$ is known (see Figure 3.2).

To start the simulation one must have an initial state estimate $\hat{\underline{x}}(t_o)$ and an associated error covariance for that estimate, $\underline{P}(t_o)$. Between time t_o and the first measurement of afferent firing at time t_1 the processor computer $\underline{P}'(t_1)$ from $\underline{\Phi}_A(\tau)$, $\underline{P}(t_o)$ and $\underline{P}_I(t_1)$ and then the Kalman gains $\underline{K}(t_1)$ from $\underline{P}'(t_1)$, $\underline{C}$ and the variance of the measurement noise $E[n^2(t_1)]$. Since we have only one measurement the inversion implies simple division. Once the measurement $y(t_1)$ is avail-

able equation 3.11 can be used to calculate the new estimate $\hat{\underline{x}}(t_1)$ and equation 3.13 can be used to calculate the associated error covariance $\underline{P}(t_1)$. While waiting for the measurement $y(t_2)$ the processor repeats the above steps calculating $\underline{P}'(t_2)$ and $\underline{K}(t_2)$, etc.

In a real time application in which the measurement noise variance $E[n^2(t_n)]$ and input power $Q(\tau)$ are known in advance it is possible to precalculate $\underline{P}'(t_n)$, $\underline{K}(t_n)$ and $\underline{P}(t_n)$ for all future times t_n, since they are independent of the measurement $y(t_n)$. For systems which are asymptotically stable and for which the measurement noise $n(t_n)$ and input power $Q(\tau) = Q$ are time invariant $\underline{P}'(t_n)$, $\underline{K}(t_n)$ and $\underline{P}(t_n)$ approach constant values (denoted $\underline{P}'_\infty$, $\underline{K}_\infty$ and $\underline{P}_\infty$). In such a case equation 3.11 becomes time invariant (upon substituting $\underline{K}_\infty$ for $\underline{K}(t_n)$) and represents the state space version of the Weiner Filter (Ref.60,73).

Appendix I lists the calculated values for the transition matrices, Kalman gains, etc., which pertain to the simulation of perception using afferent information from the semicircular canal system.

To test this model of suprathreshold vestibular perception a step in angular acceleration of $1.5°/sec^2$ was simulated. The stimulus was on for 120 seconds and then off for 120 seconds leaving a constant rotational velocity of 180 degrees/second. The response of the model (shown in Figure 3.4) peaks approximately 27 seconds after the onset of the stimulus and decreases to less than 10% of the peak response after two

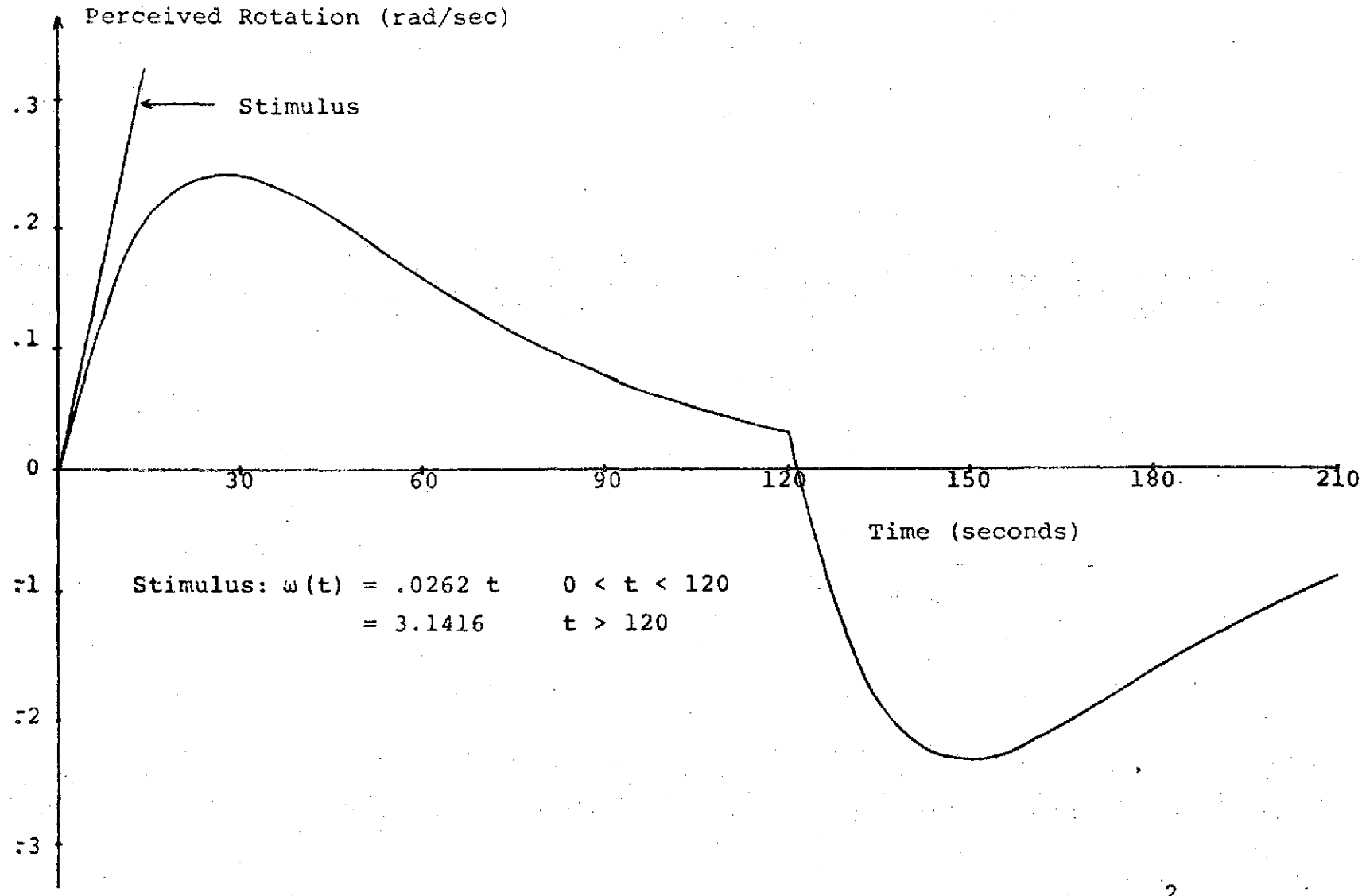

Figure 3.4 Predicted Subjective Response to 1.5 Degree/Second^2 Acceleration Step

minutes. When the acceleration ceases the predicted perception quickly changes sign with a secondary peak occuring 28 seconds after the stimulus is removed.

Clark and Stewart (Ref. 14) and Guedry and Lauver (Ref. 35) have conducted experiments to determine the subjective response for acceleration steps of $1.5°/sec^2$. Although the data from these two experiments agree in a qualitative way, there are significant quantitative differences between them. Clark and Stewart show a peak response which occurs at approximately 35 seconds with essentially no response at 120 seconds after onset. After the acceleration is removed (at 120 seconds) a reversed response with essentially the same time course but diminished in magnitude is reported. It should be noted that a linear model will not predict a reduced secondary response if the original response has stabilized at zero.

Data from Guedry and Lauver show a peak response at about 25 seconds and an adaptation time constant of approximately 30 seconds (see ref. 35). One interesting aspect of tnis data is that it indicates an initial rate of change of subjective velocity equal to approximately 2.9 (degrees/second)/second. This is almost twice tne true rate of change and would imply that the initial response to a step in angular velocity would also be twice the true rate.

The response predicted by the model reaches an initial peak at 27 seconds (consistent with Guedry and Lauver), approaches a negligible response at 120 seconds (consistent with both sets of data), has a roughly symmetrical response

after the step in acceleration is removed (dictated by its linearity) and has a gain which yields an initial perception of angular velocity consistent with the true stimulus magnitude.

In addition to the model's ability to predict subjective sensation for rotations about an earth vertical axis, it has a degree of flexibility not found in earlier models. Since all of the dynamic characteristics observed in human subjective responses are also observed in the afferent recordings made in animals the model assigned these characteristics to the human afferent. Consequently it was necessary to postulate a high bandwidth stimulus process so that the optimal filter would not contribute significantly to the overall dynamics of the subjective response. If it were discovered that the afferent dynamics in man were significantly different than the dynamics observed in man's subjective responses then the optimal estimator model for the higher centers might contribute to an explanation for the discrepancy. One example of sensory processing which contributes significantly to the overall dynamics of perception is the processing of afferent signals from the otoliths which is described in the remaining sections of this chapter.

3.2 Otolith System

Specification of the afferent dynamics for the otolith sensors differs in one fundamental respect from that of the semicircular canal system. In the case of the semicircular canals, definative data was available for the response of mammilian afferents to dynamic stimulation while no similar data is presently available for the otoliths. In this section the afferent response of the otolith sensors will be inferred from the following information

(1) The general mechanical structure of the otoliths

(2) The data available on the static response of the otoliths to a constant sheer force

(3) The limited afferent data available for dynamic stimulation plus some qualitative comments regarding the nature of the afferent response seen in the squirrel monkey by Dr. Goldberg (personal communication)

and (4) The known subjective response to accelerations from human subjects

coupled with the presumption that the higher centers process the afferent data optimally to yield a perception of specific force. Specific force is defined to be $\underline{g} - \underline{a}$ where $\underline{g}$ is the local gravitational force vector, and $\underline{a}$ is the acceleration of the body with respect to inertial space. Stated differ-

ently, specific force is the gravitoinertial reaction force per unit mass.

3.2.1 Division of Afferent Response ahd Higher Order Processing

The basic mechanical structure of the otolith sensor can be modeled as a mass (the otolithic membrane) immersed in a fluid (endolymph) and restrained by the springlike action of its mechanical restraints. Movement of the Otoconia which is presumed to be proportional to hair cell displacement can thus be described as follows:

$$M\ddot{x}(t) = -Kx(t) - V\dot{x}(t) + M\,SF(t) \qquad (3.16)$$

where $x(t)$ is the displacement of the otoconia from their resting position

M is the mass excess of the otoconia over an equal volume of endolymph

K is the effective spring constant of the system per unit displacement of the otoconia

V is the coefficient of mechanical and viscous losses due to movement of the otoconia

and SF is the specific force acting on the otoconia parallel to the plane of the macula.

Using Laplace transform notation we can solve for the transfer function relating otolith displacement to specific force:

$$\frac{x(s)}{SF(s)} = \frac{1}{s^2 + \frac{V}{M}s + \frac{K}{M}} \qquad (3.17)$$

An order of magnitude estimate can be made for the natural frequency $\omega_n = \sqrt{\frac{K}{M}}$ based upon estimates of the displacement of the otolith organ under the influence of a 1g shear force (the following procedure for estimating ω_n is due to Young Ref. 83 and through personal communication with C. Oman).

Applying the final value theorem to equation 3.17 with $SF(s) = \frac{1}{s}$ we find that the steady state displacement of the otolith organ for a 1g (10^3cm/sec^2) stimulus is

$$x(\infty) = \frac{M}{K}\, 10^3 \text{cm} \qquad (3.18)$$

Two rough estimates can be made for this displacement. The first results from assuming that the sensitivity of otolith hair cells is approximately the same as that for the semicircular canals and thus the displacement of the otoconia must be approximately the same at threshold as the threshold displacement calculated for the cupula. Oman (Ref. 58) calculated the threshold displacement of the midpoint of the cupula to be approximately 10^{-6}cm. If this were the displacement of the otoconia at threshold (approximately .005 g) then a 1g stimulus should produce a displacement of $x(\infty) = 2 \times 10^{-4}$cm. Using this figure in equation 3.18 yields a value of 2×10^{-7} for $\frac{M}{K}$ and thus $\omega_n = \sqrt{\frac{K}{M}} \approx 2240$ rad/sec. The second estimate for $x(\infty)$ is given by deVries (Ref. 20) based upon X-rays of the ruff sacculus. He found a steady state displacement of

$x(\infty) = 7 \times 10^{-3}$cm for a 1g stimulus. This value for $x(\infty)$ results in an estimate of $W_n = 374$ rad/sec.

Although these estimates differ by a factor of six they both confirm that the natural frequency of the sensor should be at least an order of magnitude above the highest frequency normally associated with vestibular stimuli. With this established we can now demonstrate that the transfer function in equation 3.17 can be represented as either a pure gain or at most a simple lag over the frequency range of interest, $\omega \in (0, \frac{\omega_n}{10})$.

Figures 3.5A and B show the Bode amplitude ratio plots and phase angle plots respectively for equation 3.17 for different damping rations $\xi = V/(2\sqrt{MK}) \leq 1.0$. If $\xi \leq 1$ then it is clear that for frequencies less than $\omega_n/10$ the system can be approximated by a gain. If $\xi > 1$ then the denominator of equation 3.17 has two real roots s_1 and s_2 which satisfy $s_1 s_2 = \omega_n^2$ which implies that one root must have a value greater than ω_n and one root a value less than ω_n. It is only the one root with a value less than ω_n which could significantly affect the frequency response of the system for $\omega < \omega_n/10$. Thus for $\omega \in (0, \frac{\omega_n}{10})$, which should include all of the normal physiologic motions, we can approximate the mechanical dynamics of the otolith organ by:

$$\frac{x(s)}{SF(s)} \propto \frac{A}{S + A} \qquad (3.19)$$

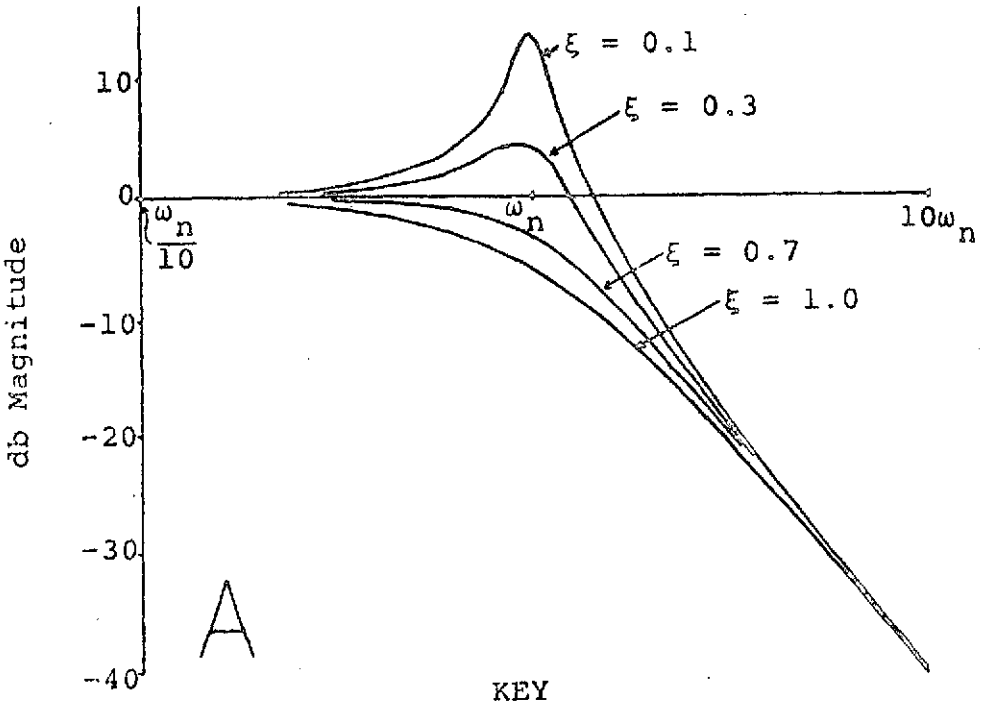

KEY

ω_n = Natural Frequency

ξ = Damping Ratio

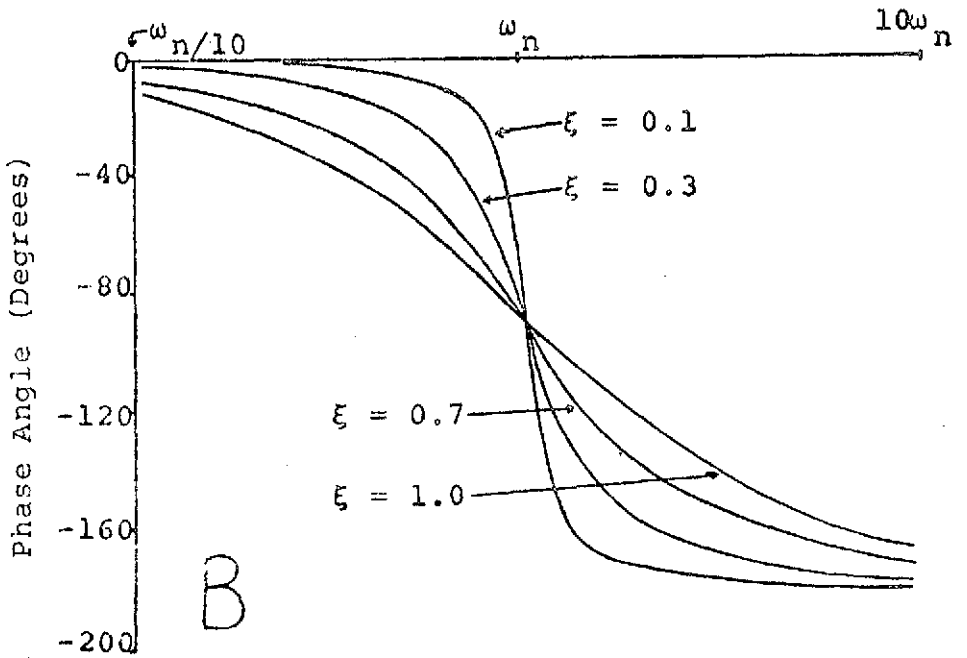

Figure 3.5 Amplitude and Phase Plots for Second Order Systems

where $A = -\frac{V}{2M} + \frac{1}{2}\left(\frac{V^2}{M^2} - \frac{4K}{M}\right)^{\frac{1}{2}}$ if $\xi > 1$

and $A = \infty$ if $\xi < 1$

The transfer dynamics from otolith displacement to afferent firing must now be considered. Vidal et al (Ref. 70) in experiments with cats found a unidirectional rate sensitivity of the form

$$\text{Firing rate} = G[\theta(t) + K\dot{\theta}(t)] \tag{3.20}$$

where $K = 0 \quad \dot{\theta}(t) \leq 0$

$K > 0 \quad \dot{\theta}(t) > 0$

and $\theta(t)$ is the tilt angle

This response nonlinearity can be removed if it is assumed that perception is a function of the difference in firing rates from cells with opposing gains. Such an assumption is reasonable based upon the work of Flurr and Mellström (Ref. 25) and leads to the following response to tilts:

$$\text{Firing rate} = G(2\theta(t) + K\dot{\theta}(t)) \tag{3.21}$$

regardless of the sign of $\dot{\theta}(t)$. We have thus retained the effect of rate sensitivity while eliminating the nonlinearity. Vidal postulated the model given in 3.20 based upon a stimulus whose frequency content was confined to $\omega < .1$ Hz and thus might not be expected to indicate the mechanical dynamics postulated in equation 3.19. In the static experiments conducted by Vidal no adaptation was reported even though recordings were made for as much as 3 minutes at a given orientation.

Fernandez and Goldberg (Ref. 24) indicated that the majority of cells from the otolith organs in the squirrel monkey achieved an essentially constant rate of firing within 30 seconds of a position change. Thus although some cells may exhibit significant adaptation a large percentage of the population does not.

While it is recognized that the otolith afferents which exhibit adaptation may contribute to the transient response (in exactly the same manner as nonadapting cells) they do not govern the long term sensations due to the otoliths which do not show significant adaptation to static tilt angles. Therefore we postulate the following form as a model for the response of a nonadapting otolith afferent to the component of specific force in the plane of the macula:

$$\left\{\begin{matrix}\text{Afferent} \\ \text{Firing Rate}\end{matrix}\right\}(s) = \left[\frac{Bs + (B+C)A}{s + A}\right]SF(s) + \frac{SFR}{s} + n(s) \quad (3.22)$$

where SFR denotes the resting discharge

$n(s)$ is the measurement noise process

and A,B,C are shown in figure 3.6

If, as in the case of the semicircular canal model, we postulate that the higher centers' <u>a priori</u> information concerning the input (in this case SF) is given by white noise through a first order filter and that the higher centers process the afferent information optimally to estimate SF then we can view the entire sensory process for the otoliths as shown in figure 3.6.

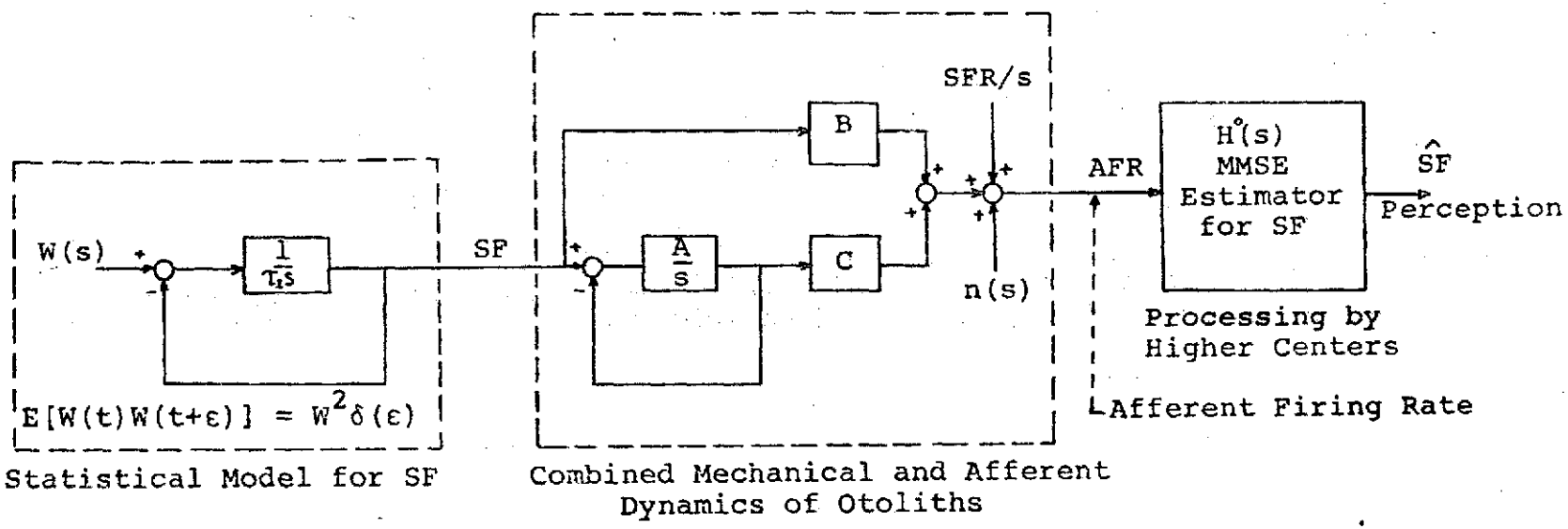

$$SF(s) = \frac{1}{\tau_I s+1} W(s)$$

$$AFR(s) = \frac{Bs+(B+C)A}{S+A} SF(s) + \frac{SFR}{s} + n(s)$$

$$\hat{SF}(s) = H(s)[AFR-\frac{SFR}{s}]$$

$$\phi_{nn}(s) = N^2$$

Figure 3.6 Model of Otolith Perception

The steady state optimal processor $H^{\circ}(s)$ can now be determined as a function of W, τ_I, A, B, C and N. Since the resting discharge SFR is independent of the input and is known by the higher centers it is presumed that it is subtracted from the afferent signal and plays no further part in the processing.

To find $H^{\circ}(s)$ we must solve the associated Wiener Hopf equation. Since $H^{\circ}(s)$ must be causal the associated Wiener Hopf equation is most easily solved by the method of spectral factorization (Ref. 60). This yields the following solution for $H^{\circ}(s)$:

$$H^{\circ}(s) = K^{\circ}\frac{S+A}{(S+F)(S+G)} \tag{3.23}$$

Where F,G and K° must satisfy

$$F^2+G^2 = \frac{B^2W^2}{\tau_I^2N^2} + \frac{1}{\tau_I^2} + A^2 \tag{3.24}$$

$$F^2G^2 = \frac{(B+C)^2A^2W^2}{\tau_I^2N^2} + \frac{A^2}{\tau_I^2} \tag{3.25}$$

$$K^{\circ} = \frac{W^2\left[(B+C)A + \frac{B}{\tau_I}\right]}{\tau_I^2N^2(F+\frac{1}{\tau_I})(G+\frac{1}{\tau_I})} \tag{3.26}$$

Now that the form of $H^{\circ}(s)$ is determined we can cascade it with the mechanical and afferent dynamics (given in 3.22) to yield a prediction for the form of the overall perceptual dynamics associated with the otoliths.

$$\frac{\{\text{Mean Perception of SF}\}}{SF(s)} = \frac{Bs + (B+C)A}{s+A} \quad K^{\circ}\frac{s+A}{(s+F)(s+G)}$$

$$= BK^{\circ}\frac{(s + \frac{(B+C)A}{B})}{(s+F)(s+G)} \qquad (3.27)$$

Equation 3.27 represents the framework within which we must be able to predict subjective perception which involves the otolith organs. Young and Meiry (Ref. 81) proposed the following model for the perception of acceleration:

$$\frac{\{\text{Perceived Lateral Acceleration}\}(s)}{\{\text{True Lateral Acceleration}\}(s)} = \frac{1.5(s+.076)}{(s+.19)(s+1.5)} \qquad (3.28)$$

It is clear that equations 3.27 and 3.28 have identical forms but it is not clear that the parameters (W, τ_I, A, B, C and N) can be chosen in such a way that the coefficients in the present model will be in essential agreement with those in 3.28.

3.2.2 Otolith Model Specification and Predictions

In this section the criteria for specifying the models' parameters will be elaborated. Based on these criteria values for the parameters will be chosen and the resultant model evaluated. Actually two sets of parameters must be developed; one for the utricle and one for the saccule. The only difference is that the resting discharge rate, the sensor gain and the measurement noise level for the saccule have been found in the squirrel monkey (Ref. 24) to be approximately

half those found for the utricle. Thus we have:

Utricle		Saccule
W	→	W
τ_I	→	τ_I
A	→	A
B	→	B/2
C	→	C/2
N	→	N/2
SFR	→	SFR/2

(3.29)

Inspection of equations 3.24, 3.25 and 3.26 reveals that F and G will remain unchanged by this transformation while $K^{\circ}_{saccule}$ will be twice the value of $K^{\circ}_{utricle}$ to make up for the difference in sensor gain. With this in mind we will proceed with the specification for the utricle model and then specify the saccular model by employing the above transformation.

Fernandez, Goldberg and Abend (Ref. 24) found an average steady state change in firing rate from the utricle due to a 1g step in specific force to be 45ips. If the final value theorem for a 1g specific force is applied to equation 3.22 we find the steady state response to be B+C. Thus, our first condition is that

$$B+C = 45 \tag{3.30}$$

Since our model of subjective sensation (equation 3.27) must fit the same data from which the Young and Meiry model

(equation 3.28) was constructed, it is reasonable to assume that the corresponding coefficients should be approximately the same. It should be noted though that any combination of differences between these parameters which preserve the essential fit of the model to the data would be perfectly acceptable. Setting corresponding coefficients in approximate equality, yields the following four conditions:

$$(B+C)\frac{A}{B} \simeq .076 \qquad (3.31)$$

$$F \simeq .19 \qquad (3.32)$$

$$G \simeq 1.5 \qquad (3.33)$$

$$BK^{\circ} \simeq 1.5 \qquad (3.34)$$

Equations 3.32, 3.33 and 3.34 should be substituted in equations 3.24, 3.25 and 3.26 to yield three nonlinear algebraic conditions in W, τ_I, A, B, C and N while eliminating F, G and K°.

Once all the parameters of the model are chosen it will be possible to calculate the afferent signal to noise ratio (S/N) which the processor has assumed in arriving at its estimate of specific force. If an unreasonable signal to noise ratio must be postulated to satisfy the other conditions that we have set, then the hypothesis of an optimal processor would have to be seriously questioned. The signal to noise ratio could conceivably be set in one of two broad regions. Either the processor would be optimally structured to interpret signals near threshold when $s/N \simeq 1$ (this choice would be best suited to tasks like the control of postural sway) or it could be structured to best handle large signals for which s/N is signifi-

cantly greater than one. The only case which would indicate a serious problem would be a case in which s/N << 1. Therefore, after calculating the signal to noise ratio at the afferent level in terms of the model parameter we can set the following restriction:

$$\frac{E[(AFR-SFR)^2]}{E[n^2]} \equiv s/N = \frac{W}{N^2} \frac{B^2/\tau_I + (B+C)^2 A}{2\{A+\frac{1}{\tau_I}\}\tau_I} \geq 1 \text{ or greater} \qquad (3.35)$$

As in the case of the semicircular canals, there is data available concerning the noise level on the afferent fibres. Fernandez et al (Ref. 24) plotted the CVs obtained from 47 otolith units and concluded that while otolith CVs are significantly lower than canal CVs there is no difference between the CVs of the utricle and saccule. Since the level of spontaneous firing at which the utricle afferents operate (≈88ips) is twice that for the saccule (≈44) we conclude that using the same CV will yield a value for $N_{saccule} \approx N_{utricle}/2$. Inspection of the CV histogram offered by Fernandez indicates that a value of CV = .04 would be representative of the most regular afferents. Using a tonic firing rate for the utricle of 88 we calculate the standard deviation of the firing rate to be $E^{1/2}[N^2] = 3.39$ ips. In the case of the semicircular canals we found that the central processor was capable of reducing the effective measurement noise by a factor of $1/\sqrt{520}$ by utilizing the large number of individual afferents available from each sensor. If we presume as a first approximation

that the central processor for the otoliths is equally capable of combining afferent signals to reduce the effective measurement noise, then we could expect:

$$E^{1/2}[N^2] = N = \frac{3.39}{\sqrt{520}} = .149 \text{ ips} \qquad (3.36)$$

Finally it is reasonable to assume that the presumed bandwidth of the input, which is governed by $1/\tau_I$, should be of the same order of magnitude as that found necessary for the semicircular canals. If there is a difference, then $1/\tau_I$ for the otoliths should be slightly lower than that for the canals since the otoliths are generally considered to be sensitive to lower frequency stimuli than are the canals. Thus we should find $1/\tau_I$ roughly in the region:

$$.5 \text{ rad/sec} = \frac{1}{10\tau_{I_{canals}}} < \frac{1}{\tau_{I_{otoliths}}} < \frac{1}{\tau_{I_{canals}}} = 5 \text{ rad/sec} \qquad (3.37)$$

After substituting the values for F, G and BK° from equations 3.32, 3.33 and 3.34 into equations 3.24, 3.25 and 3.26 we have a set of eight algebraic conditions (3.24, 3.25, 3.26, 3.30, 3.31, 3.35, 3.36 and 3.37) to be satisfied by six parameters (W, τ_I, A, B, C and N). The following values for the six parameters were found to best fulfill the stated conditions (the value of the resting discharge rate is given for completeness).

Parameter	Utricle	Saccule
W	.00268	.00268
τ_I	1.	1.
A	.2	.2
B	91.1	45.55
C	-46.1	-23.05
N	.147	.073
SFR	88	44

The consequences of using these parameter values are as follows:

(1) B+C = 45 (fulfills eqn 3.30)

(2) Equations 3.24 and 3.25 are fulfilled exactly but with

$F = .133$ (see 3.32)

$G = 1.95$ (see 3.33)

$(B+C)\frac{A}{B} = .0988$ (see 3.31)

Each of these values represents a 30% change from the approximate values specified. Since these values represent the critical frequencies of the overall subjective model, their only importance arises in how they affect the models prediction of the system's phase response. Figure 3.7 shows the phase plot for Young and Meiry's model (eqn. 3.28) and the model derived here (eqn. 3.27 with the parameter values specified above). The phase predictions of the model are quite good over the frequency range above .5 rad/sec and only slightly lower than the few data points available below .5 rad/sec.

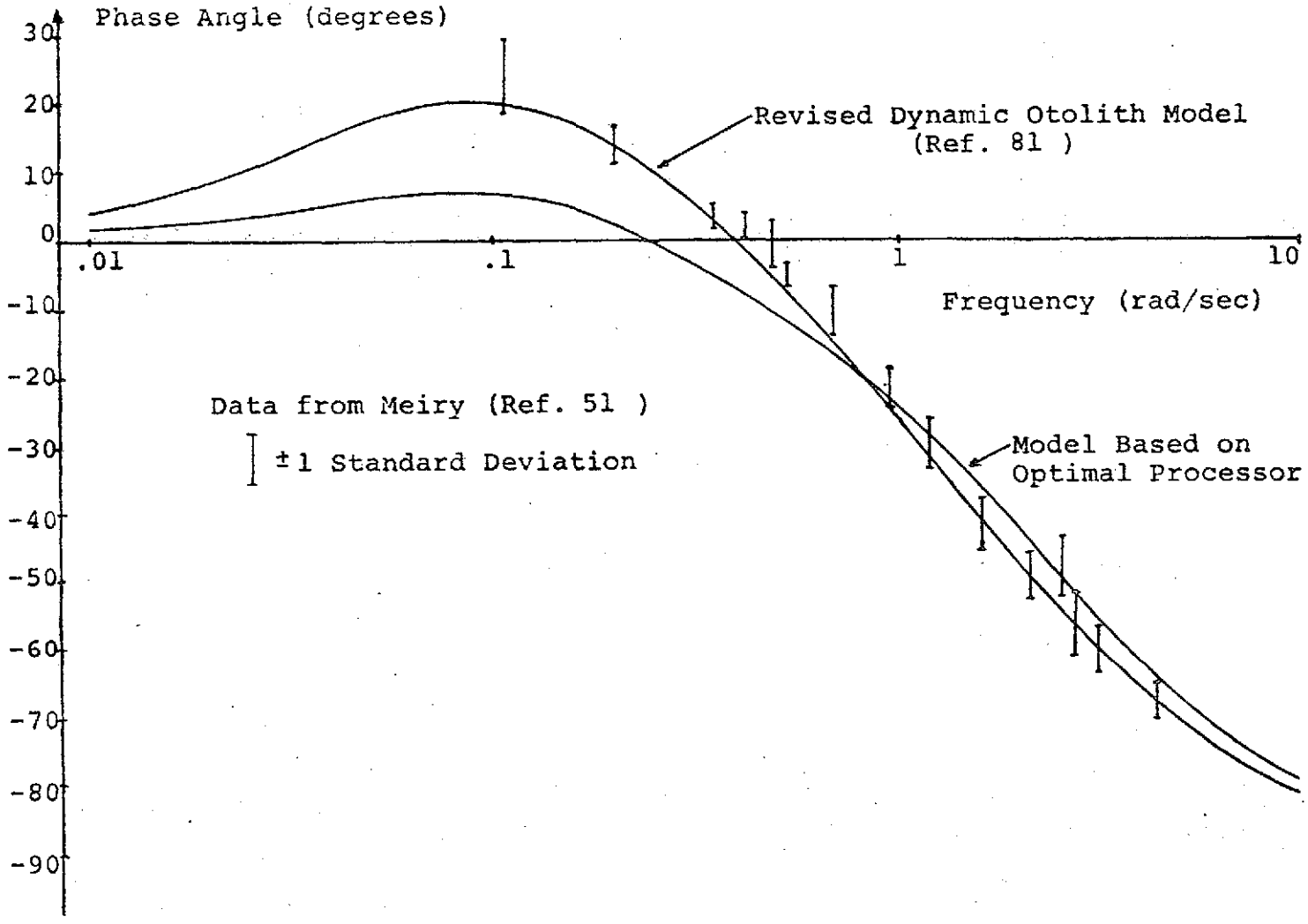

Figure 3.7 Comparison of Phase Predictions for Otolith Models

(3) $BK^{\circ} = .911$ (reasonable agreement with 3.34)

(4) $s/N = 1.21$ (sec 3.35)

(5) $N = .147$ (sec 3.36)

and (6) $\tau_I = 1$ (sec 3.37)

The resulting afferent dynamics are given by

$$\left\{\begin{matrix}\text{Afferent}\\ \text{Firing}\\ \text{Rate}\end{matrix}\right\}(s) = \frac{91.1s + 9}{s+.2}\, SF(s) + \frac{88}{s} + n(s) \qquad (3.38)$$

where $E^{1/2}[n^2(t)] = .147$

Figure 3.8 shows the change in afferent firing due to a step in acceleration of 1g. The response consists of an immediate jump of 91.1 ips which decays with a 5 second time constant to a steady state change in firing of 45 ips. It should be stressed that this five second decay could be due to either the mechanical dynamics (implying that the mechanical dynamics are very over damped) or could arise from the dynamics of the afferent processes. If more phase data becomes available on the subjective response to stimuli below .5 Hz and confirms the greater phase lead shown by Young and Meiry, the model can be altered to give an identical phase prediction. The penalty for this change is twofold. First the resulting model for the afferent response shown in figure 3.8 would jump immediately by 400 ips and then fall to 45 ips with a time constant of approximately 1.5 seconds (which at first glance seems less reasonable). Secondly, the resulting prediction for acceleration step thresholds would be signifi-

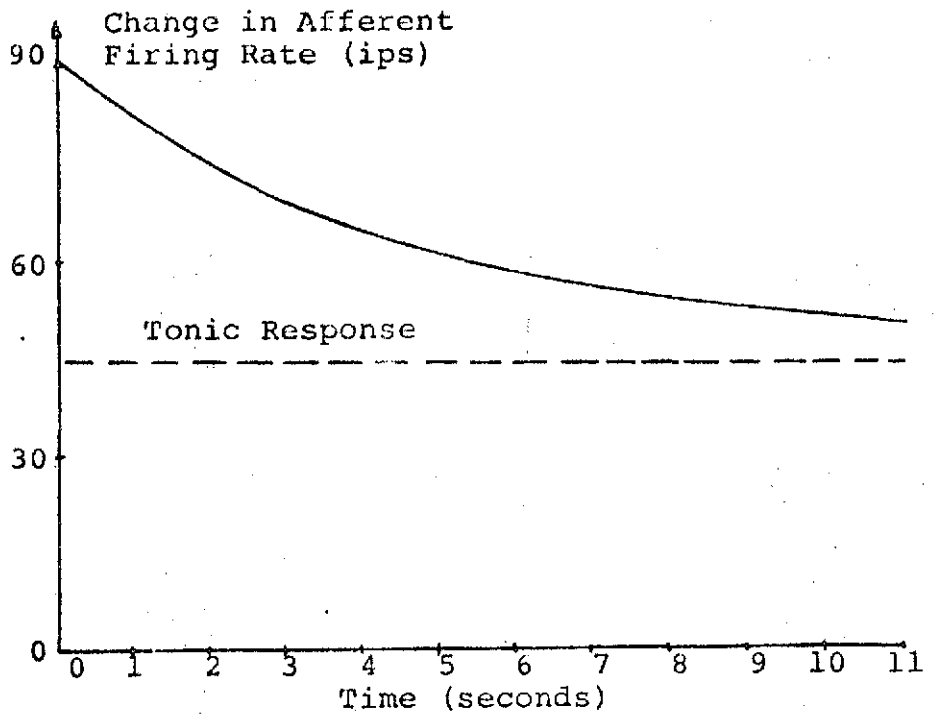

Figure 3.8 1G Step Response of Otolith Afferent Model

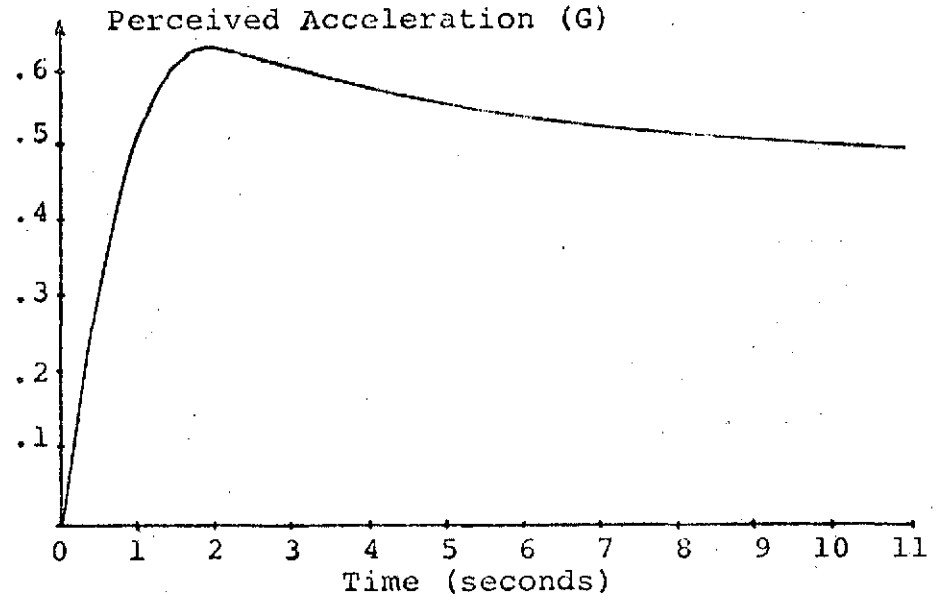

Figure 3.9 Predicted Subjective Response to 1G Step

cantly reduced below currently accepted figures.

In a personal communication with Dr. Goldberg it was learned that his current research with the otolith organs of the squirrel monkey shows a wide variety of afferent dynamics, some of which are consistent with the general prediction of Figure 3.8. When further experimental data is available concerning the dynamic response of otolith afferents an analysis similar to the one made for the semicircular canals can be undertaken. In the meantime it is interesting to note that the approach taken here can yield a model which accounts reasonably well for the available subjective data, the known physiological structure of the sensor and makes reasonable predictions concerning the afferent processes and the associated central processing.

Since for time invariant systems the steady state Kalman filter is equivalent to the Weiner filter developed above, it was decided to use the time domain formulation of the problem for the otoliths as was done for the semicircular canals. Appendix I gives the appropriate transition matrices and Kalman gains for the otolith simulation. Figure 3.9 shows the resulting subjective response of the overall system to a 1g step in acceleration. While this prediction shows less overshoot than the model by Young and Meiry there is no subjective data with which to directly compare it.

Chapter IV

QUALITATIVE NATURE OF PROCESSOR FOR DETECTION OF NEAR-THRESHOLD HORIZONTAL ROTATION

Numerous studies have been made to determine the magnitude of vestibular thresholds in the three rotational axes (with primary emphasis on the yaw axis). A comprehensive review of these experiments through 1965 is given by Clark (Ref. 10). It is interesting to note that numerous definitions of threshold are used by experimenters and thus it is difficult to compare the experimental results. An even more vexing problem is that the results of these experiments cannot be generalized to predict the probability of detection as a function of time for an arbitrary rotational stimulus. The reason that such a prediction cannot be made is that previous investigators have not proposed a stimulus-perception model adequate for arbitrary near-threshold rotations. In this chapter two fundamentally different hypotheses are considered for the nature of the threshold mechanism. The consequences of each hypothesis are explored and an experimental procedure designed and carried out to test their validity.

4.1 Processor Hypotheses

When a man is rotated, what information is available

which he can use to estimate the time course of his rotation? If the subject's eyes are open the images of a stationary environment moving across the retina provide one source of information. For those cases in which the visual environment is not inertially stable (for example, it may rotate with the subject) or in which the subject's eyes are closed, another input is needed. Although cues arising from movement of the bodily organs or from tactile sensations may be present, the most important non-visual source of information concerning rotation arises from the vestibular sensor. If a subject is denied visual cues and tactile and proprioceptive cues are ignored, then the higher centers are left with the information provided by the vestibular afferents in the form of changes in neural firing rates.

Dynamic models for the mechanical movement of the cupula and consequent afferent discharge were described in Chapter Three. Since these models were developed as part of a model of suprathreshold perception no consideration was given to either a mechanical or neural threshold nonlinearity. The existance of thresholds for rotational stimuli is sometimes accounted for by a nonlinearity at the sensor which would imply that until a certain stimulus level is reached there is no stimulus related change in afferent firing level. It is this general conception of the threshold mechanism (shown in Figure 4.1) which will be called the "simple threshold model". The

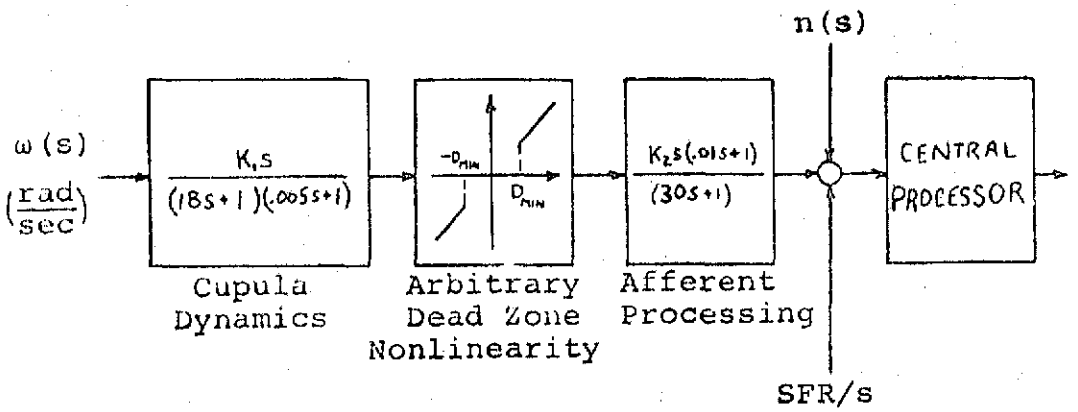

Figure 4.1 Simple Threshold Model

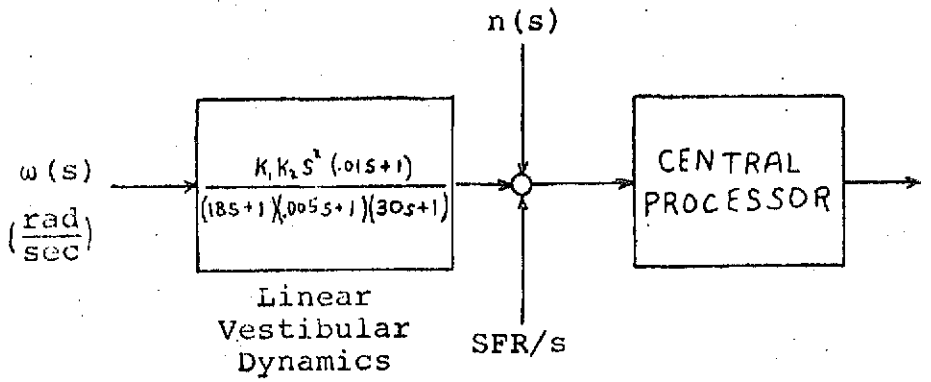

Figure 4.2 Signal in Noise Model

particular form of the nonlinearity is arbitrary except for the dead zone.

The second model will be called the "signal in noise" model since, as shown in Figure 4.2, it consists of nothing more than a measurement noise source between the sensor dynamics and the processing by the higher centers. The threshold phenomenon in this case arises from the masking effect of the measurement noise at low signal levels. The magnitude of the measurement noise is set so that a correct detection of the direction of motion will result seventy-five percent of the time.

Although these two models represent two fundamentally different approaches to modelling the phenomenon of vestibular thresholds (one including and one excluding an afferent signal correlated with subthreshold stimuli) they both predict the general variation of response latencies as a function of stimulus magnitudes. Figure 4.3 illustrates the time history of the cupula displacement (assuming a linear mechanical response) for steps in angular velocity and acceleration. For steps in angular acceleration, the displacement builds up to a steady state value with a time constant of 18 seconds. Applying the "simple threshold model" we see that if the steady state displacement is less than D_{MIN} then the output of the nonlinearity will remain zero and the performance of the processor in determining the direction of the stimulus should remain at 50%. The larger the steady state displace-

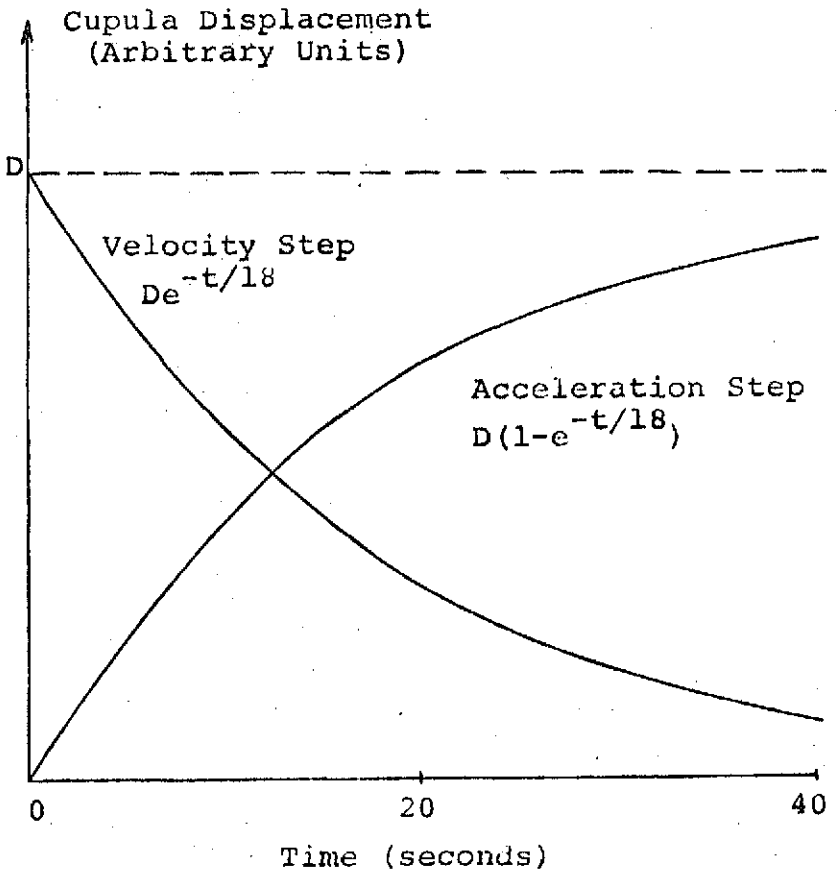

Figure 4.3 Displacement of Cupula for Velocity Step and Acceleration Step Stimuli

ment of the cupula, the sooner the output of the nonlinearity deviates from zero, which results in shorter latencies as is observed in experimental data (this is essentially a description of the classical cupulogram, Ref. 68). In the case of a velocity step input, detection will generally come quickly if the input is above threshold since the peak cupula displacement follows the stimulus onset with almost no delay.

The "signal in noise" model also predicts similar changes in latency. If the signal to noise ratio is taken as a measure of the information available to the higher centers, it is clear that for the case of an acceleration step input, the information flow peaks at about 20 seconds while in the case of a velocity step the best signal to noise ratio occurs immediately after the onset of the stimulus. If the stimulus magnitude is increased, a sufficient amount of information to make a response becomes available earlier in the case of an acceleration step, while the latency will continue to be short in the case of a velocity step.

4.2 Threshold Characteristics of the Hypothesized Models

Since both models are capable of explaining the existence of thresholds and the general trend of response latencies, it is necessary to design an experiment in which the results predicted by the two models are measurably different so that one or both of the models can be rejected.

The maximum cupula displacement for the velocity step V(t) and the acceleration step A(t) shown in figure 4.3 are the same. If this maximum value were slightly greater than D_{MIN} (figure 4.1) then the "simple threshold model" would predict that both V(t) and A(t) would be threshold level stimuli. Combining these velocity step and acceleration step stimuli at their threshold level results in a stimulus which would produce a step in cupula displacement just larger than D_{MIN}. Therefore if we define

$$\omega_c(t) = V(t) + A(t)t \qquad (4.1)$$

then the "simple threshold model" would predict that $\omega_c(t)$ would also be a threshold level stimulus.

This result does not follow for processors which deal optimally with signals in noise. If the noise-free firing rate due to $\omega_c(t)$ is compared to either that for the velocity step threshold or the acceleration step threshold it is clear that with the same level of additive noise the presence of $\omega_c(t)$ is more likely to be detected than either V(t) or A(t) alone. If the signal in noise model is correct, $\omega_c(t)$ will have to be reduced in magnitude if it is to be a threshold level stimulus. The questions which naturally arise are

1. By what factor must $\omega_c(t)$ be reduced?

and 2. Is there a sufficient difference to detect experimentally?

A measure of the information content of a signal s(t)

at a given time, when immersed in independent zero mean additive gaussian noise, n(t), is the signal to noise ratio S/N, defined as

$$\frac{S}{N} \equiv \frac{E\{s^2(t)\}}{E\{n^2(t)\}} \qquad (4.2)$$

where $E\{\cdot\}$ indicates expected value.

Let n(t) be a stationary process and define $N^2 = E\{n^2(t)\}$. Since, in the problem at hand, the signal is available over a period of time, the integrated signal to noise ratio is the appropriate measure of information content. If $FR_V(t)$ and $FR_A(t)$ denote the afferent firing rates due to threshold level velocity and acceleration step stimuli respectively, then the "signal in noise model" requires that

$$\int_0^T \frac{(FR_V{}^2(t))}{N^2}\,dt = \int_0^T \frac{(FR_A{}^2(t))}{N^2}\,dt \equiv \frac{I}{N^2} \qquad (4.3)$$

or that

$$\int_0^T FR_V{}^2(t)\,dt = \int_0^T FR_A{}^2(t)\,dt = I \qquad (4.4)$$

where (0,T) is the interval given to the subject to detect the stimulus (usually 10-15 seconds). The problem is to find a factor, K, such that $K\omega_c(t)$ gives rise to a firing rate, call it $FR_c(t)$, which has an information content equal to I. Since

$$FR_C(t) = K(FR_V(t) + FR_A(t)) \tag{4.5}$$

we can calculate its information content as follows:

$$\int_0^T FR_C^2(t)dt = K^2 \int_0^T (FR_V(t) + FR_A(t))^2 dt$$

$$= K^2 \left\{ \int_0^T FR_V^2(t)dt + \int_0^T FR_A^2(t)dt + 2\int_0^T FR_V(t)FR_A(t)dt \right\}$$

$$= 2K^2 \left\{ I + \int_0^T FR_V(t)FR_A(t)dt \right\} \tag{4.6}$$

If we set this equal to I we can solve for the required K:

$$K = \frac{1}{\sqrt{2}} \left\{ \frac{I}{I + \int_0^T FR_V(t)FR_A(t)dt} \right\}^{1/2} \tag{4.7}$$

Several facts should be noted at this point:

1. K is independent of the noise level as long as n(t) is stationary, but is implicitly a function of the sensor dynamics, $H(s)_{canal}$, through $FR_V(t)$ and $FR_A(t)$.
2. For all reasonable choices of $H(s)_{canal}$

$$\int_0^T FR_V(t)FR_A(t)dt > 0 \tag{4.8}$$

since $FR_V(t)$ and $FR_A(t)$ share the same sign in the interval (0,20) seconds.

3. Finally, using the Cauchy Schwartz inequality, we have

$$\int_0^T FR_V(t)FR_A(t)dt < \left\{\int_0^T FR_V^2(t)dt\right\}^{1/2} \cdot \left\{\int_0^T FR_A^2(t)dt\right\}^{1/2}$$

$$= I^{1/2}I^{1/2} = I \qquad (4.9)$$

Combining 4.8 and 4.9 we can conclude that

$$0 < \int_0^T FR_V(t)FR_A(t)dt < I \qquad (4.10)$$

which, utilizing 4.7 implies that

$$1/2 < K < 1/\sqrt{2} \qquad (4.11)$$

If instead of integrated signal to noise the above analysis used a first order lag $\{1/(\tau s + 1)$; for which we will use the notation $\int_0^T L\{x\}dt$ where $L\{x\}$ denotes the response of the linear system $s/(\tau s + 1)$ which is initially at rest to the input $x\}$ the results would be essentially unchanged. Specifically we have:

$$\int_0^T L\{FR_V^2\}dt = \int_0^T L\{FR_A^2\}dt \equiv I \qquad (4.12)$$

and therefore

$$\int_0^T L\{FR_C^2\}dt = \int_0^T L\{K^2(FR_V+FR_A)^2\}dt$$

$$= 2K^2(I+\int_0^T L\{FR_VFR_A\}dt) \qquad (4.13)$$

Since,

$$\int_0^T L\{FR_VFR_A\}dt > 0 \qquad (4.14)$$

and

$$\int_0^T L\{FR_VFR_A\}dt < \left\{\int_0^T L\{FR_V^2\}dt\right\}^{1/2} \cdot \left\{\int_0^T L\{FR_A^2\}dt\right\}^{1/2}$$

$$= I \qquad (4.15)$$

we can again conclude (after setting 4.13 equal to I) that

$$\frac{1}{2} < K < \frac{1}{\sqrt{2}} \qquad (4.16)$$

In fact the above analysis is valid for any linear operator, $\int_0^T L\{\cdot\}dt$, as long as it satisfies the criteria required of an inner product. This result will be useful in Chapter Five when we consider models for the detection process.

Figure 4.4 summarizes the above predictions. Every point in the figure represents a stimulus made up of a velocity step component v and an acceleration step component a. For example the point P shown in the figure represents the stimulus

$$P(t) = (\alpha + \beta t) \text{ deg/sec} \qquad (4.17)$$

The points labeled V and A represent the velocity and acceleration step threshold levels respectively for a given subject. The dotted line through the origin and the point (A,V) represents the class of stimuli over which the two models differ in their prediction of threshold levels most dramatically. The threshold prediction of the "simple threshold model", S = V + A, is illustrated along with the region consistent with the "signal in noise model".

4.3 Experimental Description

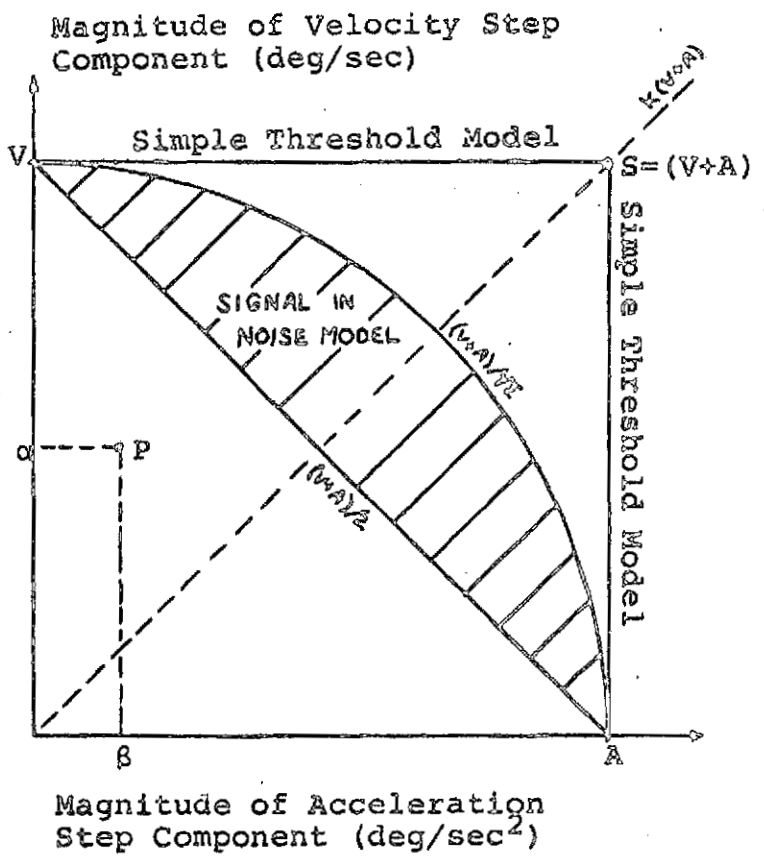

Figure 4.4 Stimulus Diagram and Threshold Predictions of Hypothesized Models

The experiment best suited to distinguish between the "simple threshold" and "signal in noise" models is now clear. Stated simply the experiment consists of finding the velocity step and acceleration step thresholds for a group of subjects and then combining these two stimuli to find the subjects' threshold along the dotted line illustrated in Figure 4.4. The predictions of the two models should then be compared to the experimental data.

The experiment was carried out at the NASA Research Center at Langely Field, Virginia using a six degree of freedom simulator called the real-time dynamic simulator (RDS). All rotations were restricted to the simulator's yaw axis which was aligned with the earth's vertical axis. The subject was seated so that the axis of rotation was through his head and the orientation of his head was varied as necessary to achieve either a rolling or yawing stimulus in head axes. An analog computer was programmed to rotate the RDS in yaw with either a velocity step or an acceleration step whose magnitude and onset time could be controlled by the experimenter. Position and velocity feedback from the simulator were recorded throughout the experiment and enabled estimation of actual stimulus magnitude with an accuracy of better than $\pm$ 2%. Two way voice communication with each subject was available in addition to two hand held switches used for subject responses.

Five men and one woman served as subjects. All attested to their good health and normal hearing. Vestibular function was tested by means of the sensitized Rhomberg test in which subjects must maintain their balance for one minute while standing toe to heel with their eyes closed.

For any one experimental session the subject's head position and the stimulus type (velocity step or acceleration step) was held constant. Experimental stimuli were presented following the random double staircase method, described by Clark and Stewart (Ref. 15) except that subjects were instructed to refrain from making responses for cases in which no positive sensation of rotation was felt and for which the response would be nothing more than a pure guess. In such cases the lack of a response was interpreted as if an incorrect response had been given. To aid in maintaining subject alertness, the subjects were asked to give a graded response which would reflect the confidence they had in the correctness of that response. If the subject was sure that he was rotating to the right (left) he would depress the switch in his right (left) hand twice in quick succession. If he was moderately confident that he was rotating to the right (left) he would depress his right (left) switch only once. If the subject was unsure, but had some basis for believing his motion was to the right (left), he would depress first his right (left) and then his left(right) switch.

One experimental session consisted of approximately 70 stimulus presentations with a short break after the first 40 were completed, and lasted slightly over an hour. All subjects wore light tight goggles and were instructed to keep their eyes open during the experiment. Each presentation began with the experimenter announcing that an experimental motion would begin within 15 seconds followed by a random stimulus onset delay of between zero and 15 seconds. The subject was allowed 13.9 seconds to make a response and the first response was the only one accepted. In a very few cases a subject reported that he had indicated opposite to that which he intended and this was generally accepted by the experimenter and corrected for.

After each presentation the simulator was returned to its zero position (in most cases the subject could detect this return and thus surmise the direction of his last motion) after which followed a period of no motion lasting at least 30 seconds.

The set of all stimulus presentations following the point at which the staircases either met or crossed served as the basis for estimates of thresholds.

Figure 4.5 shows a typical strip chart recording for a velocity step stimulus in which the subject, while unsure of his decision, indicated 2 seconds after onset that he

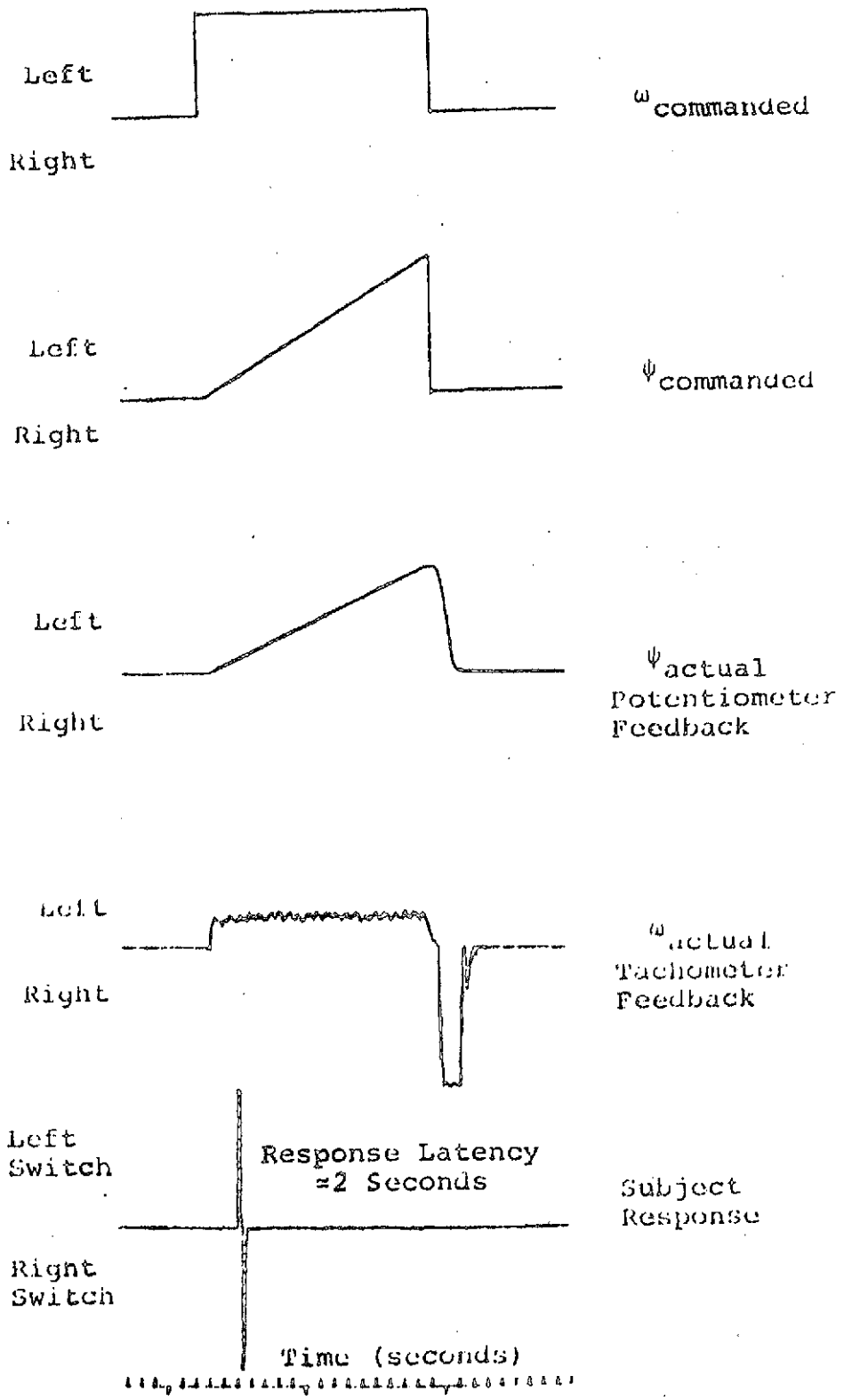

Figure 4.5 Strip Chart Recording for Velocity Step (~1.2 deg/sec) Stimulus to the Left

was rotating to the left. Although the tachometer output was quite noisy, because of the small rotation rates, it is clear that the response of the simulator was quite good. The actual rotation rates were calculated based upon the information fed back from the position potentiometers.

4.4 Analysis of Experimental Results

Figure 4.6 shows the thresholds for each of the six subjects. Thresholds were calculated as follows:

Estimated threshold =

$$TH = 10^{\left\{\frac{\sum_{i=0}^{N} \log_{10} s_i}{N+1}\right\}} \tag{4.18}$$

Upper Confidence Limit =

$$TH \times 10^{\left\{\sum_{i=0}^{N} (\log_{10}(TH)-\log_{10}s_i)^2/N\right\}} = TH\sigma \tag{4.19}$$

Lower Confidence Limit =

$$TH \times 10^{-\left\{\sum_{i=0}^{N} (\log_{10}(TH)-\log_{10}s_i)^2/N\right\}} = TH/\sigma \tag{4.20}$$

where s_i = stimulus magnitude of i^{th} stimulus since staircases met or crossed

$N+1$ = number of stimuli magnitudes $s_0, s_1, s_2, \ldots s_N$.

The value for N differed for each session since it depended on how rapidly the staircases crossed but usually

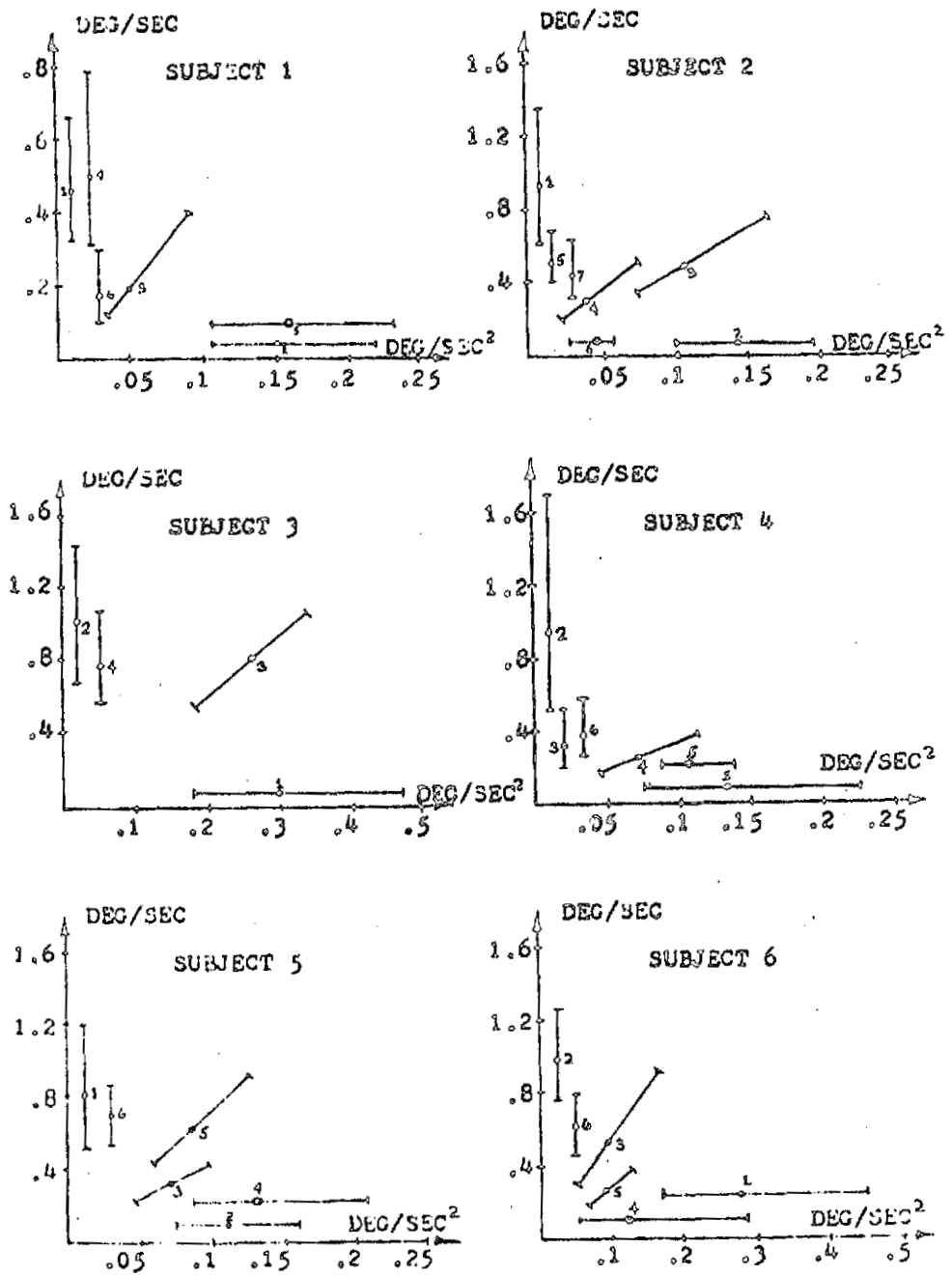

Figure 4.6 Threshold Data for Six Subjects

C - 2

it varied between 29 and 32.

Because of Weber's law (Ref. 31) all statistics were based on the log of stimulus magnitudes. For this reason the upper limit on the estimate of thresholds should be perceptually just as much greater than the estimated threshold level as the estimated threshold level is greater than the lower limit.

The number printed next to each threshold estimate represents the experiment number for that subject. Since combination stimuli for each subject could not be used until their thresholds were determined for velocity and acceleration steps, it was impossible to design the experimental presentation in such a way as to rule out order effects. To check for learning, each subject's velocity step threshold was tested several (2 or 3) times. The first velocity step experiment was always either the first or second time in the simulator. The remaining velocity step tests were scattered among the remaining tests, so that by using the results of all six subjects, a model for the effects of learning could be formulated. The assumption is made that all subjects had approximately the same learning profile and that this profile affected all experiments uniformly.

The model for learning used to correct the experimental data is given by:

$$L(N) = [K + (1 - K)e^{-(N-1)/M}] \qquad (4.21)$$

where the threshold resulting from the N^{th} session should

be L(N) times the threshold which would have been found if the same experiment had been done during the first session. Notice that after an infinite number of sessions ($N = \infty$) the threshold should be K times the initial threshold. The parameters K and M were varied to minimize the weighted variation of the models prediction from the experimental data. The optimal values of K and M were found to be

$$K^* = .52 \text{ and } M^* = 3.32 \qquad (4.22)$$

Figure 4.7 shows a plot of $\log_{10}(L^*(N))$ with the relevant estimated thresholds and confidence limits shown. Note that the confidence limits are symmetrically placed with respect to the estimated thresholds when plotted logarithmically.

It should be mentioned here that the results of one experimental session among the 35 conducted was rejected. Specifically, in the second session with subject number four, the staircases wandered to extremely high values just before the break and when questioned about it the subject admitted that he had nearly fallen asleep. After the break, the staircases immediately plummeted to reasonable levels, but the wide variation in magnitudes (note the confidence limits for this threshold) coupled with the subjects' remarks indicated that it would be reasonable to disregard this session.

The function $L^*(N)$ can now be used to adjust all threshold estimates to reflect the threshold which one would

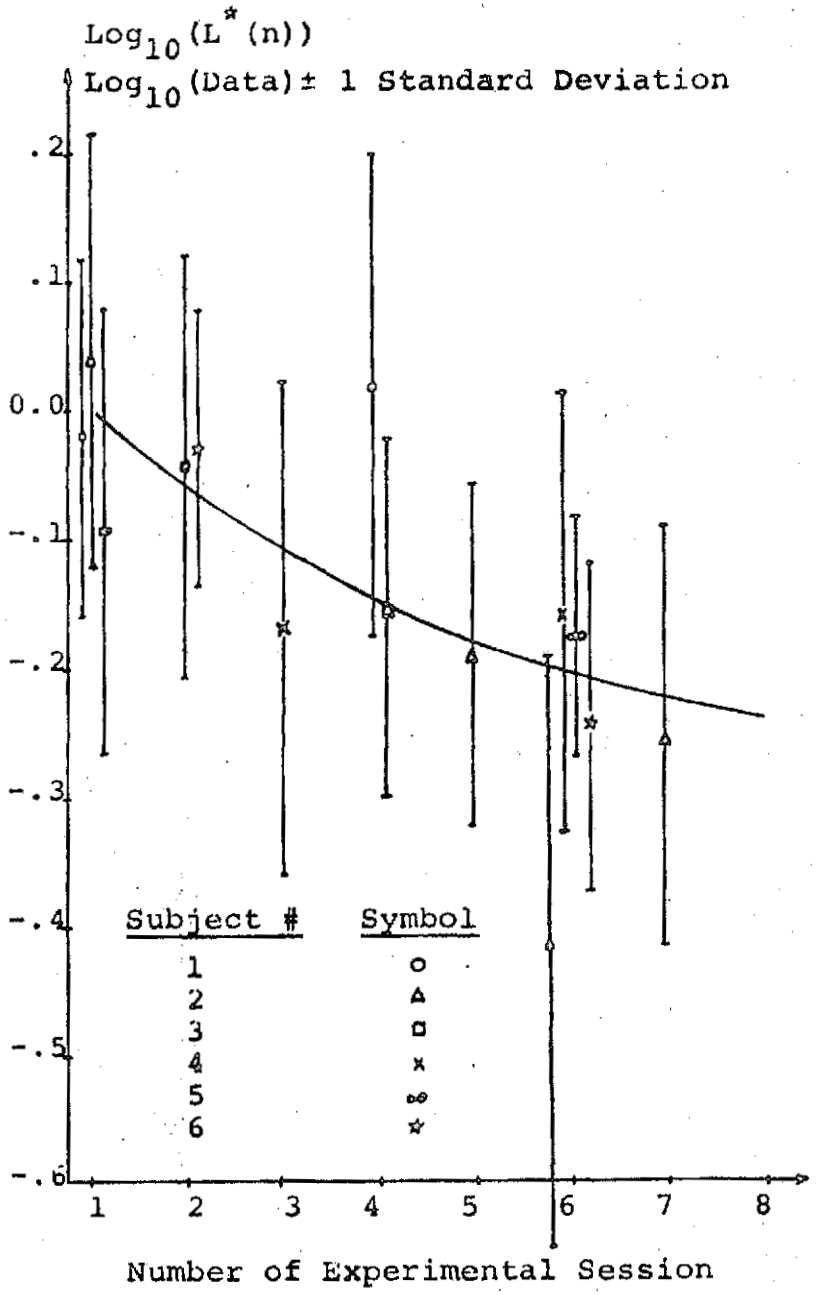

Figure 4.7 Comparison of Learning Model and Data

expect to find if the subject had been in the simulator for the first time. The data could have been adjusted to reflect any degree of experience, but it was felt that most cues which contribute to learning in these experiments are non-vestibular (tactile, audio, etc.). Table 4.1 summarizes the estimated thresholds and their corrected values. Weighted averages for each experiment type were calculated and the results are as follows (all motions are about an earth vertical axis):

Average velocity step threshold for Roll = .835°/sec

Average acceleration step threshold for Roll = .190°/sec^2

Average acceleration step threshold for Yaw = .160°/sec^2

The threshold for yaw was computed based on only five of the six subjects since subject number three was not tested. If a direct comparison is to be made between the vestibular sensitivities to acceleration steps about the yaw and roll axes the threshold for the roll axis should be calculated based upon the same five subjects. When this is done, we obtain a roll acceleration threshold of .158°/sec^2. Clearly there is no significant difference between this result and the .160°/sec^2 found for the yaw axis. This result supports conclusions made by Clark and Stewart (Ref. 16) that there are "no statistically significant differences among the thresholds about the three major body axes".

To test the validity of the "simple threshold" and

TABLE 4.1

SUBJECT NUMBER	EXP TYPE	THRESHOLD DEG/SEC (DEG/SEC^2)	CORRECTED FOR LEARNING	σ FACTOR	$\log_{10}\left(\frac{\sigma}{\text{FACTOR}}\right)$
1	V	.461	.461	1.419	.15192
	A	(.151)	(.173)	1.445	.16026
	C	.193(.054)	.247(.069)	1.585	.20038
	V	.498	.697	1.549	.18959
	Y	(.157)	(.236)	1.486	.17186
	V	.181	.289	1.724	.23665
2	V	.906	.906	1.479	.17029
	A	(.139)	(.159)	1.393	.14388
	C	.46 (.109)	.59 (.139)	1.531	.18492
	C	.30 (.044)	.42 (.062)	1.660	.21973
	V	.527	.794	1.361	.13372
	Y	(.042)	(.067)	1.387	.14235
	V	.455	.760	1.458	.16374
3	A	(.299)	(.299)	1.596	.20298
	V	1.007	1.151	1.432	.15995
	C	.75 (.237)	.96 (.303)	1.367	.13577
	V	.780	1.09	1.375	.13843
4	A	(.129)	(.129)	1.743	.24739
	V	.941	1.075	1.786	.25203
	V	.337	.431	1.574	.19692
	C	.22 (.074)	.31 (.104)	1.545	.18890
	Y	(.107)	(.161)	1.276	.10605
	V	.374	.597	1.485	.17166
5	V	.800	.800	1.491	.17352
	A	(.111)	(.127)	1.439	.15814
	C	.29 (.070)	.37 (.089)	1.380	.14003
	Y	(.131)	(.183)	1.446	.16033
	C	.63 (.081)	.95 (.122)	1.400	.14624
	V	.670	1.069	1.236	.09210
6	A	(.279)	(.279)	1.596	.20315
	V	.957	1.094	1.283	.10833
	C	.51 (.089)	.65 (.114)	1.675	.22393
	Y	(.125)	(.175)	2.061	.31411
	C	.30 (.095)	.45 (.143)	1.429	.15517
	V	.580	.926	1.337	.12607

KEY: V Roll Velocity Step; A Roll Acceleration Step; C Combination Roll; Y Yaw Acceleration Step

"signal in noise" models of central processing, the data is first corrected for learning and then transformed so that when plotted on a single stimulus graph (such as shown in figure 4.4) all velocity step thresholds fall at V_{TH} and all acceleration step thresholds fall at A_{TH}. The data from the combination stimuli can then be directly compared to the model predictions illustrated in figure 4.4.

Figure 4.8 shows the combination stimuli with their confidence limits plotted as described above. The predicted thresholds for the two models are shown (an intermediate value of K = .6 is used for the "signal in noise model") along with a curve marking the midpoints between the two predictions (the decision boundary).

Each estimated threshold point plotted can be considered the mean of a probability distribution for the true threshold value with the confidence limits being the one standard deviation points.

Since this graph shows only relative variations between experimental results, any feature of the experimental apparatus procedure or statistical technique which causes all results to be affected by a given scale factor will not affect the validity of any conclusions drawn from the graph.

If the errors which give rise to these distributions are independent (except for an arbitrary scale factor, which as noted above, will not affect the conclusions) and gaussian,

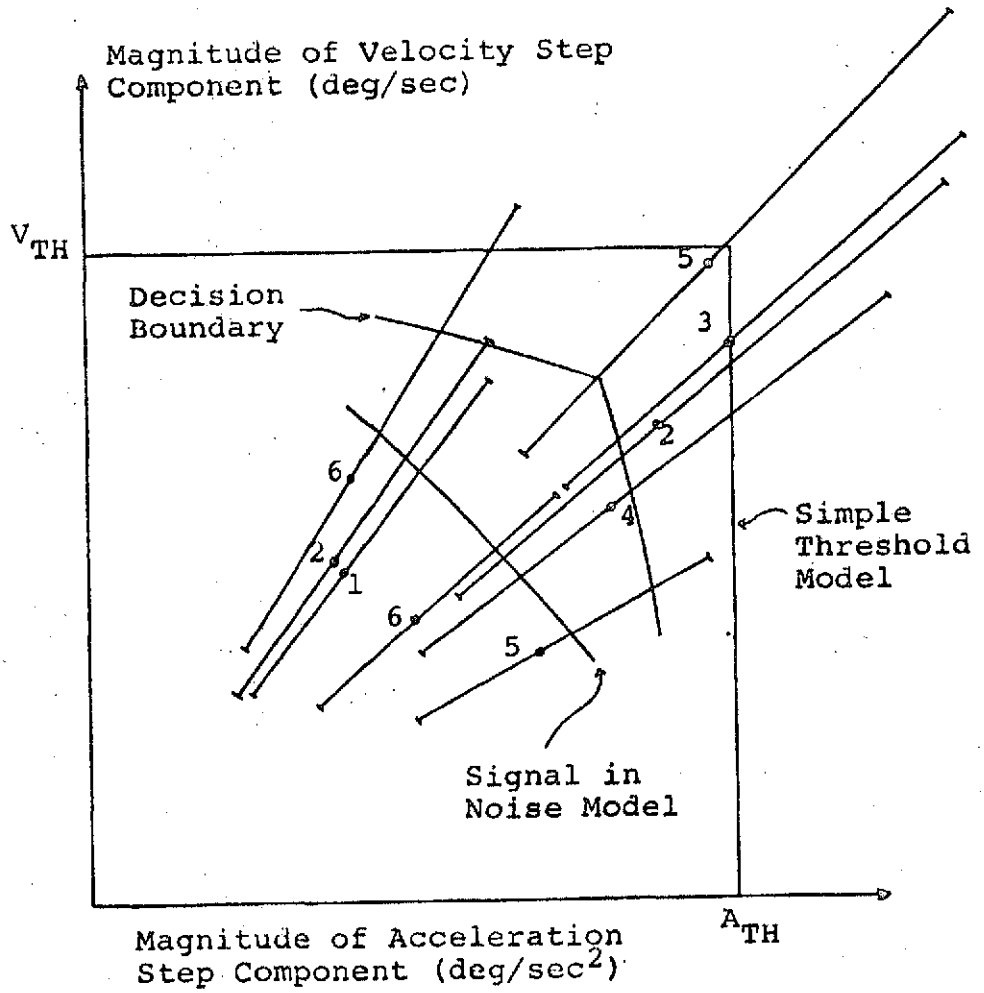

Figure 4.8 Comparison of Data to Thresholds Predicted by Hypotheses

then the relative likelihood of the two models being the source of these experimental results can be easily calculated.

One method of choosing between the two models is to ask the question: What is the probability that the true thresholds are inside the decision boundary? Using the above mentioned assumptions, the probability that the true thresholds are inside the decision boundary (favoring the "signal in noise model") is 99.8%.

It is clear from this calculation that if a choice is to be made between the proposed models, the "signal in noise model" is to be much preferred over the "simple threshold model".

4.5 Conclusions

The experiments described in this chapter yielded the following threshold information:

1. Roll velocity step threshold ≈ .835°/sec
2. Roll acceleration step threshold ≈ .190°/sec^2
3. Yaw acceleration step threshold ≈ .160°/sec^2 (4.23)

and supported the following conclusions:

1. There is no significant difference in humans between sensitivity to rotation in roll and sensitivity to rotation in yaw.
2. The phenomenon of vestibular thresholds can be accounted for by a model of central processing of

vestibular information consisting only of an optimal processing of afferent firing rates in additive noise with no necessity for peripheral dead zone nonlinearities.

Chapter V

Stochastic Model for Detection of Near Threshold Rotational Stimuli

Once the "signal in noise" hypothesis is accepted as an adequate model for the basic mechanism of the vestibular threshold phenomenon, it is possible to hypothesize a stochastic model of vestibular perception which is valid for near threshold stimuli. In the course of creating this model, several significant problems arise among which are the following:

1. Based on the response of the afferent model for the semicircular canals developed in Chapter Three, one would predict that the threshold level for a velocity step stimulus would be between 10 and 15 times greater than the threshold level for a step in acceleration. The experimental results described in Chapter Four indicate an average factor of between 4 and 5 (the ratio of velocity to acceleration step thresholds for subjects taken separately were: 2.85, 5.14, 3.94, 4.03, 7.68, and 3.64). This discrepancy between threshold and suprathreshold perception must be predicted by our model of vestibular perception.
2. While the peak afferent response for a step in angular acceleration occurs approximately 20 seconds after stimulus onset and does not drop to half peak value until 45 seconds after onset, maximum detection latencies are almost always less than 15 seconds (Ref.13,36). Therefore, some mechanism

must be found to explain why average threshold latencies do not reflect the time course of the afferent signal to noise ratio.

3. A mathematical model of the detection processes that subjects *perform during* threshold experiments when they attempt to choose between right and left moving stimuli must be formulated. It is important that a distinction be made between the process of detection and the problem of estimating stimulus magnitudes which goes on during exposures to larger stimuli. The response of this model should exhibit the same basic characteristics observed during threshold experiments and be capable of predicting response statistics as a *function of time for* arbitrary near threshold stimuli.

Section 5.1 deals with the first two problems, while sections 5.2 and 5.3 deal with the third problem. Section 5.4 summarizes the predictions which result from this model of threshold detection.

5.1. First Order Processing

If the acceleration and velocity step threshold stimuli found experimentally (.835 degree/second and .19 degree/second^2) are applied to the input of the dynamic model for the afferent response of the semicircular canals, then the responses shown in Figure 5.1 will be obtained. It is perfectly clear that no reasonable detector should find it equally difficult to detect the presence of these two signals (as it should, since both are threshold stimuli). Furthermore, the maximum detection latency for a

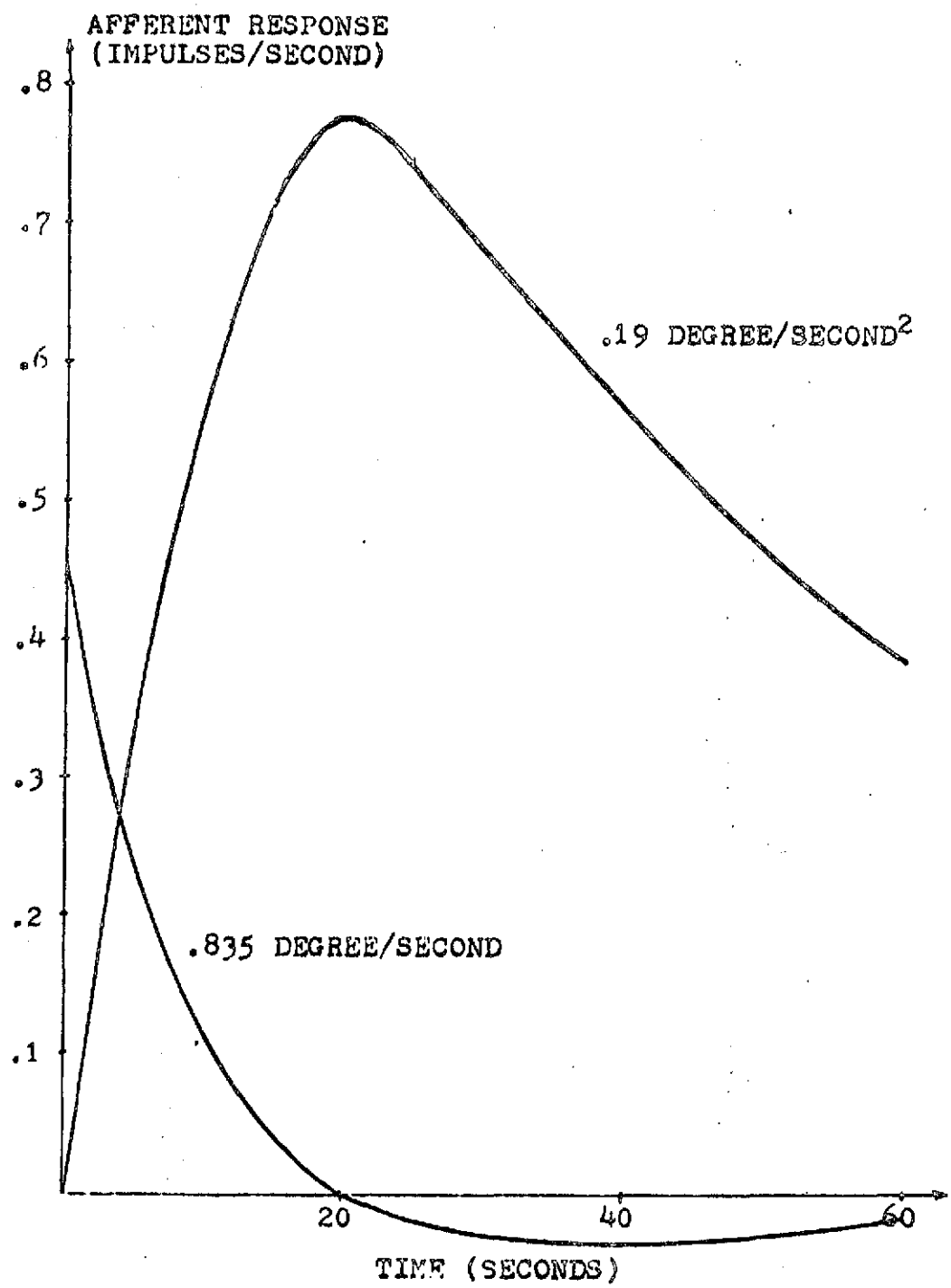

Figure 5.1 Comparison of Afferent Response to Threshold Velocity Step (.835 deg/sec) and Acceleration Step (0.19 deg/sec^2)

threshold acceleration step using these responses should be 20 seconds or greater, since it takes that long for the instantaneous signal to noise ratio to reach its peak. One relatively simple hypothesis which has a direct physical interpretation and provides an explanation for these discrepancies was found.

It is well known that in the presence of no input, there is a spontaneous firing rate of the vestibular afferent (shown as SFR in Figure 3.1) which must be subtracted before processing by the higher centers. Goldberg and Fernandez (Ref. 27) found a spontaneous rate of approximately 90 firings/second in the squirrel monkey, but the exact value is not important to the argument which follows. It is reasonable to assume that this resting discharge is not perfectly stable but has some low frequency drift associated with it, which, if large enough and allowed to remain unfiltered, will give rise to spurious sensations of motion and will contribute to the masking of low level stimuli. In the process of eliminating the spontaneous component of firing, the effect of low frequency variations can also be reduced by estimating them and subtracting them from the afferent signal. Figure 5.2 shows the proposed pathway which estimates both the spontaneous discharge (SFR) and hypothesized low frequency variations (c) and subtracts them from the afferent signal. If c and the measurement noise (n) are members of stationary Gaussian random ensembles and the signal A equals zero, then the minimum-mean-squared-error (MMSE) estimate of c is given by the output of a linear filter. It is this filter,(shown between E and F in Figure 5.2) which

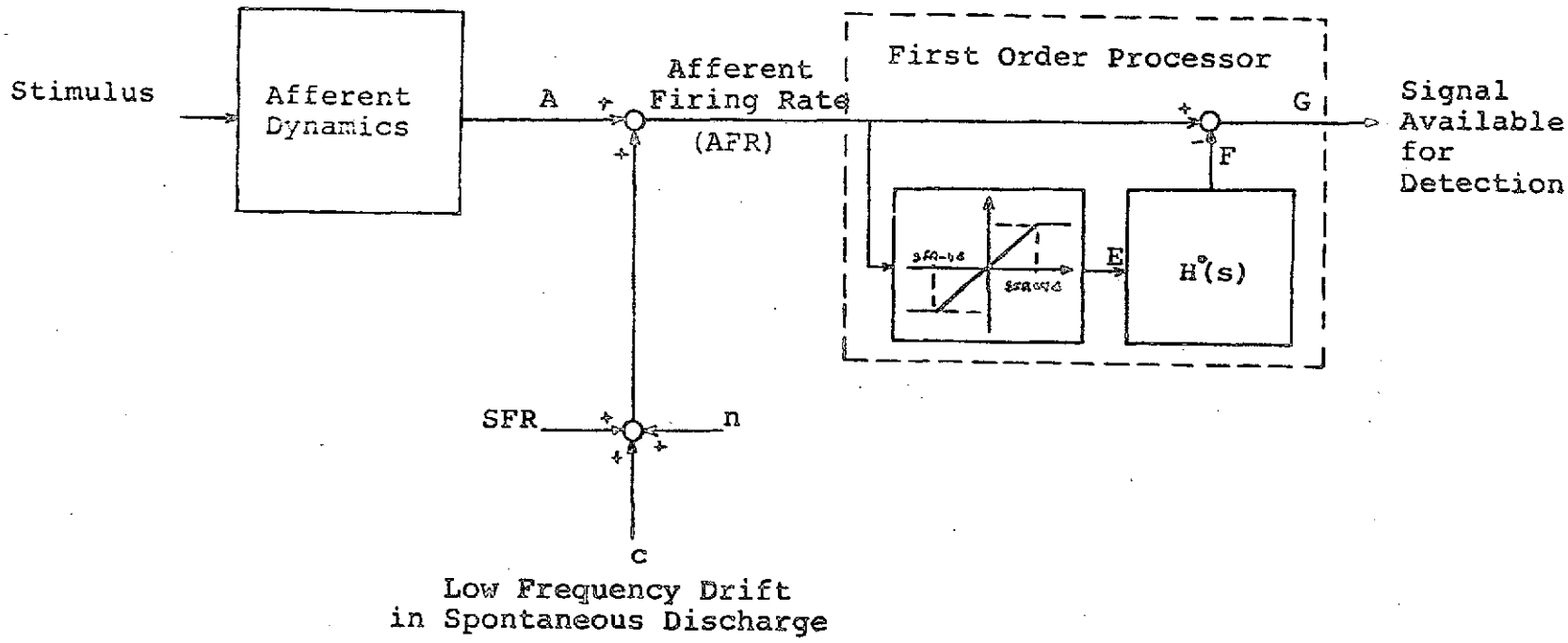

Figure 5.2 First Order Processor

accounts for the equalization of the signals shown in Figure 5.1 and which reduces the spurious sensations of motion which would occur if the signal c were processed as if it arose from a real stimulus. The assumption that the signal at A is small is, of course, not always true so some limitation must be placed on the filtering so as not to effect the processing of suprathreshold stimuli. Specifically, if the afferent firing rate (AFR) stays within ± 4σ (σ referring to the effective standard deviation of c + n) of the resting discharge rate then AFR is filtered as if A were zero, but if AFR exceeds these bounds, it is presumed that a sufficient signal to noise ratio exists to obviate the need for eliminating c. A region comprising ± 4σ was chosen since in the no stimulus case this region would, for all practical purposes, contain c + n 100% of the time. This limitation is modeled by the saturation nonlinearity which is shown between AFR and E.

The following procedure is used to specify the statistics of c and n and the resulting processor (which includes the saturation nonlinearity and the optimum processor $H^{\circ}(s)$):

1. For the purpose of maintaining simplicity the process which produces c is assumed to be such that c is exponentially correlated. This can be modelled as a white process through a first order shaping filter as follows:

$$c(s) = \{\frac{c_1}{c_2 s+1}\}W(s) \qquad (5.1)$$

where

$$\phi_{ww}(\tau) = E[W(t)W(t+\tau)] = \delta(\tau) \tag{5.2}$$

and thus

$$\phi_{cc}(t) = E[c(t)c(t+\tau)] = \frac{c_1^2}{2c_2} e^{-|\tau|/c_2} \tag{5.3}$$

The measurement noise, n, is presumed to be white and therefore:

$$\phi_{nn}(\tau) = E[n(t)n(t+\tau)] = N^2\delta(\tau) \tag{5.4}$$

Since the optimum processor $H^\circ(s)$ is determined as a function of the statistics of c(t) and n(t) we must ultimately determine only three parameters c_1, c_2, and N.

2. If the signal available for processing were c+n and the object were to produce an estimate of c with minimum squared error, then the optimal estimator would be given by the following Wiener filter:

$$H^\circ(s) = \frac{(c_1/Nc_2)^2}{(\eta^2+\eta/c_2)} \frac{1}{(\frac{s}{\eta}+1)} \tag{5.5}$$

where

$$\eta = \frac{1}{c_2}(1 + (\frac{c_1}{N})^2)^{1/2} \tag{5.6}$$

Since the actual signal available for processing is SFR + c + n and the object is to estimate (SFR + c) we must use a filter which passes a constant signal with unity gain. Thus the expression for $H^\circ(s)$ given in equation 5.5 is acceptable if

$$\frac{(c_1/Nc_2)^2}{(\eta^2+\eta/c_2)} = 1 \tag{5.7}$$

Actually, the optimal filter gain only approaches unity as $c_1/N \to \infty$. Although unity gain must be used in the ultimate model, reasonable values for c_1, c_2, and N are obtained if equation 5.7 is replaced by

$$\frac{(c_1/Nc_2)^2}{(\eta^2 + \eta/c_2)} \approx .95 \qquad (5.8)$$

The consequence of making this change is to produce a system in which SFR is estimated and eliminated with no error while the optimal filter gain for estimating c(t) is in error by only about 5%.

3. If the response of

$$1 - H^\circ(s) = \frac{s}{s+\eta} \qquad (5.9)$$

to the signals shown in Figure 5.1 are designated $s_1(t)$ and $s_2(t)$, then η is chosen such that

$$\int_0^{14} s_1(t)|s_1(t)|dt = \int_0^{14} s_2(t)|s_2(t)|dt \qquad (5.10)$$

This insures that for a given level of measurement noise and spontaneous discharge variation a .835 degree/second velocity step and a .19 degree/second^2 acceleration step will be detected with equal likelihood during a fouteen second presentation as was found experimentally. The value of η necessary to satisfy equation 5.10 was found to be

$$\eta = \frac{1}{c_2}\,(1 + (c_1/N)^2)^{1/2} = 1/3 \qquad (5.11)$$

4. Since the signals shown in figure 5.1 are threshold signals and are thus correctly detected 75% of the time, the net effect of passing them through the filter $\{1 - H^{\circ}(s)\}$ should be to produce signals $s_1(t)$ and $s_2(t)$ which when processed by the detector should yield 75% correct responses. The net effect of this condition is to adjust the level of c(t) and n(t) together so as to produce the required level of signal masking necessary to predict 75% performance for the above stimuli. The detector used for this step is developed in sections 5.2 and 5.3.

5. Equations 5.8 and 5.11 along with the procedure described in 4 yield three conditions for c_1, c_2 and N. If 5.6 is substituted into 5.8 we find that

$$\frac{(\frac{c_1}{N})^2}{[1 + (\frac{c_1}{N})^2] + [1 + (\frac{c_1}{N})^2]^{1/2}} \approx .95 \qquad (5.12)$$

or that

$$c_1/N \approx 20 \qquad (5.13)$$

If the procedure described in 4 is now carried out for different values of N while picking c_1 and c_2 to satisfy 5.13 and 5.11 then 75% performance is reached for one afferent channel when

$$\begin{aligned} c_1 &= 4.46 \\ c_2 &= 60 \\ N &= .223 \end{aligned} \qquad (5.14)$$

Since $\eta = 1/3$, the optimal filter is given by

$$H^{o}(s) = \frac{1}{3s+1} \tag{5.15}$$

The linear region for the saturation nonlinearity is bounded by SFR $\pm 4\sigma$ where σ is the effective standard deviation of the signal $c(t) + n(t)$. Since

$$4\sigma = 4\left(\frac{c_1^2}{2c_2} + N^2\right)^{1/2} \simeq 2 \text{ ips} \tag{5.16}$$

The region over which the optimal processor is allowed to operate freely is given by $(SFR - 4\sigma, SFR + 4\sigma) = (88, 92)$ ips.

Figure 5.3 summarizes the slowly varying spontaneous discharge and the first order processing. It is interesting to note that while this system was designed to meet several key criteria, it also meets several conditions which although, not specifically imposed, certainly would be expected from acceptable models of vestibular processing.

For example:

1. It might have turned out that the reasonable region for signal processing ($90 \pm 4\sigma$) would not have been sufficient to include the maximum variation in firing due to threshold stimuli. Inspection of Figure 5.1 shows that this is not the case since the peak variation in firing due to a stimulus of 0.19 degree/second^2 is 0.78 firings/second which is well within the specified region of ± 2.0 firings/second.

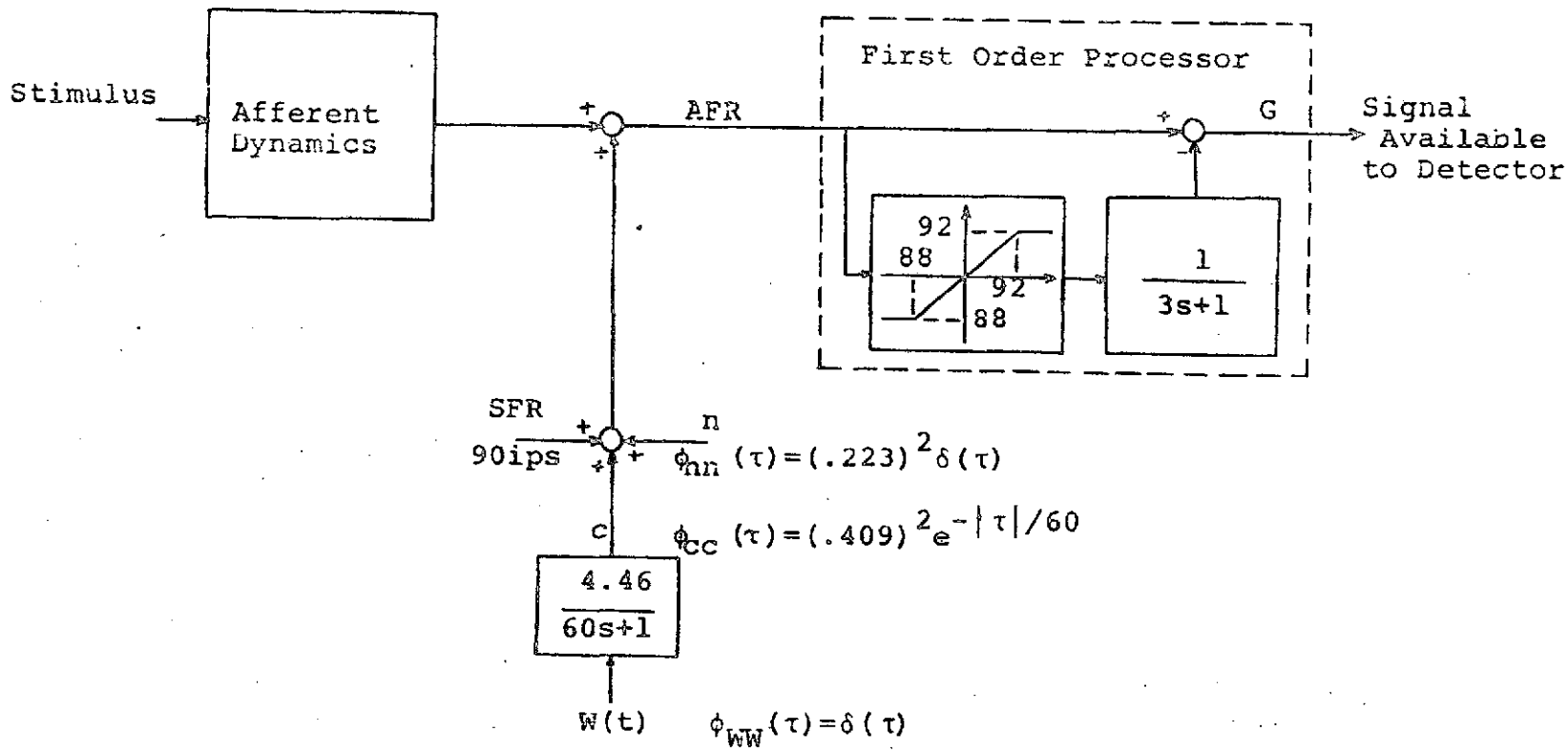

Figure 5.3 Model Of Information Available to Detector

2. On the other hand, the necessary variation in steady state firing is significantly smaller than that found in the most regular cells recorded by Goldberg and Fernandez (Ref. 27). This would lead one to the conclusion that the higher centers must be capable of combining the information from several afferent cells to achieve the threshold performance found experimentally. A discussion of this phenomenon is given in section 3.1.

3. The existence of this three second filter would explain why vestibular threshold experiments need to last only ten to fifteen seconds. As noted previously , if such a mechanism did not exist, the maximum signal level from a step in angular acceleration would occur 20 seconds after the stimulus onset and not fall to half peak amplitude until 45 seconds after onset (Figure 5.1). Figure 5.4 shows the signals available to the detector for a .835 degree/second velocity step and a .19 degree/second^2 acceleration step after the first order processing. Not only is it believable that these two signals are equally easy to detect (as opposed to those illustrated in figure 5.1) but it is also easy to understand why latencies which significantly exceed fifteen seconds are rarely encountered.

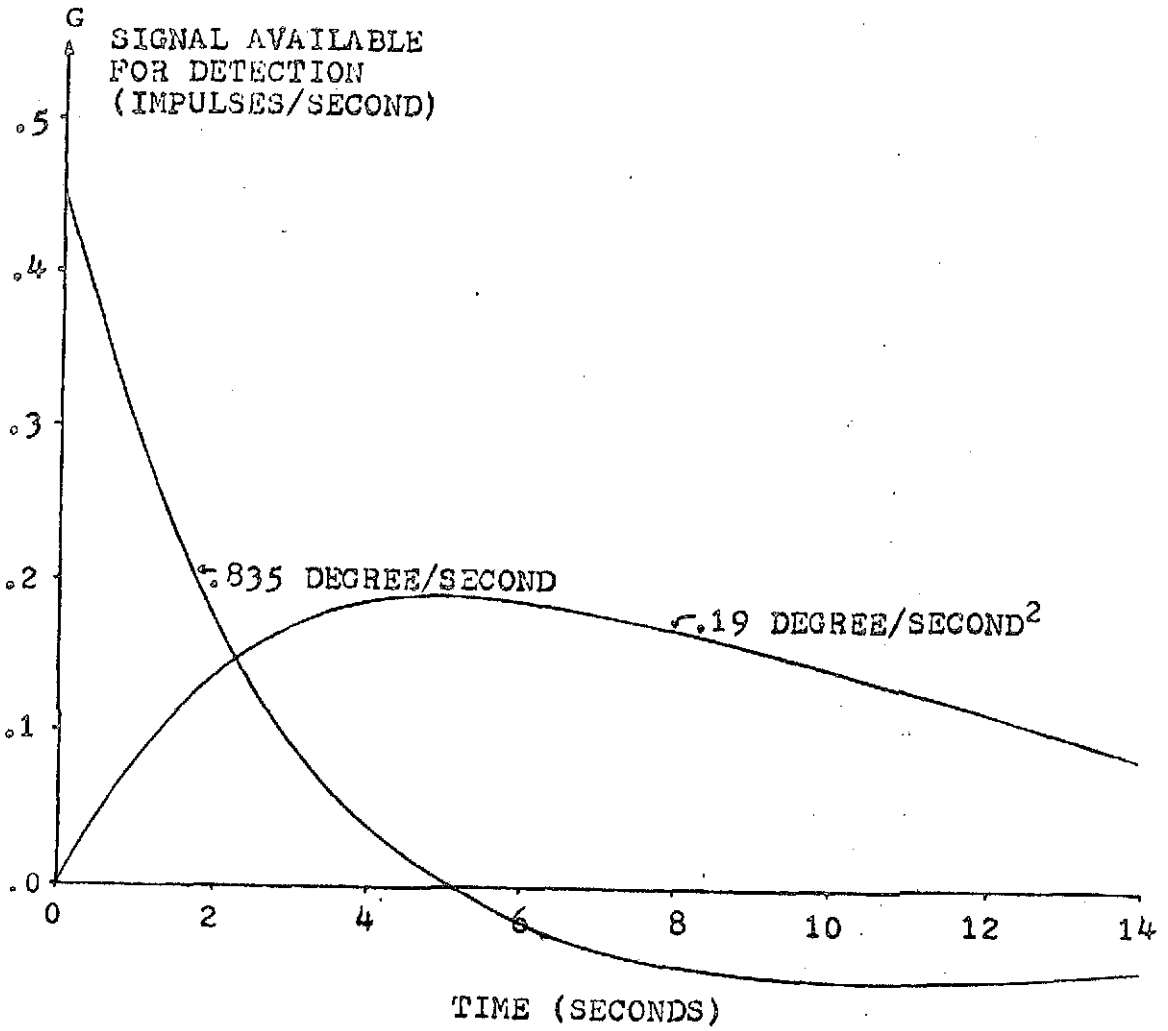

Figure 5.4 Signals Available for Detection After First Order Processing for Threshold Steps in Angular Velocity and Acceleration

5.2 Detection Using Information From The Suprathreshold Optimal Estimator

Since the first order processor insures that a threshold velocity step (.835 degree/second) and a threshold acceleration step (.19 degree/second^2) will be equally easy to detect, and since a model consistent with the "signal in noise" hypothesis insures that a combination stimuli given by

$$\omega_c(t) = K(.835 + .19t) \tag{5.17}$$

will only yield equivalent performance if

$$1/2 < K < 1/\sqrt{2} \tag{5.18}$$

we can conclude that any reasonable detector which utilizes the available signals (G in Figure 5.3) should meet all of the essential requirements. In Chapter Three a Kalman Filter was proposed as a model for the higher centers' perception of suprathreshold stimuli. Since such a processor is presumed to be operating anyway, it would make sense that it could also be used as part of the detector for near threshold signals.

If one looks at the output of the Kalman Filter associated with the semicircular canals at any given time it is seen that it consists of an estimate of the rotation rate and an error variance for the estimate. Since all processes are assumed to be Gaussian, a probability distribution for the actual stimulus magnitude conditioned on previous measurements of afferent firing rate is known.

At that instant of time, the subject could report on the probability that his instantaneous rotation is to the right or the left as illustrated in Figure 5.5. All that is needed is a way to produce such an estimate under the known conditions of a threshold experiment and to give a model of the subject's criteria for issuing a report.

In most vestibular theshold experiments a subject assumes that any motion given him will either be always to the right or always to the left and not a combination of the two, since he is expected to only give one report. If the errors in the estimate of rotation were independent from one interval to the next, it would be an easy matter to combine these estimates to produce the probability that the stimulus was to the right (or left), but since these errors exhibit significant correlation from one interval to the next, combining these estimates properly is a difficult computational task. In fact to combine N such estimates would involve the computation of two N dimensional integrals of the joint probability density for the stimulus history conditioned on the measurement history. While such a computation could be carried out by a computer, it seems unlikely that the brain would be doing anything similar, or that it would be necessary to use such a complicated detector for our model. To avoid this computational problem, the Kalman filter is applied sequentially to each measurement of afferent firing as if it were the only measurement available. In this manner we obtain a probability density for $\omega(t)$ (similar to the one shown in Figure 5.5) conditioned on only one

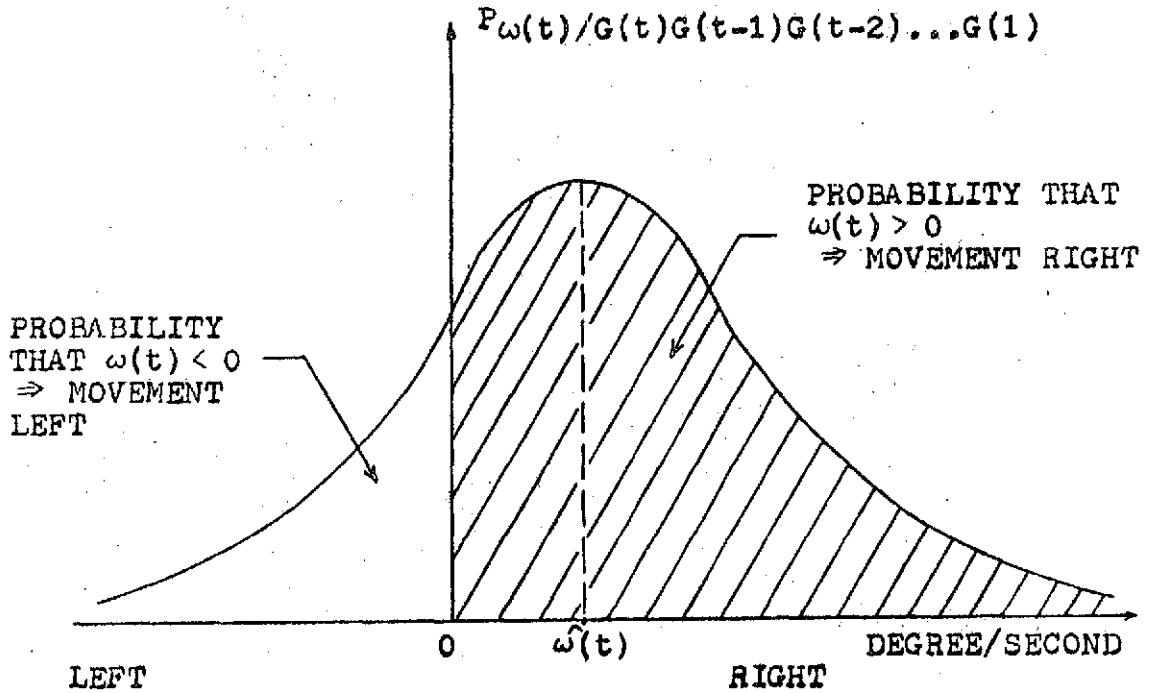

Figure 5.5 Decomposition of Probability Density Function

measurement at a time. Although this does not reduce the correlation of estimate errors from one interval to the next to zero, it does eliminate the major contribution to this correlation (the fact that in the usual Kalman filter, the estimate error at one time is propagated and becomes part of the error of subsequent estimates). With the error correlation significantly reduced the assumption of independence is reinstated and the estimates can easily be combined. If $P_{R/G(t_i)}(t_i)$ is the probability at time t_i that the motion is to the right given the measurement of G at t_i, then the combined probability that the motion is and has been to the right at time t_N is given by:

$$P_R(t_N) = \frac{A}{A+B} \tag{5.19}$$

and to the left is

$$P_L(t_N) = \frac{B}{A+B} = 1 - P_R(t_N) \tag{5.20}$$

where

$$A = \prod_{i=1}^{N} P_{R/G(t_i)}(t_i) \tag{5.21}$$

$$B = \prod_{i=1}^{N} P_{L/G(t_i)}(t_i) = \prod_{i=1}^{N}(1-P_{R/G(t_i)}(t_i)) \tag{5.22}$$

and $P_{R/G(t_i)}(t_i)$ is obtained by calculating the appropriate area under $P_{\omega(t)/G(t_i)}$ as illustrated in Figure 5.5.

Alternatively (see Ref. 7) the log of the ratio of $P_R(t_n)$ to $P_L(t_n)$ can be updated sequentially as follows:

$$\rho_n \equiv \ln\left(\frac{P_R(t)}{P_L(t)}\right) = \rho_{n-1} + \ln\left(\frac{P_{R/G(t_n)}}{P_{L/G(t_n)}}\right) \qquad (5.23)$$

$$= \rho_{n-1} + \ln(\Lambda(G(t_n)))$$

where $\Lambda(G(t_n))$ is the likelihood ratio defined as $\frac{P_{G(t_n)/R}}{P_{G(t_n)/L}}$.

The above scheme leads to an accumulated probability that the rotation was to the left or to the right, but still does not tell us what criteria a subject will use for making a report.

In the experiments conducted at Langley Research Center and reported in Chapter Four the subjects were requested to report their direction of rotation only if they had sensations of motion significant enough so that their report would not be merely a guess. For this reason the minimum criteria for issuing a report consisted of $P_R(t_N)$ either exceeding .75 or diminishing below .25 (implying that $P_L(t_N) > .75$). Another consideration which should be used in choosing a reporting criteria is that subjects are aware that they have at least 13 - 15 seconds to issue their report. Thus, before 13 seconds have elapsed the criteria for issuing a report is stricter than 75% due to the fact that a reasonably motivated subject would not report with only 75% confidence early in the experiment since he would know that his period for reporting had significant time remaining and he might as well obtain more data before committing himself. As a result of these considerations the reporting criteria shown in figure 5.6 was used. It should be made clear that any reasonable decision boundary

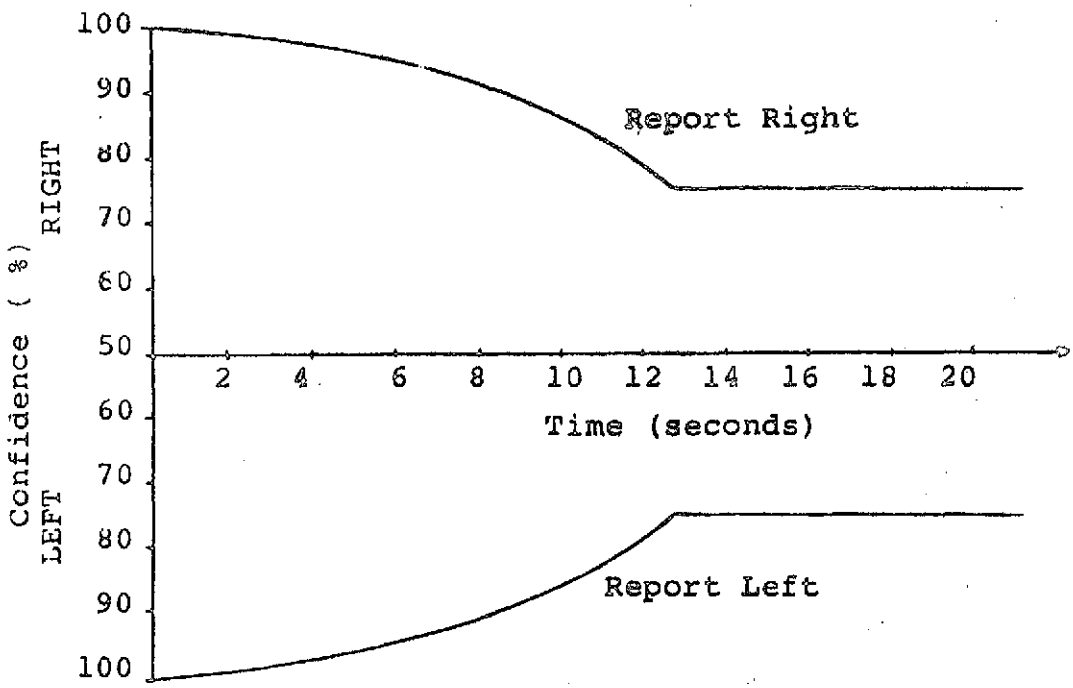

Figure 5.6 Decision Boundaries

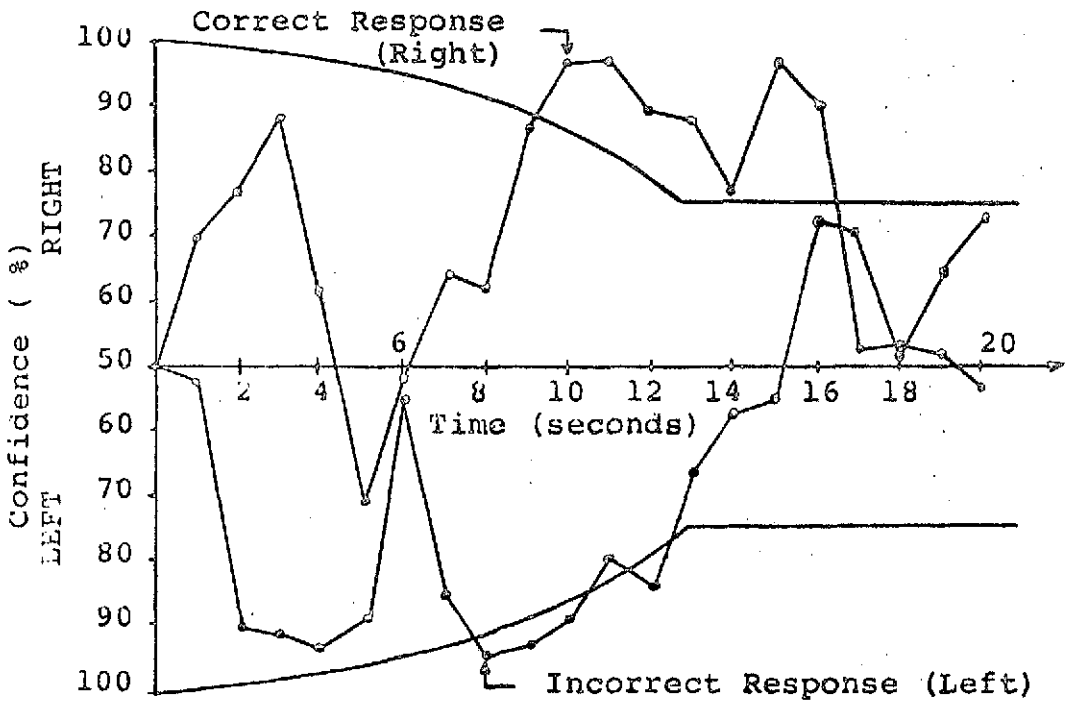

Figure 5.7 Typical Correct Response and Incorrect Response Trials

could be used since the basic integrity of the model is not dependent on this particular profile. The level of measurement noise and base rate variation was adjusted, in the manner described in the previous section, until a .19 degree/second^2 acceleration step was correctly identified approximately 75% of the time. The necessary values for c_1 and N to obtain 75% performance are given in 5.14. As expected, equivalent performance for a .835 degree/second velocity step and a combination stimuli ($W_c(t) = .67(.835 + .19t)$ degree/second) was reached for the same noise level. A typical correct response simulation and a typical incorrect response trial are shown in Figure 5.7.

Due to the numerical complexity of this detector which requires the simulation of a Kalman filter, large scale Monte Carlo simulations are impractical. Thus, while extensive latency histograms as a function of stimulus magnitude and type are not available it is possible from the number of simulations made to indicate the general nature of the response latencies. First it is clear that as stimulus magnitudes are increased, latencies uniformly decrease independent of the stimulus type. Secondly, the shortest latencies are associated with velocity step stimuli, the longest with acceleration step stimuli and intermediate latencies are found for combination stimuli. All of these predictions are consistent with the available experimental data for rotational thresholds.

5.3 Simplified Detector Model

The only major drawback of the detection model described in Section 5.2 is its numerical complexity and the resultant expense required to make a sufficient number of simulations to get meaningful statistics. For this reason an attempt was made to produce a model which gave equivalent performance, but which had sufficient simplicity to make large Monte Carlo runs realistic.

The best way to reduce the numerical complexity of the detector is to eliminate the Kalman filter and to try and use the available signal in a simpler manner to generate a decision parameter. Since any such simplified detector is likely to be less efficient in detecting the stimulus than the suboptimal Kalman detector, we can expect one of two consequences. Either

1) if the same noise level on the afferent signal is maintained then more afferent channels will have to be processed if the same performance is to be achieved,

or 2) if only one afferent channel is to be used then similar performance will require a reduction in the afferent noise level.

These consequences are not significant though, since our object is to obtain equivalent performance with a minimum of computational effort, regardless of the details of the model (e.g. noise level, number of afferent channels, etc.)

Typically, a detector consists of a decision parameter (which is a function of the available signal) and a set of

reporting criteria which the decision parameter must meet before a report is issued. One possible decision parameter could be formed by integrating the available signal and issuing a report if the parameter exceeded certain bounds. There are two problems with this solution. First, the result of integrating a zero mean random process is to produce an output similar to a random walk whose variance increases without bound as time increases. Such a model would predict a large number of reports in the absence of any stimulus input. While such reports are observed experimentally they are relatively rare. Secondly the parameter formed by simple integration does not take sufficient advantage of the initial prominent response to a velocity step stimulus. In fact, its expected value asymptotically approaches zero as t goes to infinity. Inspection of Figure 5.4 reveals that for a velocity step stimulus the available signal is of the correct sign and large for a short time and of the wrong sign and small for a much longer time. The optimum Bayes detector for the case in which one wishes to distinguish between two uncorrelated signals with different variances consists of a square law device and an integrator (Ref 69, 71). Such a detector tends to amplify the importance of large deviations more than small ones. This characteristic is useful in the case of a velocity step since it weighs the initial prominent signal much more than the small undershoot. One drawback of this procedure is that by squaring the available signal the sign of the signal is lost and thus it would be impossible to distinguish between right and left moving stimuli.

The decision parameter must therefore meet four key criteria:

1. It must be able to distinguish right moving from left moving stimuli.
2. It must have a bounded variance in response to a no-stimulus trial to reduce the probability of a false alarm to a level consistent with experimental data.
3. The processor which gives rise to the decision parameter must have a form consistent with that analyzed in Section 4.2 and therefore be consistent with the "signal in noise model" predictions illustrated in Figure 4.4.
4. It should incorporate some technique for taking advantage of the larger magnitude of the initial response as compared to any subsequent undershoot.

A detector which satisfies these four conditions and which is numerically simple is shown in Figure 5.8. The first condition is satisfied since the product $G(t_1)|G(t_1)|$ which drives the processor which generates H retains the same sign as $G(t_1)$. The variance of H is bounded in response to random processes with bounded variance since H is the output of a discrete time first order filter. A filter time constant of four seconds ($e^{-1/4} \approx .78$) was chosen to reduce the false alarm rate to less than 10%. This decay mechanism also serves as a memory limiter since it progressively discounts the importance of information as that information grows older. The third condition is fulfilled since the linear

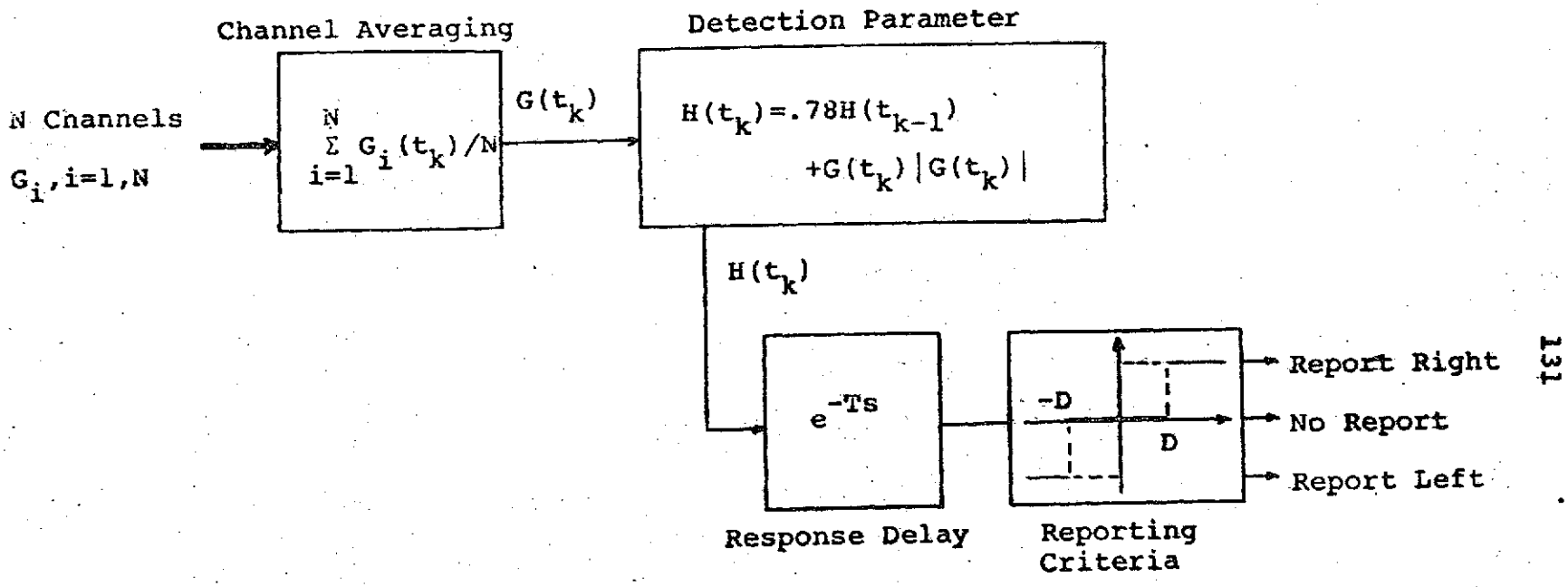

Figure 5.8 Simplified Detector

operator which processes $G(t)|G(t)|$ satisfies the requirements of a "signal in noise" processor as given in Section 4.2. Finally, since G(t)'s contribution to a change in H is proportional to the square of the magnitude of G(t), H responds with increasing sensitivity as $|G(t)|$ increases.

The minimum computational effort will be reached if only one channel is simulated. For this case (N=1) the measurement noise and resting discharge variation must be reduced by a factor of $\sim \sqrt{3}$ so that for this simplified detector

$$\begin{aligned} c_1 &= 2.58 \\ N &= .129 \end{aligned} \tag{5.24}$$

and the equivalent reduction capability of the central processor would be given by (see Section 3.1.2)

$$\text{Reduction Capability} = \left(\frac{5.1}{.129}\right)^2 = 1560 \tag{5.25}$$

which is three times greater than was necessary for the suboptimal detector using the Kalman filter. The response delay has not been modelled but it is expected that the delay is longer than typical reaction times since it arises from the conscious weighing of barely noticeable perceptions. In fact, the delay may be a function of how much the detection parameter, H, exceeds the decision boundary since a large H would imply an easier decision and thus less deliberation. In any case a Rayleigh or Maxwell distribution for the response delay with a mean delay of one or two seconds should yield reasonable predictions concerning response latencies. Finally the decision boundary (D) was adjusted

to insure that an acceleration step of 0.19 degree/second^2 would be detected 75% of the time.

The model shown in Figure 5.8 was simulated using the parameter specifications outlined above. The computational simplicity is revealed by the fact that over two thousand, twenty second simulations could be run with approximately one minute of central processor time. The results of simulations using various stimuli of differing magnitudes is summarized in the next section.

5.4 Summary of Model Predictions for Detection Probabilities and Latencies

Velocity step, acceleration step and combination stimuli were tested to determine the model's predictions concerning the probability of detection during a fourteen second trial and the distribution of detection latencies. Figure 5.9 summarizes the performance predicted by the model as determined by Monte Carlo simulation. Each point represents the results of one hundred simulated trials. Stimulus magnitudes are referred to the experimentally determined threshold levels as follows;

$$TH\sigma^N = \begin{cases} \sigma^N\ (.835)\ \text{deg/sec} & \text{velocity step} \\ \sigma^N\ (.19t)\ \text{deg/sec} & \text{acceleration step} \\ \sigma^N\ (K(.835+.19t)\ \text{deg/sec} & \text{combination} \end{cases} \quad (5.26)$$

where $\sigma = 10^{.1} = .1259$

$K = .67$ (determined from Figure 4.12)

and $N = -2, -1, 0, 1, 2$

While it is impossible to determine the precise threshold predictions in this manner it is clear that the predicted thresholds (75% correct response) are between TH/σ and $TH\sigma$ for all three stimuli. It is unnecessary to determine the exact threshold predictions with any more precision than this since much larger variations are seen experimentally among subjects.

Figures 5.10, 5.11 and 5.12 illustrate typical time histories

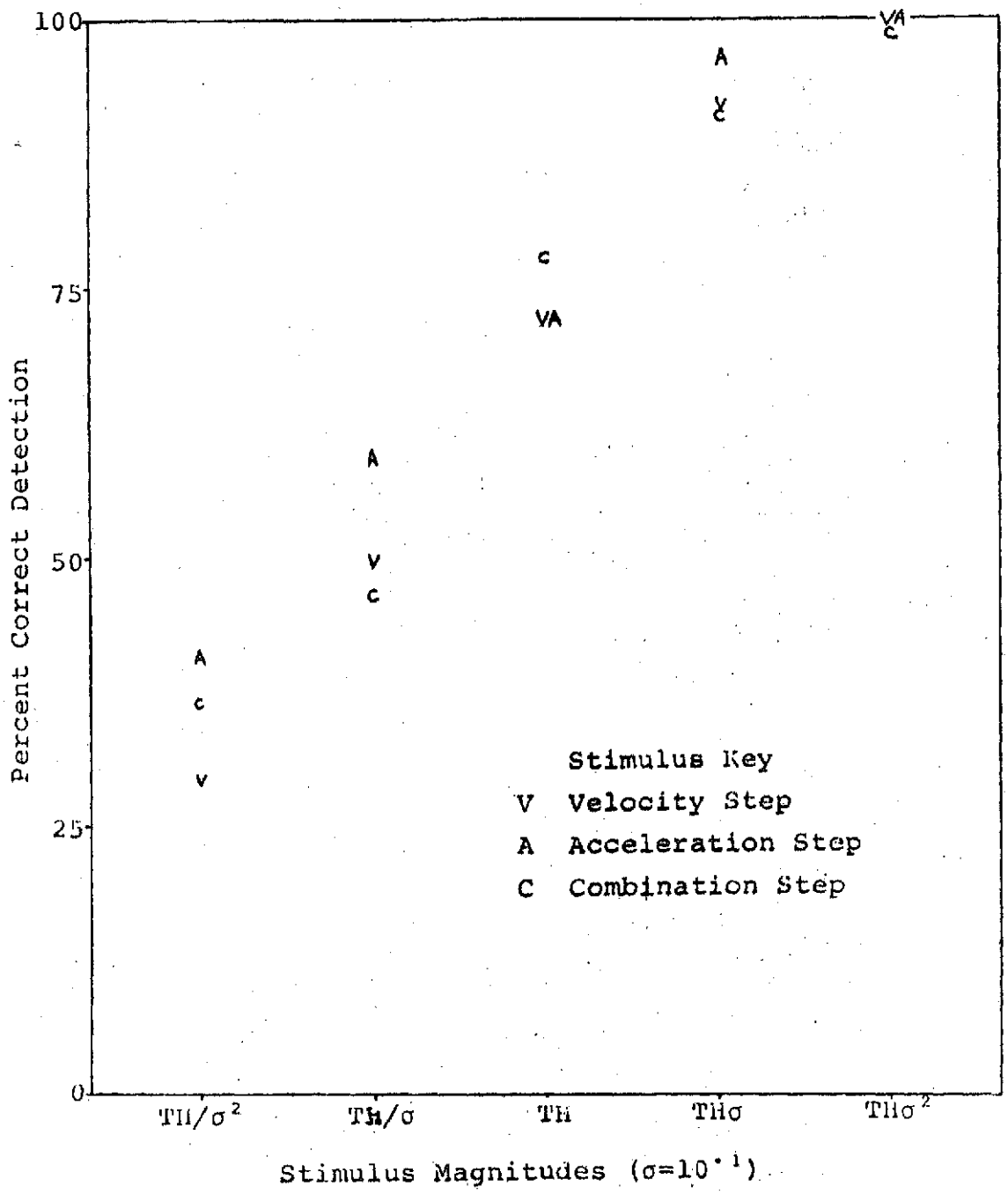

Figure 5.9 Model Predictions of Performance Variations as a Function of Stimulus Magnitudes

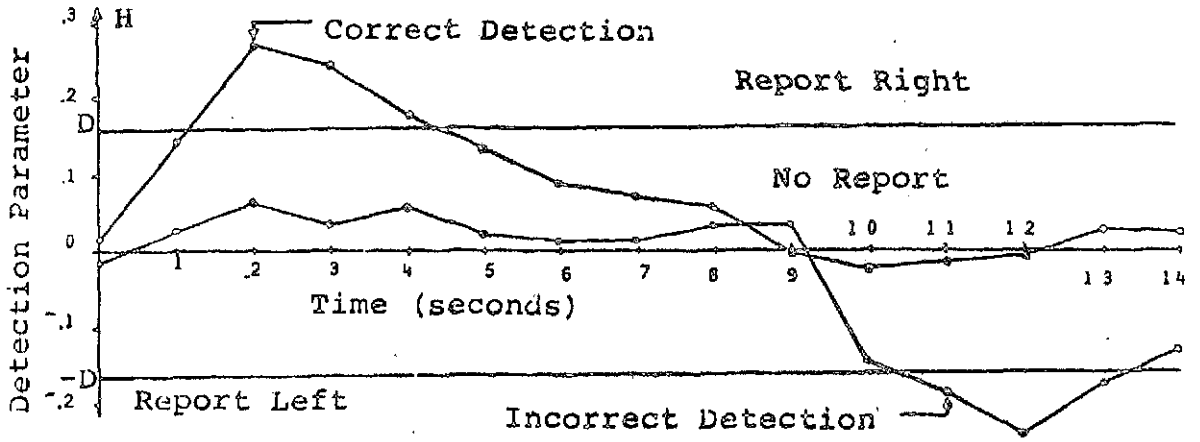

Figure 5.10 .835 Deg/Sec Velocity Step Simulations

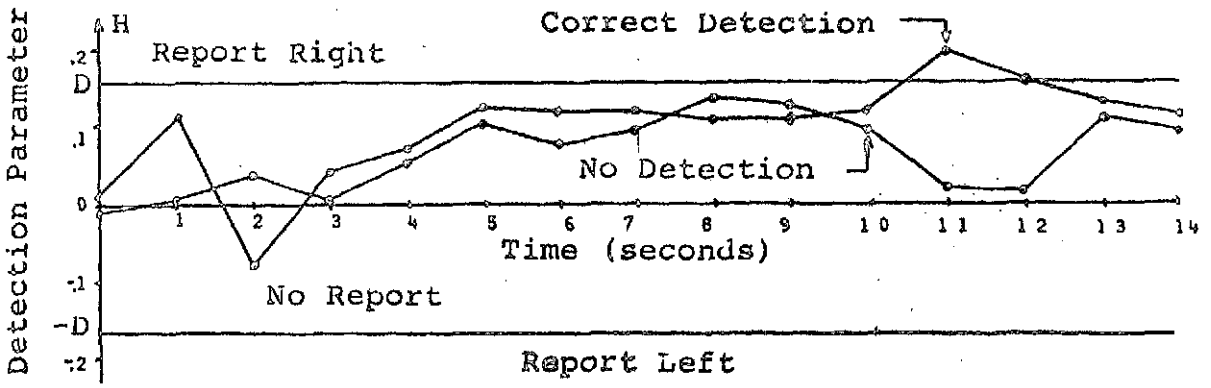

Figure 5.11 0.19 Deg/Sec^2 Acceleration Step Simulations

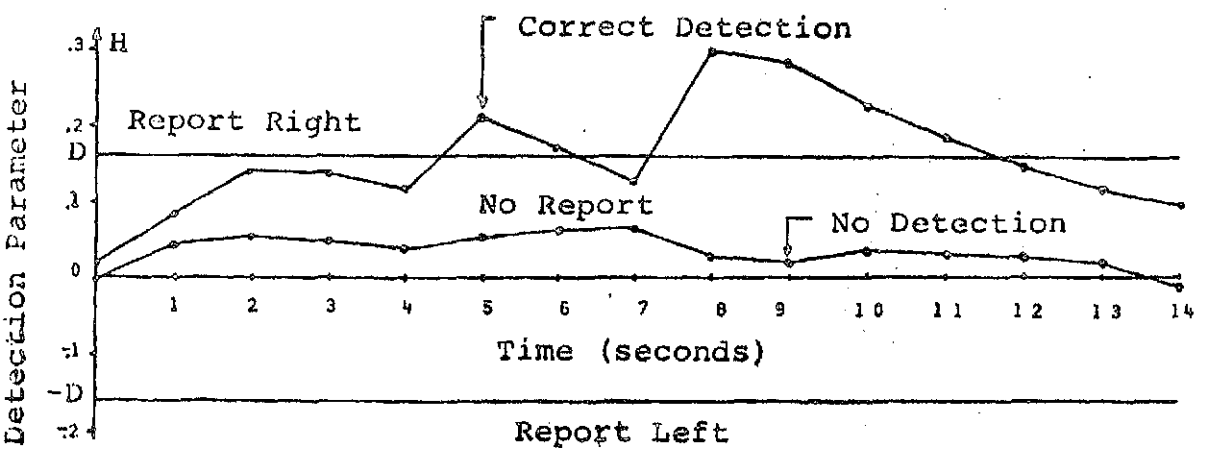

Figure 5.12 Combination Step Simulations

of H(t) for each of the three stimuli. In each case one correct response and either a false response or no response trial is shown.

Figures 5.13, 5.14 and 5.15 summarize the model's predictions for response latencies at threshold (no reaction delays are included in these figures). Short latencies for velocity steps, relatively long latencies for acceleration steps and intermediate latencies for combination stimuli are typical of the results. It is clear from the model that in all cases average latencies will decrease as stimulus magnitudes increase.

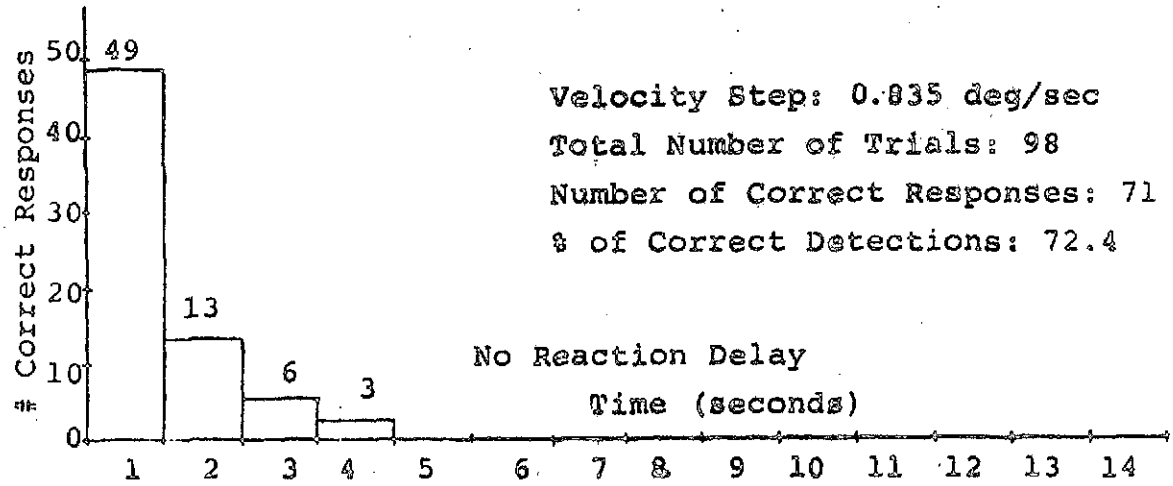

Figure 5.13 Latency Histogram for Threshold Velocity Step

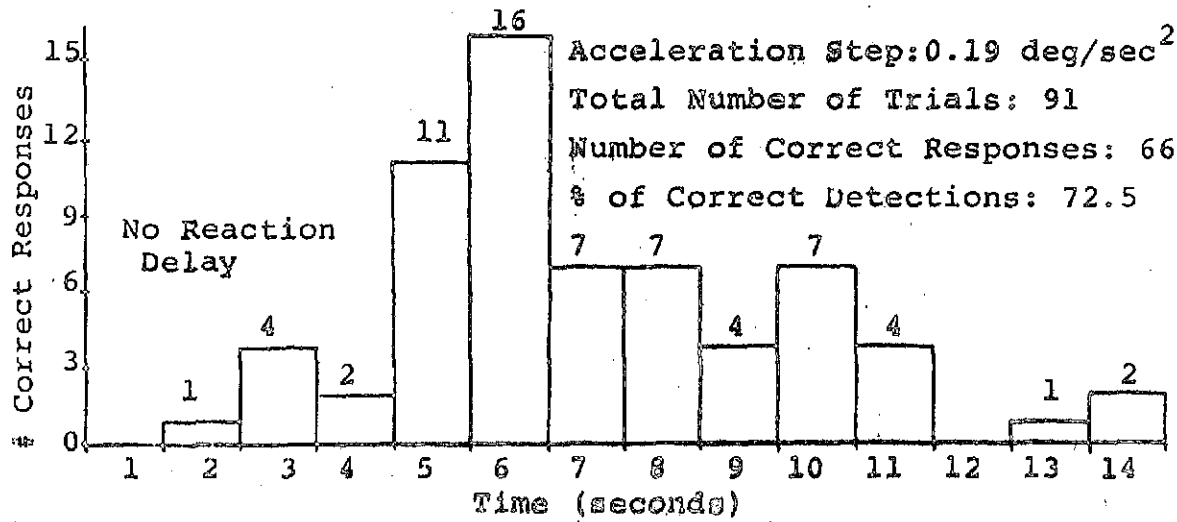

Figure 5.14 Latency Histogram for Threshold Acceleration Step

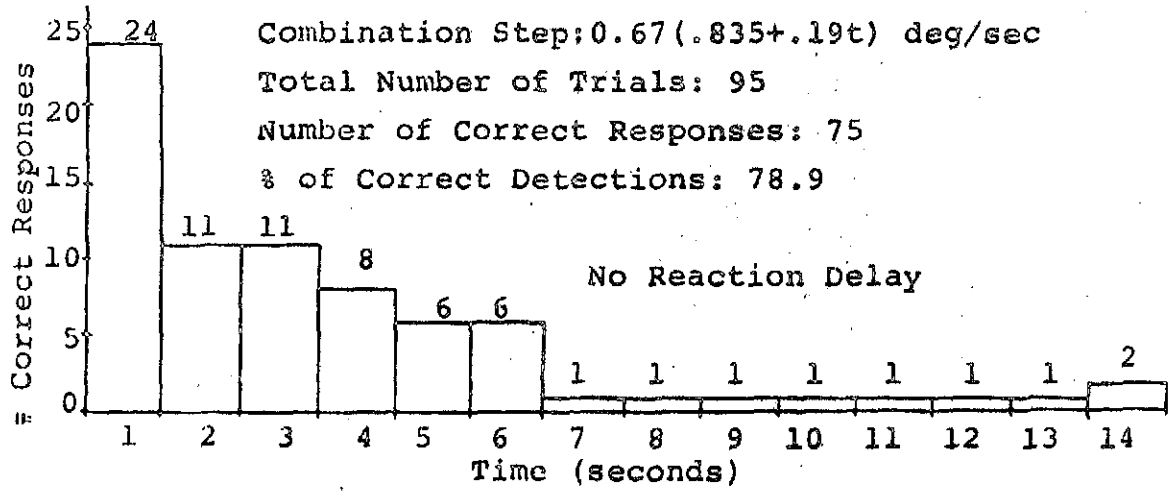

Figure 5.15 Latency Histogram for Threshold Combination Step

CHAPTER VI

STOCHASTIC MODEL FOR DETECTION OF NEAR THRESHOLD CHANGES IN SPECIFIC FORCE

The model for threshold detection of rotational stimuli was found to consist of three distinct components. The first is a linear model of the afferent response of the semicircular canals. The purpose of the second component, referred to as the first order processor, is to eliminate the spontaneous firing rate and any associated low amplitude, low frequency variations from the afferent signal. The third and final section models the detection and decision processes which utilize the signal available at the output of the first order processor. Detection of changes in specific force can be modelled using the same fundamental approach except that the relevant sensory signals are now those associated with the otolith organs.

A linear model relating changes in specific force to changes in the afferent firing rates from the utricular and saccular organs was developed in section 3.2 and will be employed here without modification. The requirement for a first order processor, similar to that found necessary for the processing of semicircular canal information, will be discussed in 6.1. While a suboptimal detector employing the appropriate Kalman filter could be developed for the otoliths in a manner similar to that done for the semicircular canals (Section 5.2) it was decided that the benefits of this approach were far

outweighed by the associated computational complexity. Instead, a successful attempt was made to implement a detector similar to the "simplified detector" developed in Section 5.3. The specifications of this detector are outlined in Section 6.2 and Section 6.3 summarizes the resulting model predictions.

6.1 Necessity for First Order Processing

The problem of detecting linear acceleration requires the higher centers to distinguish changes in the firing rate of first order otolith afferents. If, in the absence of acceleration or tilt, the discharge level was truly constant and if this level was precisely known by the higher centers than it could simply be subtracted and the resultant signal processed. On the other hand, if the spontaneous discharge level is not stable, but instead varies slowly within some known bounded region then some mechanism must be postulated to distinguish between small changes in the afferent firing caused by stimulation of the otolith organs and those caused by normal variations in the spontaneous discharge level. There are several approaches which the system could take to solve this problem. One approach would be to ignore the fact that some low frequency low amplitude changes in the afferent firing rate are not stimulus related and merely subtract the average spontaneous discharge rate from the afferent firing rate and therefore process the resulting signal as if it arose from a true input stimulus (see Figure 6.1). The problem with this approach is that one would continually be alerted to accelerations and tilts which did not actually take place. Such a high false alarm rate is unacceptable and as in the case of "the boy who cried wolf" some mechanism will arise to insure that such continual false alarms will be ignored. If these

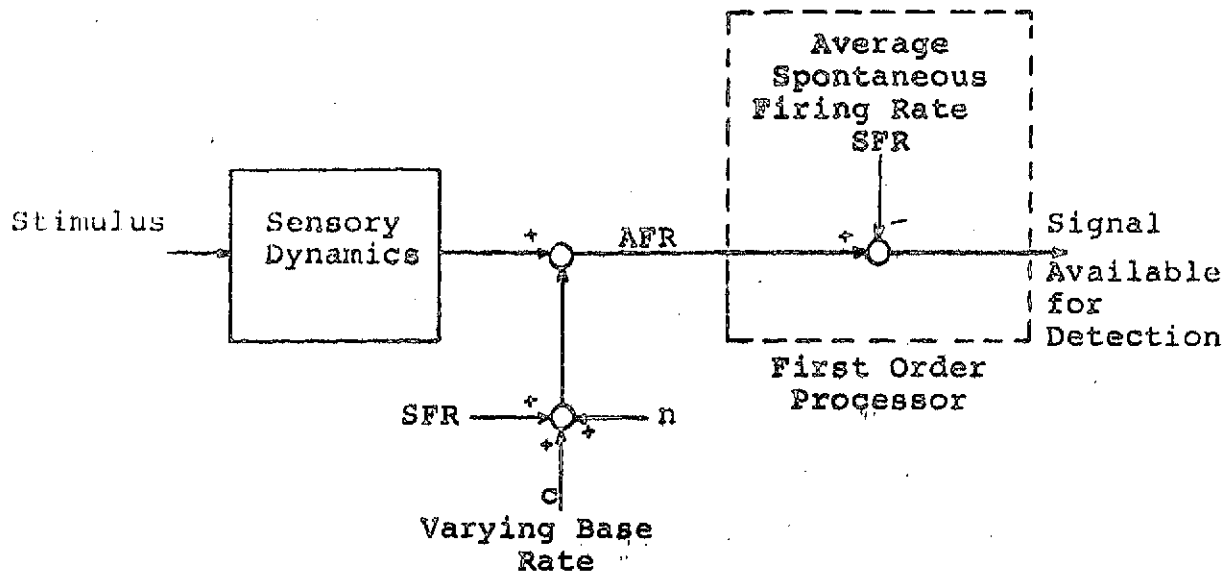

Figure 6.1 Simple First Order Processor

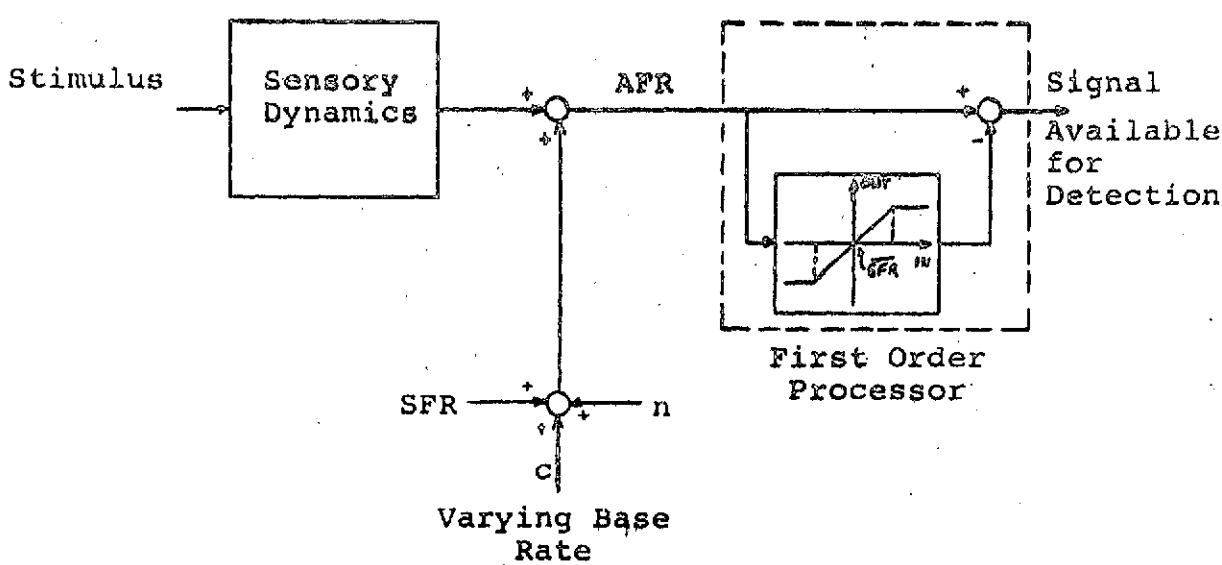

Figure 6.2 Alternate First Order Processor

low frequency variations occur, say 99% of the time within some bounded region of the average spontaneous firing rate then a second approach (see Figure 6.2) would be to ignore completely any change in the firing rate which takes place within this bounded region. This approach would solve the problem of a high false alarm rate since the signal available to the detector would only rarely differ from zero when there was no corresponding stimulus present. The problem with this approach is that too much information is thrown away unnecessarily. While it is true that small changes in the afferent firing rate which have the same spectral composition as those arising at c (Figure 6.2) but which are due to true stimulus inputs cannot be distinguished from those arising at ^{c}, it is not true that signals with a different spectral composition could not be distinguished. The simplest model for a spectral decomposition limited to variations in the firing rate near the known average rate of spontaneous discharge is shown in Figure 6.3. The model shown in Figure 6.3 is actually a compromise between the model shown in Figure 6.1 and that shown in Figure 6.2. In the first model, the presumption is that all variations in the firing rate regardless of their frequency content will be assumed to arise from stimulus inputs to the sensory organs. In the second model the presumption is that all variations within a bounded region regardless of their frequency content will be presumed to

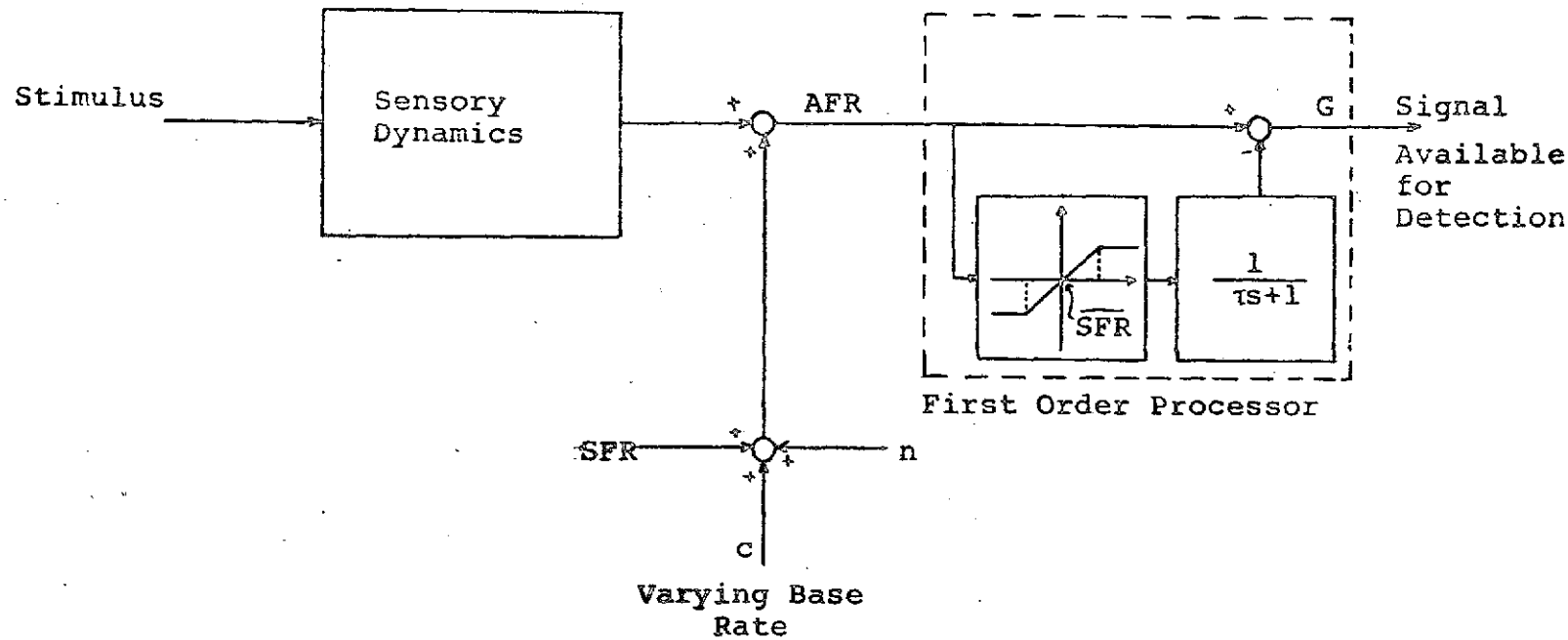

Figure 6.3 First Order Processor Based on Spectral Separation

arise from the process c and must therefore be eliminated. In the third and final model the presumption is made that for small variations in the firing rate the low frequency portion of the signal variations arise from the process c and the high frequency portion of the variations arise from a stimulus which must be detected. To this end the first order processor passes high frequency variations while eliminating low frequency variations.

It is interesting to note that this first order processor, while essentially eliminating the direct effects of any low frequency variations in the spontaneous discharge, preserves the systems ability to detect the most important class of stimulus disturbances; specifically abrupt changes in specific force which will lead most rapidly to a significant change in one's position.

The above analysis of first order processors is equally applicable to the modelling of the perception of near threshold rotational stimuli based upon semicircular canal afferents. For the case of rotational stimuli the first order processor was postulated to account for the unexpected ratio of the velocity step threshold to the acceleration step threshold (Section 5.1). No such experimental discrepancy exists for the otolith organ. The only significant implication of the first order processor for threshold detection of steps in specific force would be a slight shortening of the predicted latencies. Figure 6.4 shows the signal available for detection in the case of a

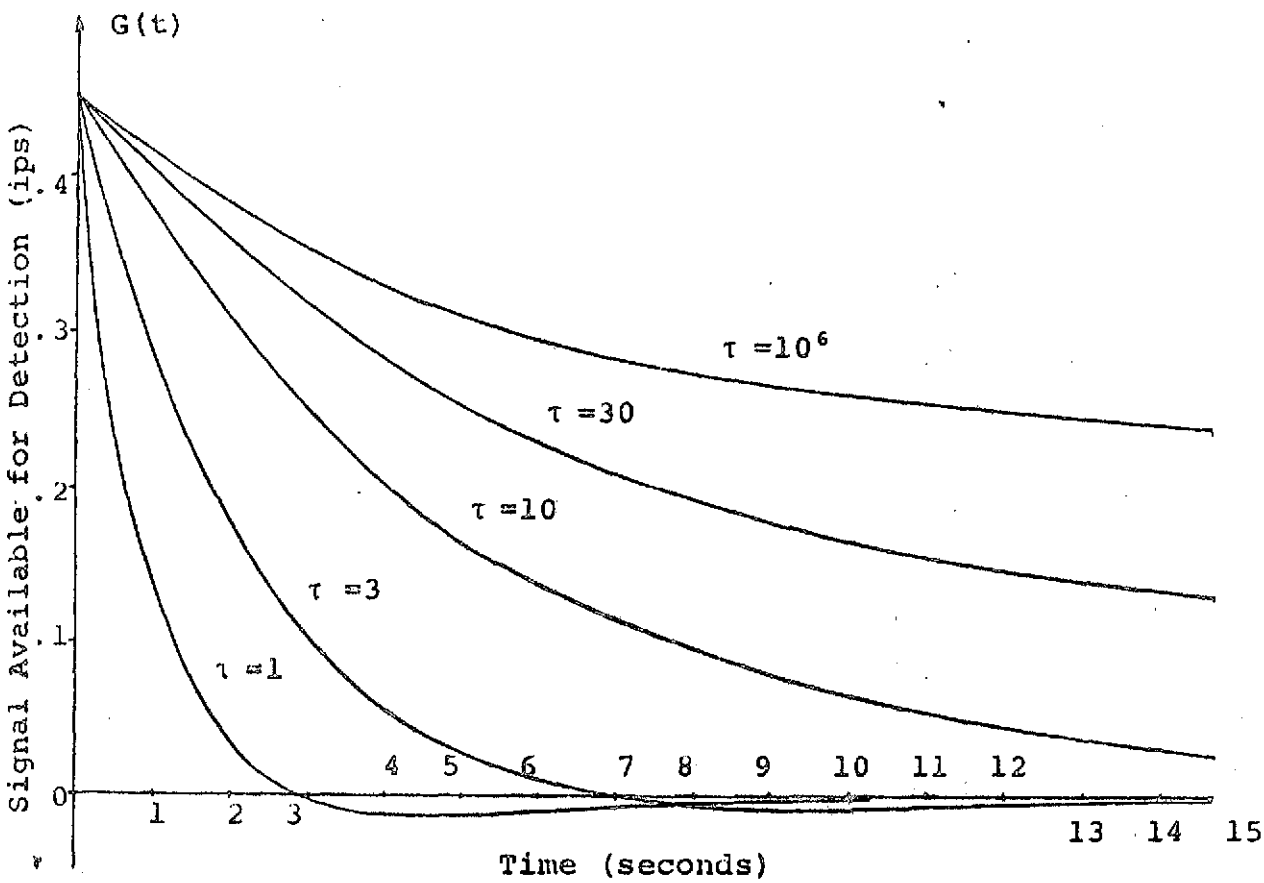

Figure 6.4 Signal Available for Detection for Various Values of τ

threshold step in specific force (.005 g) for various values of the filter time constant, τ. Figure 6.5 shows the result of passing each of these signals though the detector used for the semicircular canals (Figure 5.8, N=1) and normalizing their peak responses. Since the average detection latency will occur about the time that H(t) peaks it can be concluded that as τ decreases the average predicted latency will tend to decrease. It is difficult to choose a value for τ based on these curves since they are only approximate indicators of predicted latencies and since the predicted latencies do not change radically with changes in τ. In fact, given a small leeway in choosing the statistical distribution of the response delay T, any of the values for τ shown would be in reasonable agreement with the experimentally determined latencies (Ref.[51]). If the mean response delay were presumed to be between one and two seconds for near threshold stimuli then any value of τ greater than or equal to three seconds would be reasonable. In section 6.3 the model predictions will be given for τ=3 seconds and τ=30 seconds to show the effect of τ on the predicted latencies.

Specifications for the low frequency variations in the spontaneous firing rate can be determined in the same way as was done for the semicircular canals in Section 5.1. The equations which must be satisfied by N, c_1 and c_2 (see Figure 6.3 and Section 5.1) are:

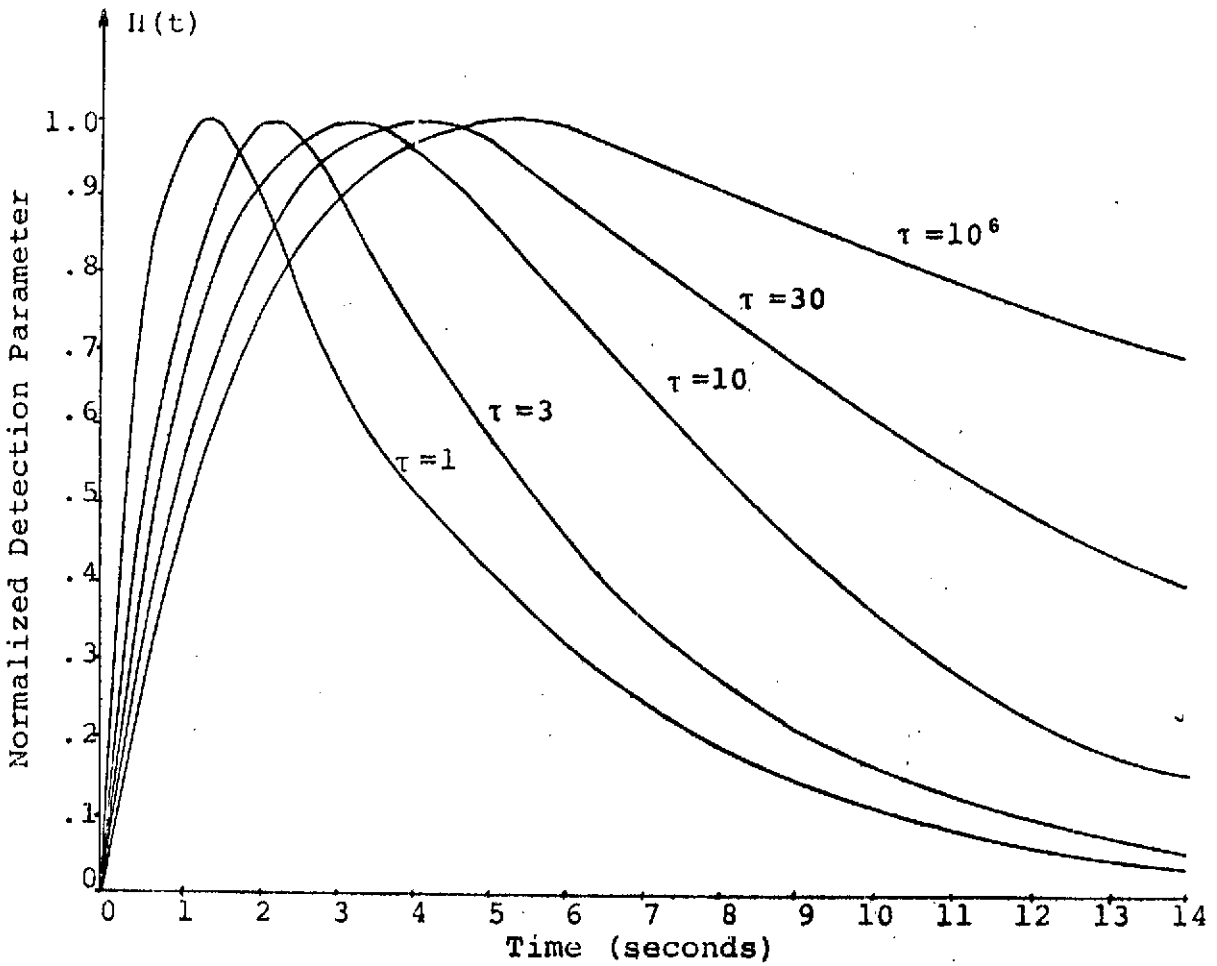

Figure 6.5 Normalized Detection Parameter for Various Values of τ

$$\frac{\left(\frac{c_1}{N}\right)^2}{\left[1 + \left(\frac{c_1}{N}\right)^2\right] + \left[1 + \left(\frac{c_1}{N}\right)^2\right]^{1/2}} = .95 \qquad (6.1)$$

or

$$\frac{c_1}{N} \approx 20 \qquad (6.2)$$

and

$$\frac{1}{c_2}\left[1 + \left(\frac{c_1}{N}\right)^2\right]^{1/2} = 1/\tau \qquad (6.3)$$

N was determined in Section 3.2 to be

$$N = .147 \qquad (6.4)$$

Thus from Equation 6.2

$$c_1 = 2.94 \qquad (6.5)$$

and from Equation 6.3

$$c_2 \approx 20\tau \qquad (6.6)$$

The only parameter which remains unspecified in Figure 6.3 is the region over which the first order processor operates linearly. The linear region for the saturation nonlinearity shown in Figure 6.3 is bounded by SFR±4σ where σ is the effective standard deviation of the nonstimulus related signal variations. σ is given by

$$\sigma = \left[N^2 + \frac{c_1^2}{2c_2}\right]^{1/2} \qquad (6.7)$$

6.2 Simplified Detector Model

The simplified detector which was used to model the detection of near threshold rotational stimuli (see Figure 5.8) is also capable of predicting threshold performance for detection of steps in lateral acceleration. Since the minimum computational effort is required when only one channel is simulated, N is set equal to 1. The motivation for the structure of this detector is outlined in detail in Section 5.3 and is not repeated here.

The response delay e^{-Ts}, which represents the sum total of all delays which are not related to the time history of the signal available for processing, is not modelled in detail here except to remark that T should be viewed as a positive random variable whose minimum value should be set equal to three or four hundred milliseconds (which represents the time normally associated with suprathreshold reaction times) and whose mean value should be set to one or two seconds. The value of D, which represents the minimum deviation of the decision parameter H(t) which will provoke a response, should not differ significantly from the value found for the semicircular canals. The exact value of D can be chosen in two ways. Either:

1. D can be adjusted to yield a threshold prediction which is the same as the experimentally determined value and then D compared to the value found for the

semicircular canals to check if it is reasonable.

or 2. D can be set to the value found for the semicircular canals, the model's theshold prediction determined and then this threshold prediction compared to the experimentally determined thresholds.

For the case τ=3 seconds, which is the same time constant used in the first order processor for the semicircular canals, there is no need to apply both procedures since for D = 0.16 (the value used for the semicircular canals) the resulting threshold (75% correct detection) is .005 g for the utricles and .010 g for the saccule. These values are in complete agreement with those of Meiry (Ref. 51). For τ=30 seconds, a value of D = .32 is necessary if the above threshold values are desired. This is only a factor of two greater than that used for the semicircular canals. If D is set equal to .16 then for τ =30 seconds the predicted utricular threshold would be approximately .0035 g and the predicted saccular threshold would be .007 g.

6.3 Summary of Model Predictions for Detection Probabilities and Latencies

Acceleration steps of five different magnitudes were tested to determine the model's predictions for the probability of detection during simulated fourteen second trials. If "TH" is used to designate an acceleration step of .005 g then the utricular model was tested with steps of magnitude TH/σ^2, TH/σ, TH, $TH\sigma$ and $TH\sigma^2$ where $\sigma = 10^{.1}$. Figure 6.6 summarizes the results of these Monte Carlo simulations. For the simulations in which τ=3 seconds the decision level D was set to .16 and for τ=30 seconds D was set to .32. The predictions are essentially equivalent with 75% performance occurring for a stimulus magnitude of .005 g. Each data point shown in Figure 6.6 is the result of 210 simulated trials. Using the same value for D in the saccular model will result in essentially the same curves shown in Figure 6.6 except that TH would have to be set equal to .010 g since the sensitivity of the saccular organ is only half that of the utricular organ (see Section 3.2). Thus the threshold prediction for the sacculos would be .010 g.

Figure 6.7 shows the time history of the detection parameter H(t) for a correct response trial and an incorrect response trial for the model with τ=3 seconds. Figure 6.8 shows the same simulations of the model for τ=30 seconds. In both figures the stimulus magntiude is .005 g.

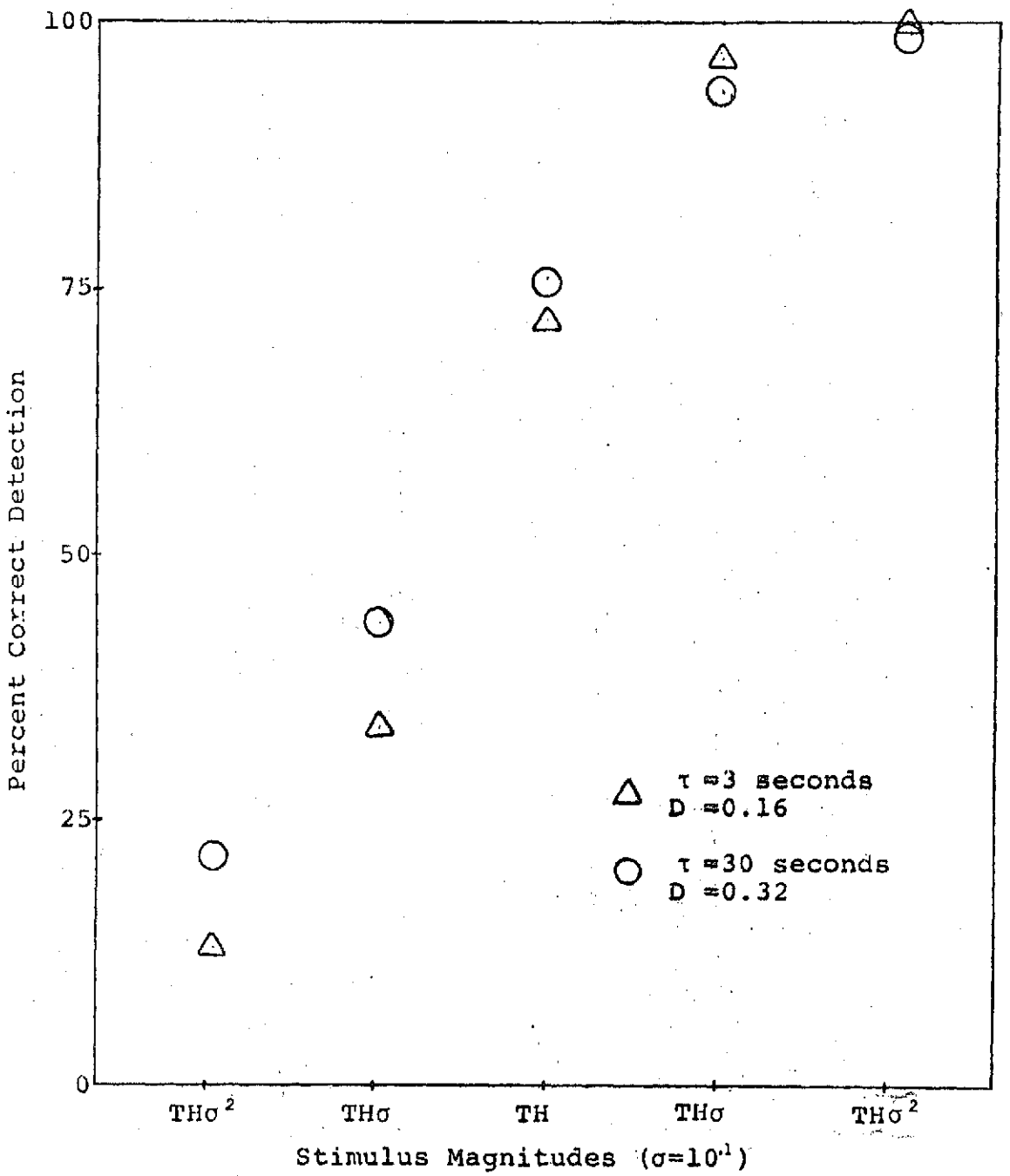

Figure 6.6 Model Predictions of Performance Variations as a Function of Stimulus Magnitudes

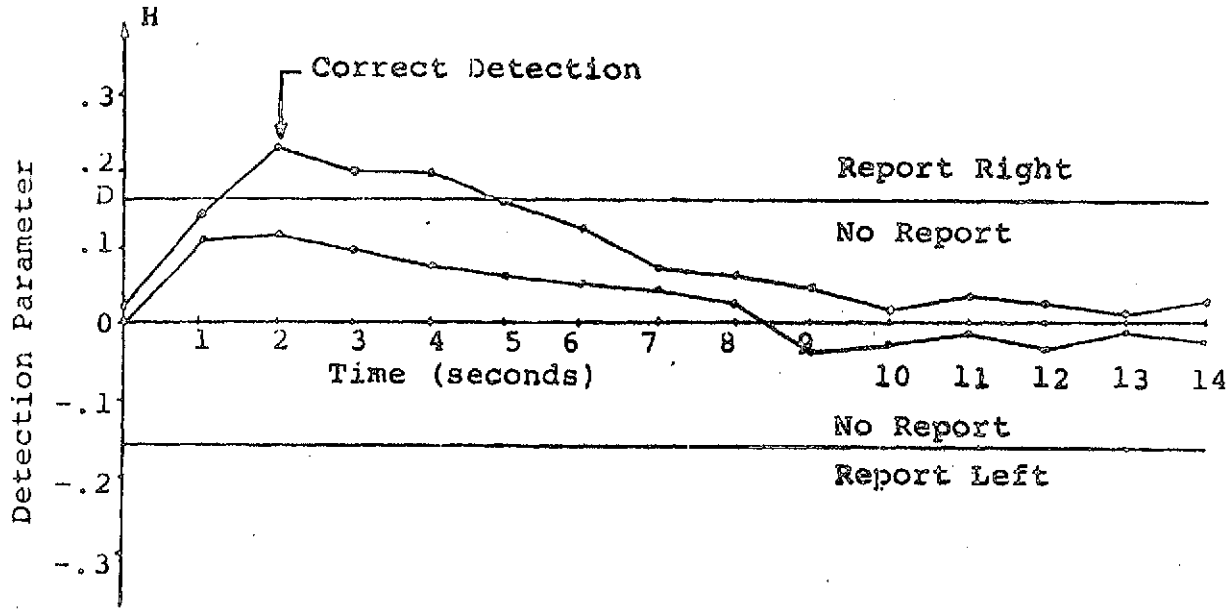

Figure 6.7 Threshold Acceleration Step Simulations
(τ =3 seconds)

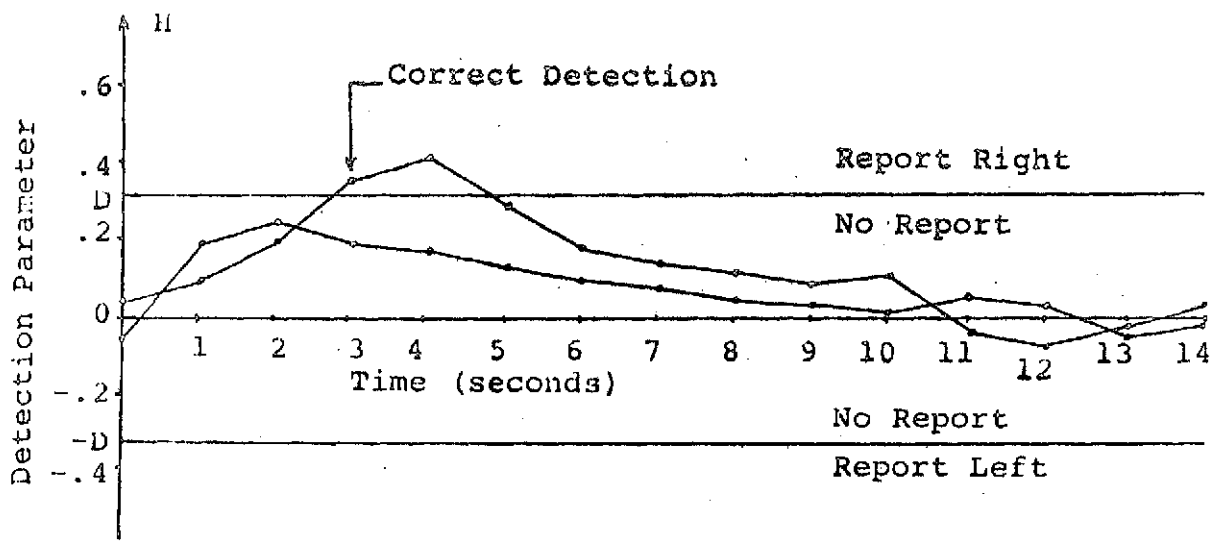

Figure 6.8 Threshold Acceleration Step Simulations
(τ =30 seconds)

Figures 6.9 (τ=3 seconds) and 6.10 (τ=30 seconds) summarize the predicted distributions of the response latencies due to the time history of the signals available for detection. These distributions do not include the response delays modelled by e^{-Ts}. Inspection of Figures 6.9 and 6.10 reveal that for a tenfold increase in τ the predicted increase in the average response latency would only be approximately one second. Since this difference in latency can just as easily be incorporated in the term e^{-Ts} the value chosen for τ is not very critical.

One of the most interesting implications of these results is that the detection processes which make use of the signals available at the afferent level for the semicircular canals and the otoliths can be modelled as if they were identical. In both cases the afferent signals were corrupted with white measurement noise and low frequency variations in the spontaneous discharge. In both cases a Weiner filter was used to estimate these low frequency variations which were then subtracted from the afferent firing level to produce a signal which presumed to consist of a white measurement noise process and possibly a signal related to a stimulus acting on the sensor. Finally, identical detectors with the same detection parameters and the same criteria for issuing a report were used to predict near threshold detection performance consistent with experimental data.

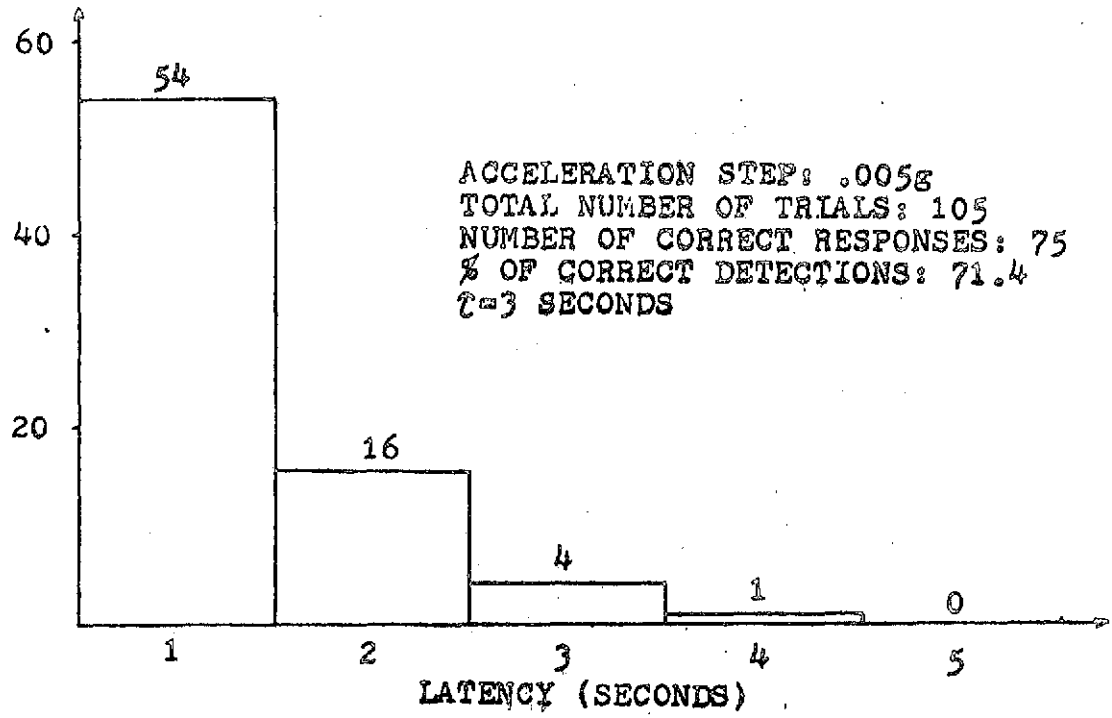

Figure 6.9 Latency Histogram for Threshold Step in Acceleration (τ=3 seconds)

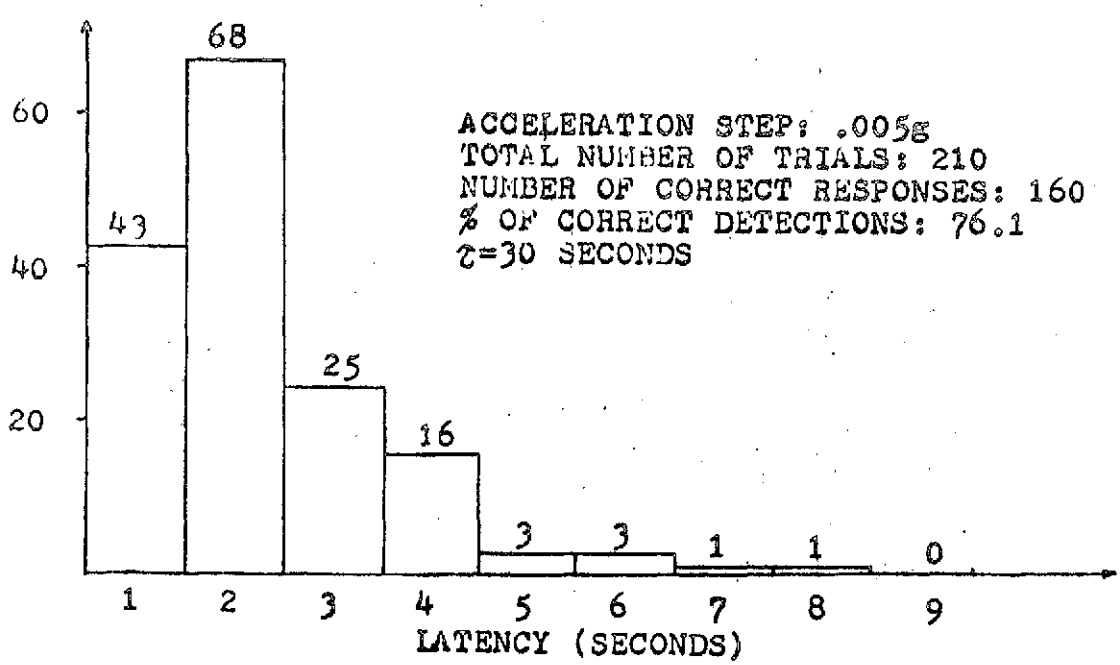

Figure 6.10 Latency Histogram for Threshold Step in Acceleration (τ=30 seconds)

CHAPTER VII

PERCEPTION OF STATIC ORIENTATION IN A CONSTANT SPECIFIC FORCE ENVIRONMENT

In previous chapters the perception of rotation or acceleration was always presumed to originate from the simple stimulation of a synergistic pair of sensors (e.g. the right posterior canal and the left superior canal) and no consideration was given to the problem of integrating the sensations arising from more than one synergistic pair (e.g. the horizontal canals and the right posterior and left superior canals). For the case of the semicircular canal system the simplest solution to this problem would be to postulate that since the planes of the three canals are roughly orthogonal that the sensations which arise from each synergistic pair can be considered the components of a vector which represents the net sensation of rotation. While it is true that the sensitive axes of the canals do not coincide with the conventional roll, pitch and yaw axes to which we tend to relate any sense of rotation, the sensation of rotation relative to the conventional body axes can be derived using a simple transformation of coordinates.

A similar approach to the problem of integrating the sensations from the utricles and the saccules would yield a model which was in agreement with the gross nature of the

steady state perception of tilt. If the sensitive axes of the otolith organs formed a mutually orthogonal set and the steady state sensitivities of these organs and their orientations with respect to the head were accurately assessed, then an unbiased estimate of the head's steady state orientation with respect to a constant specific force environment could be made. (Specific force or gravito-inertial reaction force is defined as the difference between the gravitational force vector and the vector representing the translational acceleration with respect to inertial space.) Unfortunately experimental data suggests that the perception of tilt is biased and that this bias is a function of the intensity of the specific force field (1g,2g, etc.) and the orientation of the head relative to the local direction of specific force.

The purpose of this chapter is to discuss the nature of these biases and to suggest a simple model for the integration of otolith information which will yield predictions consistent with the available experimental data.

7.1. Perceptual Illusions of Static Orientation

The first systematic investigation of man's perception of the vertical was carried out by Mach [45, 46, 47] beginning in 1873. In Mach's experiment the subject was rotated in a centrifuge at a constant rate while facing in the direction of rotation. The net specific force was such that the subject invariably felt tilted away from the center of rotation. When a plumb bob was suspended inside the centrifuge Mach reported that his sensation of the vertical was generally aligned with the direction indicated by the plumb bob (i.e. aligned with the local direction of specific force).

In more recent years numerous psychophysical experiments have been conducted, e.g.,[11, 12, 29, 30, 52, 56, 57, 63, 64, 72, 74, 75] in which subjects were tilted with respect to the local direction of specific force and then requested to indicate their perceived vertical or horizontal. In addition Cohen [17] and Schöne [63] investigated the effect of specific force magnitude and pitch orientation on the perceived angle of pitch.

The mechanism used to generate sustained tilt angles and the apparatus employed to permit the subject to indicate his orientation are crucial to the interpretation of the experimental results. For experimental results to be useful in modelling

the static sensation of orientation as a function only of the output of the otolith organs several key criteria must be met.

1. There must be no visual information available to the subject which in any way affects his perception of orientation. The ideal way to meet this condition would be to have the subject's eyes closed but unfortunately this eliminates the most reliable methods for the subject to indicate his orientation. Therefore the experimenter must strive to design an indicator which has the least influence on the subject's perception of orientation. One common solution to this problem, while probably not optimal, is to display a luminous line which the subject can manually rotate by means of a knob to indicate his perceived vertical in an otherwise darkened enclosure.
2. Data concerning the subject's perception of orientation must be collected after the experimental conditions have stabilized and have remained constant for a period sufficient to abolish all response from the semicircular canals. While one minute or more would be preferred a period of no less than thirty seconds should be adequate. There have been experiments reported in which a subject seated in a

centrifuge is slowly accelerated while instructed to continuously report his perceived orientation. While the results of three experiments are useful indicators of the phenomenon we are investigating, they should be analyzed carefully with regards to the possible contaminating effects of both canal involvement and the dynamic portion of the otolith response; especially at times just following abrupt changes in acceleration.

3. Since the effect of proprioceptive information on perceived orientation is not the object of study here, it is important that this source of information be eliminated insofar as possible through suitable head and body supports.

and

4. Instructions to the subject must clearly indicate that his task is to indicate the orientation of the earth vertical and not his perception of the direction of net force.

With these criteria met and a clear record of both the specific force magnitude and the orientation of the head with respect to the local direction of specific force a reasonably consistent set of experimental data emerges.

In a certain class of experiments in which a subject is

tilted laterally with respect to the local direction of specific force the subject perceives that his tilt angle is less than the objectively measured angle. This effect is named the Aubert effect (or A effect [3]). The Aubert effect manifests itself in several ways. If for example a subject is tilted to the right in a 1 g environment while viewing a stationary vertical line he will sense that the line has rotated counterclockwise and is now tilted to the left. Alternately if the subject is able to control the orientation of this line he will tend to rotate it in the same direction as his own tilt in order to have it appear vertical to him. In a separate class of experiments a subject will experience a sensation opposite to the one described above. An objectively vertical line will appear to tilt in the same direction as the subject's tilt and he will thus perceive his tilt to be greater than his actual tilt. This effect is known as the Müller effect (or E effect) and was first described by Müller in 1916 [53]. Although the E effect is normally associated with either a transient sensation or with experiments in which the magnitude of the specific force vector is greater than unity, some investigators [75] have reported a mild E effect for small roll angles in a 1 g environment. While the terms "Aubert effect" and "Müller effect" may be useful in discussing the outcomes

of certain experiments they do not by themselves serve to clarify the mechanism which underlies the general phenomenon associated with the perception of orientation.

For reasons which will soon become clear all of the experiments with which we are concerned will be divided into three basic categories. Figure 7.1 illustrates the three categories. Consider a coordinate system whose y axis is aligned with the head's pitch axis (pitch forward is positive), whose z axis is perpendicular to the average plane of the utricular macula (i.e., approximately θ = 25-30 degrees pitched back relative to the vertical when the head is in a normal erect position [19]) and whose x axis is defined by a right handed cross product

$$\underline{i}_x = \underline{i}_y \times \underline{i}_z \tag{7.1}$$

If the steady state specific force vector for a given experimental trial is referred to these axes as follows

$$\underline{SF} = SF_x\underline{i}_x + SF_y\underline{i}_y + SF_z\underline{i}_z \tag{7.2}$$

Where SF_x, SF_y and SF_z are expressed in g's we can categorize that experimental trial according to the following rules:

If $SF_z > -\cos(\theta)$ then designate as category A
If $SF_z = -\cos(\theta)$ then designate as category N (7.3)
If $SF_z < -\cos(\theta)$ then designate as category E.

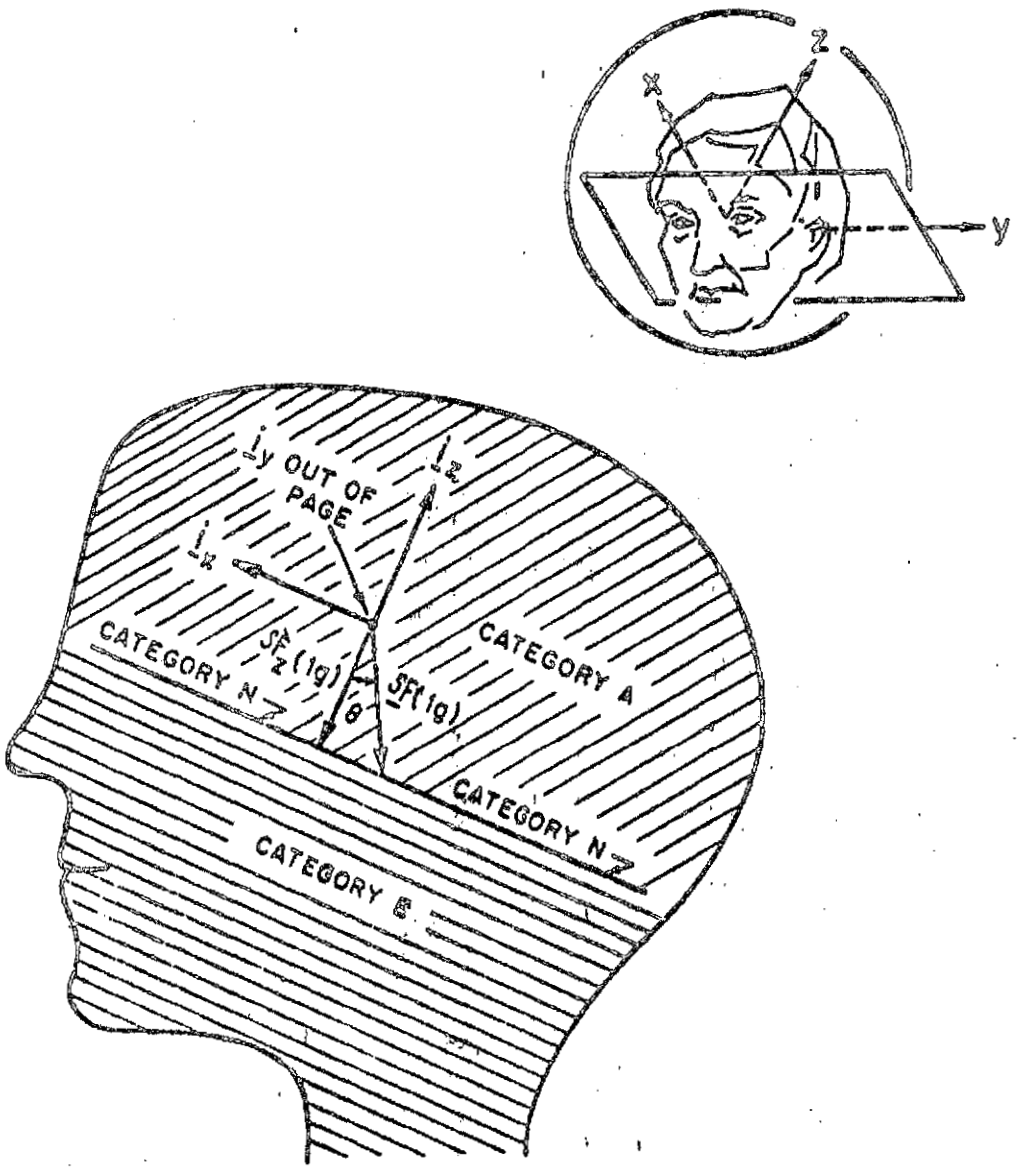

Figure 7.1 Illustration of Specific Force Stimulus Categorization

This categorization will be better understood if it is noted that for an experiment with the head erect in 1 g the stimulus is of type N. Adding any accelerations in the xy plane of the coordinate system just described will not alter the stimulus type. The crucial test is whether or not the component of specific force in the z direction is more negative (type E) or less negative (type A) than in the case in which the head is erect in 1 g.

In reviewing the results of several experiments, each trial will be assigned to the appropriate category and the direction of the mean bias in perceived orientation relative to the net specific force noted. As a preliminary example, the experiments by Mach described at the beginning of this section are of type N since the subject's head was erect in 1 g and an additional component of specific force was added in the negative y direction. Since this change in specific force did not alter the z component of specific force the category remains the same as "head erect 1 g"--namely category N. Mach's experimental result was that the vertical was aligned with the net specific force without any net bias.

More recent centrifuge experiments have confirmed Mach's results. Noble [57] in the same manner as Mach, was able to test subjects' perception of the vertical for specific force vectors making an angle of from 6 to 40 degrees with respect to the vertical. Noble concluded: "The empirical

function corroborates Mach's original hypothesis; vis., that Ss adjust V_v in accordance with the resultant of centrifugal and gravitational forces." We will find that this hypothesis is not generally true except for type N stimuli.

Clark and Graybiel [11] conducted an experiment similar to that of Noble's except that the centrifuge was slowly accelerated up to its maximum rate of rotation while the subject continuously tracked his perceived vertical. If the small tangential acceleration and the dynamic effects of the slowly changing stimulus is ignored then this experiment can also be classified as type N. Clark and Graybiel described their data as follows: "The data also show that when radial acceleration is increased slowly, as in this experiment, the subject adjusts to the resultant force accurately, with a slight tendency for the perception to lag behind the stimulus and a tendency to set the line at a position slightly greater than Ø. Insofar as the accuracy of the settings is concerned the data support the results of...Noble." Other category N experiments were conducted by Clark and Graybiel [12, 30] with similar results. Thus, for these type N experiments, the general conclusion can be drawn that the perceived vertical is aligned approximately with the specific force vector.

Schöne [63] conducted a thorough set of experiments using a centrifuge to change the magnitude of the specific force vector, SF. His experiments differed from those described

above in that he did not put his subjects in an erect position relative to the earth vertical but varied their orientation systematically with respect to SF. In doing so he conducted some trials in each of the three categories. Figure 7.2 summarizes Schöne's data for the case in which the subject's roll angle (lateral tilt) is varied in a 1 g and in a 2 g environment. The experiments in 1 g are all category A experiments (except for the case with zero roll angle which is category N). For the experiments in 2 g the z component of specific force is given by

$$SF_z = -2\cos(\phi)\cos(\theta) \tag{7.4}$$

where ϕ = roll angle of head with respect to SF

and θ = tilt angle of the utricular macule with respect to the sagital plane (approximately 25-30 degrees, see Figure 7.1).

Therefore the experiment is of category E if $\cos(\phi) > .5$ ($\phi < 60°$), category N if $\cos(\phi) = .5$ ($\phi = 60°$) and category A if $\cos(\phi) < .5$ ($\phi > 60°$). Referring again to Figure 7.2 it is clear that all category A experiments exhibit the Aubert effect, all category N experiments exhibit essentially no bias, and all category E experiments exhibit the Müller effect. Schöne repeated the tests in one g under water to test for the possible influence of the tactile sense on perception of orientation. The results of these tests are in general

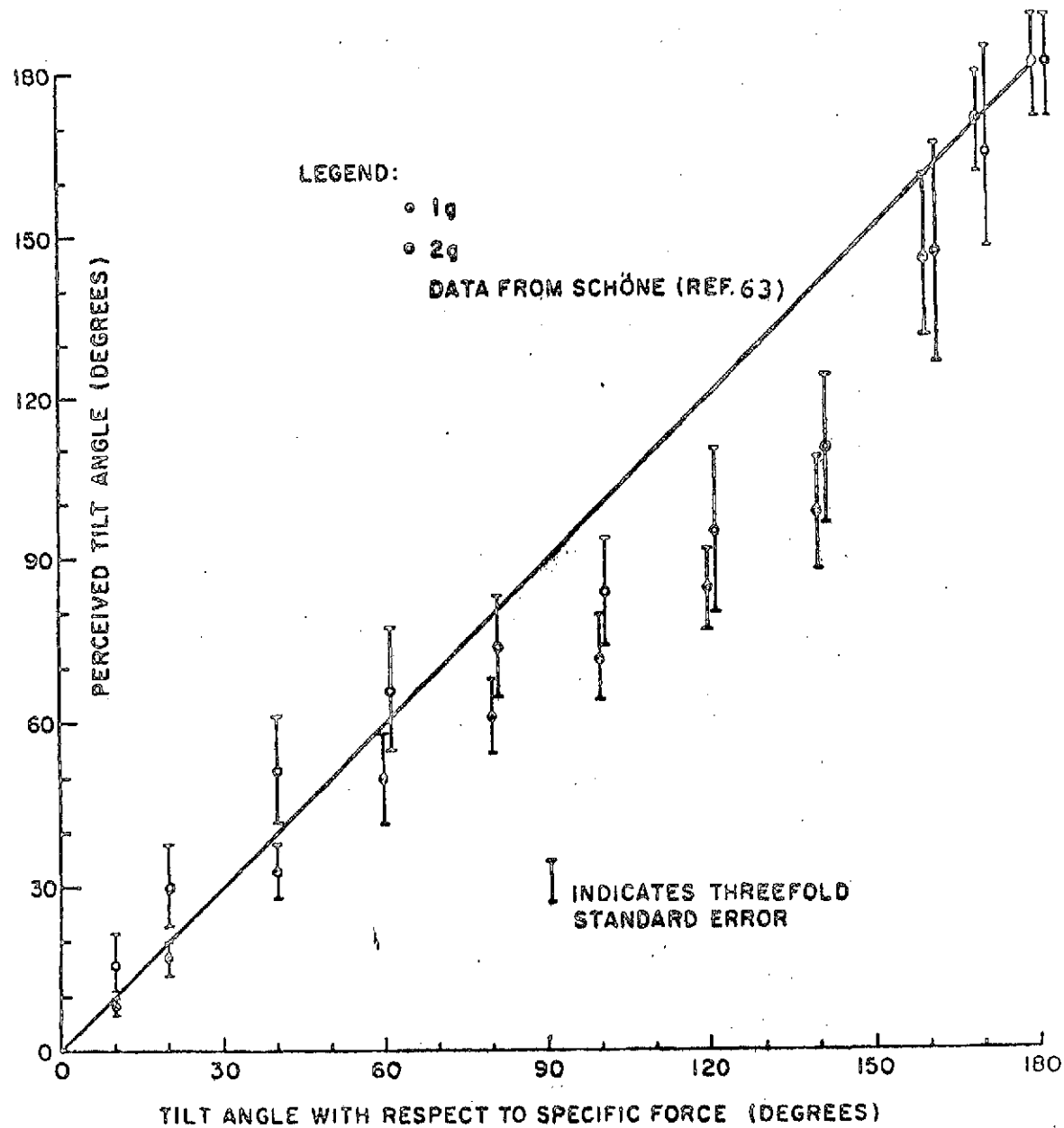

Figure 7.2 Perceived Tilt Angle as a Function of Actual Tilt Angle for 1G and 2G Specific Force Environments

agreement with the 1 g curve in Figure 7.2 with the only difference being a slightly greater Aubert effect for Ø greater than 90°.

Finally Schöne varied the pitch orientation (α) of the subject relative to the local direction of SF for different specific force magnitudes. Subjects were instructed to adjust the vertical position of a luminous spot until it was "on the horizon" or "until he sees it at eye level." Figure 7.3 summarizes the data from these experiments (constant errors have been eliminated by defining the perceived pitch angle when the head is erect in 1 g as zero).

To categorize these experimental trials it is necessary to calculate the z component of specific force.

$$SF_z(\alpha, G) = -G\cos(\theta-\alpha) \qquad (7.5)$$

where θ = 25-30 degrees

α = angle subject is pitched down (Figure 7.3)

and G = magnitude of the specific force vector (g)

All experimentally determined data points shown in Figure 7.3 ($G \geq 1$) have associated values of G and α which satisfy

$$SF_z(\alpha, G) < -\cos(\theta) \qquad (7.6)$$

and therefore the experiments which gave rise to them must be characterized as type E. To interpret these experimental

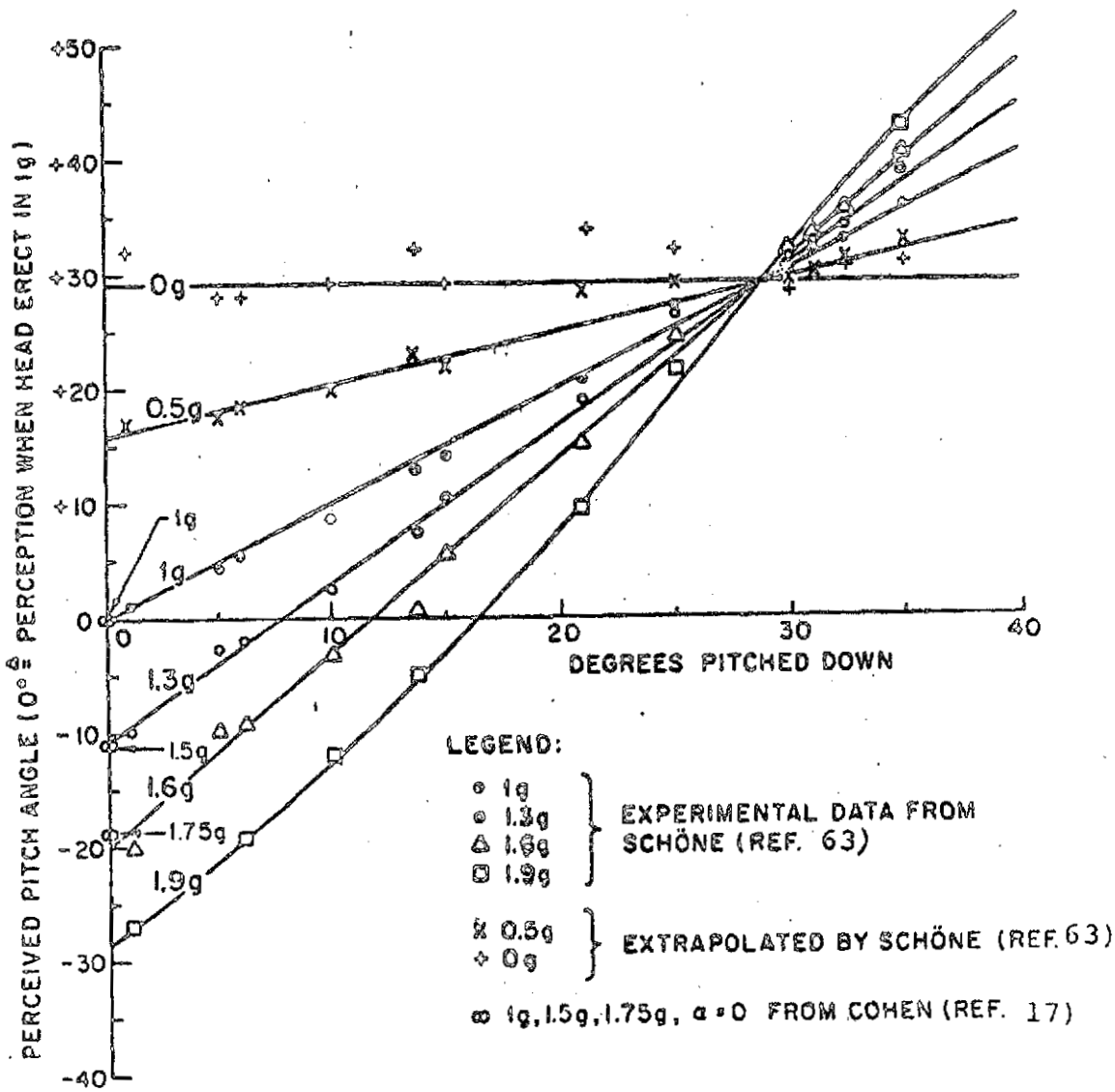

Figure 7.3 Perceived Pitch Angle as a Function of True Pitch Angle and Magnitude of Specific Force

results it is convenient to refer to the subject's perceived direction of "down," which can be derived from his indications of the horizon, and to compare this with the direction of the specific force vector. All data points confirm to the following rule: the true direction of SF is always between the perceived direction of "down" and the negative z axis ($-\underline{i}_z$). This is equivalent to a Müller effect in pitch with respect to $-\underline{i}_z$. In other words the deviation of the perceived down from $-\underline{i}_z$ will always be in the same direction but of greater magnitude than the actual deviation of the specific force from $-\underline{i}_z$ for a type E experiment. This effect is almost nonexistent for the 1 g curve but becomes progressively greater as the inequality given in 7.6 is strengthened. The fact that all the curves cross at $\alpha \approx \theta$ is to be expected since at this point $-\underline{i}_z$, SF and the perceived direction of "down" will all coincide. Finally the data points for 1.9g, 1.6g, 1.3g and 1g can be extrapolated at each value of Ø to yield a prediction for the perception of down at .5g and 0 g. In these cases

$$SF_z(\alpha, G) > -\cos(\theta) \qquad (7.7)$$

and thus the corresponding experiments would be of type A. This extrapolated data conforms to a rule just opposite to that previously stated. The rule governing this data would be: the perceived direction of "down" is always between $-\underline{i}_z$ and SF.

This is equivalent to an Aubert effect in pitch with respect to $-\underline{i}_z$. Data from Cohen [17] for which the head was erect in 1.0g, 1.25g, 1.5g, and 1.75g is also shown in Figure 7.5. Cohen's data supports the progressive increase in the error in perceived pitch orientation as the magnitude of $\underline{SF}$ increases but does not show as large an illusion of pitch as does the data from Schöne.

For the experimental evidence reviewed to this point we can infer the following correlation between stimulus type and the resulting perception of the vertical:

Category A → underestimation of tilt angle with respect to $-\underline{i}_z$ (Aubert phenomenon)
Category N → perceived vertical coincides with $\underline{SF}$ (7.8)
Category E → overestimation of tilt angle with respect to $-\underline{i}_z$ (Müller-like phenomenon)

Data from Miller and Graybiel [52] along with the experimental data described above will be compared in Section 7.3 to the predictions of a model (based on the above correlation) developed in Section 7.2.

7.2. Model Based on Altered Saccular Information

The simplest mathematical model for the steady state perception of orientation with respect to a specific force field based upon information from the otoliths would be a model consisting of three orthogonal accelerometers whose outputs correctly reflected the components of the true specific force vector. Using this model, the predicted perception of the direction "down" would always coincide with the direction of the steady state specific force vector. The experimental results presented in the previous section demonstrate that, while such a model would adequately predict responses in 1g for cases in which the head is tilted less than 20 degrees from the erect position, this simple model is inadequate for stimuli not meeting these criteria.

Before developing a model which accounts for perceptions of "down" which deviate from the steady state direction of SF it is important to illustrate how the responses of afferent nerves associated with different morphological polarizations can be combined simply to give an estimate of SF. The morphological polarization maps for the utriculus and sacculus of the squirrel monkey were illustrated in Figure 2.6. Fernandez, Goldberg, and Abend [24] demonstrated that the response of a given otolith neuron was a linear function of the component of SF in only one direction. The direction of sensitivity is designated the functional polarization vector F.

Fernandez et al. found that the distribution of the vectors $\underline{F}$ for the neurons they studied agreed closely with the morphological maps shown in Figure 2.6. If the functional polarization vector of the $i^{\underline{th}}$ cell were given by

$$\underline{F}_i = X_i \underline{i}_x + Y_i \underline{i}_y + Z_i \underline{i}_z \qquad (7.9)$$

where $X_i^2 + Y_i^2 + Z_i^2 = 1$

and $\underline{i}_x$, $\underline{i}_y$ and $\underline{i}_z$ are defined as in section 7.1, then the steady state response of this cell to a specific force stimulus $\underline{SF}$ would be given by

$$FR_i = S_i(\underline{SF} \cdot \underline{F}_i) + SFR_i \qquad (7.10)$$

where FR_i is the afferent firing rate of the $i^{\underline{th}}$ cell (ips)

S_i is the sensitivity of the $i^{\underline{th}}$ cell (ips/g)

and SFR_i is the tonic firing rate of the $i^{\underline{th}}$ cell (ips).

The firing rates from a group of such cells {i=1, N} can be combined to yield a signal which is directly related to the component of specific force along each of the three axes $\underline{i}_x$, $\underline{i}_y$, and $\underline{i}_z$. For example, an estimate of the component of specific force along $\underline{i}_z$ would be given by

$$\hat{SF}_z = \frac{\sum_{i=1}^{N} \{(FR_i - SFR_i)(\underline{F}_i \cdot \underline{i}_z)/S_i\}}{\sum_{i=1}^{N} (\underline{F}_i \cdot \underline{i}_z)^2} \qquad (7.11)$$

A simple model for the perception of "down" can then be formulated as follows:

$$\hat{\underline{DOWN}} = \frac{\hat{\underline{SF}}_x \underline{i}_x + \hat{\underline{SF}}_y \underline{i}_y + \hat{\underline{SF}}_z \underline{i}_z}{(\hat{\underline{SF}}_x^2 + \hat{\underline{SF}}_y^2 + \hat{\underline{SF}}_z^2)^{1/2}} \tag{7.12}$$

where $\hat{\underline{DOWN}}$ is a unit vector in the perceived direction of "down"

$\hat{SF}_z$ is calculated from 7.11

and $\hat{SF}_x$ and $\hat{SF}_y$ are calculated from 7.11 with "z" replaced by "x" and "y" respectively.

Since this simple model implies that

$$E[\ \hat{\underline{DOWN}} - \underline{SF}/|\underline{SF}|\ ] = 0.0 \tag{7.13}$$

where $E[\cdot]$ denotes the expectation operator. none of the deviations noted in section 7.1 will be predicted. The question of how to modify 7.12 so that the various phenomenon associated with the perception of tilt can be predicted can now be answered.

To motivate the model which will follow it should be noted that the classification of stimuli developed in section 7.1 does not depend on the components of $\underline{SF}$ along the $\underline{i}_x$ or $\underline{i}_y$ axes. In other words, a change in either SF_x or SF_y

will not alter the category of the stimuli and consequently will not change the type of response (Aubert, Müller or no deviation) predicted. It thus seems reasonable to assume that the parameter which controls the deviations which we endeavor to predict is SF_z and not SF_x or SF_y. Using this assumption we conclude that $\hat{SF}_x$ and $\hat{SF}_y$ should be calculated in accordance with equation 7.11 and they should then be used in equation 7.12 without alteration. $\hat{SF}_z$, on the other hand, must be altered to predict the illusory perceptions found experimentally. While it is relatively easy to motivate the alterations of $\hat{SF}_z$ qualitatively, the agreement of the model's predictions with the experimental data will serve as the major justification for the specific alterations proposed in the model.

Figure 7.4 illustrates stimuli from the three stimulus categories. Since for category N stimuli we want the model to predict that the direction of $\underline{SF}$ will be correctly perceived, we should use the value for $\hat{SF}_z$ calculated from 7.11. If the value substitued for $\hat{SF}_z$ in equation 7.12 is designated $\tilde{SF}_z$ then our first rule is that

1. If $\hat{SF}_z = -\cos(\theta)$ (category N) (7.14)

then set $\tilde{SF}_z = \hat{SF}_z$

For a category A stimulus we should predict a perceived direction of "down" between $\underline{SF}$ and $-\underline{i}_z$. This will be accomplished if $\hat{SF}_z$ is decreased. Therefore

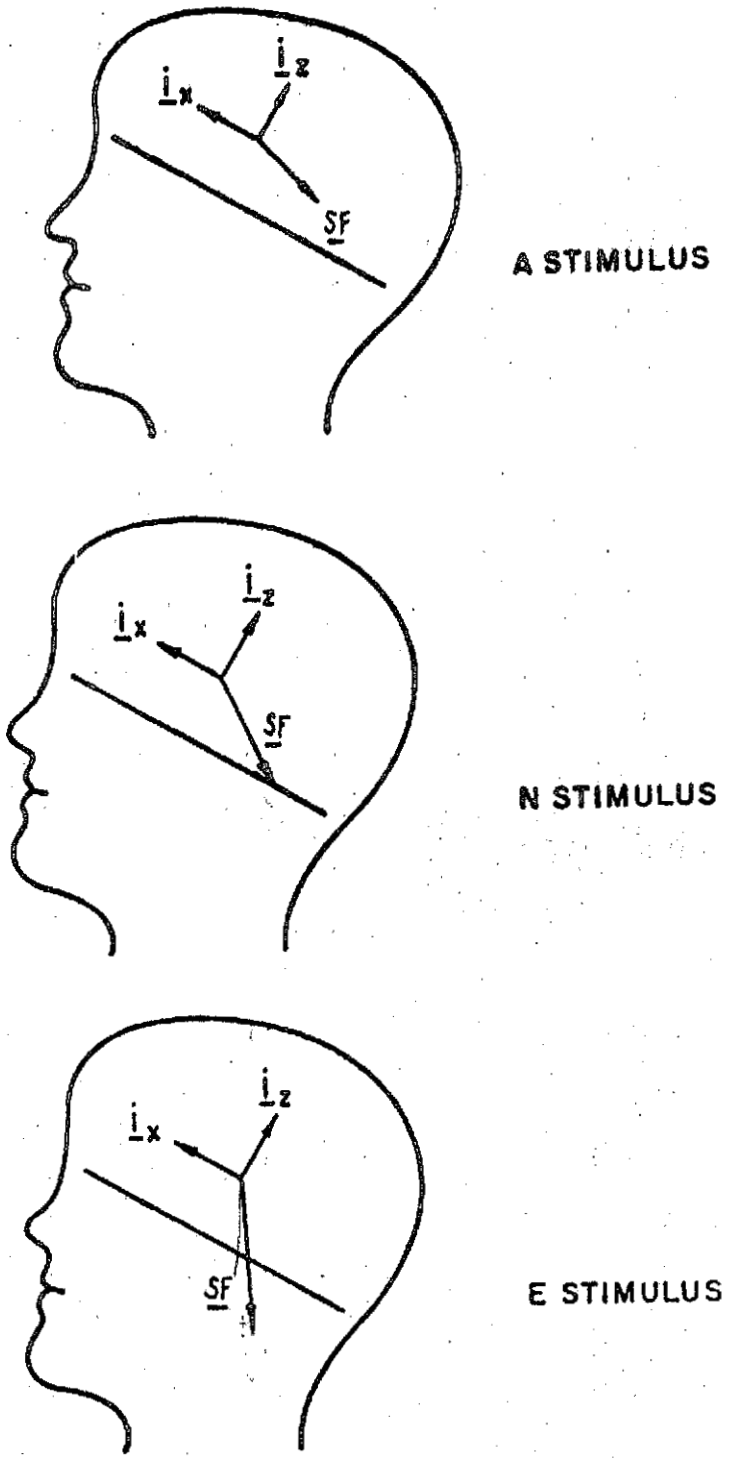

Figure 7.4 Illustration of Specific Force Stimuli for Categories A, N and E

$$2.\quad \text{If } \hat{SF}_z > -\cos(\theta) \quad \text{(category A)} \qquad (7.15)$$
$$\text{Then } \tilde{SF}_z < \hat{SF}_z$$

For a category E stimulus we must predict a perceived direction of "down" which deviates from $-\underline{i}_z$ by more than SF. This will be achieved if $\hat{SF}_z$ is increased (made less negative). Therefore

$$3.\quad \text{If } \hat{SF}_z < -\cos(\theta) \quad \text{(category E)} \qquad (7.16)$$
$$\text{Then set } \tilde{SF}_z > \hat{SF}_z$$

Figure 7.5 presents the exact alteration of $\hat{SF}_z$ which is necessary to fit the experimental data. Figure 7.6 shows the resultant model for perceived orientation. The only difference between this model and the simple model is the nonlinear alteration of $\hat{SF}_z$. In this model the accelerometers are presumed to have unity gain. Since most of the otolith neurons with functional polarization vectors which lie close to the xy plane are utricular in origin and since most of those which have significant components along $\underline{i}_z$ originate from the sacculus the accelerometers in Figure 7.6 along $\underline{i}_x$ and $\underline{i}_y$ are labeled "utricle" and the accelerometer with sensitivity along $\underline{i}_z$ is labeled "saccule." The coordinate transformation is inserted to take cognizance of the fact that our perception of "down" is usually related to the head's

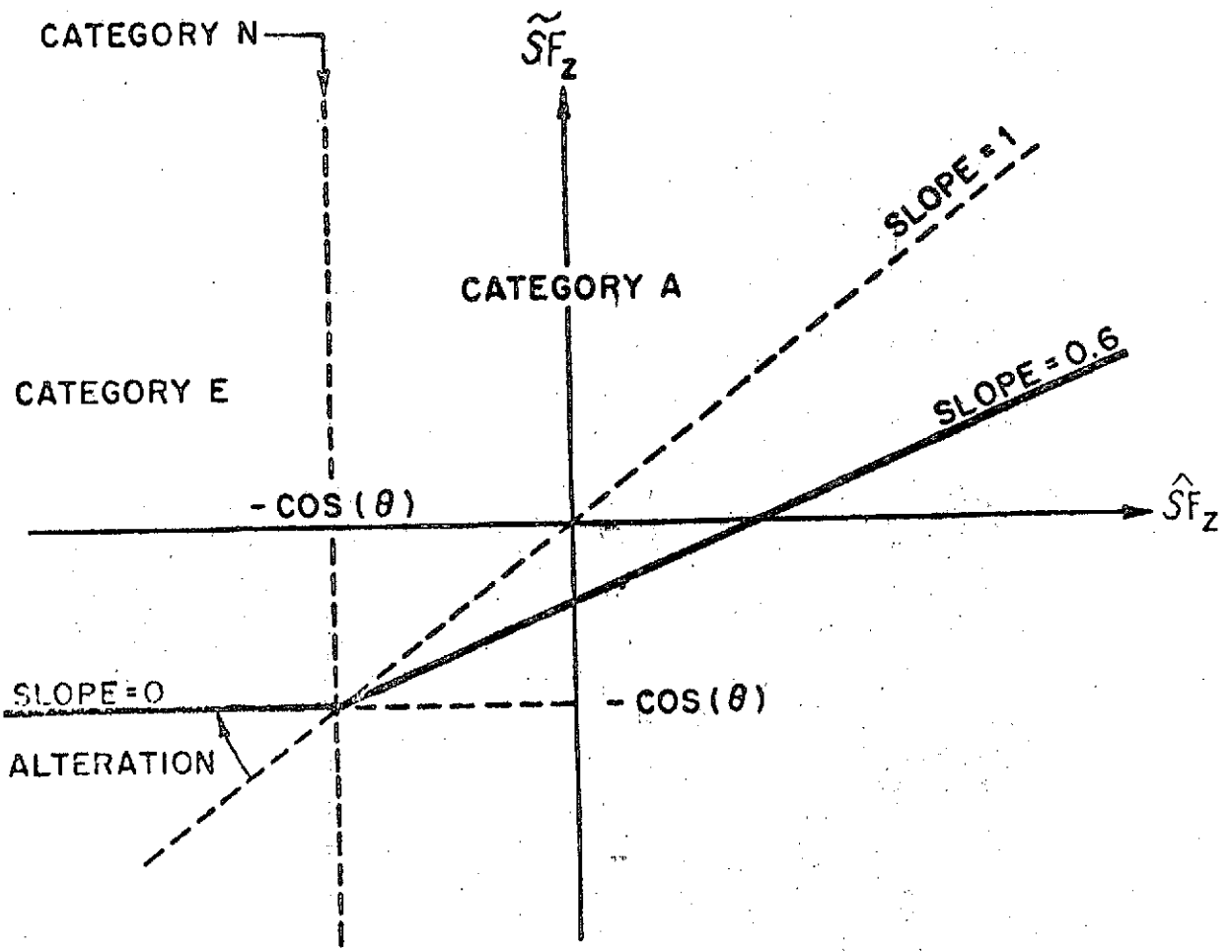

Figure 7.5 Alteration of $\hat{SF}_z$

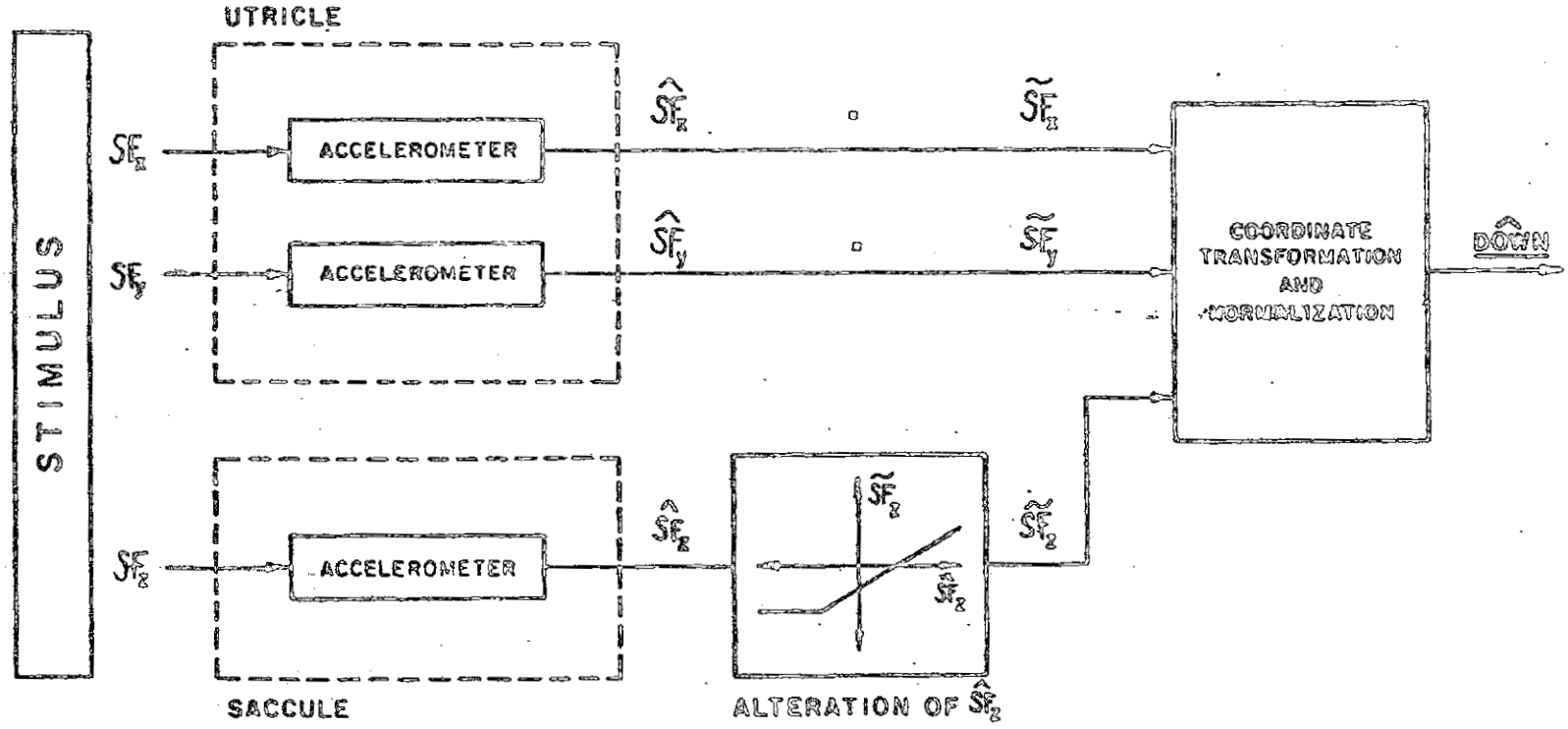

Figure 7.6 Model of Perceived Orientation

principle axes and not to $\underline{i}_x$, $\underline{i}_y$, $\underline{i}_z$. The coordinate transformation and normalization is given by:

$$\begin{bmatrix} \hat{DOWN}_{XHD} \\ \hat{DOWN}_{YHD} \\ \hat{DOWN}_{ZHD} \end{bmatrix} = \frac{\begin{bmatrix} \cos(\theta) & 0 & -\sin(\theta) \\ 0 & 1 & 0 \\ \sin(\theta) & 0 & \cos(\theta) \end{bmatrix} \begin{bmatrix} \widetilde{SF}_x \\ \widetilde{SF}_y \\ \widetilde{SF}_z \end{bmatrix}}{\left[\widetilde{SF}_z^2 + \widetilde{SF}_y^2 + \widetilde{SF}_z^2 \right]^{1/2}} \quad (7.17)$$

where $\underline{i}_{YHD} = \underline{i}_y$ (head erect pitch axis; pitch forward positive)

$\underline{i}_{ZHD}$ = yaw axis when head erect (yaw left positive)

$\underline{i}_{XHD} = \underline{i}_{YHD} \times \underline{i}_{ZHD}$ (head erect roll axis; roll right positive)

and θ = tilt angle of the average utricular plane with respect to sagital plane (25° will be used in section 7.3).

7.3. Model Predictions in Various Constant Specific Force Environments.

If the four conditions discussed in section 7.1 are presumed to be met then a given experimental trial can be fully specified by the specific force vector, $\underline{SF}$. $\underline{SF}$ will be referred to the standard head fixed coordinate system (see Figure 7.7). The orientation of $\underline{SF}$ can most easily be pictured if the angle between the median plane and a vertical plane containing $\underline{SF}$ is given (η_{SF}) and the angle between $\underline{SF}$ and $-\underline{i}_{ZHD}$ is given (μ_{SF}). Once the orientation of $\underline{SF}$ is determined the only parameter which must be known is the magnitude of $\underline{SF}$ which will be designated by G_{SF}.

The problem of how to interpret the predicted perception of "down" is somewhat more difficult. The implicit assumption made by most experimenters has been that the perceived direction of "down" will always be in a plane which includes both $\underline{i}_{ZHD}$ and $\underline{SF}$. In fact from the evidence given in the last two sections it seems more likely that the vector $\underline{\hat{DOWN}}$ lies in a plane which includes $\underline{i}_z$ and $\underline{SF}$. Typically, in a lateral tilt experiment (e.g., 90° tilt right in 1g) a subject would be asked to adjust the orientation of a luminous line in the frontal plane until it appeared vertical but no test would be given to see whether in this orientation he might not feel that he is oriented slightly face down or face up. Experimental data from Nelson [56]demonstrated that when a subject attempts to position himself to a 90° roll right

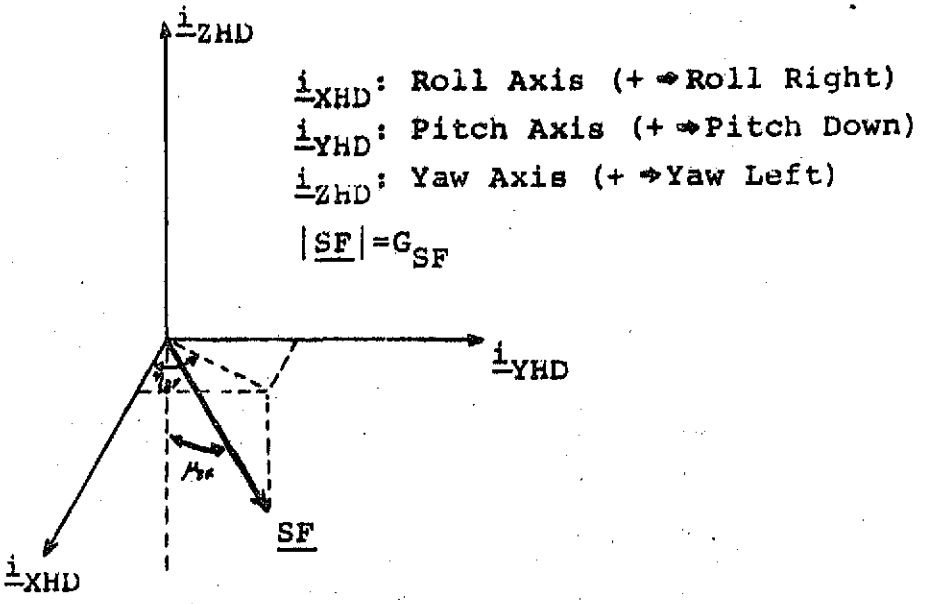

Figure 7.7 Orientation of $\underline{SF}$ With Respect to Head Axes

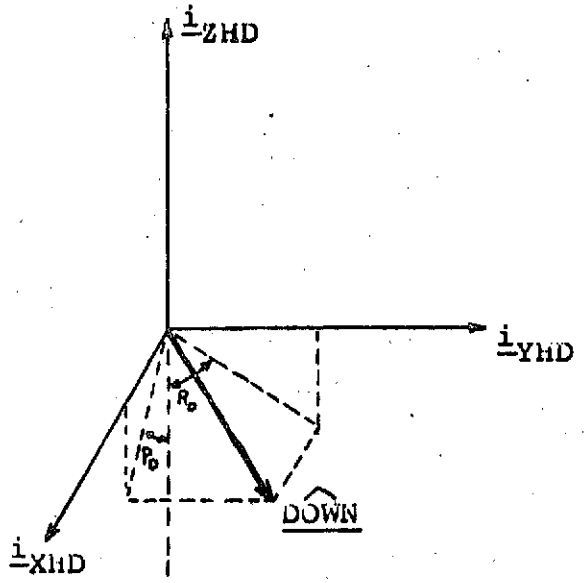

Figure 7.8 Orientation of $\hat{\underline{DOWN}}$ With Respect to Head Axes

orientation underwater he actually ends up positioning himself slightly (≈6°) face up. Since this deviation was found to be statistically significant we can assume that in an experiment in which the subject is just rolled 90° he must sense that his orientation is slightly face down. This deviation is consistent with the model shown in Figure 7.6. The problem which naturally arises is that if $\widehat{\underline{DOWN}}$ is specified in the same way as $\underline{SF}$ (by giving values for η_D and μ_D) then it cannot be readily compared to the experimental data. Figure 7.8 shows how this comparison is simplified. For an experiment in which the subject is asked to indicate his perception of the vertical by adjusting the orientation of a line in his frontal plane, the data is compared to the angle R_D (see Figure 7.8) which is the angle he must roll in order to put his perception of "down" into his median plane. For an experiment in which the subject is asked to indicate his perceived pitch angle, the data is compared to the angle P_D, which is the angle he must pitch backward to bring his perception of "down" into the $\underline{i}_{YHD}\underline{i}_{ZHD}$ plane. In any experiment in which $\underline{SF}$ is in the median plane this distinction is unnecessary since R_D will equal zero.

Figure 7.9 summarizes the model's prediction for the perception of lateral tilt ($\eta_{SF} = 90°$) in a 1g and a 2g environment. The value of R_D is plotted as a function of

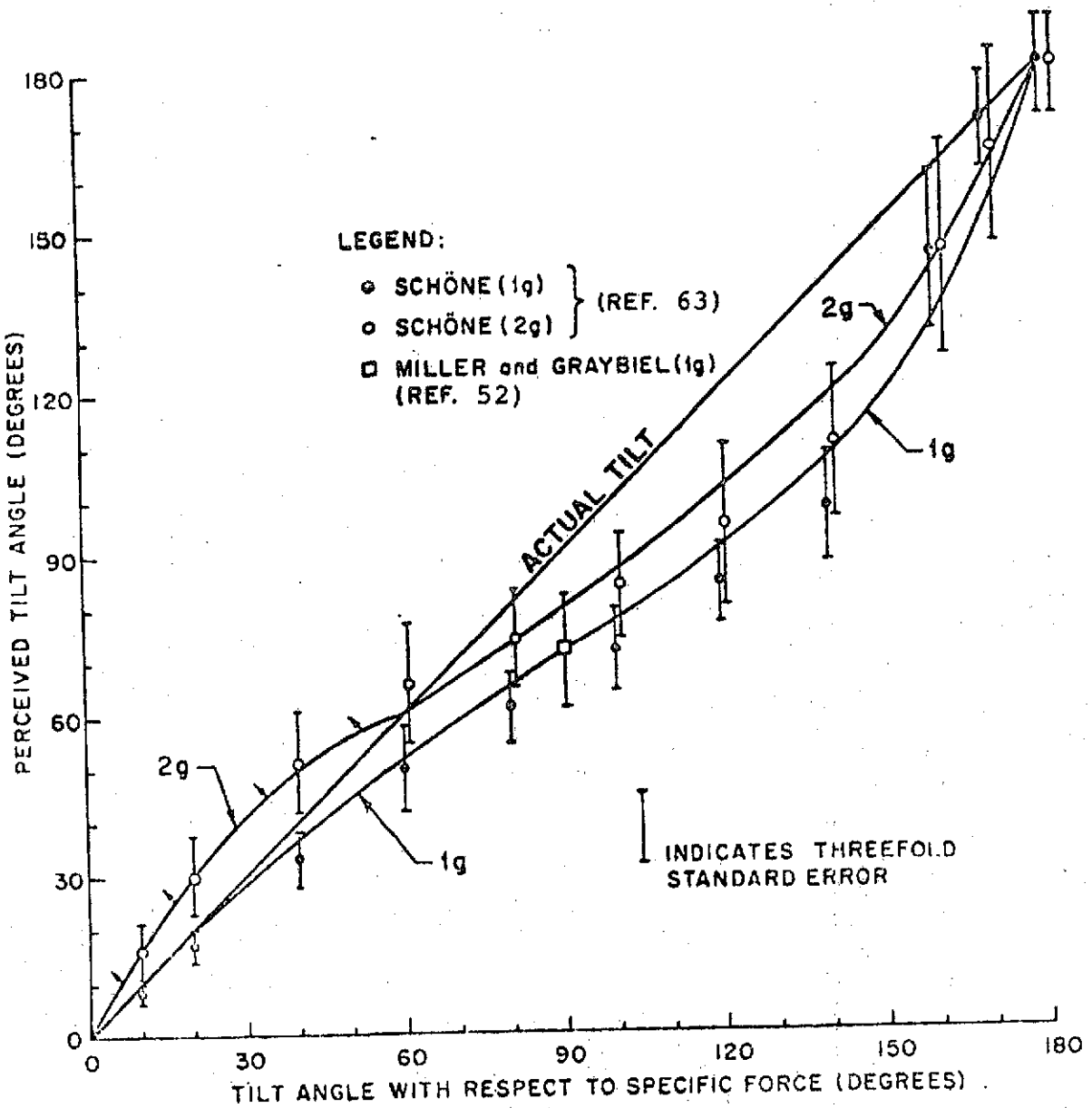

Figure 7.9 Model Predictions for Perceived Tilt Angle as a Function of Actual Tilt Angle in 1G and 2G Specific Force Environments

μ_{SF} for $G_{SF} = 1$ and $G_{SF} = 2$. The data from Schöne [63] which was given in Figure 7.2 is repeated along with data from Miller and Graybiel [52]. The small arrows indicate how these predictions would change if the alteration of $\hat{SF}_z$ shown in Figure 7.5 for type E stimuli is increased.

Figure 7.10 summarizes the model's prediction for the perception of pitch ($\mu_{SF} = 0°$) in 1g and 2g environments. The value of P_D is plotted as a function of μ_{SF} for $G_{SF} = 1$ and 2. Most of the experimental data available for the perception of pitch orientation was gathered for relatively small pitch angles ($\mu_{SF} < 40°$). Figure 7.11 shows the model's predictions of P_D as a function of μ_{SF} in the region from 0 to 40 degrees for G_{SF} = 0g, .5g, 1.0g, 1.3g, 1.6g and 1.9g. These curves should be compared to the data for Schöne and Cohen (Figure 7.3). The predicted deviations of the perception from the true pitch angle varies as a function of μ_{SF} and G_{SF} in exactly the same way as does Schöne's data except that the predicted deviations are only about 60% as great for the cases in which $G_{SF} > 1g$. On the other hand, the model accounts for 90% of the pitch perception exhibited by Cohen's data. These discrepancies can be remedied if the alteration of $\hat{SF}_z$ is increased for $\hat{SF}_z < -\cos(\theta)$ (category E stimulus) as shown in Figure 7.12. A slope of -0.4 is needed to fit Schöne's data while a slope of -0.1 is sufficient to fit Cohen's data. The small arrows perpendicular

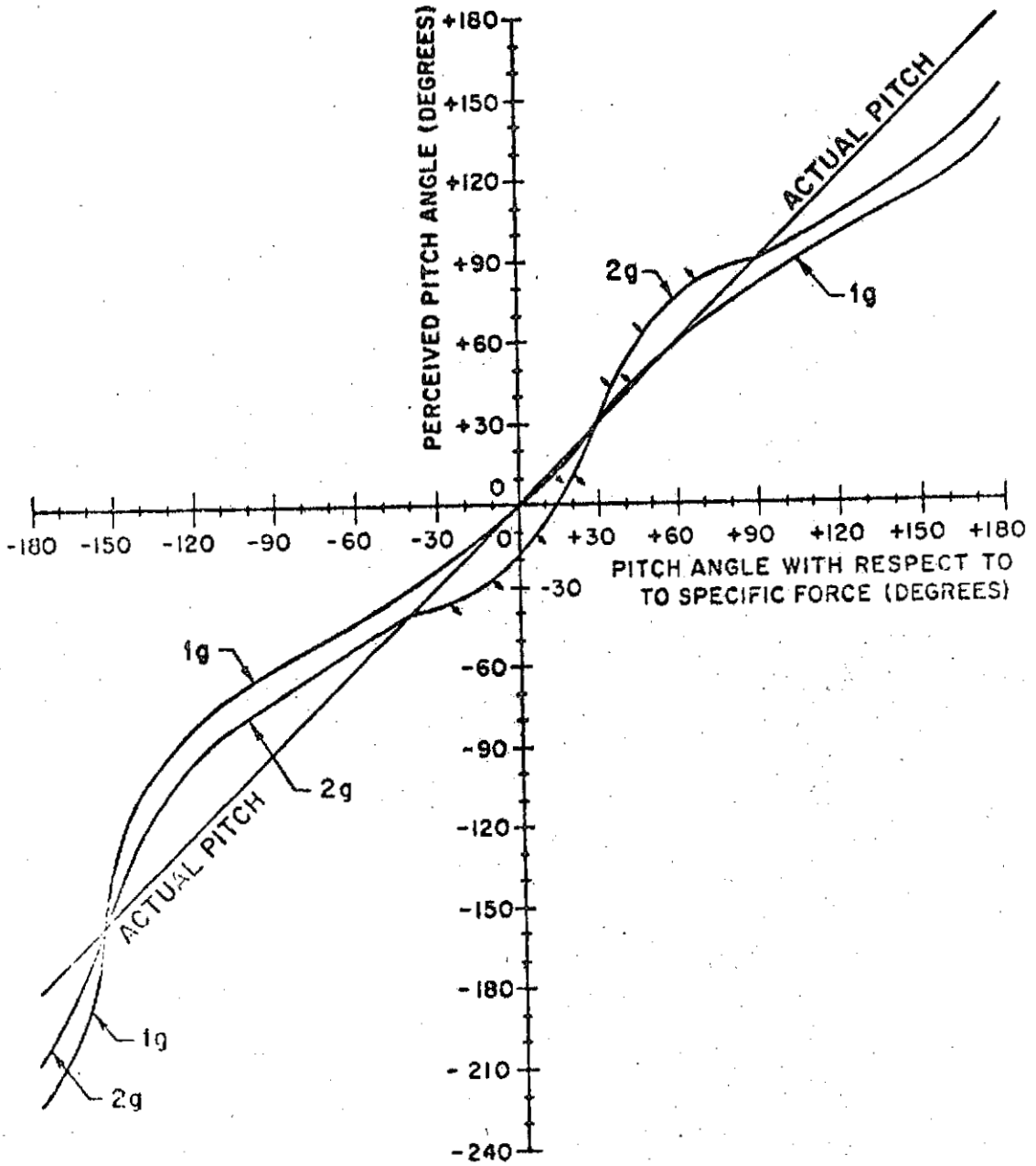

Figure 7.10 Model Predictions for Perceived Pitch Angle as a Function of True Pitch Angle in 1G and 2G Specific Force Environments

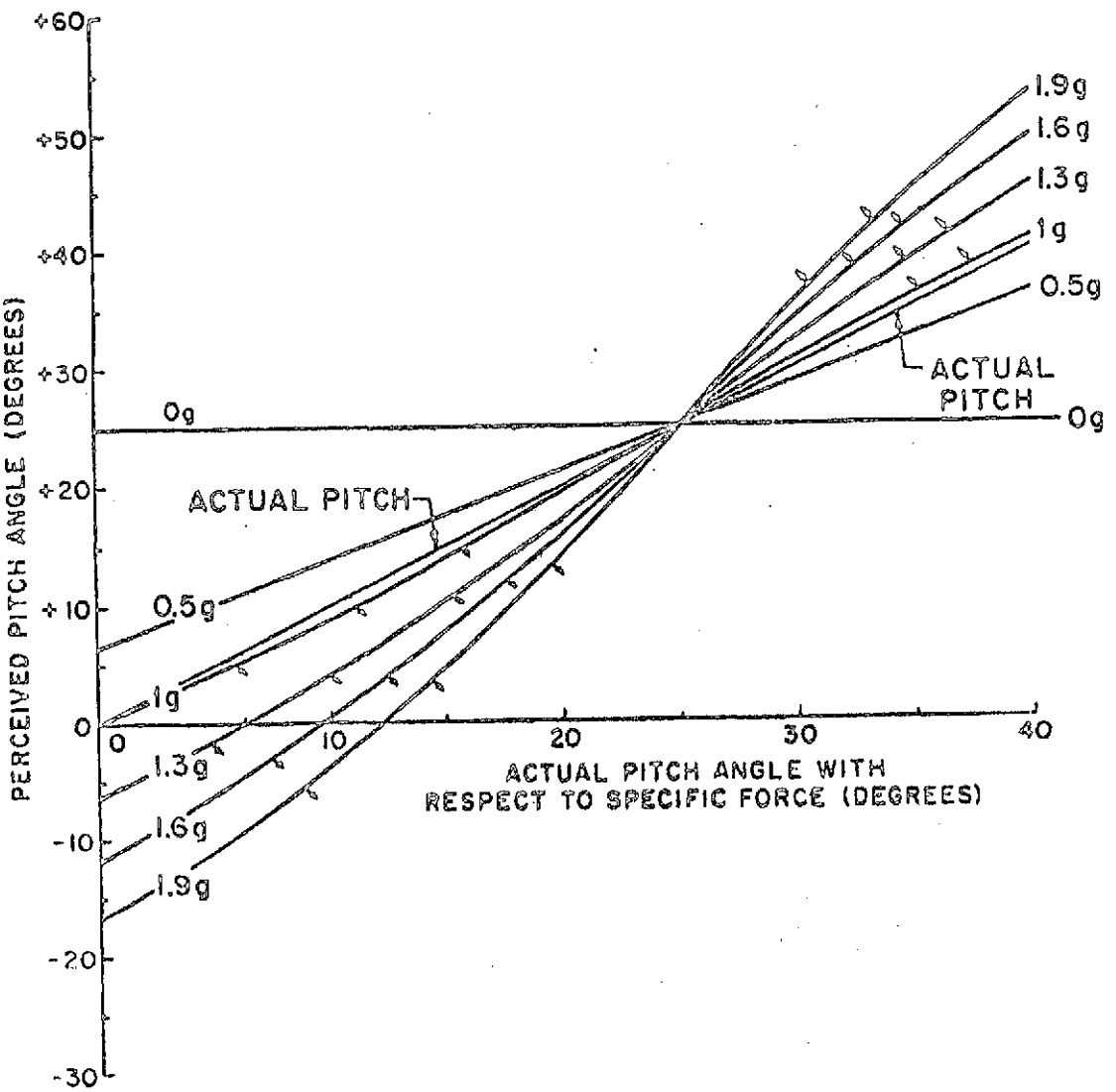

Figure 7.11 Model Predictions for Perceived Pitch Angle as a Function of True Pitch Angle in Various Specific Force Environments

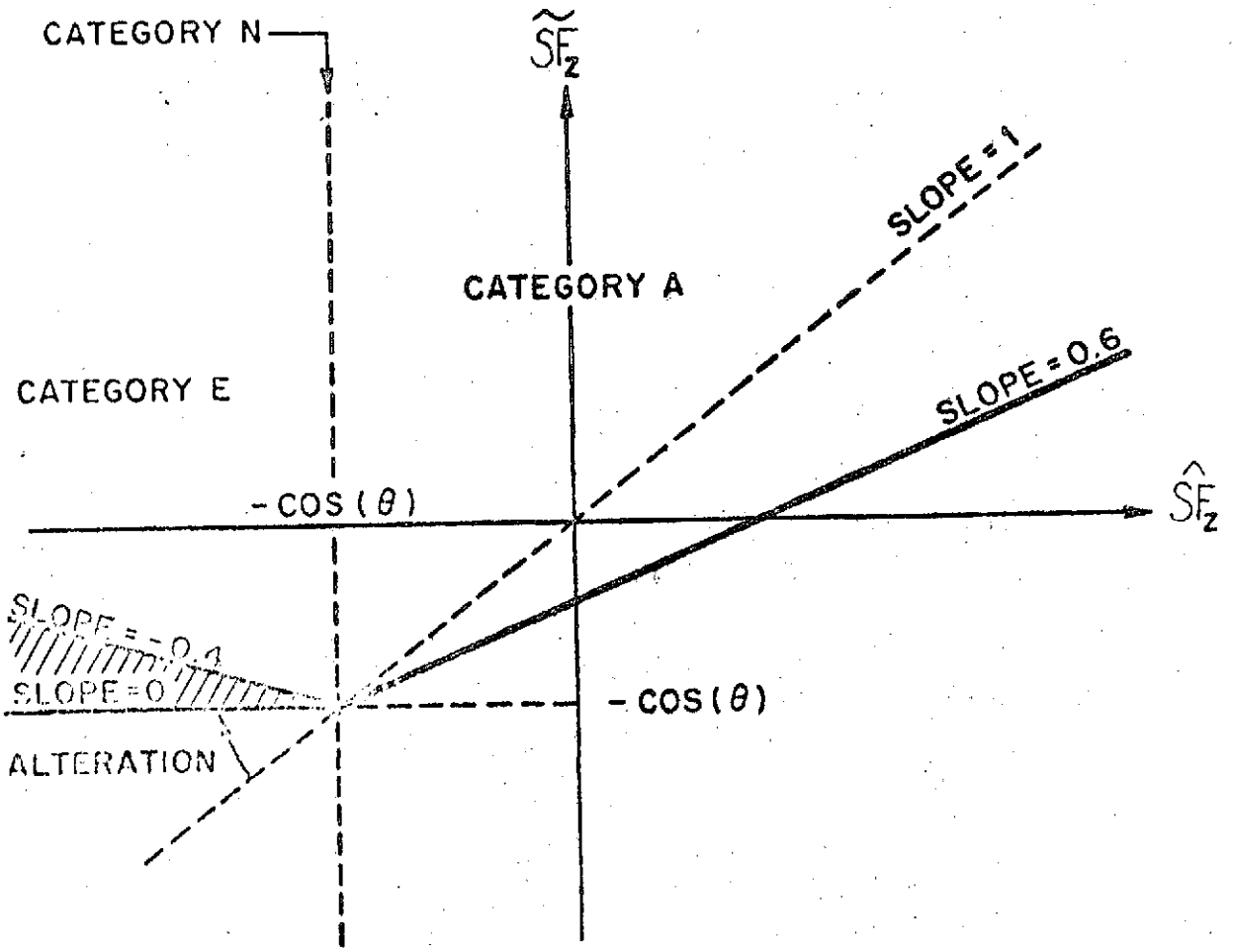

Figure 7.12 Additional Alteration of SF_z Necessary to Fit Category E Experimental Data

to the curves in Figures 7.10 and 7.11 illustrate the direction in which the predictions move as this alteration of $\hat{SF}_z$ is increased. Finally, the model predictions were generated using a value of 25 degrees for θ (the angle between the average plane of the utricles and the $\underline{i}_{XHD}$ axis) while the data from Schöne would be best fit if an angle of approximately 29 degrees were used. Since 29 degrees is within the 25-30 degree range normally associated with the orientation of the utricles this does not constitute a discrepancy.

All category N stimuli can be summed up by stating that the model correctly predicts that the perception of the vertical will be aligned with the specific force vector with essentially no error. The experimental justification for this was discussed at length in Section 7.2 [11,12,30,45,46,47,57].

While it might be noted that all model predictions and all experimental results which have been given are for cases in which the specific force vector was in the median plane (pure pitch) or in the frontal plane (pure lateral tilt) the model is capable of generating predictions for an arbitrary constant specific force vector.

7.4. Summary

The illusions associated with the perception of static tilt in various specific force environments have been reviewed and then classified in such a way that a simple perceptual model could be developed to account for the available experimental data. The fundamental conclusion to be drawn from this model is that these illusions can be accounted for by a simple nonlinear transformation of the information (mainly from the saccule) related to the component of specific force perpendicular to the average plane of the utricles.

CHAPTER VIII

INTEGRATION OF SEMICIRCULAR CANAL AND OTOLITH INFORMATION FOR MULTISENSORY STIMULI

In this chapter we consider the class of stimuli specifically excluded in Chapter Three, namely those stimuli which simultaneously excite the semicircular canals and the otoliths. In generalizing the stimulus class to include any combination of rotational acceleration and translational acceleration in three axes, a number of significant new problems arise. These problems and the philosophical approach taken to deal with them are discussed in section 8.1. A mathematical model of the perception of dynamic orientation which results from the combined effect of arbitrary angular and translational accelerations is developed in section 8.2. The model's qualitative predictions for several stimuli are also discussed. Quantitative predictions from a computer simulation of the model are presented for several stimuli in section 8.3 along with the model's frequency response for small pitch and roll angle oscillations.

8.1 Discussion of Modelling Problems and Philosophy

Before discussing any of the problems associated with the integration of sensory information from the semicircular canals and otoliths it is important to clarify what the important perceptual outputs of the model should be. Certainly we would be interested in estimating the following quantities:

1. Orientation of the head with respect to the gravitational vertical
2. Rate of rotation of the head about its three principle axes
3. The translational acceleration of the head with respect to its three principle axes

and

4. Additional quantities which are derived from the preceeding (e.g. azimuth, translational velocities and translational positions).

The most important of these is the determination of orientation with respect to the vertical. Strictly speaking, there is no way of using information which is derived only from the otoliths to determine the direction of the gravitational vertical if there is no a priori information regarding the expected variations in orientation or translational acceleration. The principle of equivalence in general relativity precludes such a separation based purely on measurements taken from linear accelerometers. In the language of modern control systems theory any system comprised only of linear

accelerometers is unobservable. How then are we capable of distinguishing a change in orientation with respect to the gravitational vertical from a change in acceleration? The answer to this question has two parts. First, we are not restricted to the use of linear accelerometers (otoliths) since we also have angular velocity transducers (the semicircular canals) which indicate with reasonable accuracy the rate of change of the head's orientation for rotational rates in the frequency range from 0.1 rad/sec to 10 rad/sec. Roughly speaking, for changes in the direction of specific force which occur in this frequency range (as determined from otolith information) the distinction between a change in oreintation with respect to the gravitational vertical and a translational acceleration (or some combination of the two) can be made by noting the output of the semicircular canals. As the frequency of the variations in the direction of the specific force vector decreases below .1 rad/sec, information from the canals becomes less and less useful. In fact as the frequency of these variations approaches zero the system is incapable of determining the gravitational vertical. The second part of our answer therefore is that for lower frequency variations the system cannot concern itself with the true gravitational vertical but must be content to estimate an "effective graviational vertical" which can serve as the practical reference for man's normal

activities. The phenomenon of associating the gravitational vertical with the perceived direction of specific force for very low frequency (essentially static) stimuli was discussed in depth in Chapter Seven.

Once the direction of the gravitational vertical is estimated, the other perceptual quantities can be derived. The sensation of rotation about an axis parallel to the perceived gravitational vertical ($\underline{\omega}_{\parallel}$) will reflect exclusively the properties of the semicircular canals described in Chapter Three.

The perception of rotation about an axis perpendicular to the perceived vertical ($\underline{\omega}_{\perp}$) should reflect the information available from the canals and the otoliths. Since the otoliths are capable of sensing a constant change in orientation with respect to the gravitational vertical the perception of constant rotation about a horizontal axis should persist indefinitely. Benson and Bodin (Ref. 4) and Guedry (Ref. 34) confirm that the perception of rotation does indeed persist for prolonged rotations about a horizontal cephalocaudal axis.

The estimate of translational acceleration is essentially determined once the direction of gravity is estimated since

$$\underline{A} = \underline{G} - \underline{SF} \tag{8.1}$$

where $\underline{A}$ = translational acceleration (g's)

$\underline{G}$ = gravitational vector (normally 1 g)

and $\underline{SF}$ = net specific force vector (g's)

C-3

The only change needed in equation 8.1 is the replacement of each term by its estimate (e.g. $\underline{A}$ by $\hat{\underline{A}}$, etc.). To maintain the notation used in Chapter Seven the estimate of $\underline{G}$ will be denoted by $\hat{\underline{DOWN}}$ since this is more descriptive of its perceptual meaning. The remaining perceptual quanitities (azimuth, translational velocity and translational position) are obtained by integration as follows:

$$\hat{\Psi}(t) = \hat{\Psi}(t_0) + \int_{t_0}^{t} |\hat{\underline{\omega}}_{\parallel}(\eta)| d\eta \tag{8.2}$$

$$\hat{\underline{V}}(t) = \hat{\underline{V}}(t_0) + \int_{t_0}^{t} \hat{\underline{A}}(\eta) d\eta \tag{8.3}$$

$$\hat{\underline{X}}(t) = \hat{\underline{X}}(t_0) + \int_{t_0}^{t} \hat{\underline{V}}(\eta) d\eta \tag{8.4}$$

where $\hat{\Psi}$ is the angle between the projection of the head's roll axis ($\underline{i}_{XHD}$) in the earth's horizontal plane and some fixed direction in that plane (e.g. a vector pointing toward true north).

$\hat{\underline{\omega}}_{\parallel}$ is the perception of rotation about an axis parallel to $\hat{\underline{DOWN}}$

$\hat{\underline{V}}$ is the perception of linear velocity

and $\hat{\underline{X}}$ is the perception of spatial position.

In all, the model should be capable of predicting 15 quantities (3 associated with $\hat{\underline{\omega}}$, 3 associated with $\hat{\underline{A}}$, 3 associated with $\hat{\underline{V}}$, 3 associated with $\hat{\underline{X}}$, 2 associated with the direction of $\hat{\underline{DOWN}}$, and 1 associated with $\hat{\Psi}$). Of these 15, the 2 associated with the direction of $\hat{\underline{DOWN}}$ are by far the most difficult to model quantitatively and for this reason

the model developed in this chapter is called the "down" estimator. Equations 8.1, 8.2, 8.3 and 8.4 determine the quantities $\hat{\underline{A}}$, $\hat{\Psi}$, $\hat{\underline{V}}$, and $\hat{\underline{X}}$ as a function of $\hat{\underline{DOWN}}$ and $\hat{\underline{\omega}}_{\parallel}$ and therefore the only estimators which are left to be modelled are those which generate $\hat{\underline{DOWN}}$ and $\hat{\underline{\omega}}$ (since $\hat{\underline{\omega}}_{||}$ is the component of $\hat{\underline{\omega}}$ parallel to $\hat{\underline{DOWN}}$).

Before considering these estimators (for $\underline{DOWN}$ and $\underline{\omega}$) in detail, several problems require consideration. The first of these is the problem of reconciling what may seem to be contradictory information from the canals and otoliths. Three examples can be cited for which there exists corresponding data. The first of these involves an abrupt change in the direction of the specific force vector relative to the head ("rotation information" from the otoliths) without any corresponding indication of rotation from the canals (e.g. aircraft catapult launch Ref. 18 , or a change in the direction of specific force due to rotation on a centrifuge Ref. 28). A second example of such a conflict would arise in the case of a constant rotation about a horizontal axis which would lead to a continuously rotating specific force vector but a zero steady state output from the canals (e.g. a barbecue-spit experiment Ref. 4 , 5 , 34). Finally, situations may arise in which the canals indicate an abrupt rotation about a horizontal axis but the otoliths indicate no change in the direction of specific force (e.g. a coordinated aircraft turn

or the abrupt cessation of rotation in a barbecue-spit experiment Ref 4 , 5 , 34). Since one or more examples from each of these categories will be treated in detail in the remaining sections of this chapter it is unnecessary at this point to give a full accounting of the perceptual responses except to say that the perception of the vertical for these stimuli is most strongly associated with:

1. The low frequency portion of the "rotation information from the otoliths

plus 2. that part of the canal information which is consistent with the high frequency portion of the "rotation information" from the otoliths.

Since the rate of movement of the perceived vertical may not be consistent with the estimate of rotation based only upon canal information the question arises whether the perception of rotation reflects the movement of $\underline{\hat{DOWN}}$ or canal information or a combination of the two. If the time histories of $\underline{\hat{DOWN}}$ and $\hat{\omega}_{\perp}$ (the component of $\underline{\hat{\omega}}$ perpendicular to $\underline{\hat{DOWN}}$) were to be consistent then in the situation in which the direction of $\underline{\hat{DOWN}}$ is constant it must follow that $\underline{\hat{\omega}}_{\perp} = \underline{0}$. The experimental evidence (Ref. 4 , 5 , 34) does not consistently support this conclusion and thus $\underline{\hat{DOWN}}$ and $\underline{\hat{\omega}}_{\perp}$ may not be in agreement. Although such a contradictory sensation (of rotating but not changing one's position) seems difficult to imagine, it is also found in cases in which otolithic and visual information conflict (Ref. 21) and during caloric

testing. The fact that these sensations are contradictory also complicates interpretation of some of the experimental data. For example, if an experimenter asked a subject if he felt himself rotating the subject could answer either "yes" or "no" (in fact an answer of yes and no would be more appropriate!).

A second problem arises in the case of stimuli which are predictable, usually because the subject is thoroughly familiar with the stimulus from past experience and is able to recognize the underlying stimulus pattern. The phenomena associated with such a situation are significantly different then those which we are attempting to model here since they involve the complex problems of pattern recognition. Furthermore, it is very likely that the processes involved in recognition are strongly dependent on the simplicity of the stimulus, the subject's past exposure and many other factors which would make an accurate prediction of the perception of dynamic orientation extremely difficult. For these reasons the stimulus class for which we are attempting to model the perceptual responses will be assumed to be unpredictable.

Finally, the information upon which the "down" estimator bases its estimate must be considered. Although the information from two sets of semicircular canals and otoliths is available to the brain it is unnecessary to waste computation time performing a dual set of sensory simulations. For this reason, the model simulates cyclopian sensors located near the

center of the skull. One case in which this simplification could make a difference is one in which a very rapid rotation of the head is made about either the yaw or roll axis, in which case the otoliths on either side of the head would normally be exposed to slightly different specific force vectors. Since no perceptual effect has been ascribed to this difference nothing is lost by eliminating it. Figure 8.1 illustrates the orientation of the three canals which are aligned with and sensitive to rotations about the three axes $\underline{i}_{XC}$, $\underline{i}_{YC}$ and $\underline{i}_{ZC}$. These axes are equivalent to the axes $\underline{i}_x$, $\underline{i}_y$ and $\underline{i}_z$ illustrated in Figure 7.1 except they are rotated +45° about $\underline{i}_z = \underline{i}_{ZC}$. The canal labeled LH has an afferent response equivalent to that of the left horizontal canal and opposite to that of the right horizontal canal. The canal labeled RS has a response equivalent to that of the right superior canal and opposite to that of the left posterior canal. Finally the canal labeled LS has a response equivalent to that of the left superior canal and opposite to that of the right posterior canal. Each canal and the optimal estimator for the rotational rate about its associated axis is modelled by the dynamic model and Kalman filter developed in section 3.1. The otolith models for the utricle and saccule along with their associated processors which were developed in section 3.2 are used to generate the estimate of specific force. One utricular sensor is aligned with its major axis of sensitivity along $\underline{i}_{XO} = \underline{i}_X$ and one along $\underline{i}_{YO} = \underline{i}_Y$ (see Figure 7.1). The saccular sensor is aligned with

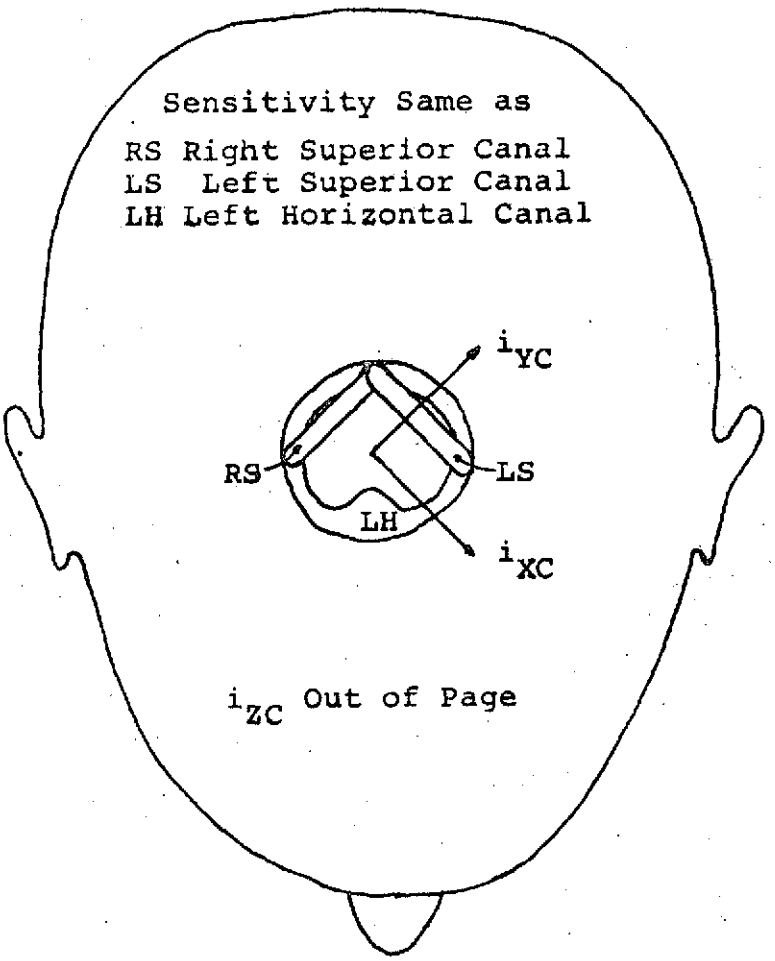

Figure 8.1 Orientation and Sensitive Axes of Cyclopian Semicircular Canal System

$\underline{i}_{ZO} = \underline{i}_{Z} = \underline{i}_{ZC}$ (see Figures 7.1 and 8.1).

Figure 8.2 summarizes the information available to the "down" estimator. The alteration of saccular information shown in Figure 8.2 is identical to that developed in Chapter Seven and its presence insures that the steady state performance of the "down" estimator for static tilts will be consistent with the predictions made in that chapter. The estimates of rotation based upon canal information and specific force based upon otolith information are transformed from sensor to head coordinates before being used by the "down" estimator since the principle head axes are the most natural coordinates to which to refer our concious perceptions of dynamic orientation.

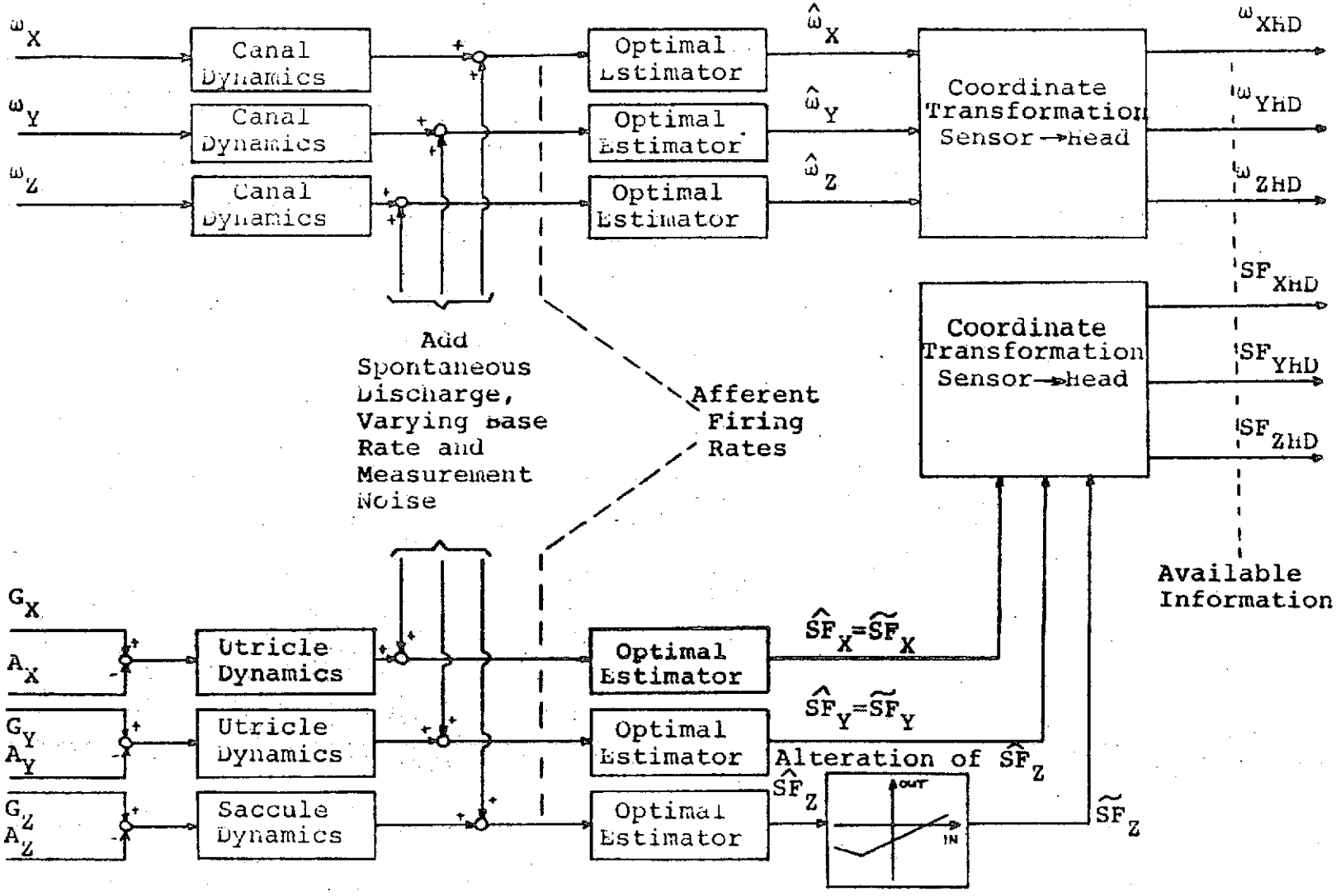

Figure 8.2 Information Available to DOWN Estimator

8.2 DOWN Estimator

After numerous algorithms were developed in an attempt to successfully produce an estimator with the desired qualifications, one was found which fulfills all of the requirements discussed in section 8.1 and which yields very reasonable quantitative results (see section 8.3). The discrete "down" estimator is illustrated in figures 8.3 and 8.4. The information available to the "down" estimator at the beginning of each update is the old estimate of down, $\underline{\hat{DOWN}}(t-\Delta t)$ and the new estimates based upon canal information ($\underline{\hat{\omega}}_{HD}(t)$) and upon otolith information ($\underline{\hat{SF}}_{HD}(t)$). Figure 8.3 illustrates the calculation of the updated perception of down, $\underline{\hat{DOWN}}(t)$ and Figure 8.4 illustrates the updated perception of rotation, $\underline{\hat{\omega}}(t)$. Each element of the model is labeled with a letter from A to L for easy reference and will be discussed in alphabetical order.

The first element, labeled A and marked with an X, represents the following computational procedure: Produce a vector $\underline{\omega}_{\hat{SF}}$ which is in the direction $\underline{\hat{SF}}_{HD}(t-\varepsilon)\times\underline{\hat{SF}}_{HD}(t+\varepsilon)$ and which has magnitude equal to the angular rate of change of the direction of $\underline{\hat{SF}}_{HD}$ at time t. In the computer simulations carried out in section 8.3, $\underline{\hat{\omega}}_{HD}$ was calculated each second (t = 1,2,3,4,...) and $\underline{\hat{SF}}_{HD}$ was calculated on the half second ($t = \frac{1}{2},\frac{3}{2},\frac{5}{2},\ldots$) so $\varepsilon = \frac{\Delta T}{2} = .5$ seconds. $\underline{\omega}_{\hat{SF}}$

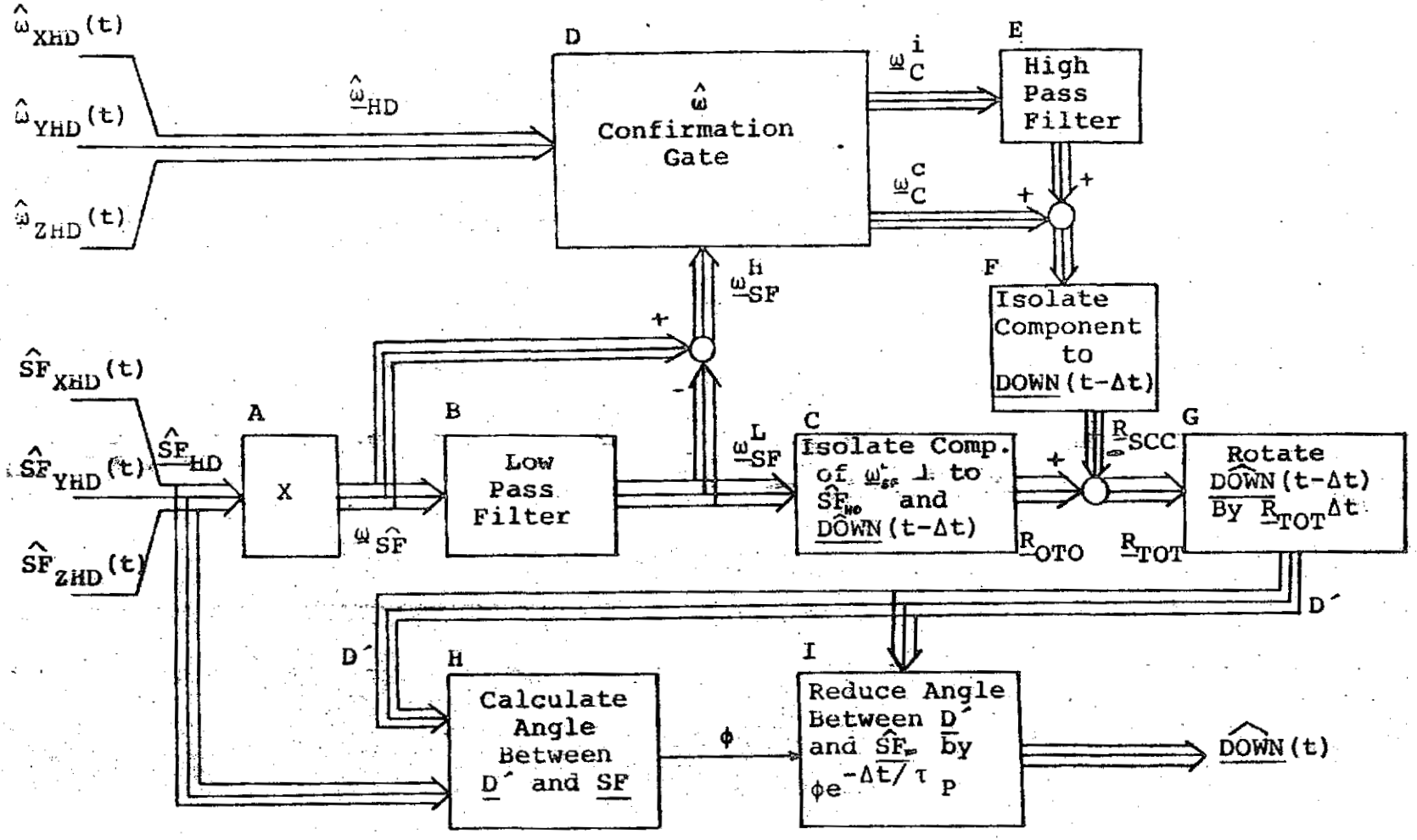

Figure 8.3 DOWN Estimator

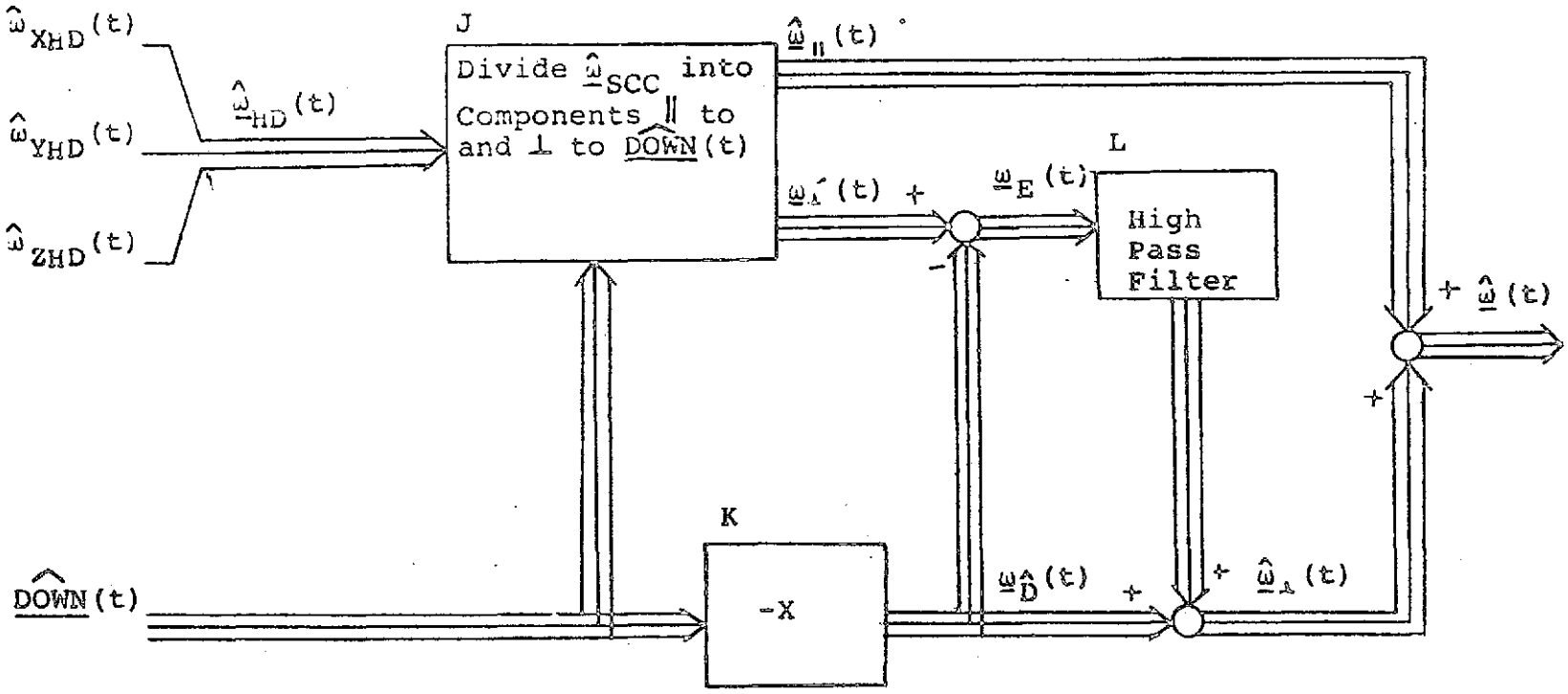

Figure 8.4 $\underline{\omega}$ Estimator

represents the information available from the otoliths concerning the rate of rotation of the head if it were assumed that SF was fixed in space.

The low pass filter, labeled B, performs the function of separating out the low frequency component of $\underline{\omega}_{SF}^{\wedge}$ which is assumed to arise from the change in the body's orientation with respect to the gravitational vertical. The output signal $\underline{\omega}_{SF}^{L}$ is intended to fill in the low frequency information missing from the canal signal $\underline{\hat{\omega}}_{HD}$ for rotations about a horizontal axis. $\underline{\omega}_{SF}^{H}$ is the high frequency component of $\underline{\omega}_{SF}^{\wedge}$ and typically arises from both transient linear accelerations and abrupt changes in the head's orientation with respect to the gravitational vertical. The best time constant for the low pass filter was found to be approximately 35 seconds.

The transformation labeled C produces a rotation vector $\underline{R}_{OTO}$ from $\underline{\omega}_{SF}^{L}$ as follows:

$$\underline{R}_{OTO} = \begin{array}{l}\text{Component of } \underline{\omega}_{SF}^{L} \text{ which is perpendicular to} \\ \text{the plane of } \underline{\hat{SF}}_{HD} \text{ and } \underline{\widehat{DOWN}}(t-\Delta t)\end{array} \qquad (8.5)$$

It may seem odd at first that this transformation allows rotations which would by themselves move $\underline{\hat{DOWN}}$ away from $\underline{\hat{SF}}$. The reason for this is that such rotations are necessary to cancel the canal signals which arise when prolonged rotations are suddenly stopped. It is this mechanism which helps to predict the stabilization of the perception of orientation

when prolonged rotations about a horizontal axis are abruptly terminated as was found experimentally by Benson and Bodin (Ref. 4, 5) and Guedry (Ref. 34). In all the simulations carried out no case has been encountered in which $\underline{R}_{SCC}$ (which will be discussed next) did not cancel completely any R_{OTO} which would move $\underline{\hat{DOWN}}$ away from $\underline{\hat{SF}}$. If such a case occurred it would appear reasonable to decrease the magnitude of $\underline{R}_{OTO}$ until the net effect of $\underline{R}_{TOT} = \underline{R}_{OTO} - \underline{R}_{SCC}$ would be to minimize the misalignment of $\hat{DOWN}$ and $\underline{SF}$ after rotation. The combined effect of elements A, B and C in figure 8.3 is to produce a rotation vector $\underline{R}_{OTO}$ from the current and past estimates of $\underline{SF}$ which represents the low frequency rotational rate information due to the otoliths.

We now turn our attention to the information available from the canals. The rotational information from the semicircular canals must be consistent with the high frequency sensations arising from the otoliths (represented by $\underline{\omega}^H_{SF}$) if it is to be used to update the sensation of orientation with respect to the vertical. The portion of $\underline{\hat{\omega}}_{HD}(t)$ which is consistent with $\underline{\omega}^H_{SF}$ is denoted by $\underline{\omega}^C_C$ and is calculated by the following procedure:

1) Calculate the component of $-\underline{\hat{\omega}}_{HD}(t)$ which is parallel to $\underline{\omega}^H_{SF}$. Call this component $\underline{C}$.
2) If $\underline{C}$ is in a direction opposite to $\underline{\omega}^H_{SF}$ then set $\underline{\omega}^C_C = \underline{0}$
3) If $\underline{C}$ is in the same direction as $\underline{\omega}^H_{SF}$ then set

$$\underline{\omega}_C^C = -\omega_{SF}^H \text{ if } |\underline{C}| > |\underline{\omega}_{SF}^H|$$

$$\underline{\omega}_C^C = -\underline{C} \quad \text{if } |\underline{C}| < |\underline{\omega}_{SF}^H| \tag{8.6}$$

The portion of $\hat{\underline{\omega}}_{HD}(t)$ which is inconsistent with $\underline{\omega}_{SF}^H$ is denoted by $\underline{\omega}_C^i$ and is given by

$$\underline{\omega}_C^i = \hat{\underline{\omega}}_{HD}(t) - \underline{\omega}_C^C \tag{8.7}$$

The reason that $-\hat{\underline{\omega}}_{HD}(t)$ (instead of $\hat{\underline{\omega}}_{HD}(t)$) was compared with $\underline{\omega}_{SF}^H$ is that for a positive perception of rotation the corresponding rotation of the g vector would be negative.

While experimental evidence clearly indicates that the effect of $\underline{\omega}_C^i$ on the perception of orientation is minimal it is not clear that it has no effect in the very short term (<1 sec). For this reason $\underline{\omega}_C^i$ is passed through a high pass filter (E) of the form $\tau s/(\tau s+1)$ where $\tau < 1$ sec. For the catapult launch simulation described in section 8.3.3 τ could be no higher than .25 seconds to retain reasonable results. A value of $\tau = 0$ would not be inconsistent with any available experimental evidence.

The rotation vector due to canal information is denoted by $\underline{R}_{SCC}$. $\underline{R}_{SCC}$ is computed by taking the sum of $\underline{\omega}_C^C$ and the result of filtering $\underline{\omega}_C^i$ and then eliminating the component which is parallel to the last estimate of down (since this component is ineffective in changing the direction of $\hat{\underline{DOWN}}$ relative to the head).

$\underline{R}_{TOT}$ is then computed by subtracting $\underline{R}_{SCC}$ from $\underline{R}_{OTO}$. $\underline{R}_{TOT}$ represents the estimate of the rotational rate of the outside world around an axis perpendicular to the last estimated direction of down for the purposes of updating that estimate. The transformation labeled G updates $\hat{\underline{DOWN}}(t-\Delta t)$ using $\underline{R}_{TOT}$. The output of G is denoted by $\underline{D}'(t)$ and satisfies:

1) $\hat{\underline{DOWN}}(t-\Delta t) \times \underline{D}'(t)$ is in the same direction as $\underline{R}_{TOT}$ and

2) the angle between $\hat{\underline{DOWN}}(t-\Delta t)$ and $\underline{D}'(t)$ is given by

$$|\underline{R}_{TOT}|\Delta t \tag{8.8}$$

Therefore, if $|\underline{R}_{TOT}| = 30$ degrees/sec, and $\Delta t = 0.5$ seconds $\hat{\underline{DOWN}}$ will be rotated about $\underline{R}_{TOT}$ by 15 degrees.

$\underline{D}'(t)$ would normally be considered the new estimate of "down" except that because it is generated through the integration of rate information it is bound to accumulate errors which must be eliminated if permanent discrepancies are to be avoided. This is accomplished through a slow reduction of any discrepancy in direction between $\underline{D}'$ and $\hat{\underline{SF}}$ (elements H and I). The time constant, τ_p, is quite large but was found to be a weak function of the magnitude of the specific force vector (as $|\hat{\underline{SF}}|$ increases, τ_p decreases and $\underline{D}'$ moves toward $\underline{SF}$ more rapidly). τ_p is given by

$$\tau_p \simeq \frac{60}{|\hat{\underline{SF}}|^{1/4}} \qquad (8.9)$$

The net effect of H and I is that in the steady state the subject adopts the estimated specific force vector, based on otolith information, as the correct direction for $\hat{\underline{DOWN}}$. This insures that the steady state response of the model will exhibit the perceptual errors modelled in Chapter Seven.

The resulting estimate of $\hat{\underline{DOWN}}(t)$ represents the model's prediction for the subject's perception of the direction of the gravitational force vector with respect to his head. This estimate is then used at time $t + \Delta t$ to generate a new estimate.

The model for predicting the perceived rate of bodily rotation is shown in Figure 8.4. $\hat{\underline{\omega}}_{\parallel}(t)$ is found simply by taking the component of $\hat{\underline{\omega}}_{HD}(t)$ parallel to $\hat{\underline{DOWN}}(t)$. $\underline{\omega}_{\hat{D}}$ is defined to be the bodily rate of rotation which would be consistent with the rate of change of the direction of $\hat{\underline{DOWN}}$. The transformation K is similar to that at A in figure 8.3 except for a minus sign. $\hat{\underline{\omega}}_{\perp}(t)$ is formed by:

1) calculating the difference between the component of $\hat{\underline{\omega}}_{HD}(t)$ which is perpendicular to $\hat{\underline{DOWN}}$ and $\underline{\omega}_{\hat{D}}$
2) passing this difference through a high pass filter (L)

and then

3) adding the resulting output to $\underline{\omega}_{\hat{D}}$.

This arrangement accepts the relatively high frequency changes in rotation rate indicated by the semicircular canal system while deferring to the rate of rotation consistent with $\hat{\underline{DOWN}}$ for lower frequency changes. Data from Benson and Bodin (Ref. 4, 5) indicates that a filter of the form $\tau S/(\tau S+1)$ with $\tau \simeq 0\text{-}5$ seconds should be sufficient (if $\tau = 0$ then $\hat{\underline{\omega}}(t) = \underline{\omega}_{\hat{D}}$ and $\hat{\underline{\omega}}_{\perp}$ would be consistent with $\hat{\underline{DOWN}}$). The total sense of rotation, $\hat{\underline{\omega}}(t)$, is given by the sum of $\hat{\underline{\omega}}_{\parallel}(t)$ and $\hat{\underline{\omega}}_{\perp}(t)$.

This completes the component by component review of the model. Before describing the quantitative results which were produced by computer simulation, several examples of qualitative predictions will be given.

First consider a standard rate aircraft turn which is abruptly stopped by rolling out of the turn rapidly into level flight. Just before the rollout the subject will perceive himself to have zero roll angle with respect to the earth vertical and a slightly pitched back orientation due to the slightly increased g force in the turn (elevator illusion). In addition he will have no sense of rotation since the canal response to the rotation of the aircraft has long since decayed to zero and $\underline{\omega}_{\hat{D}} = 0$. During the roll out the specific force vector will remain aligned with the yaw axis of the body and diminish in intensity to 1g. $\hat{\underline{SF}}$ will therefore slightly diminish in intensity and will pitch about 1 or 2

degrees (to eliminate the slight pitched back sensation). Since the direction of $\hat{\underline{SF}}$ remains practically constant the otolith pathway to $\underline{R}_{OTO}$ can be considered inactive. Since $\underline{\omega}^{H}_{SF}$ will also equal zero all of $\hat{\underline{\omega}}_{HD}$ will be considered inconsistent (both that part of $\hat{\underline{\omega}}_{HD}$ generated by the rolling out rotation and that due to the after sensation of stopping the aircraft's turn rate). Consequently all of $\hat{\underline{\omega}}_{HD}$ is passed through the high pass filter and is quickly reduced to zero. Therefore, for rough calculations $\underline{R}_{SCC} = 0$ and except for the elimination of the elevator illusion $\hat{\underline{DOWN}}$ will remain essentially unchanged and the subject should sense that he is erect.

Since $\hat{\underline{DOWN}}$ is essentially unchanged $\underline{\omega}_{D}$ in figure 8.4 is approximately zero. The component of $\hat{\underline{\omega}}_{HD}$ which arose from the roll out motion of the aircraft is $\perp$ to DOWN and will therefore be assigned to $\underline{\omega}'_{\perp}$. Since $\underline{\omega}_{D} = \underline{0}$, $\underline{\omega}_{E}$ is set equal to $\underline{\omega}'_{\perp}$ and is high pass filtered with a time constant less than 5 seconds. $\hat{\underline{\omega}}_{\perp}(t)$ equals the output of this filter (since $\underline{\omega}_{D} = 0$) which merely implies that the rolling sensation is shorter lived (due to the high pass filter) than it would have been if the otolith information had not contradicted it. The component of $\hat{\underline{\omega}}_{HD}$ which arose from the aircraft stopping its rate of turn will be in the opposite direction to the original turn and will be essentially parallel to the direction of $\hat{\underline{DOWN}}$. Therefore this component of

$\hat{\underline{\omega}}_{HD}$ will become $\hat{\underline{\omega}}_{\parallel}(t)$ and will not be diminished. The sensations described above are consistent with the illusions known to be associated with aircraft flight. Circumstances which could interfere with these illusions are the following:

1) A passenger with extensive flying experience who expected the turn or roll out might be capable of interpreting the sensations correctly.
2) The pilot who initiated the roll out would certainly have little inclination towards illusions,

or 3) Any visual information would affect the predicted perception since the model presumes that there are no visual cues.

A second example is that of a step in lateral acceleration of 1g. Initially the subject correctly perceives himself to be in an erect position in 1g. Since the subject is never rotated during the experiment the canals are not stimulated and $\hat{\underline{\omega}}_{HD} = \underline{0}$. Referring to figure 8.4 we can conclude that:

$$\hat{\underline{\omega}}(t) = \hat{\underline{\omega}}_{\perp}(t) = [1 - \frac{\tau s}{\tau s+1}]\underline{\omega}_D(t) \qquad (8.10)$$

The only active pathway in figure 8.3 is that for the information from the otoliths. $\hat{\underline{SF}}$ will move very rapidly toward $\underline{SF}$ and then stop which will induce a rapid rise in $\hat{\underline{\omega}}_{SF}$ followed quickly by a rapid decay to zero. $\underline{\omega}^{L}_{SF}$ will rise quickly during the period in which $\hat{\underline{\omega}}_{SF}$ is large and will then slowly decay to zero. Since $\underline{\omega}^{L}_{SF}$ is perpendicular

to both $\hat{\underline{DOWN}}(t-\Delta t)$ and $\hat{\underline{SF}}$, it will pass through C and $\underline{R}_{OTO} = \underline{\omega}^{L}_{SF}$. Finally $\hat{\underline{DOWN}}$ will move toward $\hat{\underline{SF}}$ at a rate proportional to the magnitude of $\underline{\omega}^{L}_{SF}$ (actually a little faster since the lower pathway in figure 8.3 will help somewhat in moving $\hat{\underline{DOWN}}$ toward $\hat{SF}$). Figure 8.5 shows a rough sketch of the approximate time course of these signals. Note that since this stimulus is of type N (see Chapter Seven) the steady state perception of down should align itself with the true specific force with no error.

The last case to be considered before presenting quantitative results is the phenomenon associated with the experiments of Benson and Bodin (Ref. 4, 5) and Guedry (Ref. 34). For a steady state rotation of $\underline{\omega}$ about a horizontal axis:

$$\begin{aligned} \hat{\underline{\omega}}_{HD} &\rightarrow \underline{0} \\ \underline{R}_{SCC} &\rightarrow \underline{0} \\ \underline{\omega}^{L}_{SF} &\rightarrow \hat{\underline{\omega}}_{SF} \simeq \underline{\omega} \\ \underline{R}_{OTO} &= \underline{\omega}^{L}_{SL} \end{aligned} \qquad (8.11)$$

and $$\hat{\underline{DOWN}} \rightarrow \hat{\underline{SF}} \simeq \underline{SF}$$

Each of these can easily be understood by reference to Figure 8.3 except possibly the last relation. It is clear that $\hat{\underline{DOWN}}$ will approach $\underline{SF}$ if it is understood that the rate of rotation of $\hat{\underline{DOWN}}(\underline{\omega}_D)$ will eventually match that of $\underline{SF}$ since $\underline{R}_{OTO}$ approaches the true rotation rate and any constant discrepancies (phase lags) will be eliminated by the lower

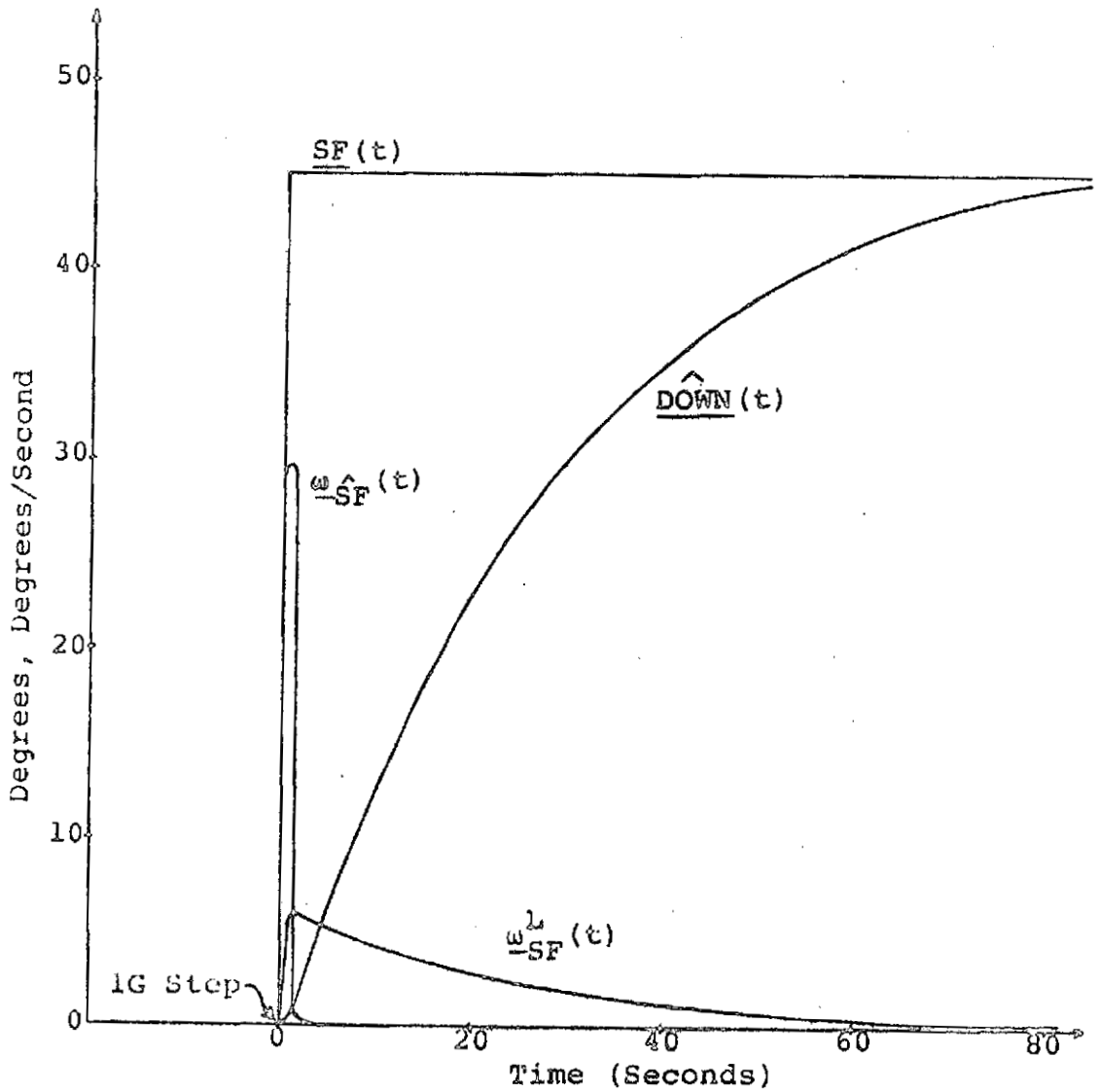

Figure 6.5 Approximate Time Course of Model Parameters and Response to 1G Step in Lateral Acceleration

pathway. Consequently the subject's steady state sensation of rotation during the period of rotation should correctly reflect the true rate of rotation ($\hat{\underline{\omega}} \approx \underline{\omega}$).

Immediately after the rotation stops we can predict that (Figure 8.3):

$\hat{\omega}_{HD}$ will quickly $\rightarrow -\underline{\omega}$ and then decays to zero (this is the typical velocity step response of the canals)

$\underline{\omega}_{SF}\hat{}$ will quickly $\rightarrow \underline{0}$

$\underline{\omega}_{SF}^{H}$ will quickly $\rightarrow +\underline{\omega}$ and then decays to zero

$\underline{\omega}_{C}^{C}$ will quickly $\rightarrow -\underline{\omega}$ and then decays to zero

$\underline{R}_{SCC}$ will quickly $\rightarrow -\underline{\omega}$ and then decays to zero

$\underline{R}_{OTO}$ will remain at $-\underline{\omega}$ and then decays to zero

$\underline{R}_{TOT} = \underline{R}_{OTO} - \underline{R}_{SCC}$ will quickly $\rightarrow \underline{0}$ (8.12)

and furthermore (figure 8.4):

$\underline{\omega}_{D}$ will quickly $\rightarrow 0$

$\underline{\omega}'_{\perp} = \hat{\underline{\omega}}_{HD}$ (since $\hat{\underline{\omega}}_{HD} \perp \hat{\underline{DOWN}}$) and $\underline{\omega}_{\parallel} = 0$

and

$$\hat{\underline{\omega}}(t) = \hat{\underline{\omega}}_{\perp}(t) = \frac{\tau s}{\tau s+1}\,\underline{\omega}'_{\perp} \qquad (8.13)$$

Therefore the model predicts that while a subject should perceive that his position with respect to the vertical is not changing after the rotation ceases he may have (depending on the value of τ chosen) a brief sensation of rotation opposite to the original rotation. Benson and

Boden (Ref. 4, 5) had some subjects who reported a brief sensation of rotation and some who didn't. Whether this discrepancy in reporting is due to the conflict between $\hat{\underline{DOWN}}$ and $\underline{\omega}$ or due to different subjects having different values of τ is unclear. That subjects perceive themselves to have a constant orientation relative to the vertical ($\hat{\underline{DOWN}}$ constant) is not in question. Benson and Bodin report "...that they (the subjects) were quite aware that the stretcher had stopped and of its position relative to the gravitational vertical..." Similar stimuli and reports of subjective responses are described in Ref. 34 .

8.3 Quantitative Model Predictions

The model developed in this chapter has been computerized so that quantitative predictions can be made for arbitrary stimulus combinations. The programs were written in Fortran IV and they include all functions shown in figures 8.2, 8.3 and 8.4. Although the model could be implemented with any update interval, $\Delta t = 1$ sec. was chosen as a reasonable compromise between computational efficiency and simulation bandwidth. One update interval takes approximately .08 seconds of central processor time when utilizing an IBM 370-165 computer.

8.3.1 Dynamic Elevator Illusion

In Chapter Seven the elevator illusion was discussed and a model which correctly predicts its occurrence and magnitude was developed. The transition from head erect in 1g to the perception of backward tilt with the head erect in 1.75 g was used as a test of the dynamic model developed in this chapter. The stimulus input to the model consists of a step in upward acceleration of .75g after the model was stabilized with head erect in 1g. No rotation stimulus was used. Figure 8.6 shows the time course of the predicted pitch sensation which resulted. Superimposed on the model's prediction is the data from Cohen (Ref. 17) in which subjects

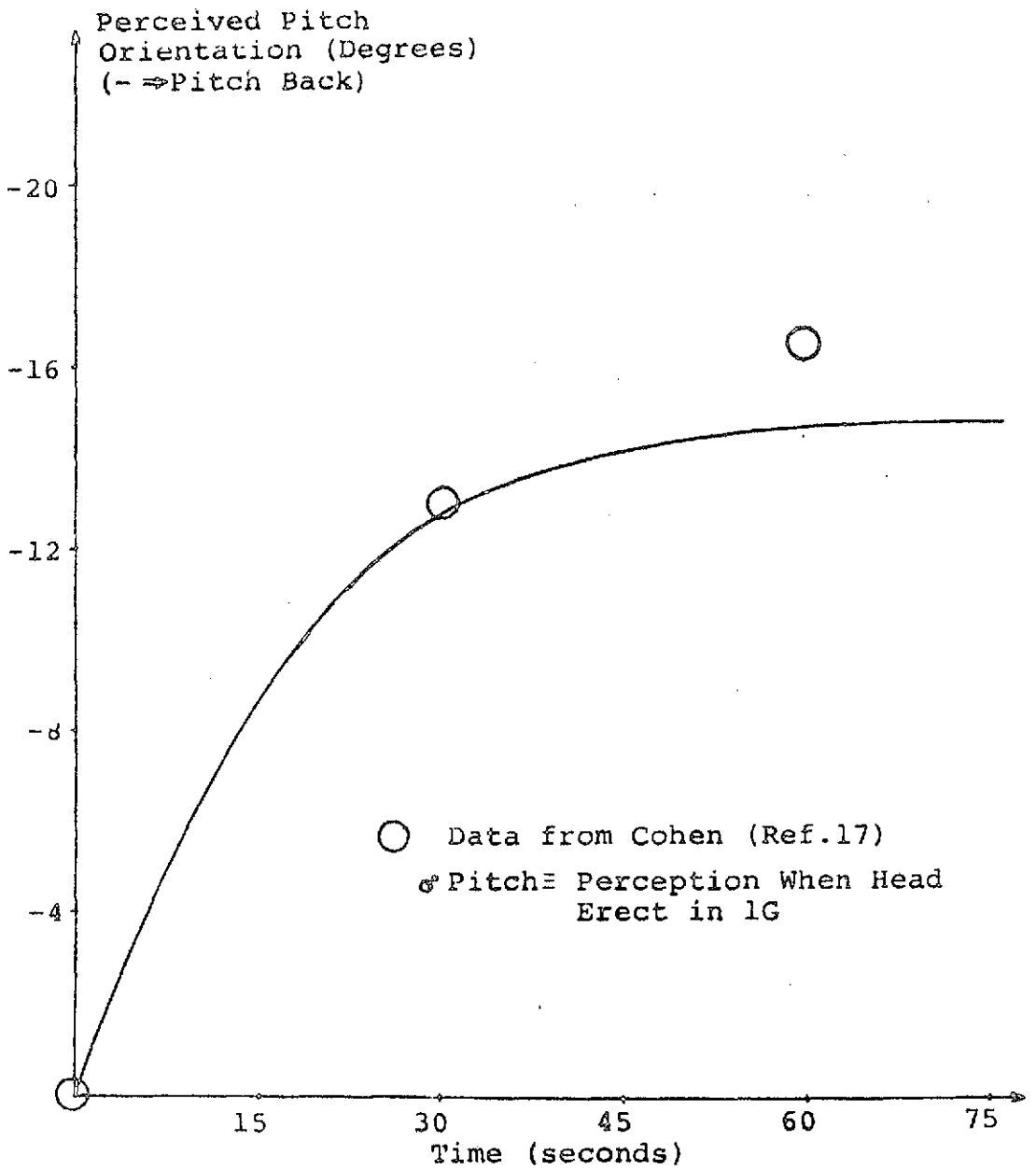

Figure 8.6 Dynamic Elevator Illusion (1.75G)

were given essentially the same stimulus except that the acceleration was produced by a centrifuge. Cohen's subjects perceived a maximum change in pitch orientation of approximately -19°. The discrepancy in the magnitude of the steady state illusion is discussed in Chapter Seven.

8.3.2 Rotation to Lateral Tilt of 5 Degrees

Experiments were conducted in the Man Vehicle Laboratory by Tang (unpublished) in which subjects who were originally erect were tilted 5° laterally over a period of 5 seconds and then held at 5° for several minutes. During the entire period of the stimulus the subjects were instructed to adjust a line to their perceived vertical while being deprived of visual cues. The orientation of the subjects' head was controlled by using a bite board. The time course of the lateral tilt was recorded and used as the stimulus input for the model shown in Figures 8.2 and 8.3. Figure 8.7 shows the stimulus and the resulting prediction of the perception of lateral tilt. The records of subject responses were used to find the average peak perception of tilt and the time of its occurrence. In addition the average perception of tilt after one minute was calculated. These experimental data points are shown in the figure.

8.3.3 Catapult Launch

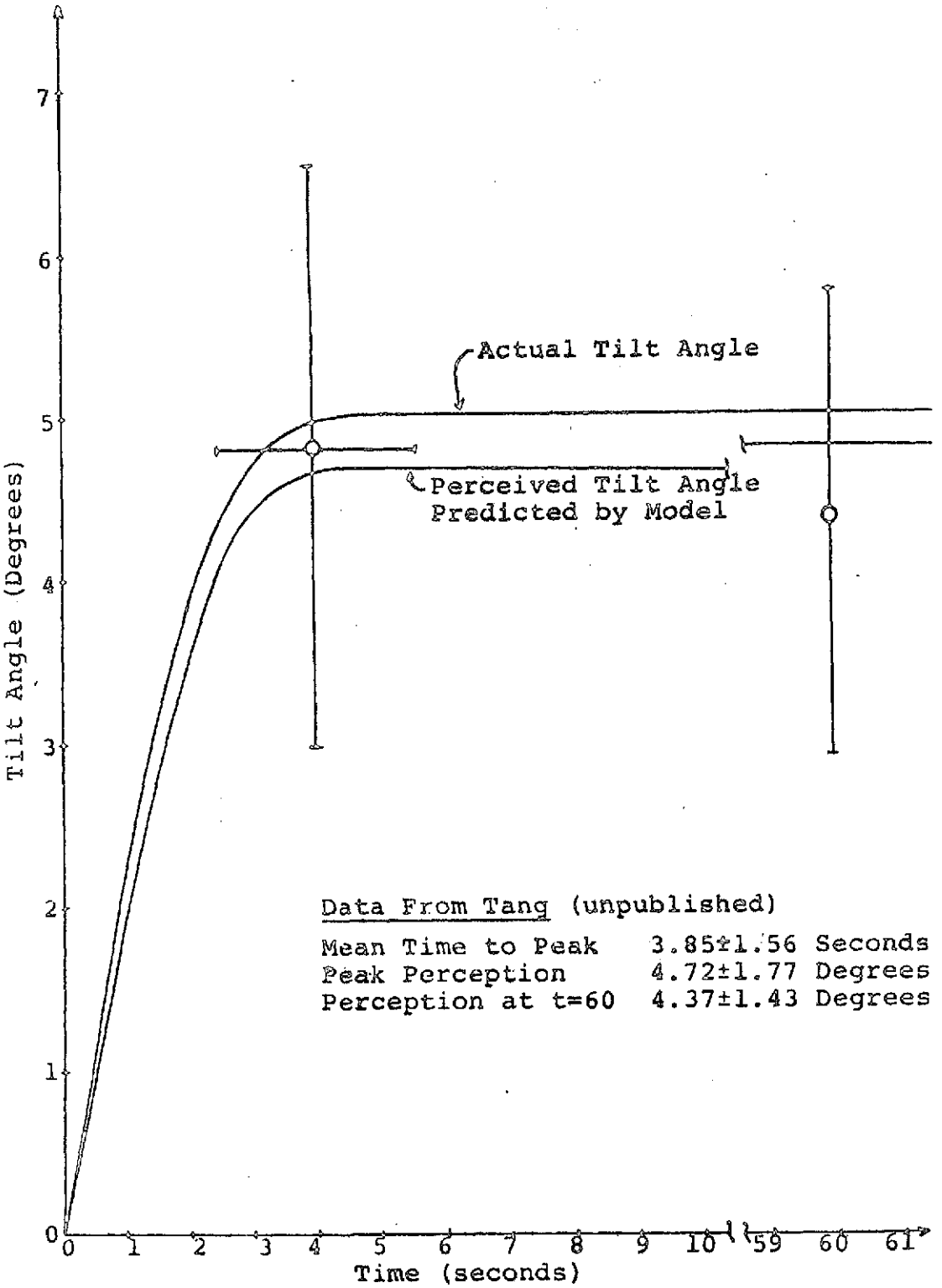

Figure 8.7 Perception of Lateral Tilt

Cohen et. al. (Ref. 18) used a centrifuge to simulate the accelerations encountered in a typical aircraft catapult launching. The average acceleration profile used by Cohen is shown in Figure 8.8 along with an actual catapult launch acceleration profile. Figure 8.9 illustrates the manner in which the acceleration was generated on the centrifuge. The following acceleration profile was used in the simulation of the "down" estimator:

$$\begin{aligned} A_{XHD} &= 3.8\,\mathrm{SIN}(\pi t/3.2)\,g \qquad && t < 3.2 \text{ seconds} \\ &= 0\ g && t > 3.2 \text{ seconds} \end{aligned} \tag{8.14}$$

The rotation profile used in the simulation is given by:

$$\begin{aligned} \omega_{ZHD} &= \frac{2\pi}{3.2}(1. - \cos(2\pi t/3.2))\ \text{deg/sec} && t < 3.2 \\ &= 0\ \text{deg/sec} && t > 3.2 \end{aligned} \tag{8.15}$$

Figure 8.10 illustrates the movement of $\hat{\underline{\text{DOWN}}}$ in response to this stimulus. In addition to the pitch sensation for which Cohen et. al. tested, the model predicts a possible rolling sensation. If this rolling sensation is truly absent then the time constant in the high pass filter (element E of figure 8.3) should be reduced to zero. If the sensation of rolling is even greater, then τ should be increased above .25 sec. Figure 8.11 compares the pitch response of the model to the data given by Cohen et. al. The above simulation was rerun with $\omega_{ZHD} = 0$ (representative of a real catapult launch) and the predicted perception of pitch was essentially the same.

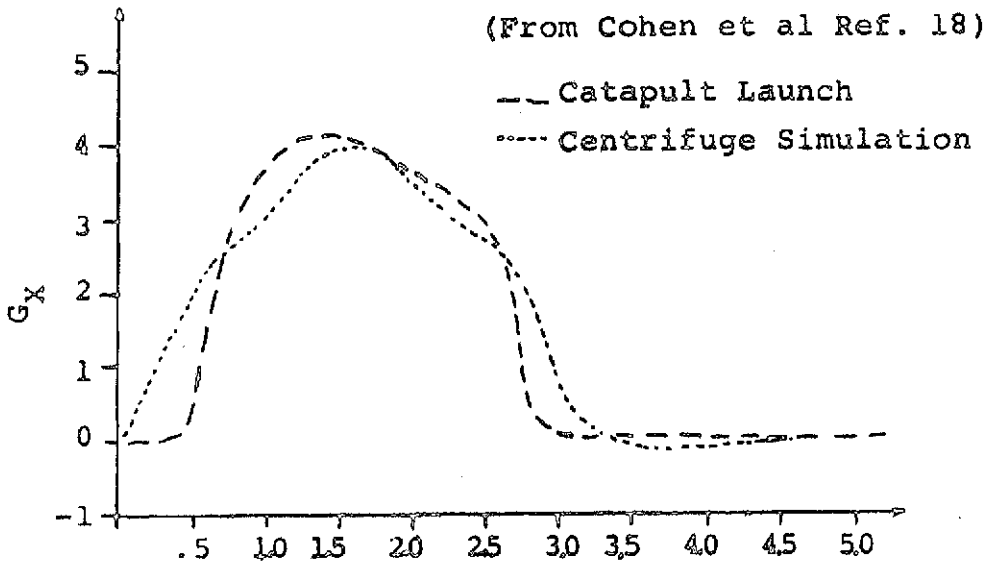

Figure 8.8 Comparison of the G_X Accelerations Recorded in Catapult Launch and Centrifuge Simulation

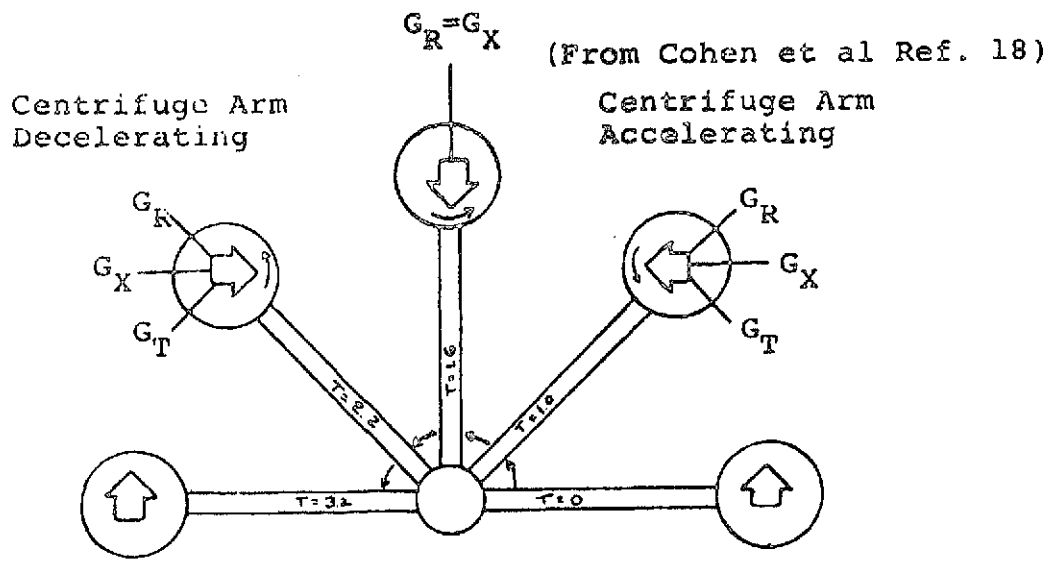

Figure 8.9 Schematic Representation of a Catapult Simulation on the Human Centrifuge

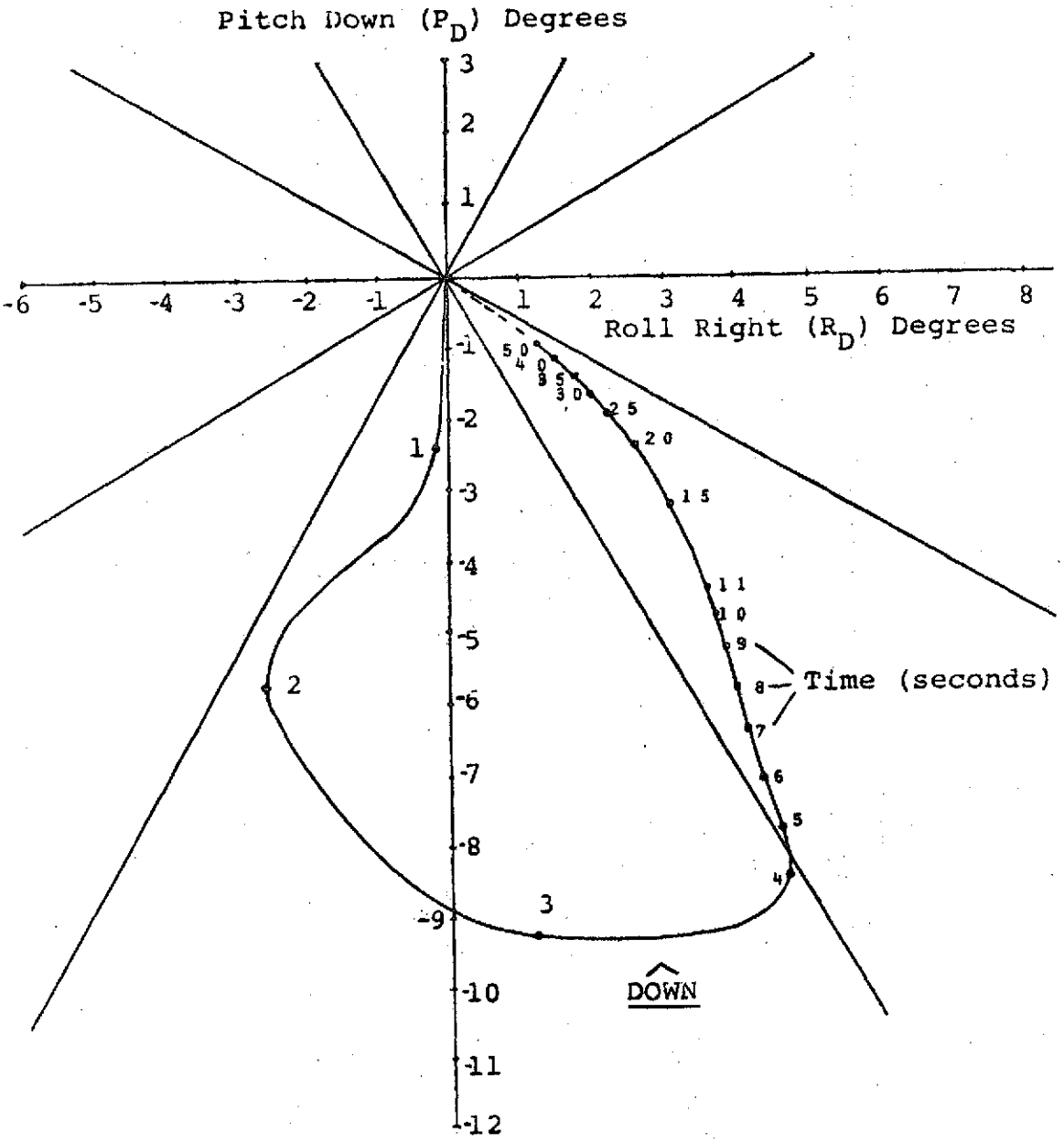

Figure 8.10 Movement of $\widehat{\text{DOWN}}$ for Catapult Launch Simulation

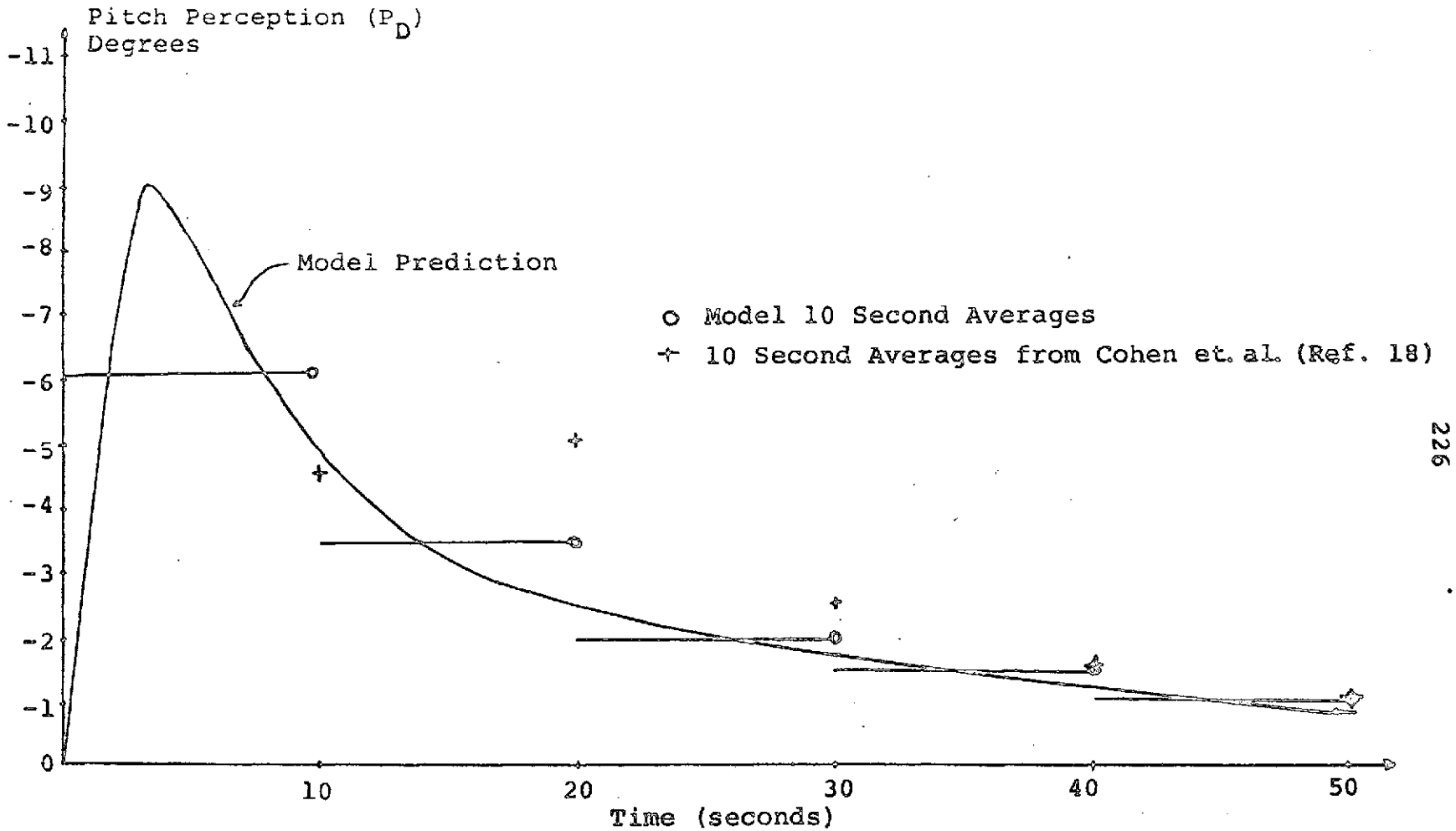

Figure 8.11 Pitch Perception for Catapult Launch Simulation

8.3.4 Frequency Response for Small Pitch and Roll Oscillations

The model's use of otolith and canal information can be best understood by comparing the frequency response of the model to that of the sensors. Since the model has nonlinearities for large tilt angles and for conflicting sensory information, it is important to confine the oscillations to small angles (<10°) and to insure that only simple tilting or pitching stimuli are used. The response is essentially the same in both pitch and roll so only the data from the roll stimuli will be illustrated. Eight frequencies from .05 to 2.1 rad/sec were tested with stimulus amplitudes of 5-10°. Lower frequencies were not tested since extremely long and therefore costly simulations would be necessary. Higher frequencies could not be tested since the update interval for the simulation was 1 second. Figure 8.12 shows the phase response of the model for these frequencies. The amplitude response of the model is within 5% of unity over the range of frequencies tested. It is clear from Figure 8.12 that for low frequency stimuli the model relies on otolith information and for higher frequency stimuli the model relies on information from the semicircular canals. The crossover frequency is approximately at .5 rad/sec. Nashner (Ref. 55) found a crossover frequency of approximately .1HZ = .628 rad/sec from experiments involving postural control of pitch orientation. Since the phase and ampli-

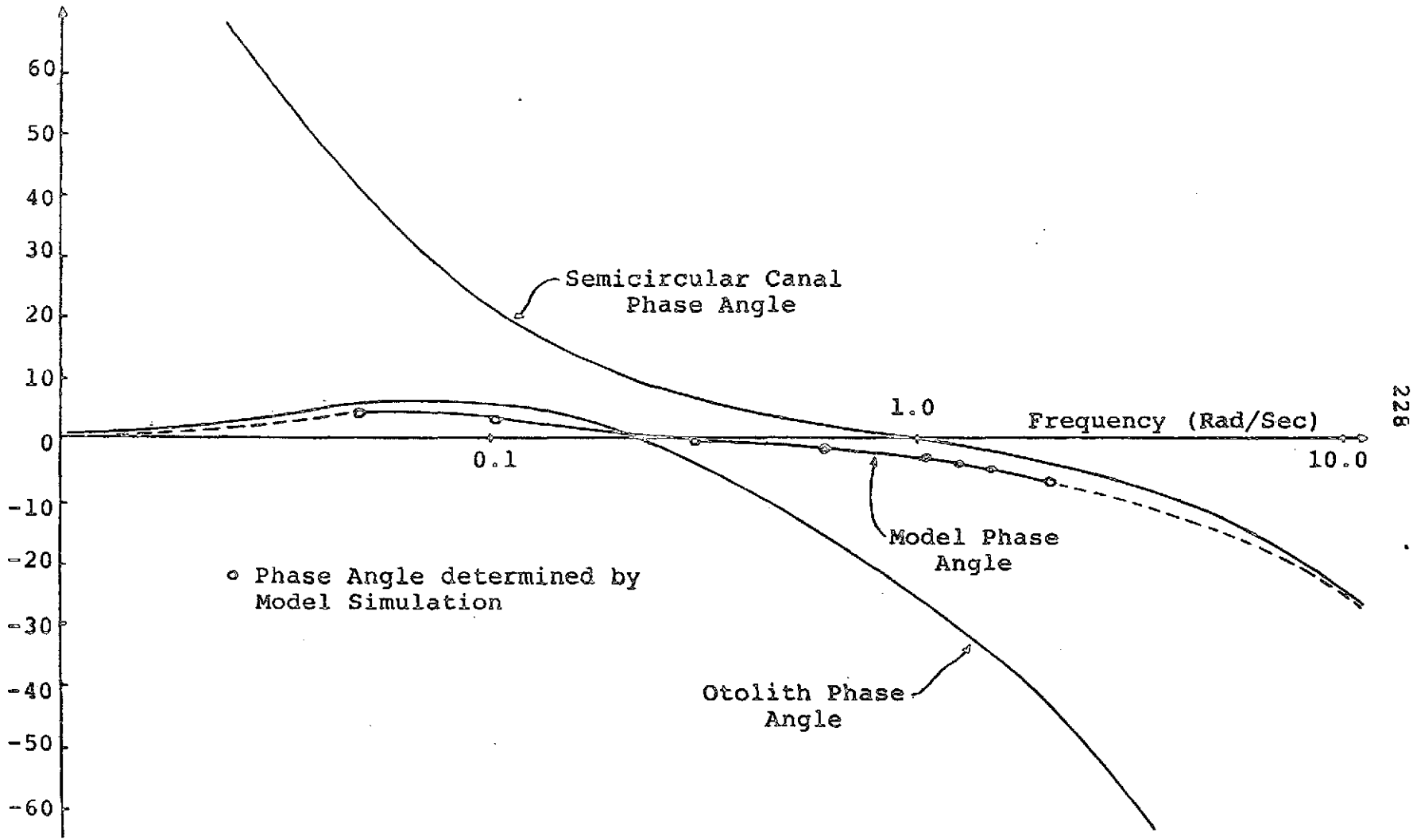

Figure 8.12 Phase Response of Combined Model to Small Tilts (<10°) in Pitch and/or Roll

tude responses are so close to that of a unity gain for frequencies up to about 3 rad/sec the model predicts that our perception for small random tilt oscillations about a head erect position in 1g should be essentially correct.

8.4 Summary

In this chapter a model for the perception of dynamic orientation resulting from stimuli which involve both the otoliths and the semicircular canals was developed. The model was applied both qualitatively and quantitatively to several such stimuli and its predictions evaluated. In all cases the model predictions were in substantial agreement with the known illusions or with the relevant experimental data.

CHAPTER IX

CONCLUSIONS AND SUGGESTIONS FOR FURTHER RESEARCH

Human perception of dynamic orientation based upon vestibular information has been modelled for near-threshold and suprathreshold stimuli. Before the processing of vestibular information could be modelled it was necessary to model the information available from the peripheral sensors. One conclusion which can be drawn from these models of afferent response is that while it is possible that little or no central processing is taking place for simple canal stimulation it is almost certain that significant dynamic processing is occurring in the case of stimuli which only involve otolith function. Furthermore, it has been demonstrated that the differences between the afferent responses observed for the otoliths and the subjective responses seen in psychophysical experiments can be reconciled and that this reconciliation is consistent with the assumption of optimal processing by the higher centers.

The conclusions which can be drawn from this research about the processing of vestibular afferent information by the brain are summarized in the following two sections. Finally, the chapter concludes with some suggestions for research which could extend the results presented in this thesis.

9.1. Summary of Threshold Modelling

Before a reasonable model could be constructed to predict

the detection probabilities for arbitrary near threshold stimuli, it was necessary to determine the basic mechanism which gave rise to sensory thresholds. Two fundamentally different mechanisms were considered. The first hypothesis, called the "simple threshold model," consisted of a dead zone nonlinearity associated with the peripheral sensor which blocked the response from any stimulus which was not sufficiently large. The second hypothesis considered was that sensory thresholds arose only because the stimulus generated afferent response was masked by the variations in afferent firing which are independent of the stimulus. These hypotheses could be distinguished experimentally by determining the threshold level (75% correct detection) associated with a stimulus which is proportional to the sum of a subject's velocity step and acceleration step thresholds. Such an experiment was carried out and the results clearly demonstrated that the second hypothesis, designated the "signal in noise model," was to be preferred to the "simple threshold model." Furthermore the data indicated that the phenomena of vestibular thresholds could be accounted for by a model of central processing of vestibular information consisting only of an optimal processing of afferent firing rates in additive noise with no necessity for peripheral dead zone nonlinearities.

Once the signal in noise hypothesis was accepted as

an adequate model for the mechanism underlying the threshold phenomenon, it was necessary to develop a model of the processor which could predict the detection probabilities as a function of time for arbitrary near threshold stimuli. The model which resulted incorporates a first order processor which attempts to eliminate the tonic discharge and any associated low frequency, low amplitude variations so that the remaining signal can be assumed to consist of only the stimulus related signals and essentially uncorrelated measurement noise. This signal can then be processed sequentially to produce either a "moving right" response, a "moving left" response or no response at the end of each measurement interval. Through the use of Monte Carlo simulations with different sample functions of the noise process, a histogram of responses as a function of time can be generated forany given stimulus which should reveal both the total probability of correctly detecting that stimulus over a given period of time and the general distribution of response latencies. The threshold model for rotational stimuli correctly predicts the threshold magnitudes for velocity steps, acceleration steps and combination stimuli (velocity step plus acceleration step) and correctly indicates the general distribution of response latencies. Finally it is interesting to note that the detector used to model rotational stimuli when coupled with the afferent models for the otoliths was

found to be adequate for predicting both the acceleration step threshold for the utricles and the saccules and in addition gave reasonable predictions for the detection latencies at threshold. While it is possible that such a finding is coincidental it seems more likely that it is indicative of the fact that the higher centers detect motion by processing near threshold canal and otolith information in a similar manner.

9.2. Summary of Suprathreshold Modelling

The problem of modeling human perception of suprathreshold stimuli was divided into three parts. The first part consisted of modelling the afferent information available from the sensors and coupling this with a model of central processing suitable for noninteracting stimuli. The results of this effort were threefold:

1. Predictions could be made for the dynamic response to simple noninteracting stimuli,
2. The best estimate of the head's rotational rate based upon information from the semicircular canals and the best estimate of the direction and magnitude of the specific force vector based upon otolith information was available for further integration for the case of interacting stimuli,

and

3. A consistent mathematical framework had been developed for the central processor which incorporated a model of the a priori information about the stimulus, a model of the sensory dynamics and a model of the variations in afferent firing, and which indicated that at least in the use of otolith information, the central processor made a significant contribution to the total dynamic response.

The second part of this investigation centered on the perception of state orientation (no canal information) with respect to a constant specific force field. A thorough review of the illusions of static orientation indicated that they were consistent with a simple vector transformation which could be associated with differences in the processing of signals arising from stimuli in and stimuli perpendicular to the "utricle plane." Based on these observations a model was developed which incorporated this difference in processing and which was capable of predicting the direction and magnitude of the experimentally determined illusions of orientation. Finally it was observed that the alteration of saccular information required by the model was similar to the nonlinear response to static tilts seen by Fernandez et al. (Ref. 24) in otolith afferents in the squirrel monkey. This similarity suggests that the mechanism which gives rise to these illusions may have at least part of its origin in the peripheral sensor.

Finally the problem of integrating information from the semicircular canals and the otolith for the general class of interacting stimuli was considered. The major difficulty encountered in modelling the perception of dynamic orientation for motions which involve rotations about a horizontal axis was the problem of deriving the transformation of canal and otolith information which produces a perception of orientation with respect to the vertical. Once such a transformation is derived, predictions for the other perpetual outputs (rotation rates, accelerations, etc.) follow in a relatively straightforward manner. The model for the perception of the vertical relies primarily on the otolith sensors for low frequency ($< \sim .5$ rad/sec) changes in orientation and relies primarily on canal information which is confirmed by changes in the direction of the perceived specific force sensed by the otoliths for more rapid changes ($> \sim .5$ rad/sec) in orientation. This spectral division of responsibility is quite reasonable in light of the frequency characteristics of the sensors and the problems associated with any attempt to differentiate between translational accelerations and a change in orientation with respect to the vertical. The response of the model to small variations in tilt angle with respect to the vertical in a 1 g environment indicate that under these conditions the perception of tilt should be essentially correct for frequencies from zero to about three

radians per second. Accuracy in this region of operation should be expected since this is the region in which most head movements take place in daily life.

The model's usefulness in predicting, without detailed simulation, the qualitative nature of the response to be expected from relatively simple interacting stimuli was demonstrated with several examples. Furthermore the accuracy of the model's quantitative predictions were shown for several stimuli for which data was available. While suggestions for further research to improve this model will be given in the next section, the results of the simulations carried out indicate that the model in its present form should be very useful in predicting the perceptual response to a wide variety of stimuli which up until now could not be confidently predicted.

9.3. Suggestions for Further Research

The results presented in this thesis could be extended by further research in the following areas:

1. There is a great need for further information about the dynamic response of otolith afferents to time varying changes in specific force. The model of otolith information developed in Chapter Three is consistent with qualitative descriptions of otolith response but should be compared to more qualitative data. Specifically, a systematic study of the response of first order afferents to stimuli of various frequencies would be very useful.

2. Investigation of possible afferent vestibular thresholds might be conducted by studying the response of afferent fibers to stimuli which are near the perceptual threshold. One difficulty which would arise would be that the noise on a single afferent fiber would be significantly greater than the response due to the stimulus. The only way to circumvent this problem would be to average the responses of many stimulus trials.
3. The statistics of afferent noise should be investigated much more thoroughly than has been done up to this point. Not only should the autocorrelation of the noise process on a single afferent be studied but also its correlation with the noise processes on other sensory afferents. Such an investigation should indicate if the low frequency variation of the tonic discharge which was postulated in this thesis is present and would also suggest the degree to which afferent channels can be considered independent.
4. Further psychophysical experiments should be carried out to determine the effect of a suprathreshold stimulus to one sensor on the detection probabilities associated with a near threshold stimulus to another sensor. The results of such a study might have significant implications concerning the applicability of subthreshold stimuli for the improvement of simulator fidelity.

5. The amount of quantitative data available from psychophysical experiments in which subjects are exposed to interacting stimuli and for which they are requested to indicate their perception of the vertical is quite limited. Any experimental program which systematically investigates these responses would provide very useful information for the modelling of the perceptual response to interacting stimuli.
6. Neurophysiologic studies of the interaction of semicircular canal and otolith information might be very productive. Since the otoliths provide the steady state response to continuous rotations about a horizontal axis in the same way that the visual system does for rotations about a vertical axis, it would be reasonable to assume that higher order vestibular neurons exist (most likely in the medial vestibular nucleus since this is the first nucleus which receives significant projections from both the semicircular canals and the otoliths) which depend upon both semicircular canal afferents and otolith afferents and which correctly reflect the true rotation about a horizontal axis (see Dischgans et al Ref. 22 and Henn, Young, Finley Ref. 37 for evidence of such an interaction between semicircular canal and visual information for rotations about a vertical axis).

7. Finally an attempt should be made to incorporate visual information into the model of human perception of dynamic orientation. While there is not sufficient information at this time to develop a definitive model of visual-vestibular perception of dynamic orientation there is a great need for a preliminary model which includes visual information. Such a model would be useful to suggest critical psychophysical and neurophysiological experiments and could be modified or if necessary radically altered in light of new experimental results. Even if the model underwent several radical changes the explicit nature of such a mathematical model helps to clarify both the issues involved and the underlying assumptions which too often are made but not explicitly recognized or understood.

Appendix A

SUMMARY OF PARAMETERS FOR PERCEPTUAL MODELS

I. SEMICIRCULAR CANAL MODEL

The response of semicircular canal afferents is modelled by the following linear dynamical system (see section 3.1).

$$\dot{\underline{x}}_c = \underline{A}_c\underline{x}_c + \underline{B}_c\omega \tag{A.1}$$

$$y_c = \underline{C}_c\begin{bmatrix}\underline{x}_c \\ \hline \omega\end{bmatrix} + SFR_c + n_c \tag{A.2}$$

where $$\underline{A}_c = \begin{bmatrix} 0 & 1 & 0 \\ 0 & 0 & 1 \\ -.37037 & -17.7966 & -200.0888 \end{bmatrix} \tag{A.3}$$

$$\underline{B}_c = \begin{bmatrix} 0 \\ 0 \\ 1 \end{bmatrix} \tag{A.4}$$

$$\underline{C}_c = [-23.5785, -1131.89, -6371.86, 63.6620] \tag{A.5}$$

SFR_c is the spontaneous firing rate (90 ips) including low frequency variations (A.6)

n_c is a white measurement noise process which is discussed in the section 3.1

ω is the effective stimulus to the canal in (rad/sec)

and y_c is the first order afferent response of the canal (ips)

In the computer simulations used to test the model the afferent response was updated every .1 sec. by the following discrete model:

$$\underline{x}_c(t + .1) = \underline{\Phi}_c(t+.1,t)\underline{x}_c(t) + \underline{D}_c\omega(t+.1) \tag{A.7}$$

$$y_c(t+.1) = \underline{C}_c \begin{bmatrix} \underline{x}_c(t+.1) \\ \hline \omega(t+.1) \end{bmatrix} + SFR_c + n_c \qquad (A.8)$$

where

$$\underline{\Phi}_c = \begin{bmatrix} .9999912 & .09959244 & .47296x10^{-3} \\ -.17517x10^{-3} & .9915322 & .00496791 \\ -.00183626 & -.0879745 & -.440444x10^{-3} \end{bmatrix} \qquad (A.9)$$

$$D_c = \begin{bmatrix} .2241507x10^{-4} \\ .4730012x10^{-3} \\ .4958018x10^{-2} \end{bmatrix} \qquad (A.10)$$

$\underline{C}_c$, SFR and n_c are the same as previously defined and ω is the effective stimulus (rad/sec)

Since the Kalman filter was designed to process one measurement each second and to estimate not only the internal states of the sensor but also the stimulus input, ω, it must have a model of the canal dynamics and the input process. This is accomplished by augmenting the state vector of equation A.1 with a state $x_c(4)$ which represents the input ω (see figure 3.3). The resulting linear model which represents the internal model used by the Kalman estimator is given by:

$$\dot{\underline{x}}_{CI} = \underline{A}_{CI}\underline{x}_{CI} + \underline{B}_{CI}W_{CI} \qquad (A.11)$$

$$y_{CI} = \underline{C}_{CI}\underline{x}_{CI} + SFR_{CI} + n_{CI} \qquad (A.12)$$

where

$$\underline{A}_{CI} = \begin{bmatrix} 0 & 1 & 0 & 0 \\ 0 & 0 & 1 & 0 \\ -.37037 & -17.7966 & -200.0888 & 1 \\ 0 & 0 & 0 & -5 \end{bmatrix} \qquad (A.13)$$

$$B_{CI} = \begin{bmatrix} 0 \\ 0 \\ 0 \\ 5 \end{bmatrix} \tag{A.14}$$

W_{CI} *is a unit white noise process* (A.15)

and y_{CI}, $\underline{C}_{CI}$, SFR_{CI}, n_{CI} are the same as y_c, $\underline{C}_c$, SFR_c, n_c

The discrete version of the Kalman filter (see equations 3.11, 3.13, 3.14 and 3.15) requires the transition matrix associated with $\underline{A}_{CI}$ which is given by

$$\Phi_{CI} = \begin{bmatrix} .99911 & .95698 & .004760 & .767\text{x}10^{-3} \\ -.001763 & .91448 & .004573 & .924\text{x}10^{-3} \\ -.001694 & -.07953 & -.415\text{x}10^{-3} & -.490\text{x}10^{-4} \\ 0.0 & 0.0 & 0.0 & .006738 \end{bmatrix} \tag{A.16}$$

The resultant steady state Kalman Gains are given by

$$\underline{K}_{\infty C} = \begin{bmatrix} -.9191772\text{x}10^{-3} \\ +.8141562\text{x}10^{-5} \\ +.1503512\text{x}10^{-3} \\ +.3055998\text{x}10^{-1} \end{bmatrix} \tag{A.17}$$

Finally the steady state Kalman filter for the semi-circular canal system is given by

$$\hat{\underline{x}}(t+1) = \underline{\Phi}_{CI}\hat{\underline{x}}_C(t) + \underline{K}_{\infty C}[(y_{CI}-SFR_{CI}) - \underline{C}_{CI}\underline{\Phi}_{CI}\hat{\underline{x}}_C(t)] \tag{A.18}$$

where $\hat{\underline{x}}_{C4}(t+1)$ *is the minimum mean squared error estimate of the rotational rate* $\omega(t+1)$

y_{CI} is the afferent measurement at t+1

and $\underline{\Phi}_{CI}$, $\underline{K}^{\infty}_{C}$, SFR_{CI}, $\underline{C}_{CI}$ are defined above.

II. OTOLITH MODEL

The response of utricular afferents is modelled by the following linear dynamical system (see section 3.2).

$$\dot{\underline{x}}_u = \underline{A}_u\underline{x}_u + \underline{B}_u f \tag{A.19}$$

$$y_u = \underline{C}_u\underline{x}_u + SFR_u + n_u \tag{A.20}$$

where

$$A_u = \begin{bmatrix} 0 & 1 \\ -40. & -200.2 \end{bmatrix} \tag{A.21}$$

$$B_u = \begin{bmatrix} 0 \\ 1 \end{bmatrix} \tag{A.22}$$

$$C_u = [1800,\ 18000] \tag{A.23}$$

SFR_u is the spontaneous firing rate (88 ips) including low frequency variations (A.24)

n_u is a white measurement noise process which is discussed in section 3.2

f is the effective specific force acting on the sensor (g's)

and y_u is the afferent response of the utricle (ips).

The discrete version of equations (A.19) and (A.20) for an update interval of .1 seconds is given by

$$\underline{x}_u(t+.1) = \underline{\Phi}_u(t+.1,t)\underline{x}_u(t) + \underline{D}_u\, f(t+.1) \tag{A.25}$$

$$y_u(t+.1) = \underline{C}_u\underline{x}(t+.1) + SFR_u + n_u \tag{A.26}$$

where

$$\underline{\Phi}_U(t+.1,t) = \begin{bmatrix} .98118 & .0049059 \\ -.19624 & -.00098118 \end{bmatrix} \quad (A.27)$$

$$\underline{D}_U = \begin{bmatrix} .47050\text{x}10^{-3} \\ .49059\text{x}10^{-2} \end{bmatrix} \quad (A.28)$$

$\underline{C}_u$, SFR_u and n_u are as previously defined and f is the specific force stimulus (g's). The internal model of the otolith dynamics augmented with the internal model of the stimulus statistics is given by

$$\underline{x}_{UI} = \underline{A}_{UI}\underline{x}_{UI} + \underline{B}_{UI}W_{UI} \quad (A.29)$$

$$y_{UI} = \underline{C}_{UI}\underline{x}_{UI} + SFR_{UI} + n_{UI} \quad (A.30)$$

where

$$\underline{A}_{UI} = \begin{bmatrix} 0 & 1 & 0 \\ -40. & -200.2 & 1 \\ 0 & 0 & -1 \end{bmatrix} \quad (A.31)$$

$$\underline{B}_{UI} = \begin{bmatrix} 0 \\ 0 \\ 1 \end{bmatrix} \quad (A.32)$$

W_{UI} is a unit white noise process (A.33)

and y_{UI}, C_{UI}, SFR_{UI}, n_{UI} are the same as y_U, C_U, SFR_U and n_U

The transition matrix associated with $\underline{A}_{UI}$ for a 1 second update interval is given by:

$$\underline{\Phi}_{UI} = \begin{bmatrix} .81955 & .0040977 & .0028114 \\ -.16391 & -.81955\text{x}10^{-3} & .0012864 \\ 0.0 & 0.0 & .36788 \end{bmatrix} \qquad (A.34)$$

The steady state Kalman gains for the system defined by (A.29) and (A.30) are

$$\underline{K}_{\infty U} = \begin{bmatrix} .1283\text{x}10^{-4} \\ .2792\text{x}10^{-4} \\ .6102\text{x}10^{-2} \end{bmatrix} \qquad (A.35)$$

Finally the steady state Kalman filter for the utricle is given by

$$\hat{\underline{x}}_U(t+1) = \underline{\Phi}_{UI}\hat{\underline{x}}_U(t) + \underline{K}_{\infty U}[(y_{UI}-SFR_{UI}) - \underline{C}_{UI}\underline{\Phi}_{UI}\hat{\underline{x}}_U(t)] \qquad (A.36)$$

y_{UI} is the afferent measurement at t+1

and Φ_{UI}, $\underline{K}_{\infty U}$, SFR_{UI}, C_{UI} are defined above.

The saccular model is identical to that of the utricle except that the afferent response is only half as great ($y_S = y_U/2$) and the resulting Kalman gains are twice as great ($\underline{K}_{\infty S} = 2\underline{K}_{\infty U}$).

REFERENCES

1. Abbott Laboratories, "The Internal Ear", Drawings by Biagio J. Melloni, Abbotts Medical Journal, No. 199, Spring 1957.

2. Aschan, G. and Bergstedt, M., "The Genesis of Secondary Nystagmus Induced by Vestibular Stimuli", Acta. Soc. Med. Upsaliensis, 60, 1955.

3. Aubert, H., "Eine Scheinbare Bedeutende Drehung von Objecten bei Neigung des Kopfes Noch Rechts Oder Links", Arch. Path. Anat. Physiol, 20, 1861.

4. Benson, A.J., Bodin, M.A., "Interaction of Linear and Angular Accelerations on Vestibular Receptors in Man", Aerospace Med., 37, 1966.

5. Benson, A.J. Bodin, M.A., "Effect of Orientation to the Gravitational Vertical on Nystagmus Following Rotation About a Horizontal Axis", Acta. Otobryng., 61, 1966.

6. Benson, A.J., "Interactions Between Semicircular Canals and Gravireceptors", Recent Adv. in Aerospace Med., D.E. Busby Ed., D. Reidel, Holland, 1970.

7. Birdsall, T.G. and Roberts, R.A., "Theory of Signal Detectability: Deferred-Decision Theory", Acous. Soc. Am., 37, 1965.

8. Brockett, R.W., Finite Dimensional Linear Systems, John Wiley and Sons, N.Y., 1970.

9. Brodal, A. and Pompeiano, O. Ed., Basic Aspects of Central Vestibular Mechanisms, Progress in Brain Research, Vol. 37, Elseuier, Amsterdam, 1972.

10. Clark, B., "Thresholds for the Perception of Angular Acceleration in Man", Aerospace Med., 38, 1967.

11. Clark, B., Graybiel, A., "Visual Perception of the Horizontal Following Exposure to Radial Acceleration on a Centrifuge", J. Comp. Physiol. Psychol., 44, 1951.

12. Clark, B., Graybeil, A., "Congributing Factors in the Perception of the Oculogravic Illusion", Amer. J. Psychol., 76, 1963.

13. Clark, B. and Stewart, J.D., "Perception of Angular Acceleration About the Yaw Axis of a Flight Simulator", Aeorspace Med., 33, 1962.

14. Clark, B. and Stewart, J.D., "Magnitude Estimates of Rotational Velocity During and Following Prolonged Increasing, Constant and Zero Acceleration", J. Exp. Psych, 78, 1968.

15. Clark, B. and Stewart, J.D., "Comparison of Three Methods to Determine Thresholds for Perception of Angular Acceleration", Am. J. Psych., 81, 1968.

16. Clark, B. and Stewart, J.D., "Thresholds for the Perception of Angular Acceleration About the Three Major Body Axes", Forth Symposium on the Role of the Vestibular Organs in Space Exploration, NASA SP-187, 1968.

17. Cohen, M.M., "Elvator Illusion: Influence of Otolith Organ Activity and Neck Proprioception", Perception and Psychophysics, (in press).

18. Cohen, M.M., Crosbie, R.I. and Blackburn, L.H., "Disorienting Effects of Aircraft Catapult Launchings", Aerospace Med., 44, 1973.

19. Corvera, J., Hallpike, C.S., and Schuster, E.H.J., "A New Method for the Anatomical Reconstruction of the Human Macular Planes", Acta. Otolaryng., 49, 1958.

20. de Vries, H1., "The Mechanics of the Labyrinth Otoliths", Acta. Otolaryng, 38, 1950.

21. Dichgans, J., Held, R., Young, L.R. and Brandt, T., "Moving Visual Scenes Influence the Apparent Direction of Gravity", Science, 178, 1972.

22. Dichgans, J., Schmidt, C.L. and Graf, W., "Visual Input Improves the Speedometer Function of the Vestibular Nuclei in Goldfish", Exp. Pr. Res., 1973.

23. Dohlman, G., "On the Mechanism of Transformation into Nystagmus on Stimulation of the Semicircular Canals", Acta Otolaryng., 26, 1938.

24. Fernandez, C., Goldberg, J.M. and Abend, W.K., "Response to Static Tilts of Peripheral Neurons Innervating Otolith Organs of the Squirrel Monkey", J. Neurophysiology, 35, 1972.

25. Fluur, E. and Mellström, A., "Vestibular Nystagmus - A Differential Reaction", Acta. Otolaryng., 71, 1971.

26. Gacek, R.R., "Anatomical Evidence for an Efferent Vestibular Pathway", Third Symposium on the Role of Vestibular Organs in Space Exploration, NASA SP-152, 1967

27. Goldberg, J.M. and Fernandez, C., "Physiology of Peripheral Neurons Innervating Semicircular Canals of the Squirrel Monkey, I, II and III", J. Neurophysiology, 34, 1971.

28. Graybiel, A. and Brown, R. H., "The Delay in Visual Reorientation Following Exposure to a Change in Direction of Resultant Force on a Human Centrifuge", J. Gen. Psychol., 45, 1951.

29. Graybiel, A. and Clark, B., "Perception of the Horizontal or Vertical with Head Upright, On the Side, and Inverted Under Static Conditions and During Exposure to Centripetal Force", Aerospace Med., 33, 1962.

30. Graybiel, A., Clark, B., "Validity of the Oculogravic Illusion as a Specific Indicator of Otolith Function", Aerospace Med., 36, 1965.

31. Green, D.M. and Swets, J.A., Signal Detection Theory and Psychophysics, John Wiley, N.Y., 1966.

32. Groen, J.J., Lowenstein, O. and Vendrick, A.J., "The Mechanical Analysis of the Responses from the End Organs of the Horizontal Semicircular Canals in the Isolated Elasmobranch Labyrinth", Physiol., Vol. 117, 1952.

33. Groen, J.J., "The Semicircular Canal Systems of the Organs of Equilibrium, I and II", Physics in Medicine and Biology, 1956-1957.

34. Guedry, F.E., "Orientation of the Rotation Axis Relative to Gravity. Its Influence on Nystagmus and the Sensation of Rotation", Acta. Otolaryng., 60, 1965.

35. Guedry, F.E. and Lauver, L.S., "Vestibular Reactions During Prolonged Constant Angular Acceleration", J. Applied Physiol., 16, 1961.

36. Guedry, F.E., Richmond, G., "Differences in Response Latency with Different Magnitude Angular Acceleration", U.S. Army Medical Research Lab., Report No. 301

37. Henn, V., Young, L.R. and Finley, C., "Visual Input in the Nucleus Vestibularis of the Alert Monkey", Pflügers Arch. Suppl., 343, 1973.

38. Igarashi, M., "Dimensional Study of the Vestibular Apparatus", Laryngoscope, 77, 1967.

39. Jazwinsky, A.H., Stochastic Processes and Filtering Theory, Academic Press, 1970.

40. Johnson, W.H., "The Importance of Otoliths in Disorientation", Aerospace Med., 35, 1964.

41. Kalman, R.E. and Bucy, R.S., "New Results in Linear Filtering and Prediction Theory", Trans. Am. Soc. Mech. Engn., J. Basic Eng., 83, 1961.

42. Lindeman, H.H., "Studies on the Morphology of the Sensory Regions of the Vestibular Apparatus", Ergeb. Anat. Entwickl. Gersch., Vol. 42, 1969.

43. Lowenstein, O. and Sand, A., "The Mechanism of the Semicircular Canal. A Study of Responses of Single-Fibre Preparations to Angular Accelerations and to Rotations at Constant Speed.", Proc. Roy. Soc., London, Ser. B., 129 , 1940.

44. Lowenstein, O. and Sand, A., "The Individual and Integral Activity of the Semicircular Canals of the Elasmobranch Labyrinth", J. Physiol., 99, 1940.

45. Mach, E., "Physikalische Versuche über den Gleichgewichtssin des Menshen", Sitzungber, Math. Nat. Kl. Akad, Wiss. Wien, III Abt., 68, 1873.

46. Mach, E., "Grandlinien der Lehre von den Bewegungsemfindungen", Leipzig: Wilhelm Engelmann, No. 4, 1875.

47. Mach, E., "On Sensations of Orientation", Popular Scientific Lectures (3rd Ed.), McCormack, T.J. (trans.), 1898.

48. Malcolm, R. and Melvill Jones, G., "A Quantitative Study of Vestibular Adaptation in Humans", Acta. Otolaryng., 70, 1970.

49. Mayne, R., "The Audiogyral Illusion and the Mechanism of Spatial Orientation", Bulletin of Mathematical Biophysics, 14, 1952.

50. Mayne, R., "The Analogy of the Vestibular Organs to an Inertial Guidance System", Oto-Rhino-Laryngology, Proc. of the Ninth Intern. Conf., Mexico, 1969.

51. Meiry, J.L., "The Vestibular System and Human Dynamic Space Orientation", ScD.Thesis, MIT, 1965.

52. Miller, E.F., Graybiel, A., "Rotary Autokinesis and Displacement of the Visual Horizontal Associated with Head (Body) Position", Aerospace Medicine, 34, 1963.

53. Müller, G.E., "Uber das Aubertsche Phanomen", Z. Sinnesphysiol., 49, 1916.

54. Nashner, L.M., "Sensory Feedback in Human Postural Control", ScD. Thesis, MIT, 1970.

55. Nashner, L.M., "A Model Describing Vestibular Detection of Body Sway Motion", Acta Otolaryng, 72, 1971.

56. Nelson, J.G., "Effect of Water Immersion and Body Position upon Perception of the Gravitational Vertical", Aerospace Medicine, 39, 1968.

57. Noble, C.E., "The Perception of the Vertical: III the Visual Vertical as a Function of Centrifugal and Gravitation Forces", J. Exp. Psychol., 39, 1949.

58. Oman, C.M., "Dynamic Response of the Semicircular Canal and Lateral Line Organs", PhD. Thesis, MIT, 1972.

59. Oman, C.M. and Young, L.R., "The Physiologic Range of Pressure Difference and Cupula Deflections in the Human Semicircular Canal", Acta. Otolaryng., 74, 1972.

60. Papoulis, A., Probability, Random Variables and Stochastic Processes, McGraw Hill, 1965.

61. Peters, R.A., "Dynamics of the Vestibular System and Their Relation to Motion Perception", Systems Technology Inc., Technical Report, No. 168-1, 1968.

62. Schmid, R., Stefanelli, M. and Mira, E., "Mathematical Modelling: A Contribution to Clinical Vestibular Analysis", Acta. Otolaryng., 72, 1971.

63. Schöne, H., "On the Role of Gravity in Human Spatial Orientation", Aerospace Med., 35, 1964.

64. Schöne, H. and Wade, N.J., "The Influence of Force Magnitude on the Perception of Body Position", Br. J. Psychol., 62, 1971.

65. Steer, R.W., Jr., "The Influence of Angular and Linear Acceleration and Thermal Stimulation on the Human Semicircular Canal", ScD. Thesis, MIT, 1967.

66. Steinhausen, W., "On the Proof of the Movement of the Cupula in the Complete Arcade-ampulla of the Labyrinth Under Rotary and Caloric Stimulation", Pfluger's Archiv. ges Physiol., 22, 1931.

67. Steinhausen, W., "Observations of the Cupula in the Ampullae of the Semicircular Canals of the Labyrinth of a Living Pike", Pfluger's Archiv. ges Physiol., 232, 1933 (MASA Translation TTF-13, 665).

68. van Egmond, A.A.J., Groen, J.J. and Jongkees, L.B.W., "The Mechanics of the Semicircular Canal", J. Physiol., 110, 1949.

69. Van Trees, H.L., Detection, Estimation and Modulation Theory Part I, John Wiley, N.Y., 1968.

70. Vidal, J., Jennerod, M., Lifschitz, W., Leviton, H. and Sequendo, J.P., "Static and Dynamic Properties of Gravity Sensitive Receptors in the Cat Vestibular System", Kybernetik, 9, 1971.

71. Wainstein, L.A., Zubakov, V.D., Extraction of Signals from Noise, Prentice Hall, 1962.

72. Whitkin, H.A., "Perception of the Upright When Direction of Force Acting on the Body is Changed", J. Exp. Psychol., 40, 1950.

73. Wiener, N., Extrapolation, Interpolation, and Smoothing of Stationary Processes, Wiley, 1949.

74. Witkin, H.A., "Further Studies of the Perception of the Upright When the Direction of the Force Acting on the Body is Changed", J. Exp. Psychol., 43, 1952.

75. Witkin, H.A. and Asch, S.E., "Studies in Space Orientation. III Perception of the Upright in the Absence of a Visual Field", J. Exp. Psychol., 38, 1948.

76. Wong, E., Stochastic Processes and Filtering Theory, Academic Press, 1970.

77. Young, L.R., "Effects of Linear Acceleration on Vestibular Nystagmus", Third Symposium on the Role of the Vestibular Organs in Space Exploration, NASA SP-152, 1967.

78. Young, L.R., "The Current Status of Vestibular System Models", Automatica, Vol. 5, 1969.

79. Young, L.R., "Cross Coupling Between Effects of Linear and Angular Acceleration on Vestibular Nystagmus", Bibl. Opthal., 82, 1972.

80. Young, L.R., "Role of the Vestibular System in Posture and Movement", Medical Physiology V., Montecastle ed., Mosby St. Louis, 1974.

81. Young, L.R. and Meiry, J.L., "A Revised Dynamic Otolith Model", Aerospace Med., 39, 1968.

82. Young, L.R. and Oman, C.M., "Model for Vestibular Adaptation to Horizontal Rotation", Aerospace Med., 40, 1969.

83. Young, L.R., "Developments in Modelling Visual-Vestibular Interaction", Whittaker Corp. Report Number AMRL-TR-71-14, 1971.